



**Neide Marisa Costa Gomes**

Licenciada em Ciências da Engenharia Química

## **Advanced Supported and Non Supported Polyoxometalate Materials for Oxidative Catalytic Reactions**

Dissertação para obtenção do Grau de Mestre em  
Engenharia Química e Bioquímica

**Orientador:** Doutor Luís Branco, Investigador Principal, Faculdade de Ciências e  
Tecnologia – Universidade NOVA de Lisboa

**Co-orientadora:** Doutora Sandra Gago, Investigadora Auxiliar, Faculdade de Ciências e  
Tecnologia – Universidade NOVA de Lisboa

### **Júri:**

**Presidente:** Doutor Mário Fernando José Eusébio, Professor Auxiliar (FCT-UNL)

**Arguente:** Doutora Isabel Maria de Figueiredo Ligeiro da Fonseca,  
Professora Associada (FCT-UNL)

**Vogal:** Doutor Luís Alexandre Almeida Fernandes Cobra Branco,  
Investigador Principal (FCT-UNL)





Universidade Nova de Lisboa  
Faculdade de Ciências e Tecnologia

Neide Marisa Costa Gomes  
Licenciada em Ciências da Engenharia Química

## Advanced Supported and Non Supported Polyoxometalate Materials for Oxidative Catalytic Reactions

Dissertação para obtenção do Grau de Mestre em  
Engenharia Química e Bioquímica

**Orientador:** Doutor Luís Branco, Investigador Principal, Faculdade de Ciências e  
Tecnologia – Universidade NOVA de Lisboa

**Co-orientadora:** Doutora Sandra Gago, Investigadora Auxiliar, Faculdade de Ciências e  
Tecnologia – Universidade NOVA de Lisboa

### Júri:

**Presidente:** Doutor Mário Fernando José Eusébio, Professor Auxiliar (FCT-UNL)

**Arguente:** Doutora Isabel Maria de Figueiredo Ligeiro da Fonseca,  
Professora Associada (FCT-UNL)

**Vogal:** Doutor Luís Alexandre Almeida Fernandes Cobra Branco,  
Investigador Principal (FCT-UNL)



**ADVANCED SUPPORTED AND NON SUPPORTED POLYOXOMETALATE MATERIALS  
FOR OXIDATIVE CATALYTIC REACTIONS**

Copyright @ Neide Marisa Costa Gomes, Faculdade de Ciências e Tecnologia (FCT),  
Universidade NOVA de Lisboa (UNL)

A Faculdade de Ciências e Tecnologia e a Universidade Nova de Lisboa têm o direito, perpétuo e sem limites geográficos, de arquivar e publicar esta dissertação através de exemplares impressos reproduzidos em papel ou de forma digital, ou por qualquer outro meio conhecido ou que venha a ser inventado, e de a divulgar através de repositórios científicos e de admitir a sua cópia e distribuição com objectivos educacionais ou de investigação, não comerciais, desde que seja dado crédito ao autor e editor.



## **Acknowledgments**

Começo por agradecer aos meus orientadores, Dr.<sup>a</sup> Sandra Gago e Dr.<sup>o</sup> Luís Branco. Obrigada Sandra, por todo o apoio e (incrível!) paciência. Obrigada por responder às dezenas de telefonemas e e-mails com dúvidas, sempre mostrando disponibilidade, carinho e simpatia. Obrigada Luis por toda a ajuda prestada, disponibilidade, apoio, paciência e conhecimento científico transmitido, demonstrando sempre boa disposição e boa vontade. Obrigada aos dois por todo o tempo despendido da vossa parte, assim como as incríveis oportunidades que me proporcionaram durante estes últimos meses. Era impossível encontrar melhores orientadores.

Quero agradecer também aos integrantes do laboratório do grupo de Fotoquímica, em especial à Andreia e à Noémi pela ajuda prestada para realizar este trabalho, e claro, por todo o carinho e boa disposição.

Um especial obrigado à Dr.<sup>a</sup> Salete Balula, ao Dr.<sup>o</sup> Carlos Granadeiro, à Fátima Mirante e a todos os integrantes do laboratório onde trabalhei na Faculdade de Ciências da Universidade do Porto, por me receberem na sua linda cidade e por me permitirem realizar parte do estudo no seu laboratório. Obrigada pela incrível hospitalidade e por me fazerem sentir confortável enquanto estive longe de casa.

Aos meus pais. Obrigada pelo vosso amor e encorajamento desde... que me consigo lembrar. Obrigada por me levarem (e irem buscar) de carro até à estação quase todos os dias para poder dormir mais um bocadinho. Obrigada por me ajudarem a investir no meu futuro e educação, e principalmente por acreditarem nas minhas capacidades. Gosto muito de vocês, o vosso apoio fez toda a diferença.

À minha irmã Neuza, a minha “role model”. Por inspirar-me constantemente, guiar-me e a ensinar-me o verdadeiro significado de trabalhar arduamente.

Ao meu Fábio, o meu pilar. Por tudo. Nunca poderei agradecer o suficiente por todo o apoio e amor que me dá todos os dias. Obrigada por me apoiares em tudo e por me maneres motivada durante este percurso, principalmente quando as coisas ficavam complicadas. Não consigo imaginar como teria sido se não te tivesse comigo. Obrigada por estares sempre do meu lado, gosto muito muito muito de ti.

Um obrigado muito especial à minha Velinha. A melhor amiga e companheira que alguma vez poderia ter tido durante os meus anos de faculdade, e, espero eu, para o resto da minha vida. Obrigada por estares sempre do meu lado, e por estares presente nesta grande vitória (não só minha, mas tua também! Parabéns!).

A todos os meus bons amigos, por todo o apoio, força e motivação que bem foi precisa. Ah, e por me aturarem constantemente!

A toda a gente que contribuiu para a minha felicidade durante estes 5 anos de faculdade. Cada um de vocês tem um lugar especial no meu coração.





## Abstract

In this work, new heterogeneous catalysts based on mesoporous silica nanoparticles (MSNPs) with different cations of ionic liquids (ILs) covalently bonded to their surface, 1-butyl-3-methylimidazolium ( $[C_4MIM]^+$ ), 1-butylpyridinium ( $[C_4Py]^+$ ) and tetrabutylammonium ( $[N_{4,4,4,4}]^+$ ), and with the polyoxometalate (POM) derived from phosphomolybdic acid ( $[H_{(3-x)}PMo_{12}O_{40}]^{x-}$ ) as anions were prepared. Their analogous homogeneous compounds were also prepared for comparison (POM-ILs),  $[N_{4,4,4,4}]_3[PMo_{12}O_{40}]$ ,  $[C_4MIM]_3[PMo_{12}O_{40}]$  and  $[C_4Py]_3[PMo_{12}O_{40}]$ .

The catalysts were characterized by elemental analysis, in solution ( $^1H$  and  $^{31}P$ ) and solid-state ( $^{13}C$  and  $^{31}P$ ) NMR spectroscopy, DLS (for the silica nanoparticles), SEM, TEM, EDS, X-ray fluorescence spectroscopy, FTIR spectroscopy and ICP-MS.

The homogeneous catalysts were applied in the preliminary oxidation reactions of two lignin model compounds, cinnamyl alcohol and guaiacol, varying the reaction conditions (time, presence of hydrogen peroxide and use of conventional heating or microwave heating). The results obtained were characterized by solution  $^1H$  NMR spectroscopy. The oxidation of cinnamyl alcohol seems to be promissory using microwave heating process in comparison to conventional process.

All catalysts prepared were also applied in the oxidative desulfurization reactions of a multicomponent model diesel, composed by 1-benzothiophene, dibenzothiophene, 4-methyldibenzothiophene and 4,6-dimethyldibenzothiophene in order to study the performance of each catalyst in the removal of sulfur compounds present in fuels. This part of the study was performed in Faculdade de Ciências from Universidade do Porto, and the catalytic performance was evaluated by gas chromatography.

The heterogeneous catalysts had the most promising results, in particular MSNPs- $[N_{4,4,4,4}]POM$  achieving 100% of total desulfurization after only 2 hours. Its recycling ability was evaluated for three consecutive cycles and it was observed an increase of the catalytic efficiency for the second and third cycles reaching the complete desulfurization of the model diesel after just 1h instead of the 2h. The catalysts with cation tetrabutylammonium had the best results in both heterogeneous and homogeneous catalysis in comparison to the other two catalysts. In general, all catalysts tested had interesting results.

**Keywords:** Green Chemistry, Polyoxometalate based Ionic Liquids (POM-ILs), Mesoporous Silica Nanoparticles (MSNPs), Lignin valorization, Oxidative Desulfurization.



## Resumo

Neste trabalho foram preparados novos catalisadores heterogêneos suportados em Nanopartículas Mesoporosas de Sílica (NPMs) com diferentes catiões de líquidos iônicos ligados covalentemente às suas superfícies (1-butil-3-metilimidazólio ( $[C_4MIM]^+$ ), 1-butilpiridínio ( $[C_4Py]^+$ ) e tetrabutilamônio ( $[N_{4,4,4,4}]^+$ )), e com o anião derivado do polioxometalato ácido fosfomolibdico ( $[H_{(3-x)}PMo_{12}O_{40}]^{x-}$ ). Os compostos homogêneos análogos (sem as nanopartículas de sílica) foram também preparados para comparação (LI-POM),  $[N_{4,4,4,4}]_3[PMo_{12}O_{40}]$ ,  $[C_4MIM]_3[PMo_{12}O_{40}]$  e  $[C_4Py]_3[PMo_{12}O_{40}]$ .

Os catalisadores homogêneos e heterogêneos foram caracterizados por análise elemental, espectroscopia de RMN de sólidos ( $^{13}C$  e  $^{31}P$ ) e em solução ( $^1H$  e  $^{31}P$ ), DLS, análises SEM e TEM, EDS, fluorescência de raios-X, espectroscopia de infravermelhos e ICP-MS.

Na segunda parte do trabalho experimental, os catalisadores homogêneos preparados foram aplicados em reações preliminares de oxidação de dois compostos modelo da lignina, álcool cinamil e guaiacol, variando as condições de reação (tempo, presença de peróxido de hidrogênio e uso de aquecimento convencional ou de microondas). Os resultados destes ensaios foram caracterizados por  $^1H$  RMN em solução. A oxidação do álcool cinamílico parece ser promissora utilizando microondas, em comparação com o processo de aquecimento convencional.

Todos os catalisadores preparados foram aplicados em reações de dessulfurização oxidativa de um gasóleo modelo multicomponente, contendo na sua composição 1-benzotiofeno, dibenzotiofeno, 4-metildibenzotiofeno e 4,6-dimetildibenzotiofeno. O objectivo foi estudar as suas eficiências na eliminação de compostos de enxofre presentes nos combustíveis. Esta parte do estudo foi realizada na Faculdade de Ciências da Universidade do Porto, e os resultados foram caracterizados por cromatografia de gás. Os catalisadores heterogêneos tiveram os resultados mais promissores, particularmente o catalisador MSNPs- $[N_{4,4,4,4}]POM$ , que após apenas 2 horas obteve uma dessulfurização total de 100%. A sua capacidade de reciclagem foi avaliada para três ciclos consecutivos e observou-se um aumento da eficiência catalítica para o segundo e terceiro ciclos, atingindo-se uma dessulfurização completa após apenas 1 hora em vez de 2 horas. Os catalisadores com o catião tetrabutilamônio tiveram os melhores resultados em ambos os tipos de catalisadores, em comparação aos outros dois catiões utilizados. No geral, todos os catalisadores tiveram resultados muito interessantes.

**Palavras-chave:** Química Verde, Líquidos Iônicos baseados em polioxometalatos (POM-LIs), Nanopartículas de Sílica Mesoporosa, Valorização de Lignina, Dessulfurização Oxidativa.



# **Table of Contents**

	<b>Page</b>
Acknowledgments.....	vii
Table of Contents .....	xiii
Tables Index .....	xv
Figures Index.....	xvi
Abbreviations List .....	xxi
Compound List.....	xxiii
1. Introduction.....	1
1.1. Green Chemistry .....	1
1.2. Biomass.....	2
1.2.1. Application of Biomass .....	3
1.2.2. Biomass and Sustainability .....	4
1.3. Lignin.....	4
1.4. Catalytic Oxidation.....	7
1.4.1. Homogeneous and Heterogeneous Catalysis .....	8
1.4.2. Oxidative Desulfurization .....	9
1.5. Ionic Liquids.....	9
1.6. Polyoxometalates .....	12
1.7. Mesoporous Silica Nanoparticles.....	13
2. Experimental Section .....	15
2.1. Materials and Equipments .....	15
2.2. Synthesis of POM-IL catalysts .....	17
2.2.1. Synthesis of Ionic Liquids .....	17
2.2.2. Synthesis of POM-IL catalysts .....	20
2.3. Synthesis of MSNPs-POM-ILs catalysts .....	21
2.3.1. Synthesis of Mesoporous Silica Nanoparticles (MSNPs) .....	21
2.3.2. Synthesis of MSNPs-POM-IL catalysts.....	23
2.4. Catalytic Reactions .....	28
2.4.1. Oxidation of Lignin Model Compounds .....	28
2.4.1.1. Conventional Heating using acetonitrile as solvent .....	28
2.4.1.2. Microwave Heating using acetonitrile as solvent.....	29
2.4.2. Oxidative Desulfurization of a Model Diesel.....	30
2.4.2.1. Homogeneous Catalysts.....	30
2.4.2.2. Heterogeneous Catalysts .....	31

3. Results and Discussion.....	33
3.1. Objectives.....	33
3.2. Preparation and characterization of IL and POM-IL catalysts.....	34
3.2.1. Preparation and characterization of Ionic Liquids.....	34
3.2.1.1. N-(3-trimethoxysilylpropyl)pyridinium iodide.....	35
3.2.1.2. N-(3-trimethoxysilylpropyl)-3-methylimidazolium iodide .....	37
3.2.1.3. N-(3-trimethoxysilylpropyl)tributylammonium iodide .....	39
3.2.1.4. 1-butylpyridinium chloride .....	40
3.2.2. Preparation and characterization of POM-IL catalysts .....	43
3.2.2.1. [N <sub>4,4,4,4</sub> ] <sub>3</sub> [PMo <sub>12</sub> O <sub>40</sub> ] catalyst.....	43
3.2.2.2. [C <sub>4</sub> MIM] <sub>3</sub> [PMo <sub>12</sub> O <sub>40</sub> ] catalyst .....	46
3.2.2.3. [C <sub>4</sub> Py] <sub>3</sub> [PMo <sub>12</sub> O <sub>40</sub> ] catalyst .....	48
3.3. Preparation and characterization of MSNPs and MSNPs-POM-IL catalysts..	52
3.3.1. Preparation and characterization of Mesoporous Silica Nanoparticles (MSNPs).....	52
3.3.2. Preparation and characterization of MSNPs-POM-IL catalysts.....	54
3.3.2.1. MSNPs-[C <sub>4</sub> MIM]POM .....	54
3.3.2.2. MSNPs-[C <sub>4</sub> Py]POM catalyst .....	61
3.3.2.3. MSNPs-[N <sub>4,4,4,4</sub> ]POM.....	64
3.4. Catalysis.....	68
3.4.1. Oxidation of Lignin Model Compounds .....	68
3.4.1.1. Conventional Heating .....	68
3.4.1.2. Microwave Heating .....	69
3.4.2. Oxidative Desulfurization of a multicomponent model diesel.....	71
3.4.2.1. Homogeneous Catalysts in ODS .....	72
3.4.2.2. Heterogeneous Catalyst in ODS .....	75
4. Conclusion.....	85
5. Future Perspectives.....	87
Annexes.....	89
Bibliography.....	99

## Tables Index

	<b>Page</b>
<b>Table 1.1.</b> - Principles of Green Chemistry and Green Engineering. ....	1
<b>Table 1.2.</b> - Average distribution of the three main biopolymers in softwood, hardwood and switchgrass (Adapted from <i>McKendry et al.</i> <sup>13</sup> ).....	4
<b>Table 1.3.</b> - Comparison of main advantages/disadvantages of Homogeneous and Heterogeneous catalysts (adapted from <sup>25</sup> ). ....	8
<b>Table 3.1.</b> - Reaction conditions and results of the synthesis of the prepared ionic liquids. ....	35
<b>Table 3.2.</b> - Elemental Analysis calculated and determined results (C, N and H) for [N <sub>4,4,4,4</sub> ] <sub>3</sub> [PMo <sub>12</sub> O <sub>40</sub> ] catalyst.....	44
<b>Table 3.3.</b> - Elemental Analysis calculated and determined results (C, N and H) for [C <sub>4</sub> MIM] <sub>3</sub> [PMo <sub>12</sub> O <sub>40</sub> ] catalyst.....	46
<b>Table 3.4.</b> - Elemental Analysis calculated and determined results (C, N and H) for [C <sub>4</sub> Py] <sub>3</sub> [PMo <sub>12</sub> O <sub>40</sub> ] catalyst. ....	49
<b>Table 3.5.</b> - ICP-MS results for P and Mo for MSNPs-[C <sub>4</sub> MIM]POM catalyst.....	58
<b>Table 3.6.</b> - ICP-MS results for Mo content of MSNPs-[C <sub>4</sub> MIM]POM catalyst. ....	58
<b>Table 3.7.</b> - Elemental Analysis results in mmol/g of material for C and N content in MSNPs-[C <sub>4</sub> MIM]POM catalyst. ....	58
<b>Table 3.8.</b> - ICP-MS results for Molybdenum for MSNPs-[C <sub>4</sub> Py]POM catalyst. ....	62
<b>Table 3.9.</b> - ICP-MS results for Molybdenum for MSNPs-[C <sub>4</sub> Py]POM catalyst. ....	62
<b>Table 3.10.</b> - Elemental Analysis results in mmol/g of material for C and N content in MSNPs-[C <sub>4</sub> Py]POM catalyst. ....	62
<b>Table 3.11.</b> - ICP-MS results for Molybdenum of MSNPs-[N <sub>4,4,4,4</sub> ]POM catalyst.....	65
<b>Table 3.12.</b> - ICP-MS results for Molybdenum for MSNPs-[N <sub>4,4,4,4</sub> ]POM catalyst. ....	65
<b>Table 3.13.</b> - Elemental Analysis results in mmol/g of material for C and N content for MSNPs-[N <sub>4,4,4,4</sub> ]POM catalyst. ....	65
<b>Table 3.14.</b> - Quantities of solvent (acetonitrile), oxidant (hydrogen peroxide), model oil and standard solution used in the study of the Homogeneous catalysts in ODS. ....	72
<b>Table 3.15.</b> - Results and comparison of the performance of Homogeneous catalysts in ODS. Representation of the oxidation of the model oil compounds (ppm) and total desulfurization (%), over time (min).....	74
<b>Table 3.16.</b> - Quantities of solvent ([BMIM][PF <sub>6</sub> ]), oxidant (hydrogen peroxide), model oil and standard solution used in the study of the Heterogeneous catalyst in ODS, in 3 equal cycles, half the solvent quantity and half oxidant quantity studies. ....	75
<b>Table 3.17.</b> - Results and comparison of the performance of the Heterogeneous catalyst in ODS in 3 cycles and half the solvent quantity and half oxidant quantity. Representation of the oxidation of the model oil compounds (ppm) and total desulfurization (%), over time (min). ....	77
<b>Table 3.18.</b> - Results and comparison of the performance of MSNPs-[C <sub>4</sub> Py]POM catalyst in ODS in 3 cycles Representation of the oxidation of the model oil compounds (ppm) and total desulfurization (%), over time (min).....	78
<b>Table 3.19.</b> - Results and comparison of the performance of MSNPs-[N <sub>4,4,4,4</sub> ]POM catalyst in ODS in 3 cycles Representation of the oxidation of the model oil compounds (ppm) and total desulfurization (%), over time (min).....	79
<b>Table 3.20.</b> - Comparison of the performance of Homogeneous catalysts in ODS, over time (min). ....	80
<b>Table 3.21.</b> - Comparison of the performance of Heterogeneous catalysts and Heterogeneous catalyst in ODS, over time (in minutes). ....	81

## Figures Index

	<i>Page</i>
<b>Fig. 1.1.</b> - Representation of Biomass sources: Agricultural and forest residues, industrial residues, urban waste and livestock waste (Adapted from <i>Kunakawan Group</i> ).....	2
<b>Fig. 1.2.</b> - Photosynthesis process (Adapted from <i>Wisegeek</i> ).....	3
<b>Fig. 1.3.</b> - Comparison between the use of fossil fuels and the use of biomass to produce fuel, chemical products and biomaterials (adapted from <i>GLW Energy</i> ). ....	3
<b>Fig. 1.4.</b> - Phenylpropanoid monomers, <i>p</i> -coumaryl alcohol, coniferyl alcohol and sinapyl alcohol of lignin polymer.....	5
<b>Fig. 1.5.</b> - Lignin Chemical structure (Adapted from <i>Lignoworks</i> ).....	6
<b>Fig. 1.6.</b> - Lignin Model Compounds, Cinnamyl Alcohol and Guaiacol.....	7
<b>Fig. 1.7</b> - Chemical representation of some types of sulfur-organic compounds present in fuel: 1-benzothiophene (1-BT), dibenzothiophene (DBT), 4-methyldibenzothiophene (4-MDBT) and 4,6-dimethyldibenzothiophene (4,6-DMDBT).....	9
<b>Fig. 1.8.</b> - Common structures of cations and anions present in ionic liquids (R, R <sub>1</sub> , R <sub>2</sub> , R <sub>3</sub> and R <sub>4</sub> are alkyl groups). ....	10
<b>Fig. 1.9.</b> - Some of the applications of Ionic Liquids (Adapted). ....	11
<b>Fig. 1.10.</b> - Chemical representation of an isopolyanion (Linqvist) and heteropolyanions (Keggin, Wells-Dawson and Anderson-Evans) ( <i>Adapted from</i> ).....	12
<b>Fig. 1.11.</b> - Schematic representation of the functions of two surfactants for assembly of the MSNPs (adapted from <i>Wu et al</i> ). ....	13
<b>Fig. 2.1.</b> – Calcination of Mesoporous Silica Nanoparticles (MSNPs) at a temperature of 550 °C for 5 h, using a heating rate of 1 °C/min.....	22
<b>Fig. 2.2.</b> – Sample preparation for DLS analysis. Use of bidistilled water (left), Ultrasonication to disperse particles (middle) and analysis using a Horiba Scientific Nano Particle Analyzer SZ-100 (right). ....	22
<b>Fig. 2.3.</b> – FTIR tablet preparation using KBr as a solid solvent. ....	24
<b>Fig. 3.1.</b> - Chemical structures of the desired Ionic Liquids. ....	34
<b>Fig. 3.2.</b> - Schematic representation of the synthesis of ionic liquid N-(3-trimethoxysilylpropyl)pyridinium iodide with pyridine and 3-iodopropyltrimethoxysilane. ....	35
<b>Fig. 3.3.</b> - Fourier-Transform Infrared Spectrum of N-(3-trimethoxysilylpropyl)pyridinium iodide (blue), pyridine (grey) and 3-iodopropyltrimethoxysilane (green). ....	36
<b>Fig. 3.4.</b> - Solution <sup>1</sup> H NMR Spectrum of N-(3-trimethoxysilylpropyl)pyridinium iodide, in deuterated chloroform. ....	36
<b>Fig. 3.5.</b> - Schematic representation of the synthesis of ionic liquid N-(3-trimethoxysilylpropyl)-3-methylimidazolium iodide using 1-methylimidazole and 3-iodopropyltrimethoxysilane. ....	37
<b>Fig. 3.6.</b> - Fourier-Transform Infrared Spectra of N-(3-trimethoxysilylpropyl)-3-methylimidazolium iodide (blue), 1-methylimidazole (grey) and 3-iodopropyltrimethoxysilane (green). ....	37
<b>Fig. 3.7.</b> - Liquid State <sup>1</sup> H NMR Spectrum of N-(3-trimethoxysilylpropyl)-3-methylimidazolium iodide, in deuterated chloroform.....	38
<b>Fig. 3.8.</b> - Schematic representation of the synthesis of ionic liquid N-(3-trimethoxysilylpropyl)tributylammonium iodide using tributylamine and 3-iodopropyltrimethoxysilane.....	39
<b>Fig. 3.9.</b> - Fourier-Transform Infrared Spectrum of N-(3-trimethoxysilylpropyl)tributylammonium iodide (green), tributylamine (blue) and 3-iodopropyltrimethoxysilane (grey). ....	39
<b>Fig. 3.10.</b> - Liquid State <sup>1</sup> H NMR Spectrum of N-(3-trimethoxysilylpropyl)tributylammonium iodide, in deuterated chloroform.....	40
<b>Fig. 3.11.</b> - Schematic representation of the synthesis of ionic liquid 1-butylpyridinium chloride using pyridine and 1-chlorobutane. ....	40



<b>Fig. 3.12.</b> - Fourier-Transform Infrared Spectrum of solid 1-butylpyridinium chloride (blue), pyridine (grey), liquid 1-butylpyridinium chloride (green) and 1-clorobutane (light blue). .....	41
<b>Fig. 3.13.</b> - Liquid State <sup>1</sup> H NMR Spectrum of 1-butylpyridinium chloride, in deuterated chloroform.....	41
<b>Fig. 3.14.</b> - Chemical structures of the prepared Homogeneous Catalysts, [N <sub>4,4,4,4</sub> ] <sub>3</sub> [PMo <sub>12</sub> O <sub>40</sub> ], [C <sub>4</sub> MIM] <sub>3</sub> [PMo <sub>12</sub> O <sub>40</sub> ] and [C <sub>4</sub> Py] <sub>3</sub> [PMo <sub>12</sub> O <sub>40</sub> ]. .....	43
<b>Fig. 3.15.</b> - Schematic representation of ion exchange from [N <sub>4,4,4,4</sub> ][Br] to [N <sub>4,4,4,4</sub> ] <sub>3</sub> [PMo <sub>12</sub> O <sub>40</sub> ], using ion exchange resin Amberlyst® A26 (OH <sup>-</sup> ) and polyoxometalate H <sub>3</sub> PMo <sub>12</sub> O <sub>40</sub> .....	43
<b>Fig. 3.16.</b> - Fourier-Transform Infrared Spectra of catalyst [N <sub>4,4,4,4</sub> ] <sub>3</sub> [PMo <sub>12</sub> O <sub>40</sub> ] (blue), [N <sub>4,4,4,4</sub> ][Br] (green) and polyoxometalate H <sub>3</sub> PMo <sub>12</sub> O <sub>40</sub> (grey).....	44
<b>Fig. 3.17.</b> - Solution <sup>1</sup> H NMR Spectrum of [N <sub>4,4,4,4</sub> ] <sub>3</sub> [PMo <sub>12</sub> O <sub>40</sub> ], in DMSO-d <sub>6</sub> .....	45
<b>Fig. 3.18.</b> - Solution <sup>31</sup> P NMR Spectrum of [N <sub>4,4,4,4</sub> ] <sub>3</sub> [PMo <sub>12</sub> O <sub>40</sub> ], in DMSO-d <sub>6</sub> . .....	45
<b>Fig. 3.19.</b> - Schematic representation of ion exchange from [C <sub>4</sub> MIM][Cl] to [C <sub>4</sub> MIM] <sub>3</sub> [PMo <sub>12</sub> O <sub>40</sub> ], using ion exchange resin Amberlyst® A26 (OH <sup>-</sup> ) and polyoxometalate H <sub>3</sub> PMo <sub>12</sub> O <sub>40</sub> .....	46
<b>Fig. 3.20.</b> - Fourier-Transform Infrared Spectra of [C <sub>4</sub> MIM][Cl] (blue), polyoxometalate H <sub>3</sub> PMo <sub>12</sub> O <sub>40</sub> (green) and catalyst [C <sub>4</sub> MIM] <sub>3</sub> [PMo <sub>12</sub> O <sub>40</sub> ] (grey). .....	47
<b>Fig. 3.21.</b> - Solution <sup>1</sup> H NMR Spectrum of [C <sub>4</sub> MIM] <sub>3</sub> [PMo <sub>12</sub> O <sub>40</sub> ], in DMSO-d <sub>6</sub> . .....	47
<b>Fig. 3.22.</b> - Solution <sup>31</sup> P NMR Spectrum of [C <sub>4</sub> MIM] <sub>3</sub> [PMo <sub>12</sub> O <sub>40</sub> ], in DMSO-d <sub>6</sub> . .....	48
<b>Fig. 3.23.</b> - Schematic representation of ion exchange from [C <sub>4</sub> Py][Cl] to [C <sub>4</sub> Py] <sub>3</sub> [PMo <sub>12</sub> O <sub>40</sub> ], using ion exchange resin Amberlyst® A26 (OH <sup>-</sup> ) and polyoxometalate H <sub>3</sub> PMo <sub>12</sub> O <sub>40</sub> .....	48
<b>Fig. 3.24.</b> - Fourier-Transform Infrared Spectra of 1-butylpyridinium chloride [C <sub>4</sub> Py][Cl] (blue), polyoxometalate H <sub>3</sub> PMo <sub>12</sub> O <sub>40</sub> (green) and catalyst [C <sub>4</sub> Py] <sub>3</sub> [PMo <sub>12</sub> O <sub>40</sub> ] (grey). .....	49
<b>Fig. 3.25.</b> - Solution <sup>1</sup> H NMR Spectrum of [C <sub>4</sub> Py] <sub>3</sub> [PMo <sub>12</sub> O <sub>40</sub> ], in DMSO-d <sub>6</sub> . .....	50
<b>Fig. 3.26.</b> - Solution <sup>31</sup> P NMR Spectrum of [C <sub>4</sub> Py] <sub>3</sub> [PMo <sub>12</sub> O <sub>40</sub> ], in DMSO-d <sub>6</sub> . .....	51
<b>Fig. 3.27.</b> - DLS analysis of the Mesoporous Silica Nanoparticles size distribution with three measurements.....	52
<b>Fig. 3.28.</b> - TEM images of the Mesoporous Silica Nanoparticles used for the production of the catalysts magnified to 500 nm, 200 nm and 100 nm, using water as solvent.....	53
<b>Fig. 3.29.</b> - Fourier-Transform Infrared Spectra of Mesoporous Silica Nanoparticles before (green) and after (blue) calcination process.....	53
<b>Fig. 3.30.</b> - Schematic representation of the three-step synthesis method of heterogeneous catalyst MSNPs-[C <sub>4</sub> MIM]POM.....	54
<b>Fig. 3.31.</b> - TEM images of the heterogeneous catalyst MSNPs-[C <sub>4</sub> MIM]POM, in resolutions 500 nm and 100 nm, using water as solvent.....	55
<b>Fig. 3.32.</b> - SEM images of heterogeneous catalyst MSNPs-[C <sub>4</sub> MIM]POM, magnified in resolutions 4 μm, 1 μm and 500 nm.....	55
<b>Fig. 3.33.</b> - EDS analysis of the elements present in the heterogeneous catalyst MSNPs-[C <sub>4</sub> MIM]POM prepared.....	56
<b>Fig. 3.34.</b> - X-Ray Fluorescence Spectroscopy results of the heterogeneous catalyst MSNPs-[C <sub>4</sub> MIM]POM. ....	57
<b>Fig. 3.35.</b> - X-Ray Fluorescence Spectroscopy results magnified, of the heterogeneous catalyst MSNPs-[C <sub>4</sub> MIM]POM. ....	57
<b>Fig. 3.36.</b> - Fourier-Transform Infrared Spectra of MSNPs-[C <sub>4</sub> MIM]POM catalyst (blue), MSNPs-[C <sub>4</sub> MIM][OH] (green) and polyoxometalate H <sub>3</sub> PMo <sub>12</sub> O <sub>40</sub> (grey).....	59
<b>Fig. 3.37.</b> - Solution <sup>1</sup> H NMR Spectrum of MSNPs-[C <sub>4</sub> MIM]POM, in Deuterium Oxide basified with sodium hydroxide and 1,3,5-trioxane as internal standard.....	59
<b>Fig. 3.38.</b> - Solid State <sup>13</sup> C CP MAS NMR Spectrum of MSNPs-[C <sub>4</sub> MIM]POM.....	60
<b>Fig. 3.39.</b> - Solid State <sup>31</sup> P NMR Spectrum of MSNPs-[C <sub>4</sub> MIM] <sub>3</sub> [PMo <sub>12</sub> O <sub>40</sub> ]. .....	61
<b>Fig. 3.40.</b> - Schematic representation of the three-step synthesis method of heterogeneous catalyst MSNPs-[C <sub>4</sub> Py]POM. ....	61
<b>Fig. 3.41.</b> - TEM images of the heterogeneous catalyst MSNPs-[C <sub>4</sub> Py]POM, in resolutions 500 nm, 200 nm and 100 nm, using water as solvent.....	62

<b>Fig. 3.42.</b> - Fourier-Transform Infrared Spectra of MSNPs-[C <sub>4</sub> Py]POM catalyst (blue), MSNPs-[C <sub>4</sub> Py][OH] (green) and polyoxometalate H <sub>3</sub> PMo <sub>12</sub> O <sub>40</sub> (grey).....	63
<b>Fig. 3.43.</b> - Solution <sup>1</sup> H NMR Spectrum of MSNPs-[C <sub>4</sub> Py]POM, in Deuterium Oxide basified with sodium hydroxide and 1,3,5-trioxane as internal standard. ....	63
<b>Fig. 3.44.</b> - Schematic representation of the three-step synthesis method of heterogeneous catalyst MSNPs-[N <sub>4,4,4,4</sub> ]POM.....	64
<b>Fig. 3.45.</b> - TEM images of the heterogeneous catalyst MSNPs-[N <sub>4,4,4,4</sub> ]POM, in resolutions 500 nm, 200 nm and 100 nm, using water as solvent.....	64
<b>Fig. 3.46.</b> - Fourier-Transform Infrared Spectra of MSNPs-[N <sub>4,4,4,4</sub> ]POM catalyst (blue), MSNPs-[N <sub>4,4,4,4</sub> ][OH] (green) and polyoxometalate H <sub>3</sub> PMo <sub>12</sub> O <sub>40</sub> (grey). ....	66
<b>Fig. 3.47.</b> - Solution <sup>1</sup> H NMR Spectrum of MSNPs-[N <sub>4,4,4,4</sub> ]POM, in Deuterium Oxide basified with sodium hydroxide and 1,3,5-trioxane as internal standard.....	66
<b>Fig. 3.48.</b> - Solid State <sup>13</sup> C CP MAS NMR Spectrum of MSNPs-[N <sub>4,4,4,4</sub> ]POM.....	67
<b>Fig. 3.49.</b> - Solid State <sup>31</sup> P NMR Spectrum of MSNPs-[N <sub>4,4,4,4</sub> ]POM.....	67
<b>Fig. 3.50.</b> - Oxidation of cinnamyl alcohol using polyoxometalate H <sub>3</sub> PMo <sub>12</sub> O <sub>40</sub> as catalyst, without using hydrogen peroxide, with conventional heating.....	68
<b>Fig. 3.51.</b> - Oxidation of cinnamyl alcohol using catalyst [N <sub>4,4,4,4</sub> ] <sub>3</sub> [PMo <sub>12</sub> O <sub>40</sub> ], using hydrogen peroxide with conventional heating. ....	69
<b>Fig. 3.52.</b> - Oxidation of cinnamyl alcohol using polyoxometalate H <sub>3</sub> PMo <sub>12</sub> O <sub>40</sub> , using hydrogen peroxide and microwave heating.....	69
<b>Fig. 3.53.</b> - Oxidation of cinnamyl alcohol using catalyst [C <sub>4</sub> MIM] <sub>3</sub> [PMo <sub>12</sub> O <sub>40</sub> ], using hydrogen peroxide and microwave heating.....	70
<b>Fig. 3.54.</b> - Oxidation of cinnamyl alcohol using catalyst [C <sub>4</sub> Py] <sub>3</sub> [PMo <sub>12</sub> O <sub>40</sub> ], using hydrogen peroxide and microwave heating.....	70
<b>Fig. 3.55.</b> - Schematic representation of Oxidative Desulfurization (ODS) of 1-benzothiophene (1-BT), dibenzothiophene (DBT), 4-methyldibenzothiophene (4-MDBT) and 4,6-dimethyldibenzothiophene (4,6-DMDBT) using a catalyst, a solvent and an oxidant.....	71
<b>Fig. 3.56.</b> - Representation of the initial extraction of the Oxidative Desulfurization of sulfur compounds.....	72
<b>Fig. 3.57.</b> - Reactors with acetonitrile, model oil and standard solution used in the study of the Homogeneous catalysts in ODS. ....	73
<b>Fig. 3.58.</b> - Graphic of the development of the Oxidative Desulfurization process of sulfur compounds using [N <sub>4,4,4,4</sub> ] <sub>3</sub> [PMo <sub>12</sub> O <sub>40</sub> ] catalyst. ....	73
<b>Fig. 3.59.</b> - Graphic representation of the Gas Chromatography results of the Oxidative Desulfurization of petroleum model compounds using Homogeneous Catalysts.....	75
<b>Fig. 3.60.</b> - Paraffin bath setting for the ODS reactions.....	76
<b>Fig. 3.61.</b> - Gas Chromatograph used to analyze the ODS samples.....	76
<b>Fig. 3.62.</b> - Graphic representation of the Gas Chromatography results of the Oxidative Desulfurization of petroleum model compounds using MSNPs-[C <sub>4</sub> MIM]POM as a Heterogeneous Catalyst.....	78
<b>Fig. 3.63.</b> - Graphic representation of the Gas Chromatography results of the Oxidative Desulfurization of petroleum model compounds using MSNPs-[C <sub>4</sub> Py]POM as a Heterogeneous Catalyst.....	79
<b>Fig. 3.64.</b> - Graphic representation of the Gas Chromatography results of the Oxidative Desulfurization of petroleum model compounds using MSNPs-[N <sub>4,4,4,4</sub> ]POM as a Heterogeneous Catalyst.....	80
<b>Fig. 3.65.</b> - Graphic representation of the total desulfurization obtained (in percentage) of Homogeneous Catalysts after 6 hours of oxidation. ....	81
<b>Fig. 3.66.</b> - Graphic representation of the total desulfurization obtained (in percentage) of Heterogeneous Catalysts after 2 hours of oxidation. ....	82
<b>Fig. A.1.1.</b> - <sup>1</sup> H NMR (400.13 MHz, D <sub>2</sub> O + NaOH, 25 °C) of MSNPs-[C <sub>4</sub> MIM][I].....	89
<b>Fig. A.1.2.</b> - <sup>1</sup> H NMR (400.13 MHz, D <sub>2</sub> O + NaOH, 25 °C) of MSNPs-[C <sub>4</sub> MIM][OH]. ....	89
<b>Fig. A.1.3.</b> - <sup>1</sup> H NMR (400.13 MHz, D <sub>2</sub> O + NaOH, 25 °C) of MSNPs-[C <sub>4</sub> Py][I].....	90

<b>Fig. A.1.4.</b> - $^1\text{H}$ NMR (400.13 MHz, $\text{D}_2\text{O}$ + NaOH, 25 °C) of MSNPs-[ $\text{C}_4\text{Py}$ ][OH].	90
<b>Fig. A.1.5.</b> - $^1\text{H}$ NMR (400.13 MHz, $\text{D}_2\text{O}$ + NaOH, 25 °C) of MSNPs-[ $\text{N}_{4,4,4,4}$ ][I].	91
<b>Fig. A.1.6.</b> - $^1\text{H}$ NMR (400.13 MHz, DMSO $d_6$ , 25 °C) of lignin model compound, cinnamyl alcohol.	91
<b>Fig. A.1.7.</b> - $^1\text{H}$ NMR (400.13 MHz, DMSO $d_6$ , 25 °C) of the catalysis of cinnamyl alcohol using $\text{H}_3\text{PMo}_{12}\text{O}_{40}$ as catalyst, in conventional heating.	92
<b>Fig. A.1.8.</b> - $^1\text{H}$ NMR (400.13 MHz, DMSO $d_6$ , 25 °C) of the catalysis of cinnamyl alcohol using $\text{H}_2\text{O}_2$ (30%) and [ $\text{N}_{4,4,4,4}$ ] $_3$ [ $\text{PMo}_{12}\text{O}_{40}$ ] as catalyst, in conventional heating.	92
<b>Fig. A.1.9.</b> - $^1\text{H}$ NMR (400.13 MHz, DMSO $d_6$ , 25 °C) of the catalysis of cinnamyl alcohol using $\text{H}_3\text{PMo}_{12}\text{O}_{40}$ as catalyst, in microwaves.	93
<b>Fig. A.1.10.</b> - $^{31}\text{P}$ NMR (100.61 MHz, DMSO $d_6$ , 25 °C) of [ $\text{N}_{4,4,4,4}$ ] $_3$ [ $\text{PMo}_{12}\text{O}_{40}$ ] catalyst.	93
<b>Fig. A.1.11.</b> - $^{31}\text{P}$ NMR (100.61 MHz, DMSO $d_6$ , 25 °C) of [ $\text{C}_4\text{MIM}$ ] $_3$ [ $\text{PMo}_{12}\text{O}_{40}$ ] catalyst.	94
<b>Fig. A.1.12.</b> - $^{31}\text{P}$ NMR (100.61 MHz, DMSO $d_6$ , 25 °C) of [ $\text{C}_4\text{Py}$ ] $_3$ [ $\text{PMo}_{12}\text{O}_{40}$ ] catalyst.	94
<b>Fig. A.1.13.</b> - Solid State $^{13}\text{C}$ CP MAS NMR (162 MHz, 25 °C) of MSNPs-[ $\text{C}_4\text{MIM}$ ]POM catalyst.	95
<b>Fig. A.1.14.</b> - Solid State $^{13}\text{C}$ CP MAS NMR (162 MHz, 25 °C) of MSNPs-[ $\text{N}_{4,4,4,4}$ ]POM catalyst.	95
<b>Fig. A.1.15.</b> - Solid State $^{31}\text{P}$ CP MAS NMR (100.61 MHz, 25 °C) of MSNPs-[ $\text{C}_4\text{MIM}$ ]POM catalyst.	96
<b>Fig. A.1.16.</b> - Solid State $^{31}\text{P}$ CP MAS NMR (100.61 MHz, 25 °C) of MSNPs-[ $\text{N}_{4,4,4,4}$ ]POM catalyst.	96
<b>Fig. A.2.1.</b> - FTIR spectra of MSNPs-[ $\text{C}_4\text{MIM}$ ][I], N-(3-trimethoxysilylpropyl)-3-methylimidazolium iodide and MSNPs.	97
<b>Fig. A.2.2.</b> - FTIR spectra of MSNPs-[ $\text{C}_4\text{MIM}$ ][I] and MSNPs-[ $\text{C}_4\text{MIM}$ ][OH].	97
<b>Fig. A.2.3.</b> - FTIR spectra of MSNPs-[ $\text{C}_4\text{Py}$ ][I], MSNPs-[ $\text{C}_4\text{Py}$ ][OH], MSNPs and N-(3-trimethoxysilylpropyl)pyridinium iodide.	98
<b>Fig. A.2.4.</b> - FTIR spectra of MSNPs-[ $\text{N}_{4,4,4,4}$ ][I], MSNPs and N-(3-trimethoxysilylpropyl)tributylammonium iodide.	98



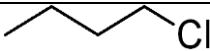
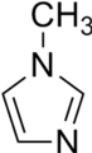
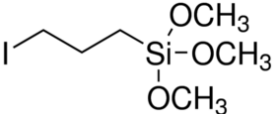
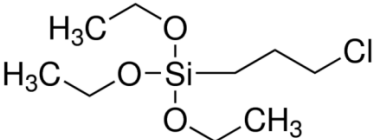
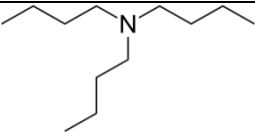
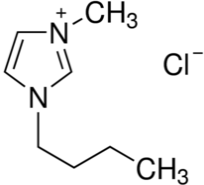
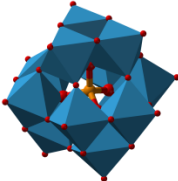
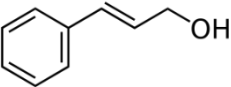
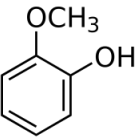
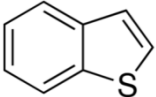
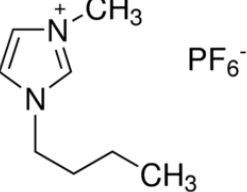
## Abbreviations List

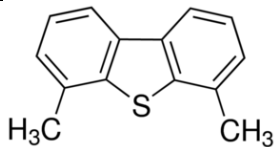
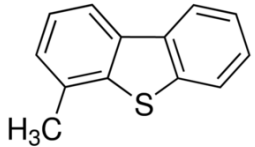
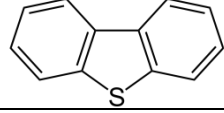
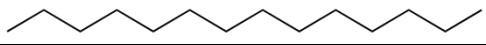
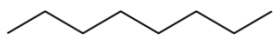
<sup>1</sup> H NMR	Proton Nuclear Molecular Resonance
1-BT	1-Benzothiophene
4-MDBT	4-Methyldibenzothiophene
4,6-DMDBT	4,6-Dimethyldibenzothiophene
<sup>13</sup> C NMR	Carbon Nuclear Molecular Resonance
<sup>31</sup> P NMR	Phosphorus Nuclear Molecular Resonance
μ	Micron
BTEB	1,4-Bis(triethoxysilyl) benzene
[C <sub>4</sub> MIM][Cl]	1-Butyl-3-methylimidazolium chloride
cm	Centimeter
CTAB	n-Cetyltrimethylammonium bromide
CTAC	Cetyltrimethylamine chloride
DBT	Dibenzothiophane
DLS	Dynamic Light Scattering
DMSO	Dimethylsulfoxide
EDS	Energy Dispersive X-ray Spectroscopy
FTIR	Fourier-transform infrared spectroscopy
GC	Gas Chromatography
h	Hour
ICP-MS	Inductively Coupled Plasma Mass Spectrometry
IL	Ionic Liquid
IUPAC	International Union of Pure And Applied Chemistry
M	Molar
MW	Molecular Weight
MIM	1-Methylimidazolium
min	Minute
mM	miliMolar
MOSNPs	Mesoporous Organosilica Nanoparticles
MSNPs	Mesoporous Silica Nanoparticles
nm	Nanometer
ODS	Oxidative Desulfurization
POM	Polyoxometalate
ppm	Parts per million
Py	Pyridinium
rpm	Rotations per minute
s	Second
SEM	Scanning Electron Microscopy
T	Temperature
t	Time
TEA	Triethanolamine
TEM	Transmission Electron Microscopy
TEOS	Tetraethyl orthosilicate
UV	Ultra-violet
Vis	Visible
XRF	X-Ray Fluorescence



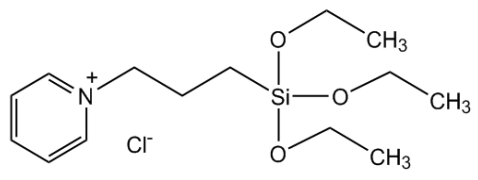
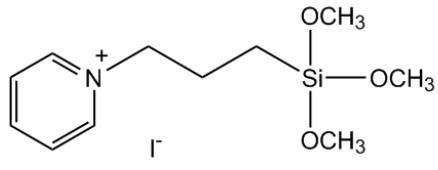
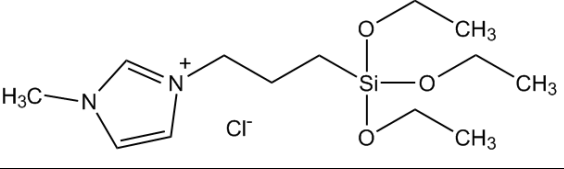
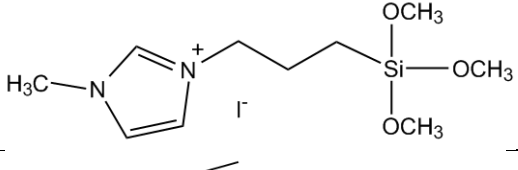
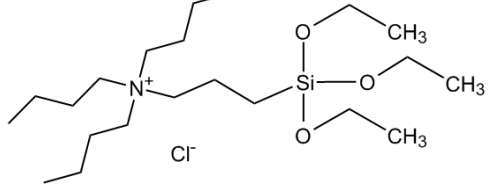
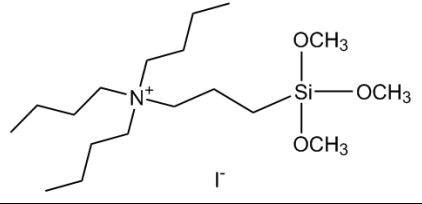
## Compound List

### *Reagents and Model Compounds*

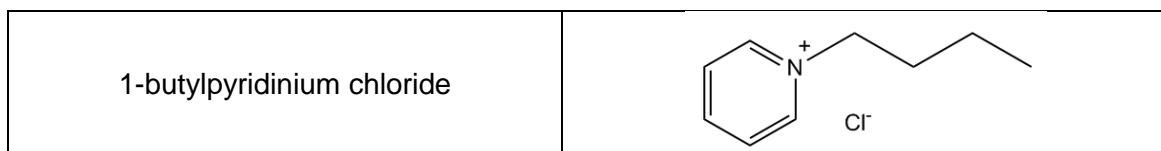
1-Chlorobutane	
1-Methylimidazole	
3-Iodopropyltrimethoxysilane	
(1-Chloropropyl)triethoxysilane	
Tributylamine	
1-Butyl-3-methylimidazolium chloride ([C <sub>4</sub> MIM][Cl])	
Phosphomolybdic acid	
Cinnamyl Alcohol	
Guaiacol	
1-Benzothiophene	
1-Butyl-3-Methylimidazolium hexafluorophosphate	

4,6-Dimethyldibenzothiophene	
4-Methyldibenzothiophene	
Dibenzothiophene	
Tetradecane	
n-Octane	

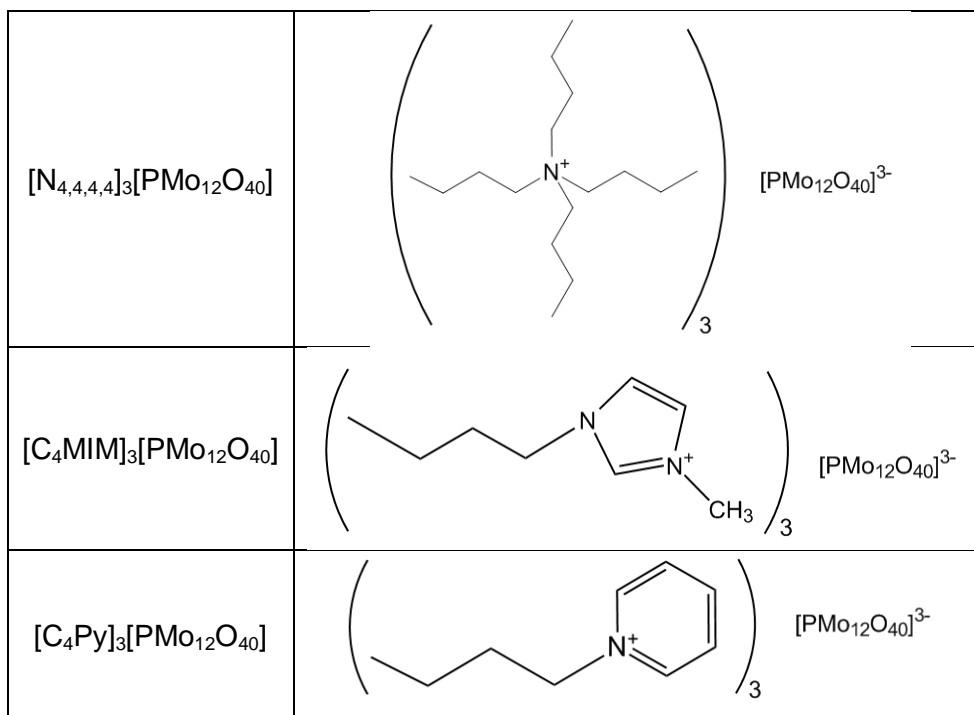
### ***Ionic Liquids***

N-(3-triethoxysilylpropyl)pyridinium chloride	
N-(3-trimethoxysilylpropyl)pyridinium iodide	
N-(3-trimethoxysilylpropyl)-3-methylimidazolium chloride	
N-(3-trimethoxysilylpropyl)-3-methylimidazolium iodide	
N-(3-trimethoxysilylpropyl)tributylammonium chloride	
N-(3-trimethoxysilylpropyl)tributylammonium iodide	

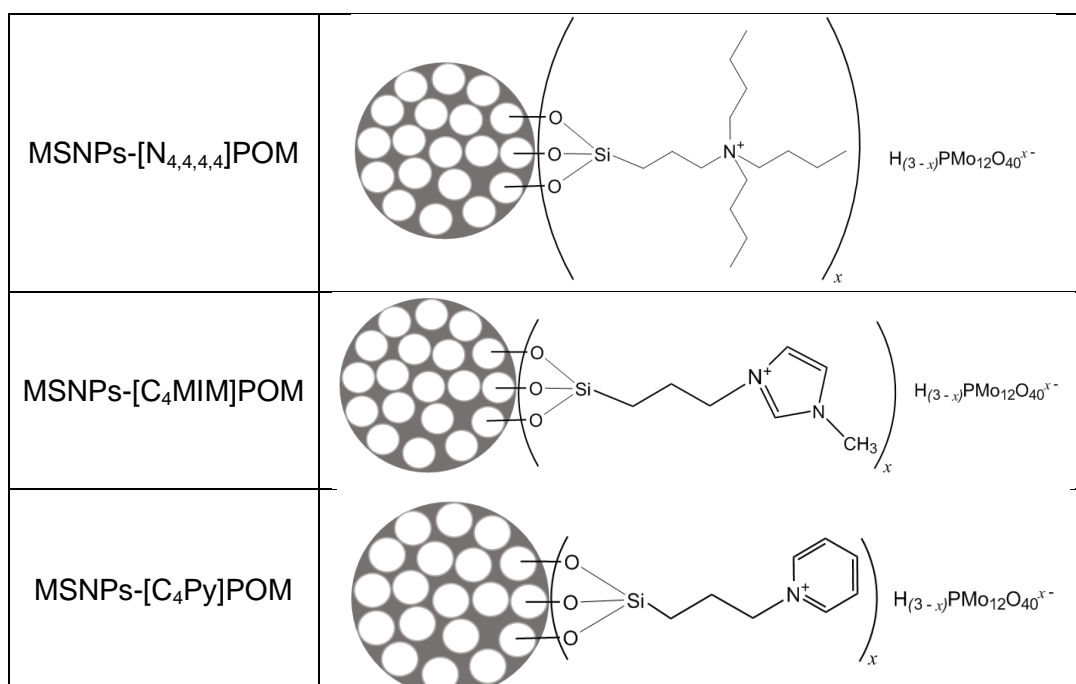




### Homogeneous Catalysts



### Heterogeneous Catalysts





# 1. Introduction

## 1.1. Green Chemistry

Nowadays, the society in general, has developed using natural resources, which brought some consequences. In the last years, it has been notice an increase in the use of non-renewable resources that now are scarce. Some of the long-term negative effects of these advancements could not be ignored. Pollution ruined oceans and acid rains deteriorated forests worldwide. The air is contaminated and the Earth's ozone layer has significant holes. Also, as consequence, the residues formed with the constant use of fossil fuels and chemical products are accumulating and harming the environment as well as public health. Some of these chemicals were suspected of causing human cancer and other health outcomes. In our efforts to improve crop protection, commercial products, and medicines, we also caused inadvertent harm to the environment. It is important that there are changes in human behavior to acknowledge the importance of maintaining our planet a safe place.

Chemistry was always considered a dangerous science for society and the environment. Therefore, it is important to change that mindset, showing that there are ways to adopt safer and sustainable practices in syntheses processes and treatment of toxic residues.<sup>1</sup> The United States of America (USA) formed the Environmental Protection Agency (EPA) in 1970, responsible for protecting human and environmental health. Later, the concept of Green Chemistry (or Sustainable Chemistry) was created by EPA with the intent to reduce or eliminate the dangers associated to handling, synthesizing and treating chemical products.<sup>2</sup> To encourage industries to adopt a "greener" and sustainable technology and practice, it was proposed twelve principles of Green Chemistry and twelve principles of Green Engineering.<sup>3,4</sup> The following table (**Table 1.1.**) represents the principles of Green Chemistry and Green Engineering.

**Table 1.1.** - Principles of Green Chemistry and Green Engineering.

Principles of Green Chemistry	Principles of Green Engineering
Prevent waste - <b>P</b>	<b>I</b> - Inherently non-hazardous and safe
Renewable materials - <b>R</b>	<b>M</b> – Minimize material diversity
Omit derivatization steps - <b>O</b>	<b>P</b> – Prevention instead of treatment
Degradable chemical products - <b>D</b>	<b>R</b> – Renewable material and energy inputs
Use safe synthetic methods - <b>U</b>	<b>O</b> – Output-led design
Catalytic Reagents - <b>C</b>	<b>V</b> – Very simple
Temperature, Pressure ambient - <b>T</b>	<b>E</b> – Efficient use of mass, energy, space and time
In-process Monitoring - <b>I</b>	<b>M</b> – Meet the need
Very few auxiliary substances - <b>V</b>	<b>E</b> – Easy to separate by design
E-factor, maximize feed in product - <b>E</b>	<b>N</b> – Networks for exchange of local mass & energy
Low Toxicity of chemical products - <b>L</b>	<b>T</b> – Test the life cycle of the design
Yes, it's safe - <b>Y</b>	<b>S</b> – Sustainability throughout product life cycle

Green Chemistry principles were firstly described in 1998 by Paul Anastas and John Warner, with the intent to turn the methods applied to chemical compounds more sustainable.<sup>5</sup> Since these principles don't cover all the important aspects for the environmental impact, Green Engineering principles were also proposed. Sustainable engineering allows the development of products and processes economically viable and the reduction pollution since the beginning of the process, avoiding risks to human health and to the environment.

Some examples about the impact of Green Chemistry on the environment are: the discovery of a catalytic chemical process that uses less energy and possess a great potential to reduce greenhouse gas emissions at normal temperature and pressure conditions; the use of supercritical carbon dioxide in one of the steps of computer chip preparation, and it significantly reduces the quantities of chemicals, energy, and water needed to produce chips; the pharmaceutical industry is continually seeking ways to develop medicines with less harmful side-effects and less toxic waste; Several companies have been working to develop plastics that are made from renewable, biodegradable sources; mixture of soya oil and sugar that replaces fossil-fuel-derived paint resins and solvents, among others.<sup>6</sup>

The previous examples showed the importance of Green Chemistry in the distinct types of industry, offering a pathway to a sustainable world. Even though nowadays these principles are still not being used in all industries, there is a constant growing effort to manipulate chemical compounds in a safe way and to operate in an eco-friendly manner.

## 1.2. Biomass

Biomass is a renewable source of energy originated from the energy stored in chemical bonds by materials that stem from organic matter. It can be found in different forms like wood and respective waste products, agricultural crops and respective waste, food, animal manure and human sewage (**Fig. 1.1.**)<sup>7</sup>

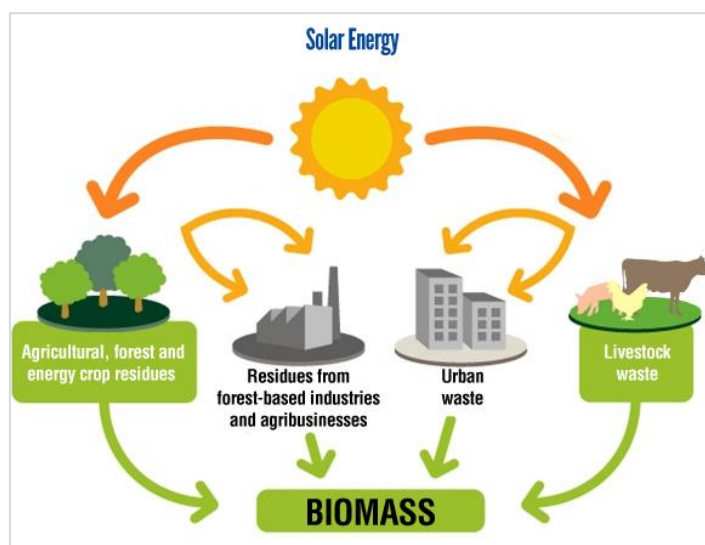


**Fig. 1.1.** - Representation of Biomass sources: Agricultural and forest residues, industrial residues, urban waste and livestock waste (Adapted from *Kunakawan Group*<sup>8</sup>).

Biomass is composed mainly by long chain natural polymers, cellulose (representing 40 to 50% of the biomass by weight), hemicellulose (representing 20 to 40% of the biomass by weight) and lignin.<sup>9</sup>

In plants, solar energy is captured by chlorophyll by photosynthesis and, in the presence of carbon dioxide ( $\text{CO}_2$ ) and water,  $\text{CO}_2$  converts into carbohydrates that form building blocks of biomass (**Fig. 1.2.**). When the carbon, hydrogen and oxygen molecule bonds are broken, the solar energy that was once captured and stored in the chemical bonds is released.<sup>2</sup> Biomass is considered a renewable source of energy because it is a cyclical process. The  $\text{CO}_2$  can be available again in short period of time, in comparison with fossil fuels.<sup>10</sup>

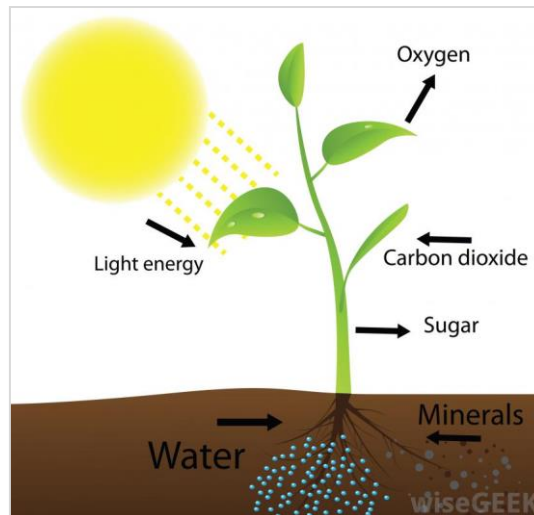


**Fig. 1.2.** - Photosynthesis process (Adapted from *Wisegeek*<sup>11</sup>).

Currently, fossilized biomass is exploited as coal and oil. Since it takes millions of years to convert biomass into fossil fuels, these cannot be considered a renewable source of energy, since burning “old” biomass and converting it into “new” CO<sub>2</sub> contributes to the greenhouse effect.

### 1.2.1. Application of Biomass

In the process of producing energy, there are two alternatives. Either biomass is burned and the energy is released as heat, or it is converted to a different form of energy like liquid biofuels such as ethanol and biodiesel, or biogas so it can be later burned as a fuel (e.g. methane). Ethanol is produced by fermentation of corn and sugar cane, biodiesel is produced from vegetable oil and animal fat, and methane is produced in digesters from agricultural and human waste.<sup>1</sup>

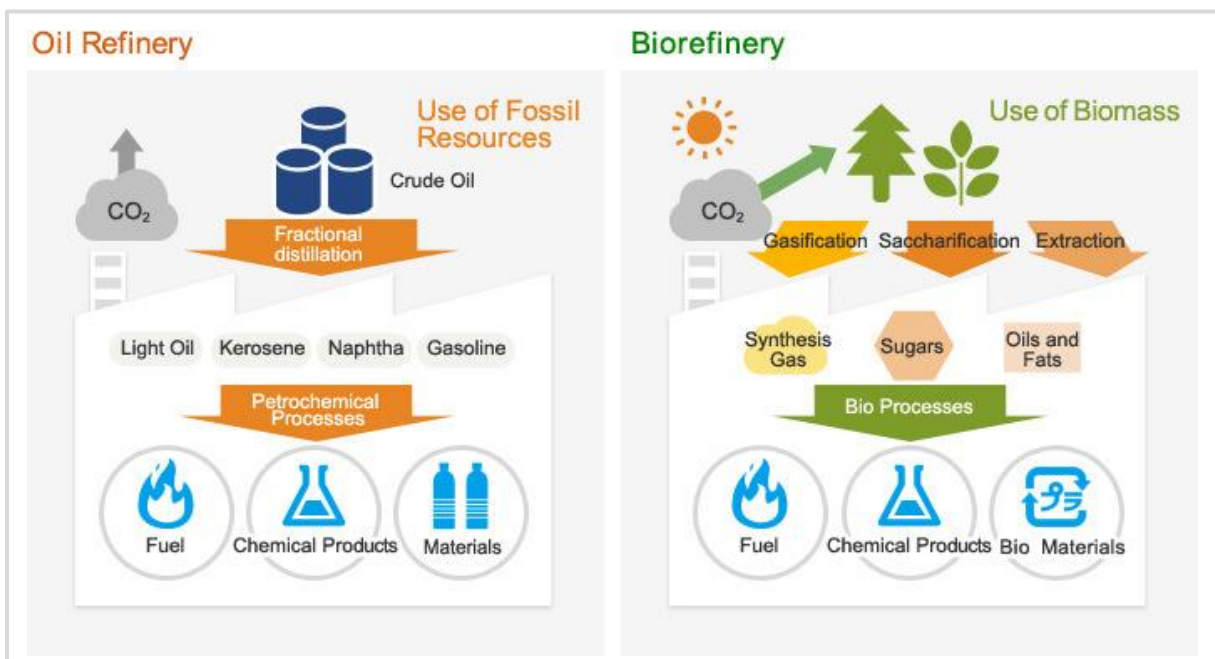


**Fig. 1.3.** - Comparison between the use of fossil fuels and the use of biomass to produce fuel, chemical products and biomaterials (adapted from *GLW Energy*<sup>12</sup>).

Using biomass as a source of energy has gotten a lot of attention for several reasons: The application of biomass can be done at a lower cost and at a higher conversion efficiency, since biomass residues can be used as fuel. In this context, the production of food surpluses in Western Europe and in the United States, which promotes the introduction of alternative non-crops desirable; and the production of biomass as a sustainable renewable source of energy since it does not contribute to a buildup of CO<sub>2</sub> in the atmosphere.<sup>2</sup>

Knowing the properties of the biomass source and the type of energy required, it is possible to determine the adequate conversion process. Therefore, specific properties become important depending of the selected energy conversion process. The main interest properties are related to moisture content, calorific value, proportions of fixed carbon and volatiles, ash/residue content, alkali metal content and cellulose/lignin ratio.

### 1.2.2. Biomass and Sustainability

Biomass energy can be harmful to the environment if harvested at unsustainable rates and damage ecosystems. It can have negative outcomes, such as the production of harmful air pollution, large consumption of water and large global warming emissions. For these reasons, it is important to manage and monitored carefully the production of energy from biomass. In order to understand the potential role of biomass as a primary energy source, it is necessary to look at the carbon emissions and compare it to the most important competitor, fossil fuels.<sup>3</sup>

Nowadays, there are researchers worldwide trying to develop several ways to develop the use of biomass for fuel, since it is presently estimated to contribute of the order 10% to 14% of the world's energy supply.<sup>2</sup> In 2016, biomass provided 5% of the primary energy consumed in the USA in the forms of biofuels (mainly ethanol, in a total of 48%), wood and derived products of wood (41%) and municipal waste (11%).<sup>1</sup>

### 1.3. Lignin

Lignin is a natural polymer derived from lignocellulosic biomass (composed by cellulose, hemicellulose and lignin) of plants and some algae (**Table 1.2.**). The main function of this polymer is to provide structure to the plant and protect against degradation.

**Table 1.2.** - Average distribution of the three main biopolymers in softwood, hardwood and switchgrass (Adapted from *McKendry et al.*<sup>9</sup>).

	Softwood	Hardwood	Switchgrass
Lignin	27–30%	20–25%	5–20%
Cellulose	35–40%	45–50%	30–50%
Hemicellulose	25–30%	20–25%	10–40%

This polymer's complex amorphous structure is the result of the polymerization of three phenylpropanoid monomers: *p*-coumaryl alcohol, coniferyl alcohol and sinapyl alcohol

(Fig. 1.4).<sup>13</sup> These monomers are bonded with C-O and C-C linkages to form a complex three-dimensional structure.

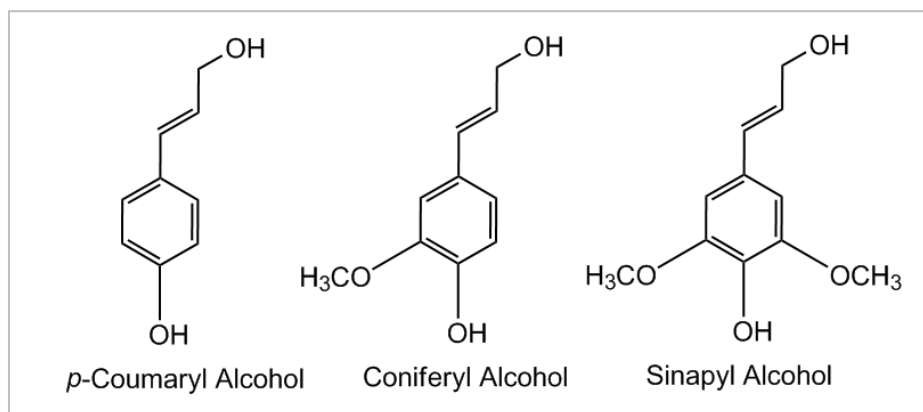


**Fig. 1.4.** - Phenylpropanoid monomers, *p*-coumaryl alcohol, coniferyl alcohol and sinapyl alcohol of lignin polymer.

Although representing more than 20 % of Earth's biosphere, about 98 % of this polymer is currently burned for paper and pulp industry.<sup>14</sup> This happens because of its complex structure. Structural studies (such as NMR and GC-Mass Spectra) indicated that more than 50% of lignin components are aromatic hydrocarbons. This way, it represents an attractive source of aromatic compounds in chemistry, being the only renewable source of key and high-volume aromatic compounds for the chemical industry.<sup>15</sup>

Although most lignin is burned, it is currently used to produce low-value products such as foams and resins, not being used for the production of high-value products. The main reason is that its molecular structure is very stable and there is no efficient depolymerization method to modify the molecule.

In the context of green chemistry, lignin valorization to produce value-added chemical products, fuels and materials, represent a challenge to environmental protection and sustainability. The conversion of this polymer into aromatic molecules has become the center of scientists especially for the decline in fossil fuels resources. Lignin does not compete with food production, therefore causing no detrimental social and ecological consequences.<sup>16</sup>

One of the issues in lignin valorization is not knowing the exact composition and correct structure, since the biomass source, type of wood, season and growing parameters vary.<sup>17</sup> There are diverse types of lignin (kraft lignin, lignosulfonated lignin, organosolv lignin, pyrolytic lignin, steam-explosion lignin, acidolysis lignin, etc), depending on parameters such as polarity, purity, molecular weight, frequent linkages and specific chemical groups.<sup>18</sup> Another difficulty is that this polymer structure is very stable (**Fig. 1.5**), so it is difficult to depolymerize it.

The first step for lignin valorization is to make a pretreatment. This way, lignin is separated from other components, making the isolation an easier step. The choice of the type of lignin influences the valorization process, since the cost, presence of impurities, compounds obtained can vary. From all types of lignin, kraft lignin and organosolv lignin have potential to produce high value products.

Using oxidation reactions to modify lignin bring advantages such as the production of complex platform aromatic compounds with additional functionalities, as well as an easy product separation. The use of homogeneous catalysts is focused in biocatalysis, biomimetic catalysis and organometallic processes. Even being an efficient process, biocatalysis requires specific conditions due to the presence of enzymes. (laccases, manganese peroxidases and lignin peroxidases).<sup>19,20</sup> Biomimetic catalysis is essentially

based on the use of metalloporphyrins in the presence of hydrogen peroxide or molecular oxygen.<sup>21</sup>

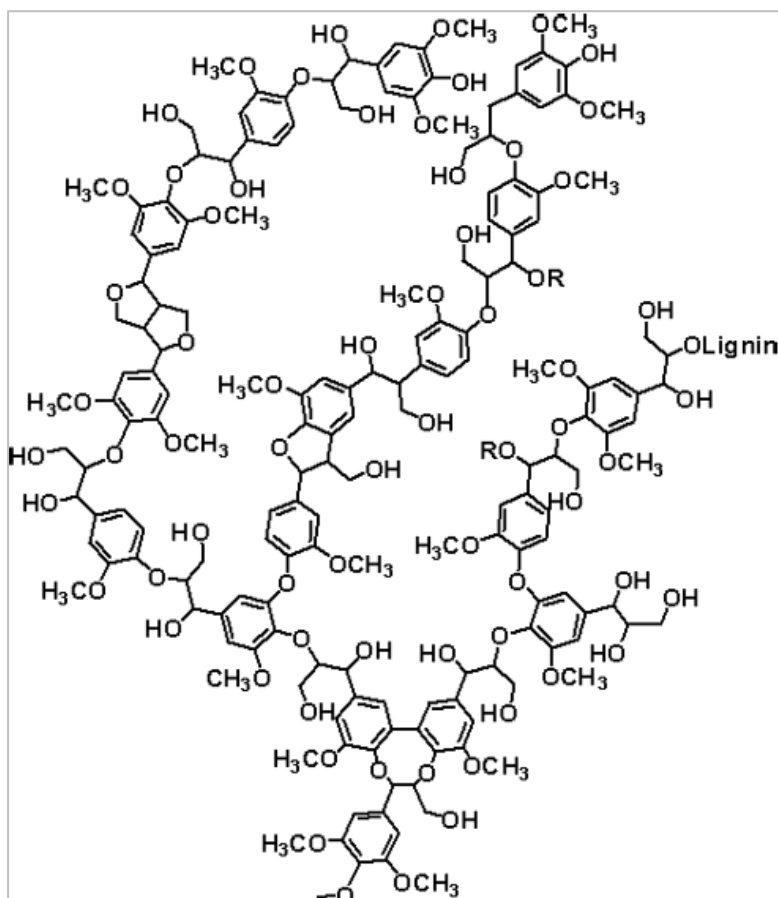


**Fig. 1.5.** - Lignin Chemical structure (Adapted from *Lignoworks*<sup>22</sup>).

Organometallic catalysis is performed using metal-organic complex or material such as methyltrioxorhenium, cobalt/manganese salen complexes, iron tetraamido macrocyclic complex, polyoxometalates, and catalysts with various ligand systems, etc.<sup>23</sup> A wide range of ligands that can affect the electronic and steric properties of the catalysts, which are directly linked to their activity, solubility and stability, is available.

Although interesting results have been reported, most of these homogeneous catalysts suffer from catalyst decomposition, or lack of selectivity for lignin. In addition, the recyclability of the catalyst cannot be envisaged. These problems could be solved by using heterogeneous catalysts, that are currently being study worldwide.

When using lignin for studies, it is common the use of lignin model compounds. The most reported model compounds in the literature are guaiacol, vanillyl alcohol, apocynol, syringyl alcohol, veratryl alcohol, etc. Using these model compounds as substrates showed the advantage to study the reactivities and selectivity's of the multifunctional groups, as well as how specific bonds can be broken.

In the present work, two lignin model compounds, guaiacol and cinnamyl alcohol (**Fig. 1.6.**) are selected to be used as substrates in catalytic oxidations.



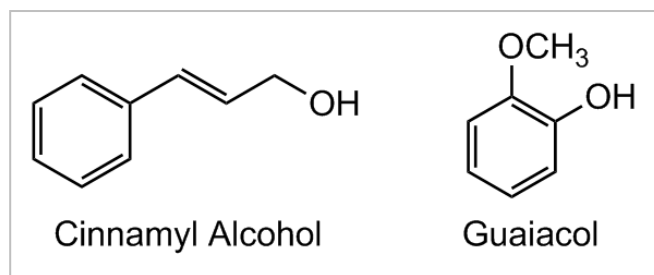


**Fig. 1.6.** - Lignin Model Compounds, Cinnamyl Alcohol and Guaiacol.

Nowadays, lignin valorization is investigated with oxidation reactions in raw lignin and model compounds. The coupling of heterogeneous catalysts is promising for exhibiting several advantages such as easier separation, recyclability and for being eco-efficient processes. There are challenges to be addressed by the scientific community to develop new and efficient process in industrial scale, making lignin a fair competitor with the current energy sources tested.

#### 1.4. Catalytic Oxidation

The word “catalysis” was employed in 1836 to refer to an entity that is capable to promote the occurrence of chemical reactions by contact, to speed up the rate of the reaction without being consumed. Though the word was created at that time, there were already used catalytic processes in more ancient times, for example, the fermentation process (example of biocatalysis). Catalytic reactions only started to gain weight in the beginning of the 20<sup>th</sup> century, and now, 95 % of chemicals are produced, at least, with one catalytic step.

A catalytic oxidation is a process that consists on oxidizing compounds by the addition of a catalyst. The catalyst contributes to the product formation by increasing the reaction rate by reducing the activation energy of the oxidation. It is not present in the stoichiometry of the reaction and it is not consumed. It is important that the catalyst is eco-friendly and easy to recycle, this way, choosing the right oxidizing agent for oxidation catalysis is a key step. It is also important to consider the cost and commercial availability, as well as properties of the oxidizing agent like high selectivity, high reaction rate, sustainability and percentage of active oxygen.

The most used “green” oxidants are molecular oxygen and oxygen peroxide. Using molecular oxygen is very difficult to control in a reaction, it results in low selectivity. Oxygen peroxide is also a very eco-friendly choice and it is also capable of oxidizing organosulfides compounds in low and high pH values. This oxidant is commonly used for being a liquid and it is easy to implement in standard batch equipment. The disadvantages of using this oxidant are the slow reaction with aromatic hydrocarbons and it is very unstable when in aqueous solution, decomposing in water and oxygen. To be useful, catalysts should be effective with 30% aqueous hydrogen peroxide, but many systems described in the literature do not fulfill this requirement.

The oxidation of hydrocarbons such as alkanes, alkenes and aromatics is the most important process to apply in the conversion of oils and natural gas feedstocks to industrial organic chemicals. Even though heterogeneous and homogeneous catalytic oxidations are already practiced industrially, the pressure of Green Chemistry, is stimulating the deployment of catalytic oxidations in order to produce fine chemicals. This application is more difficult, but in some cases, such technologies have been successfully applied. An example of this is the BASF process for the synthesis of a citral (used for fragrances and vitamins), since it uses a catalytic vapor phase oxidation with a silver catalyst.

### 1.4.1. Homogeneous and Heterogeneous Catalysis

Catalytic oxidations can be conducted with heterogeneous or homogeneous catalysts. In heterogeneous processes, the catalyst is in a different phase from that of the reactants. Heterogeneous catalysts still have low selectivity rates and low chemical stability at low temperature and pressure, but can be recovered and recycled. Usually, these catalysts are made of platinum, vanadium and molybdenum, and in some cases, these are modified with additives to enhance selectivity. Therefore, when using heterogeneous catalysts, it is important to optimize the surface area and the access from the solvent to the active center of the catalyst. The fact that the catalysts is in a distinct phase with respect to the reaction medium, accounts for the major advantage of the heterogeneous catalysts over the homogenous as it makes the separation e reutilization of heterogeneous catalysts simple and cheaper compared to the homogenous catalysts.

Homogeneous catalysis is characterized by all reactants, products and catalyst at the same phase, usually in liquid phase. Some common homogeneous catalysts used for organic catalysis are carboxylates of cobalt, iron and manganese. Though this type of catalysis has advantages, such as higher selectivity, activity and manipulation, but there are some problems associate to homogeneous catalysis. This type of catalysis showed lower productivity and chemical stability and limitations in the recovering of the catalyst, which have a negative impact in the development of sustainable chemistry. Today, a variety of homogeneous catalysts are known, such as Brønsted and Lewis acids, metal complexes, metals ions, organometallic complexes, etc.

The main advantages and disadvantages of these catalysts are described in **Table 1.3.**

**Table 1.3.** - Comparison of main advantages/disadvantages of Homogeneous and Heterogeneous catalysts (adapted from <sup>24</sup>).

Property	Homogeneous Catalysts	Heterogeneous Catalysts
Recovery	Difficult, high cost	Easy, low cost
Thermal Stability	Poor	Good
Selectivity	Excellent	Poor

In general, the main difference between homogeneous and heterogeneous catalysts is the fact that in homogeneous catalysts, each catalytic entity acts as an individual active site. Therefore, these catalysts are more active and selective, in comparison to heterogeneous catalysts.

It is very difficult to separate homogeneous catalysts from the reaction medium, and it requires intensive and expensive processes. After recognizing the limitations of homogeneous catalysts, scientists all over the world had the need to study the complementary capacities that heterogeneous catalysts could bring. There are constant attempts to combine the advantages of both catalysts, such as activity, selectivity and recyclability.

It is also important to consider the different steps of the catalytic reaction when choosing the use of heterogeneous catalysts, such as: external diffusion, internal diffusion, adsorption of reagents, surface reaction, desorption of products, internal

diffusion and external diffusion. Since homogeneous catalysts are molecularly dispersed in the reaction medium, there is no internal diffusion.

#### 1.4.2. Oxidative Desulfurization

When fuels are burned, sulfur compounds can be converted in SO<sub>x</sub> and contribute to acid rain, corrosion and global warming. In order to minimize the environmental impact, it has been studied the removal of organosulfides compounds present in fossil fuels. Therefore, in the last years, different methods of desulfurization to remove 1-benzothiophene compounds (1-BT) and derivatives (**Fig. 1.7.**) from fuels have been developed.

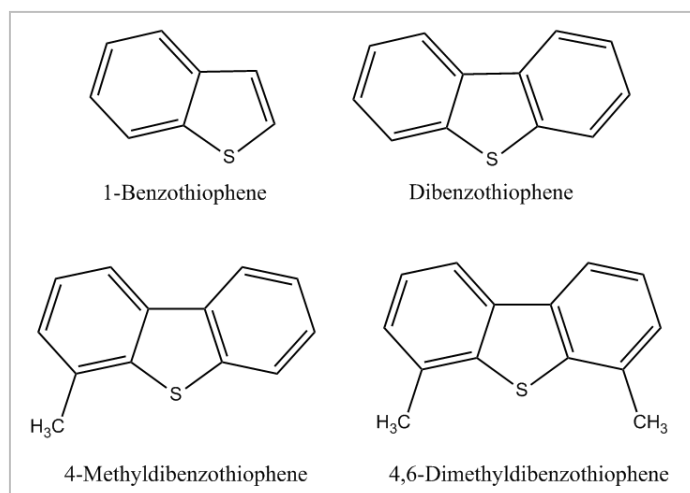


**Fig. 1.7** - Chemical representation of some types of sulfur-organic compounds present in fuel: 1-benzothiophene (1-BT), dibenzothiophene (DBT), 4-methyldibenzothiophene (4-MDBT) and 4,6-dimethyldibenzothiophene (4,6-DMDBT).

The most effective method to remove the sulfur-organic compounds from fuels is Oxidative Desulfurization (ODS). In this method, a catalytic reaction occurs in a two-phase system composed by a phase of oil and another as organic phase of solvent, oxidant (usually oxygen peroxide) and catalyst, according to the Green Chemistry Principles.

This method demonstrated high selectivity and performance in removing compounds like DBT, by oxidizing sulfur to sulfoxides and sulfones. These are extracted to the solvent phase by the increase of polarity. Other desulfurization methods included Hydrodesulfurization (HDS)<sup>25</sup>, Desulfurization by adsorption (ADS)<sup>26</sup>, Desulfurization by extraction (EDS)<sup>27</sup> and Biodesulfurization<sup>28</sup>.

#### 1.5. Ionic Liquids

Even though ionic liquids (ILs) gain more attention with the beginning of Green Chemistry in the 90's, these compounds are older than what people think. The first example of an ionic liquid known was in 1888, synthesizing ethanolanmonium nitrate, with a melting point at 12.5 °C.<sup>29</sup>

More recently, Parshall in the 70's, published the use of ionic liquids as a homogeneous catalysis media, and Osteryoung who developed an alkylation method of Friedel-Crafts, with a reaction medium as a salt with a low melting point.<sup>30,31</sup>

There were a lot of discoveries in the last 100 years, but the last 20 years there was a significant increase of the use and investigation of these compounds in different areas.

Ionic Liquids are organic salts with a melting point lower than 100 °C, having potential to be applied in diverse areas in industrial and academic levels. These compounds exhibit high ionic conductivity, consisting of organic cations and organic or inorganic anions.<sup>32</sup>

The fact that they are in liquid state at room temperature is justified by its composition and crystalline structure. The weak intermolecular interactions are the cause for the low melting points, depending on the combination of organic cations and anions. These class of peculiar materials possess negligible vapour pressures, non-flammability, high range of solubilities, higher chemical and thermal stability as well as a wide electrochemical window.<sup>33</sup>

Due to these properties, ILs can be distinguished from other used salts, and can be attractive in terms of a Green Chemistry context. Through its use, ionic liquids contribute for the reduction of environmental pollution by reducing the greenhouse gases to the atmosphere.<sup>34</sup> One of the most interesting characteristics of the ILs is related to their ability to alter the final properties according to the suitable cation-anion combinations.<sup>32</sup>

In the last years, different ionic liquids have been developed based on organic cations such as imidazolium, pyridinium, ammonium, pyrrolidinium, phosphonium, sulfonium, guanidinium, thiazolium, triazolium, etc., combined with a variety of organic or inorganic anions.<sup>33</sup> The following figure (**Fig. 1.8.**) represents some examples of the most common cations and anions used in ionic liquids.

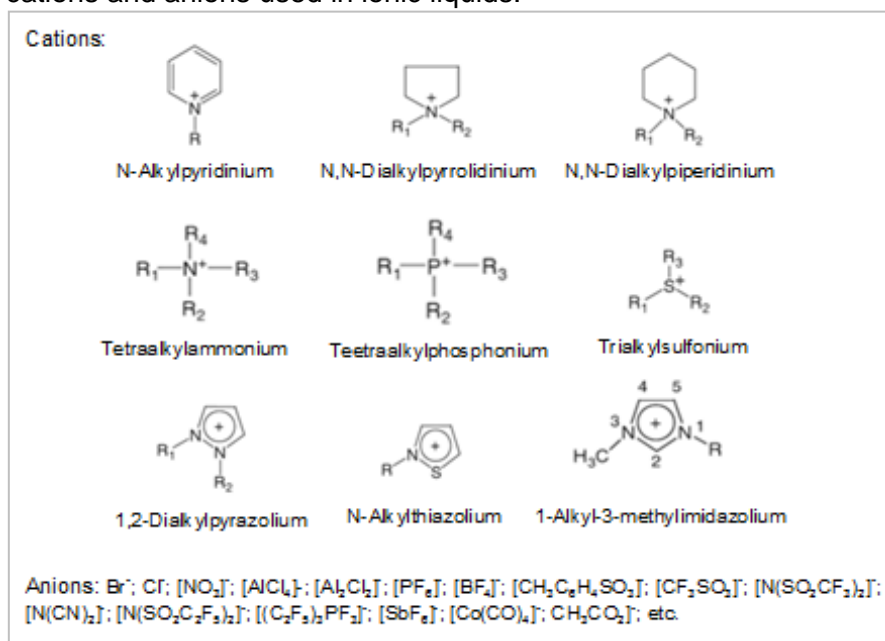


**Fig. 1.8.** - Common structures of cations and anions present in ionic liquids (R, R<sub>1</sub>, R<sub>2</sub>, R<sub>3</sub> and R<sub>4</sub> are alkyl groups<sup>35</sup>).

Some examples of ILs included the cations: 1-alkyl-3-methylimidazolium, [C<sub>n</sub>MIM]<sup>+</sup> and 1-alkylpyridinium cations, [C<sub>n</sub>Py]<sup>+</sup>, tetraalkylammonium, [N<sub>n,n,n,n</sub>]<sup>+</sup> and tetraalkylphosphonium, [P<sub>n,n,n,n</sub>]<sup>+</sup>.

There is a subclass of ionic liquids designated *Room Temperature Ionic Liquids (RTIL)*. These ionic liquids are characterized for being liquids at room temperature, having asymmetric and bulky ions.<sup>36</sup> This specific subclass of ILs is relevant in some applications where the liquid state is a great advantage.

ILs are commonly used in catalysis and biocatalysis, separation processes as solvents, pharmaceutical chemistry, biotechnology and production of new functionalized materials (**Fig. 1.9.**)<sup>32</sup> This way, throughout the years, ionic liquids have been used more often, increasing the possible applications, as well as publications and citations.

In the last years, ionic liquids have been studied as an alternative to the use of conventional organic solvents in organic reactions. Therefore, new reactions involving C-C linkage were explored, as well as linkages of carbon with nitrogen, oxygen, sulfur and halogenates.<sup>37</sup>

In general, ionic liquids are considered “green solvents” because of their ability to substitute toxic, volatile and flammable organic solvents in phase transfer processes, with low reaction time, high yields and easier purification. Ionic liquids can also be inserted in homogeneous and heterogeneous catalytic reactions. By dissolving transition metal catalysts in IL media, it is possible to improve the catalytic activity as well as the possibility to reuse the reaction medium many times.<sup>38</sup> Catalytic processes that use organic solvents to dissolve the final product and not the ionic liquid catalyst are preferred.<sup>38</sup> The low solubility of ionic liquids in supercritical CO<sub>2</sub> and high solubility of CO<sub>2</sub> in ionic liquids make the use of these as a sustainable process to extract products.<sup>39</sup> Ionic Liquids are also developed to be incorporated in cations or anions of catalysts, as well as the development of chiral ionic liquids in asymmetric reactions.

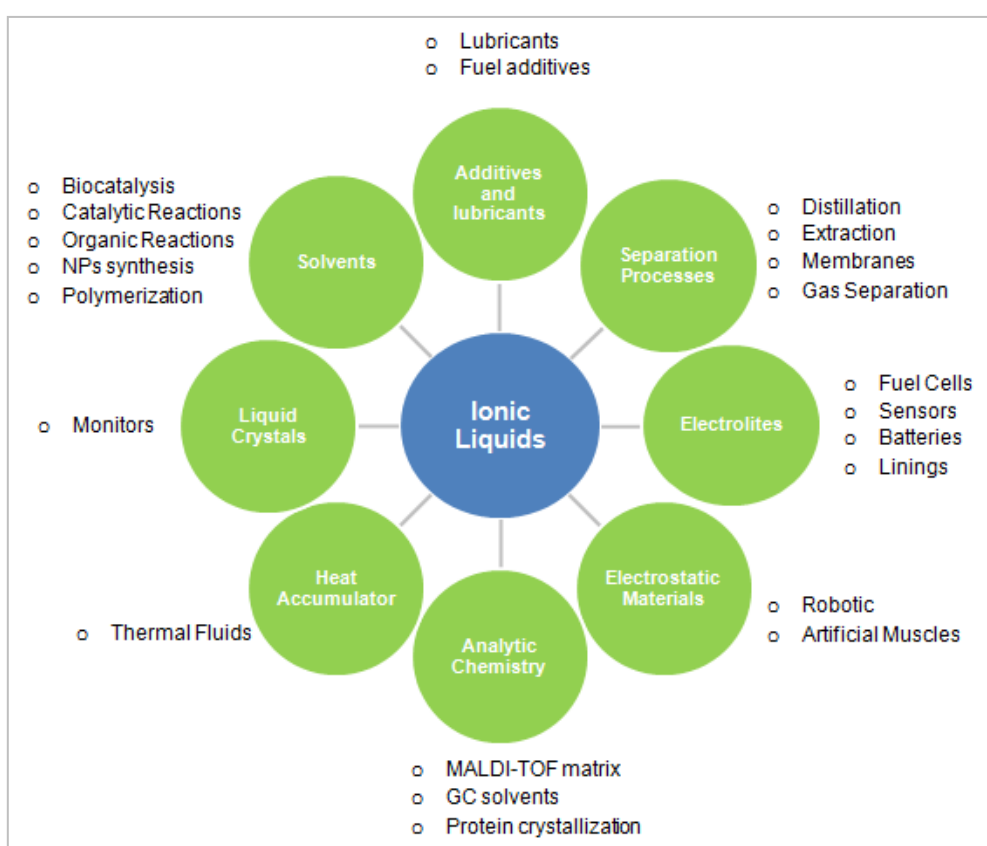


**Fig. 1.9.** - Some of the applications of Ionic Liquids (Adapted<sup>40</sup>).

The use of ionic liquids is also beneficial for the environment, due to the capacity to replace other toxic organic solvents, capacity to reduce chemical waste and the improvement of safety of chemical processes and products, according to Green Chemistry.<sup>33</sup>

Even though the study of ionic liquids has increased in the last years, there is still the possibility to develop new methods and technologies in some investigation fields. The contribute of sciences such as physics, biology, biochemistry, medicine and materials can help the application of IL in a global way. The properties of IL are relevant to developing new purification processes of biological components as well as functionalization of specific materials.<sup>32</sup>

## 1.6. Polyoxometalates

Polyoxometalates (POM) are nanoclusters with transition metals from groups 5 and 6 in the highest oxidation state, and oxygen atoms in its constitution.<sup>41</sup> These complexes are very attractive to scientists all over the world because of their morphology and size (up to 4 nm of dimension and 40.000 g/mol of molecular mass), oxidation/reduction properties, as well as magnetic and electric properties.

These complexes have also a significant role in overcoming environmental struggles, since they can be used to retain toxic gases and radioactive residues. The synthesis of these complexes is a low-cost process and doesn't use toxic reagents. Polyoxometalates are currently used in medicine, electronics and in the development of new materials.<sup>42</sup>

Polyoxometalates consist in a metallic oxide with the structure  $M_xO_y$ . M represents the metal in the complex, designated by addenda atom, usually Molybdenum (Mo), Tungsten (W), Vanadium (V) or Tantalum (Ta). These complexes can be divided in two distinct groups: isopolyanions ( $[M_xO_y]_n^-$ ) and heteropolyanions ( $[X_zM_xO_y]_n^-$ ). The difference between the two types, is that there is another essential atom (X) to complete the structure. An example of an isopolyanion is the anion Linqvist, represented by the structure  $[M_6O_{19}]_n^-$ , and some examples of heteropolyanions are the anions Keggin, Wells-Dawson and Anderson-Evans, represented respectively by the structures  $[XM_{12}O_{40}]_n^-$ ,  $[X_2M_{18}O_{62}]_n^-$  and  $[XM_6O_{24}]_n^-$  (**Fig. 1.10**).

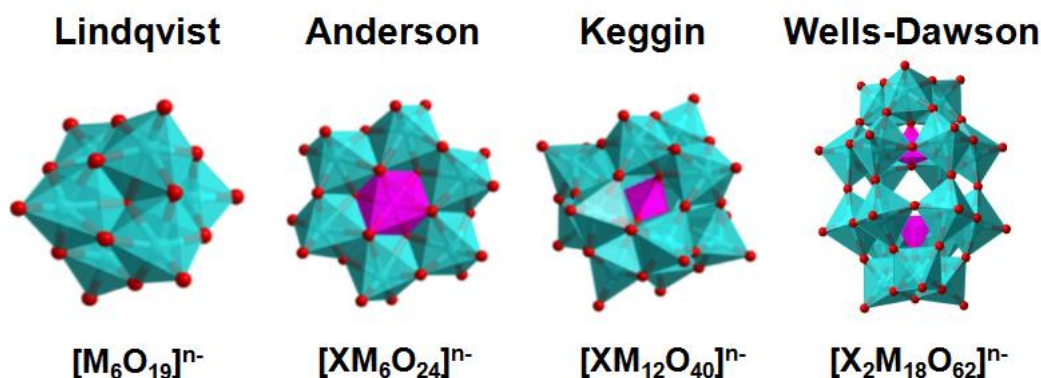


**Fig. 1.10.** - Chemical representation of an isopolyanion (Linqvist) and heteropolyanions (Keggin, Wells-Dawson and Anderson-Evans) (*Adapted from* <sup>43</sup>).

For the present work, the Keggin anion is going to be used. This heteropolyanion is represented by the structure  $[XM_{12}O_{40}]_n^-$ , having a tetrahedral central structure ( $XO_4$ ) connected by oxygen atoms to twelve octahedrons ( $MO_6$ ).<sup>44</sup> Keggin polyoxometalates are stable at high temperatures and can be synthesized in large quantities at a low cost and low toxicity.

Due to their high capacity to oxidize, polyoxometalates have been studied in order to be applied in catalytic reactions to overcome problems such as cost, chemical stability, thermal stability and recycling.

Even being efficient in oxidation processes, polyoxometalates can be hard to be recovered and recycled. This way, it is important to keep developing immobilization methods to produce new heterogeneous catalysts. The incorporation of metallic complexes in supported materials is a sustainable alternative to the conventional heterogeneous catalysts.

The materials that are most utilized in the immobilization of polyoxometalates are mesoporous silica nanoparticles, activated carbon and zeolites. In this work, mesoporous silica nanoparticles are used as a support material.

## 1.7. Mesoporous Silica Nanoparticles

In the last years, silica-based nanoparticles have attracted much attention because of their different applications and versatility. Silica nanoparticles are known for having low toxicity, therapeutic delivery, biocompatibility, scalable synthetic availability, and high chemical and thermal stability.<sup>45</sup> These can be altered to have precise measures of size, high surface area, morphology, shape, pore size (2 to 30 nm), particle size and crystallinity, to be applied in different nanotechnological applications. This way, by functionalizing these nanoparticles and modifying their properties, it is possible to obtain specific materials targeted to different chemical reactions.<sup>46</sup>

MSN are very attractive in nanotechnology because of their structural basis, since it can be applied in processes of nanomedicine, nanomaterials, adsorption, separation processes, biomedical systems, drug delivery systems, biological imaging and chromatography.<sup>47</sup>

Currently, nanoparticles are the most promising nanomaterial for drug delivery applications. This is due to MSNPs high surface area and pore volume, high biocompatibility *in vitro* and *in vivo*, tunable particle size.<sup>48</sup> Their large pore volume can transport large quantities of drugs into perfused organs.<sup>49</sup> Nowadays, the main challenge in the use of MSNPs is the design of optimal carries that could more specifically bind to and/or accumulate in the targeted organs or tissues, such as tumors. This would imply more selective drug doses, the need to control charges and sizes (determines the cell uptake of MSNPs and ability to penetrate through tissues), as well as minimizing toxicity and side effects.<sup>50</sup> Since the nanoparticle size is important to be controlled in these cases, it is important ensure the requirements for synthesizing smaller particles.

In the following work, MSNPs were synthesized using the protocol reported by *Bouchoucha et al*<sup>51</sup>, in which an altered version of the synthesis reported by *Kim et al*<sup>52</sup> was used, tuning the concentration of the triblock copolymer Pluronic F127 as a non-ionic surfactant. Triethanolamine (TEA) was added to the synthesis as a dispersion agent, as co-inhibitor of particle growth and/or as the base catalyzing hydrolysis and condensation reactions of silicate species.<sup>52</sup>

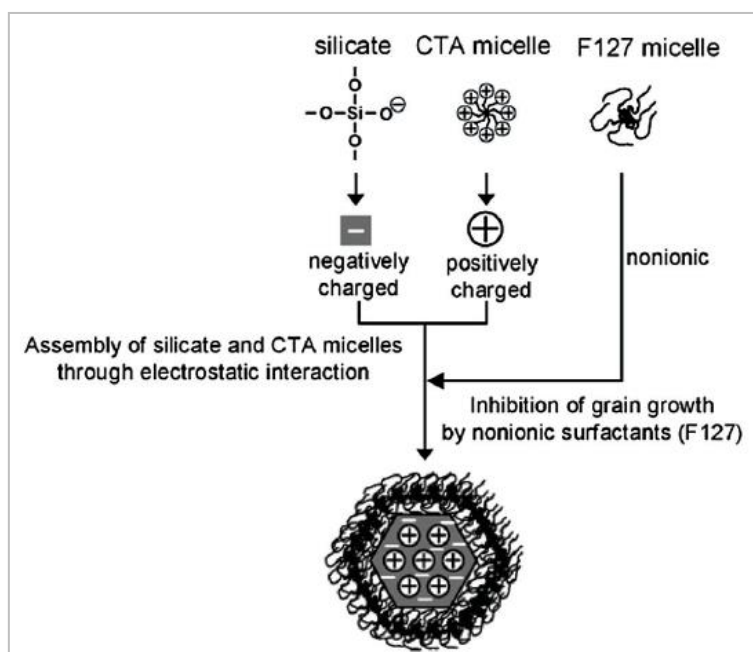


**Fig. 1.11.** - Schematic representation of the functions of two surfactants for assembly of the MSNPs (adapted from *Wu et al*<sup>53</sup>).

It has been studied the immobilization of transition metallic complexes in solid supports, such as mesoporous silica, activated carbon and zeolites. This way, barriers such as higher cost, low chemical and thermal stability and recovery in homogenous catalysis are overcome.<sup>54</sup>

The use of mesoporous silica increases the ratio area/volume, which increasing the accessibility of reagent molecules to the catalytic centers. Silica nanoparticles are also a sustainable alternative to the conventional heterogeneous catalysts.

Even though using polyoxometalates as catalysts increases the efficiency of the reaction, its recovering and recycling is problematic. These problems can be overcome by immobilizing the catalysts in solid supports. One of the most used materials for immobilizing polyoxometalates is mesoporous silica.

By functionalizing silica nanoparticles with cationic groups, there is a higher electrostatic interaction with polyoxometalates as anions. In this work, heterogeneous catalysts are prepared by using functionalized mesoporous silica nanoparticles as a solid support by immobilization of different ionic liquids (providing the cation) and polyoxometalate phosphomolybdic acid,  $H_3PMo_{12}O_{40}$  (providing the anion).



## **2. Experimental Section**

### **2.1. Materials and Equipments**

#### **Solvents and Reagents**

All the listed products were used without previous purification: 1-Benzothiophene (Merck KGaA); 1-Butyl-3-methylimidazolium chloride, [BMIM]Cl (Solchemar, >99%); 1-Butyl-3-methylimidazolium hexafluorophosphate, [BMIM][PF<sub>6</sub>] (Sigma-Aldrich, ≥97%); 1-Chlorobutane (Alfa Aesar, >99%); (1-chloropropyl)triethoxysilane (Sigma-Aldrich, 95%); 1-Methylimidazole (Sigma-Aldrich, 99%); 1,3,5-Trioxane (Sigma-Aldrich, ≥99%); 3-Iodopropyltrimethoxysilane (Sigma-Aldrich, >95%); 4-Methyldibenzothiophene (Sigma-Aldrich, 96%); 4,6-Dimethyldibenzothiophene (Alfa Aesar, 97%); Acetonitrile (J. T. Baker, p.a.); Acetonitrile Anhydrous (Sigma-Aldrich, 99.8%); Amberlyst® A15 (H<sup>+</sup>) (Fluka); Amberlyst® A26 (OH<sup>-</sup>) (Alfa Aesar); BTEB (Fluorochem); Chloroform (Carlo Erba, >99%); Cinnamyl Alcohol (BDH Chemicals); n-cetyltrimethylammonium bromide, CTAB (BDH Chemicals, >99%); n-cetyltrimethylammonium chloride, CTAC (Sigma-Aldrich, 25 wt% in H<sub>2</sub>O); Dibenzothiophene (Sigma-Aldrich, 98%); Deuterated Dimethylsulfoxide (DMSO d<sub>6</sub>) (Euriso-top, 99.80 D Water <0.02%); Deuterium Chloroform (Euriso-top, 99,80 D Water <0.01%); Deuterium Oxide (Sigma-Aldrich, 99.9 atom %); Dichloromethane (Sigma-Aldrich, >99.9%); Diethyl ether (Honeywell |Riedel-de Haën®r®, ≥99.8%); DOWEX® 50WX8-100 (H<sup>+</sup>) (Sigma-Aldrich); Ethanol absolute anhydrous (Carlo Erba, p.a.); Glycerol (Fisher Chemical); Guaiacol (Janssen Pharma); Hydrochloric Acid (Sigma-Aldrich, p.a.); Methanol (Sigma-Aldrich, p.a.); n-Octane (Acros Organics, +99%); NaOH (pellets) (Eka); Perdrogen 30% H<sub>2</sub>O<sub>2</sub> (w/w) (Sigma-Aldrich, p.a.); Phosphomolybdic acid (Merck, p.a.); Pluronic F127 (Sigma-Aldrich); Pyridine (Merck, p.a.); Sodium phosphomolybdate hydrate (Sigma-Aldrich, ≥99.9%); Sodium Sulfite (Sigma-Aldrich, p.a.); Tetradecane (Sigma-Aldrich, ≥99.0%); Tetraethylorthosilicate (TEOS) (Sigma-Aldrich, 98%); Triethanolamine (TEA) (Alfa Aesar, >98%); Toluene (Valente e Ribeiro Lda., synthesis grade); Tributylamine (Fluka, >98%).

#### **Equipment and Techniques**

##### ***Dynamic Light Scattering (DLS)***

DLS analyses were performed in a Horiba Scientific Nano Particle Analyzer SZ-100.

##### ***Elemental Analyses (EA)***

Elemental Analyses for C, H and N were performed in a Thermofinnigan Flash EA 112 series at Laboratório de Análises (LAQV/UCIBIO – REQUIMTE) and the Mo analyses were performed by ICP-OES on a Perkin-Elmer Optima 4300 DV instrument at the University of Santiago de Compostela.

##### ***FTIR Spectroscopy***

FTIR spectra were obtained on a Bruker Tensor 27 infrared spectrophotometer using KBr pellets for solid samples and NaCl cells for the liquid samples.

##### ***Gas Chromatography (GC)***

The Oxidative Desulfurization was tracked by Gas Chromatography, using the chromatograph Bruker, model 430-GC, in Faculdade de Ciências from Universidade do Porto.

### ***NMR Spectroscopy***

Solution NMR spectroscopy was used to obtain  $^1\text{H}$  NMR and  $^{31}\text{P}$  NMR spectra, operating, respectively, at 400.13 MHz ( $^1\text{H}$ ) and 162 MHz ( $^{31}\text{P}$ ). The equipment used was a Bruker Avance III 400, part of the National NMR Facility supported by Fundação para a Ciência e a Tecnologia (RECI/BBB-BQB/0230/2012).

Solid State  $^{13}\text{C}$  CP MAS and  $^{31}\text{P}$  CP MAS NMR spectra were acquired with a 7 T (300 MHz) AVANCE III Bruker spectrometer operating respectively at 75 MHz ( $^{13}\text{C}$ ) and 121 MHz ( $^{31}\text{P}$ ) equipped with a BBO probehead. The samples were spun at the magic angle at a frequency of 5, 6 or 10 kHz in 4 mm-diameter rotors at room temperature. The  $^{13}\text{C}$  CP MAS NMR experiments were acquired with proton cross polarization (CP MAS) with a contact time of 1.2 ms and the recycle delay was 2.0 s. The  $^{31}\text{P}$  MAS NMR spectra were obtained by a single pulse sequence with a  $90^\circ$  pulse of 5.0  $\mu\text{s}$  at a power of 20 W and a relaxation delay of 2.0 s.

### ***Scanning Electron Microscopy (SEM)***

SEM and energy dispersive X-ray spectroscopy (EDS) studies were performed at Centro de Materiais da Universidade do Porto (CEMUP) using a high-resolution (Schottky) scanning electron microscope with X-ray microanalysis and electron backscattered diffraction analysis Quanta 400 FEG ESEM/EDAX Genesis X4M. The samples were studied as powders and were coated with an Au/Pd thin film by sputtering using the SPI Module Sputter Coater equipment.

### ***Transmission Electron Microscopy (TEM)***

TEM images were obtained using a Hitachi transmission electron microscope model H-8100, with thermionic emission (LaB6) and 200 kV acceleration voltage at MicroLab (Instituto Superior Técnico). Digital image acquisition with a CCD MegaView II bottom-mounted camera. The samples were supported on a carbon-coated copper grid.

### ***X-ray Fluorescence (XRF)***

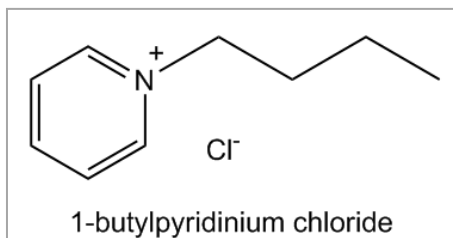
The X-Ray Fluorescence results were obtained by energy dispersive X-ray fluorescence ( $\mu$ -EDXRF) using a portable  $\mu$ -XRF spectrometer ArtTAX 800, Bruker in FCT-UNL. It operates with a molybdenum (Mo) X-ray source, focusing polycapillary lens and electro-thermally cooled xFlash (Si drift) detector, with 170 eV resolution (Mn K $\alpha$ ).

In this experimental work, it was also used the complementary equipments: Centrifuge (20.000 rpm; Beckman Avanti J-25 Centrifuge); Centrifuge (5.000 rpm, Tehtnica Centric 150, 650 2006); Domestic Microwave (Laser); Muffle (Nabertherm L5/11/C6D); pH Meter (Crison pH-Meter BASIC 20+; Scale, Sartorius Analytic Research R200D); Ultrasonic Bath (Elma S 100H Elmasonic) and Vortex Mixer (Janke & Kunkel IKA Labortechnik VF2).

## 2.2. Synthesis of POM-IL catalysts

### 2.2.1. Synthesis of Ionic Liquids

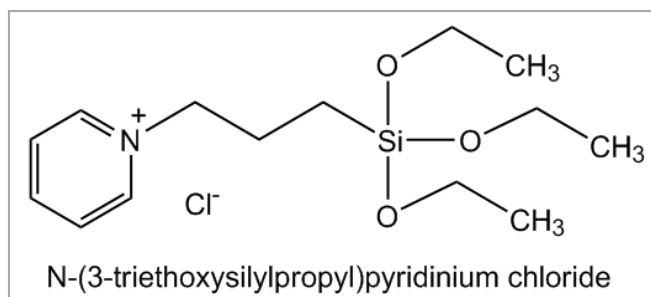
#### Synthesis of 1-butylpyridinium chloride



This synthesis was performed in 1.4:1 molar ratio, by reflux of 1-chlorobutane (9.3 mL, 88.5 mmol) and pyridine (5.1 mL, 63.2 mmol) without additional solvent. The reaction mixture was kept in reflux under stirring conditions for 48 h. Then, the final product was washed with diethyl ether (2x20 mL), decanted and dried under vacuum. The final product was obtained as a brownish solid (3.69 g, 28 %).

**<sup>1</sup>H NMR** (400.13 MHz, CDCl<sub>3</sub>, 25 °C)  $\delta$  = 9.70 (d, J = 4.0 Hz, 2H), 8.50 (t, J = 4.0 Hz, 1H), 8.16 (t, J = 8.0 Hz, 2H), 5.02 (t, J = 8.0 Hz, 2H), 2.05 (m, 2H), 1.40 (m, 2H), 0.93 (t, J = 8.0 Hz, 3H) ppm. **FTIR** (NaCl cell,  $\bar{\nu}/\text{cm}^{-1}$ ): 3417 (m); 3079 (m); 3025 (m); 3000 (m); 2961 (m, -CH<sub>2</sub>); 2934 (m, -CH<sub>2</sub>); 2874 (m, -CH<sub>3</sub>); 2361 (m); 1986 (m); 1920 (m); 1868 (m); 1580 (s, C=N<sub>arom</sub>); 1482 (m); 1438 (s); 1380 (m, C-N<sub>arom</sub>); 1313 (m); 1287 (m); 1242 (m); 1216 (m); 1146 (m); 1068 (m); 1030 (m); 991 (m); 931 (m); 873 (m); 747 (m); 704 (m); 649 (m); 602 (m).

#### Synthesis of N-(3-triethoxysilylpropyl)pyridinium chloride

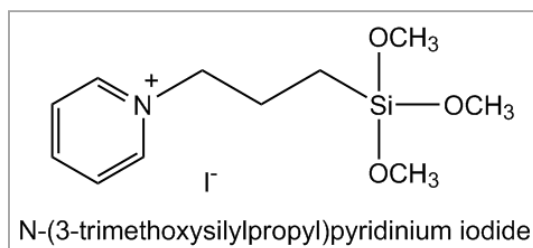


The synthesis was performed in 1:1 molar ratio, by reflux of (3-chloropropyl)triethoxysilane (0.5 mL, 2.08 mmol) and pyridine (0.168 mL, 2.08 mmol). The reaction was stirred under nitrogen atmosphere at 80 °C for 24 hours. The resultant liquid was washed with diethyl ether (2x20 mL) and dried under vacuum with stirring at 50 °C for 3 hours. FTIR and <sup>1</sup>H NMR spectra allowed to conclude that the reaction did not occur according to single presence of the reagent (3-chloropropyl)triethoxysilane in the spectra. The possible cause for this is the lower reactivity of the chloro- derivative reagent.

#### Synthesis of N-(3-trimethoxysilylpropyl)pyridinium iodide

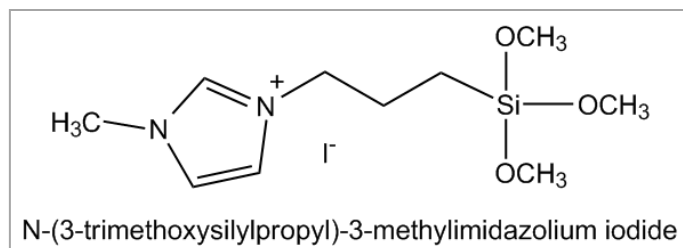
The synthesis was performed in 1:1 molar ratio, by reflux of 3-iodopropyltrimethoxysilane (0.404 mL, 1 mmol) with pyridine (0.167 mL, 1 mmol). The reaction was stirred under nitrogen atmosphere at 80 °C for 3 h. The product was

washed with diethyl ether (2x20 mL). The pure product was obtained as a viscous brownish yellow oil after dried in vacuum for 2 h (0.72 g, 94 %).



**<sup>1</sup>H NMR** (400.13 MHz, CDCl<sub>3</sub>, 25 °C) δ = 9.36 (d, J = 4.0 Hz, 2H), 8.62 (t, J = 8.0 Hz, 1H), 8.20 (t, J = 8.0 Hz, 2H), 4.99 (t, J = 16.0 Hz, 2H), 3.59 (s, 9H), 2.22 (m, 2H), 0.73 (t, J = 4.0 Hz, 2H) ppm. **FTIR** (NaCl cell,  $\bar{\nu}/\text{cm}^{-1}$ ): 3441 (m); 3128 (m); 3028 (m, -CH<sub>2</sub>); 2943 (s, -CH<sub>2</sub>); 2839 (s, -CH<sub>2</sub>); 1632 (s, C=N<sub>arom</sub>); 1579 (m); 1486 (s); 1460 (m); 1413 (m); 1350 (m, C-N<sub>arom</sub>); 1317 (m); 1245 (m); 1191 (s); 1079 (s, Si-OR); 889 (m); 815 (s); 776 (s); 682 (s); 646 (m).

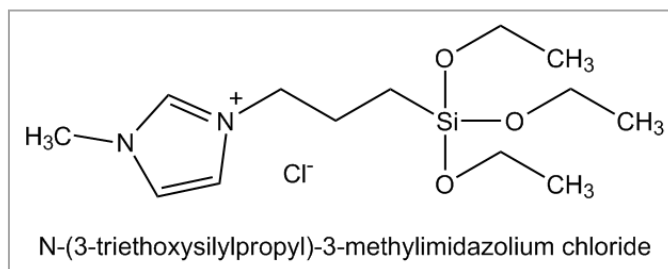
### Synthesis of N-(3-trimethoxysilylpropyl)-3-methylimidazolium iodide



The synthesis of N-(3-trimethoxysilylpropyl)-3-methylimidazolium iodide was performed in 1:1 molar ratio, by reflux of 1-methylimidazole (0.165 mL, 2.068 mmol) and 3-iodopropyltrimethoxysilane (0.405 mL 2.068 mmol). The reaction was stirred for 24 h under nitrogen atmosphere at 100 °C. The viscous brown liquid was then washed with diethyl ether (2x20 mL) and dried in vacuum for 3 h (0.75 g, 98 %).

**<sup>1</sup>H NMR** (400.13 MHz, CDCl<sub>3</sub>, 25 °C) δ = 9.89 (s, 1H), 7.59 (s, 1H), 7.45 (s, 1H), 4.34 (t, J = 8.0 Hz, 2H), 4.11 (s, 3H), 3.55 (s, 9H), 2.02 (t, J = 4.0 Hz, 2H), 0.65 (t, J = 8.0 Hz, 2H) ppm. **FTIR** (NaCl cell,  $\bar{\nu}/\text{cm}^{-1}$ ): 3456 (m); 3142 (m); 3076 (m, -CH<sub>2</sub>); 2945 (s, -CH<sub>2</sub>); 2840 (s, -CH<sub>2</sub>); 2360 (m); 2356 (m); 1571 (m, C=N); 1459 (m); 1348 (m); 1188 (s); 1170 (s); 1079 (s, Si-OR); 916 (m); 821 (s); 775 (m); 619 (m).

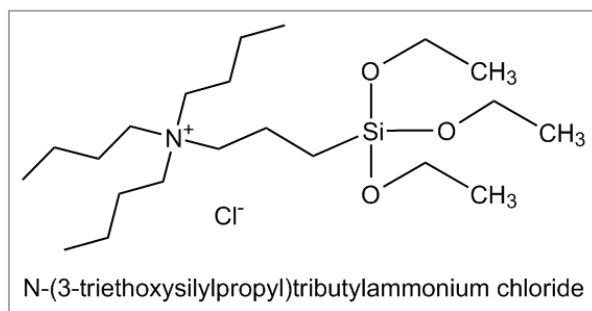
### Synthesis of N-(3-triethoxysilylpropyl)-3-methylimidazolium chloride



1-Methylimidazole (0.298 mL, 3.74 mmol) was added in excess to (3-chloropropyl)triethoxysilane (0.6 mL, 2.49 mmol) and stirred at 100 °C for 24 h under nitrogen atmosphere. The next day, the final product was washed several times with diethyl ether (2x20 mL) and dried in vacuum for 3 h at 50 °C (0.86 g, 95 %).

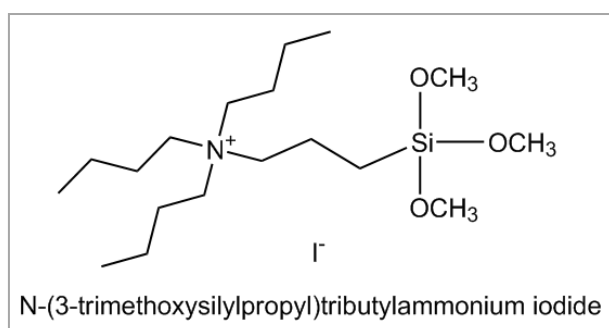
**<sup>1</sup>H NMR** (400.13 MHz, CDCl<sub>3</sub>, 25 °C) δ = 7.65 (s, 1H), 7.34 (s, 1H), 4.27 (t, J = 4.0 Hz, 2H), 4.06 (d, J = 8.0 Hz, 3H), 3.76 (m, 6H), 3.63 (t, J = 4.0 Hz, 1H), 1.97 (m, 2H), 1.16 (t, J = 8.0 Hz, 9H), 0.55 (t, J = 8.0 Hz, 2H) ppm. **FTIR** (NaCl cell,  $\bar{\nu}/\text{cm}^{-1}$ ): 3385 (m); 3181 (m); 3055 (m); 2974 (s, -CH<sub>2</sub>); 2928 (s, -CH<sub>2</sub>); 2888 (s, -CH<sub>2</sub>); 2734 (m, -CH<sub>2</sub>); 1635 (m, C=N); 1571 (m); 1445 (m); 1390 (m); 1295 (m); 1248 (m); 1167 (s); 1078 (vs, Si-OR); 987 (m); 958 (s, C-N<sub>alif</sub>); 876 (m); 781 (s); 623 (m).

### Synthesis of N-(3-triethoxysilylpropyl)tributylammonium chloride



The synthesis was performed in 1:1 molar ratio, by reflux of (3-chloropropyl)triethoxysilane (0.6 mL, 2.5 mmol) and tributylamine (0.592 mL, 2.5 mmol). The reaction was stirred under nitrogen atmosphere at 100 °C for 48 h. The obtained brown oil was washed several times with diethyl ether (2x20mL) and then dried in vacuum for 3 hours. The reaction was not complete due the lower reactivity of the chloro- derivative reagent. FTIR and <sup>1</sup>H NMR spectra indicated a mixture of compounds.

### Synthesis of N-(3-trimethoxysilylpropyl)tributylammonium iodide

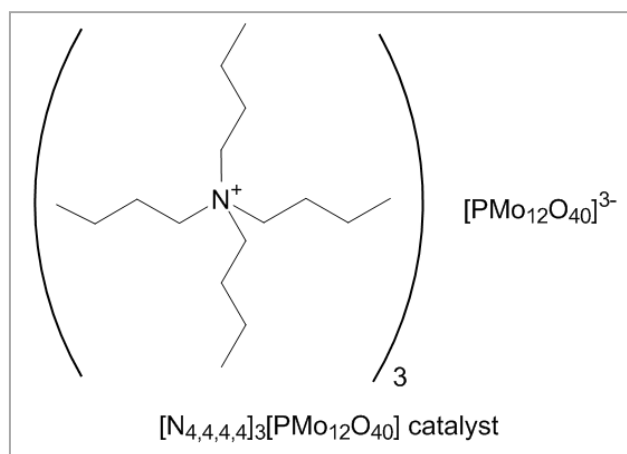


Tributylamine (0.491 mL, 2.07 mmol) and 3-iodopropyltrimethoxysilane (0.405 mL, 2.07 mmol) were mixed in 1:1 molar ratio. The mixture was kept under stirring and nitrogen conditions, at 80 °C for 24h. The desired product was washed with diethyl ether (2x20 mL) and then dried in vacuum for 3 hours. The final product was obtained viscous pale-yellow liquid (0.49 g, 50 %).

**<sup>1</sup>H NMR** (400.13 MHz, CDCl<sub>3</sub>, 25 °C) δ = 3.60 (s, 9H), 3.40 (m, 8H), 1.72 (m, 8H), 1.51 (m, 6H), 1.05 (t, J = 8.0 Hz, 9H), 0.78 (t, J = 8.0 Hz, 2H) ppm. **FTIR** (NaCl cell,  $\bar{\nu}/\text{cm}^{-1}$ ): 3432 (s); 3193 (s); 2948 (vs, -CH<sub>2</sub>); 2723 (s, -CH<sub>2</sub>); 2626 (s, -CH<sub>3</sub>); 2520 (s, -CH<sub>3</sub>); 2397 (s); 2167 (s); 1908 (s); 1724 (s); 1614 (s); 1467 (vs); 1407 (s); 1380 (s); 1077 (vs, Si-OR); 933 (s, C-N<sub>alif</sub>); 884 (s); 823 (vs); 683 (s); 645 (s).

## 2.2.2. Synthesis of POM-IL catalysts

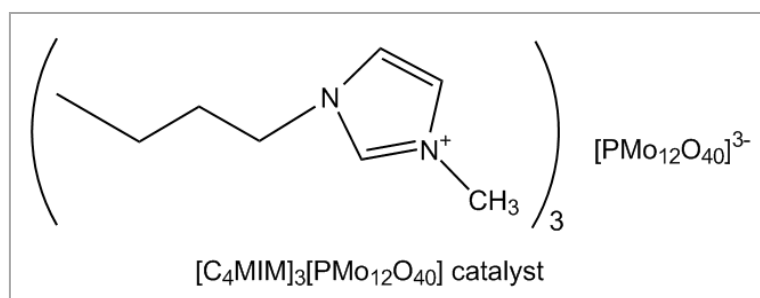
### Synthesis of $[N_{4,4,4,4}]_3[PMo_{12}O_{40}]$ catalyst



Tetrabutylammonium bromide (0.8026g, 2.48 mmol) was dissolved in methanol, and added to ion exchange resin Amberlyst® A26 (OH<sup>-</sup>) (10 mL, 7.44 mmol). The mixture was stirred, and after 1 h the resin was filtered and washed with methanol, obtaining tetrabutylammonium hydroxide. H<sub>3</sub>PMo<sub>12</sub>O<sub>40</sub> (0.8049 g, 0.44 mmol) was slowly added in excess dissolved in methanol and the solution was stirred for 20 min. Then, a yellow precipitate is formed, filtered and washed with methanol. The final product was obtained as a yellow solid after dried in vacuum for 24 hours at 85 °C (0.67 g, 42 %).

<sup>1</sup>H NMR (400.13 MHz, DMSO d<sub>6</sub>, 25 °C) δ (ppm) = 3.19 (t, J = 8.0 Hz, 8H), 1.58 (s, 8H), 1.35 (m, 8H), 0.96 (t, J = 8.0 Hz, 12H) ppm. <sup>31</sup>P NMR (162 MHz, DMSO d<sub>6</sub>, 25 °C) δ = -4.10 ppm. FTIR (KBr,  $\bar{\nu}/\text{cm}^{-1}$ ): 3451 (m); 2963 (s, -CH<sub>2</sub>); 2934 (s, -CH<sub>2</sub>); 2874 (m, -CH<sub>2</sub>); 1923 (w); 1635 (m); 1481 (m); 1469 (m); 1380 (m); 1282 (m); 1150 (m); 1106 (m); 1062 (s); 1030 (m); 954 (s, C-N<sub>alif</sub>); 880 (s); 807 (s); 740 (m); 617 (m); 505 (m); 465 (m). **Elemental analysis** calculated for (C<sub>16</sub>H<sub>36</sub>N)<sub>3</sub>PMo<sub>12</sub>O<sub>40</sub> (2549.63): C, 23.18; H, 4.39; N, 1.65; Found: C, 22.59; H, 4.24; N, 1.65.

### Synthesis of $[C_4MIM]_3[PMo_{12}O_{40}]$ catalyst

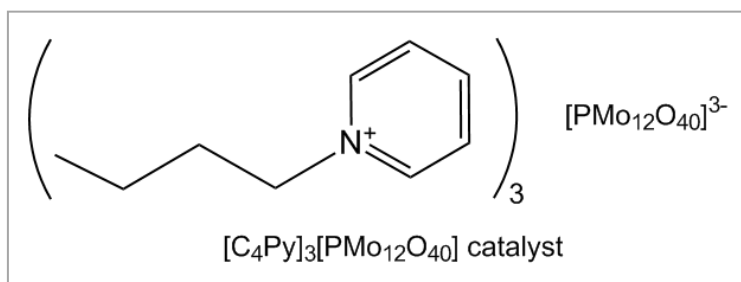


1-Butyl-3-methylimidazolium chloride, [C<sub>4</sub>MIM][Cl], (0.2309 g, 1.3 mmol) was dissolved in methanol, and then added to the ion exchange resin Amberlyst® A26 (OH<sup>-</sup>) (8.4 mL, 6.7 mmol) for 1 h with continuous stirring. The product was filtered and the resin was washed with methanol. H<sub>3</sub>PMo<sub>12</sub>O<sub>40</sub> (0.9047 g, 0.43 mmol) was slowly added in excess dissolved in methanol and the solution was stirring for 24 hours. Then, a yellow precipitate is formed, filtered and washed with methanol. The final product was obtained as a yellow solid after dried in vacuum for 24 hours at 85 °C (0.84 g, 73 %).

<sup>1</sup>H NMR (400.13 MHz, DMSO d<sub>6</sub>, 25 °C) δ = 9.10 (s, 1H), 7.77 (s, 1H), 7.70 (s, 1H), 4.19 (t, J = 8.0 Hz, 2H), 3.86 (s, 3H), 1.81 (m, 2H), 1.28 (t, J = 8.0 Hz, 2H), 0.93 (t, J =

8.0 Hz, 3H) ppm.  $^{31}\text{P}$  NMR (162 MHz, DMSO  $d_6$ , 25 °C)  $\delta$  = -4.11 ppm. FTIR (KBr,  $\bar{\nu}$  / $\text{cm}^{-1}$ ): 3454 (s); 3146 (s); 3110 (s); 3089 (s); 2959 (s, -CH<sub>2</sub>); 2931 (s, -CH<sub>2</sub>); 2867 (s, -CH<sub>2</sub>); 2356 (m); 1924 (m); 1602 (m, C=N); 1563 (m); 1462 (m); 1425 (m); 1379 (m); 1334 (m); 1165 (s); 1105 (s); 1062 (s, Si-OR); 1020 (s); 956 (s, C-N<sub>alif</sub>); 878 (s); 796 (s); 648 (s); 620 (s); 504 (s); 464 (m). **Elemental analysis** (%) calculated for (C<sub>8</sub>H<sub>15</sub>N<sub>2</sub>)<sub>3</sub>PMo<sub>12</sub>O<sub>40</sub> (2239.88): C, 13.20; H, 3.72; N, 1.99; Found: C, 12.86; H, 3.75; N, 2.00.

### Synthesis of [C<sub>4</sub>Py]<sub>3</sub>[PMo<sub>12</sub>O<sub>40</sub>] catalyst

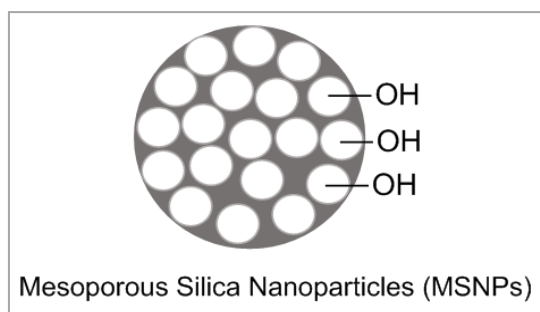


1-butylpyridinium chloride (0.2580 g, 1.46 mmol) was dissolved in methanol. Ion exchange resin Amberlyst® A26 (OH<sup>-</sup>) (9.13 mL, 7.3 mmol) was added to the ionic liquid with stirring conditions for 1 h. The product was filtered and washed with methanol. H<sub>3</sub>PMo<sub>12</sub>O<sub>40</sub> (0.9729 g, 0.53 mmol) was slowly added in excess dissolved in methanol and the solution was stirring for 30 min. Then, a yellow precipitate is formed, filtered and washed with methanol. The final product was obtained as a yellow solid after dried in vacuum for 24 hours at 85 °C (0.92 g, 74 %).

$^1\text{H}$  NMR (400.13 MHz, DMSO  $d_6$ , 25 °C)  $\delta$  = 9.10 (d, J = 4.0 Hz, 2 H), 8.63 (t, J = 8.0 Hz, 1H), 8.19 (t, J = 8.0 Hz 2H), 4.63 (t, J = 8.0 Hz, 2H), 1.95 (m, J = 8.0 Hz, 2H), 1.31 (m, 2H), 0.94 (t, J = 8.0 Hz, 3H) ppm.  $^{31}\text{P}$  NMR (162 MHz, DMSO  $d_6$ , 25 °C)  $\delta$  = -4.11 ppm. FTIR (KBr,  $\bar{\nu}$  / $\text{cm}^{-1}$ ): 3454 (s); 3124 (s); 3080 (s); 3063 (s); 2963 (s, -CH<sub>2</sub>); 2929 (s, -CH<sub>2</sub>); 2869 (s, -CH<sub>2</sub>); 2361 (m); 2333 (m); 1922 (m); 1632 (m, C=N); 1581 (m); 1485 (m); 1462 (m); 1384 (m); 1316 (m); 1278 (m); 1247 (m); 1209 (m); 1168 (m); 1063 (s, Si-OR); 956 (s, C-N<sub>alif</sub>); 878 (s); 795 (s); 682 (s); 644 (m); 594 (m); 504 (m). **Elemental analysis** calculated for (C<sub>9</sub>H<sub>14</sub>N)<sub>3</sub>PMo<sub>12</sub>O<sub>40</sub> (2230.87): C, 15.04; H, 1.88; N, 1.87; Found: C, 14.52; H, 1.88; N, 1.88.

## 2.3. Synthesis of MSNPs-POM-ILs catalysts

### 2.3.1. Synthesis of Mesoporous Silica Nanoparticles (MSNPs)



The following method for the synthesis of Mesoporous Silica Nanoparticles was described by *Bouchoucha et al*<sup>52</sup>.

For this synthesis, CTAB (0.6632 g, 1.82 mmol), Pluronic F127 (2.68 g) and Triethanolamine (15.64 g, 0.105 mmol) were dissolved in a solution composed by 57 mL of ethanol and 125 mL of distilled water. The solution was then stirred at room temperature for 24 hours. The next day, TEOS (2.56 mL, 11.48  $\mu\text{mol}$ ) was added to the solution at room temperature under vigorous stirring conditions for 1 min. The final solution was aged without stirring and at room temperature for 24 hours. After adding 100 mL of ethanol to the solution, the product was centrifuged at 20.000 rpm at room temperature, and washed after with distilled water. After the centrifugations, the white solid obtained was dried at 80 °C. Once dried, the MSNPs were calcinated (**Fig. 2.1.**) at 550 °C for 5 h, using a heating rate of 1 °C/min (1.3081 g).

**FTIR** (KBr,  $\bar{\nu}/\text{cm}^{-1}$ ): 3442 (s); 1706 (m); 1631 (m); 1084 (vs, *Si-OR*); 807 (m); 455 (s).



**Fig. 2.1.** – Calcination of Mesoporous Silica Nanoparticles (MSNPs) at 550 °C for 5 h, using a heating rate of 1 °C/min.

For the preparation of the samples for DLS analysis (**Fig.2.2.**), 3 mL of filtered bidestilled water were added to 5 mg of MSNPs. The sample was put in an ultrasonic bath for 15 minutes and then was shaken in a vortex equipment for 5 minutes to disperse the nanoparticles. This process was repeated several times. Several dispersions with different concentrations of MSNPs were prepared (with 1 mg and 2 mg of MSNPs).

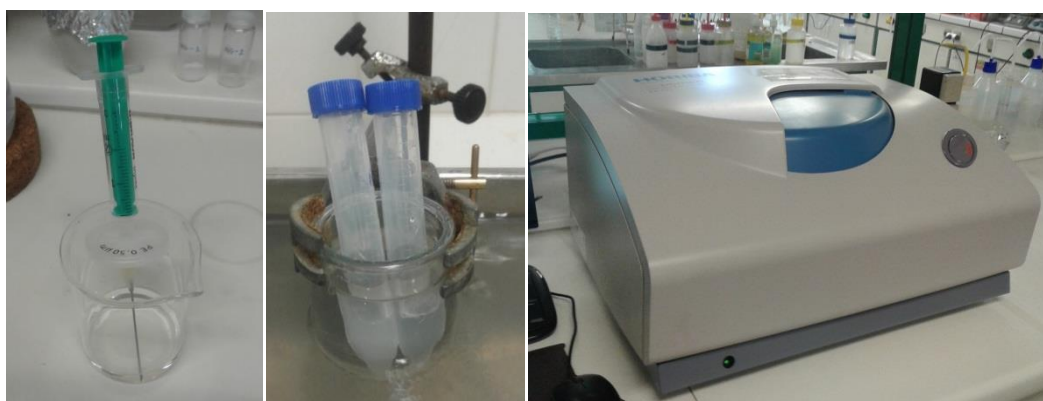


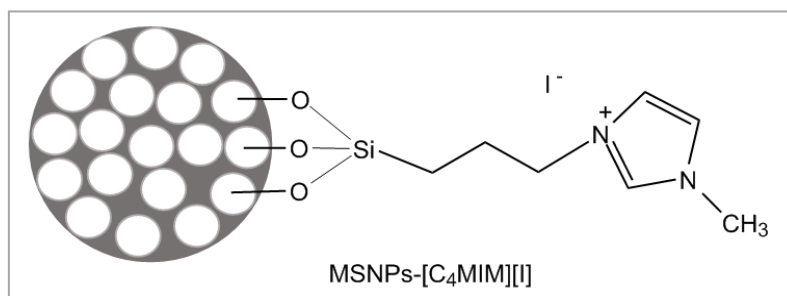
**Fig. 2.2.** – Sample preparation for DLS analysis. Use of bidestilled water (left), Ultrasonnd to disperse particles (middle) and analysis using a Horiba Scientific Nano Particle Analyzer SZ-100 (right).



### 2.3.2. Synthesis of MSNPs-POM-IL catalysts

- Synthesis of MSNPs-[C<sub>4</sub>MIM]POM catalyst

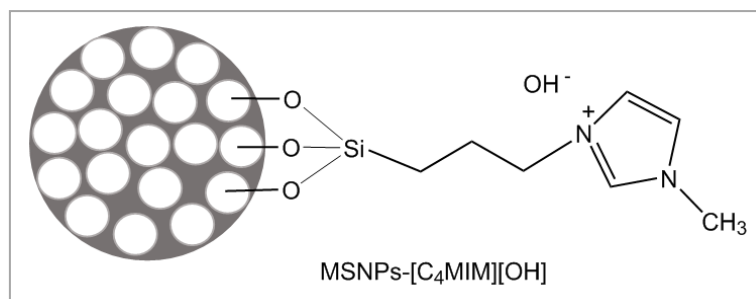
#### Synthesis of MSNPs-[C<sub>4</sub>MIM][I]



After drying 0.4513 g of MSNPs at 180 °C for 2 h under vacuum, it was added to ionic liquid N-(3-trimethoxysilylpropyl)-3-methylimidazolium iodide with 20 mL of dichloromethane as solvent. The reaction occurred for 24 hours at 40 °C and under stirring conditions. The product was then centrifuged several times with chloroform, and was left drying under vacuum (0.68 g, 57 %).

<sup>1</sup>H NMR (400.13 MHz, D<sub>2</sub>O + NaOH, 25 °C) δ = 7.35 (s, 1H), 7.28 (s, 1H), 4.6 (t, J = 8.0 Hz, 2H), 3.76 (s, 3H), 3.22 (s, 1H), 1.84 (m, 2H), 0.30 (t, J = 8.0 Hz, 2H) ppm. FTIR (KBr,  $\bar{\nu}/\text{cm}^{-1}$ ): 3444 (m); 1634 (m, C=N); 1573 (m); 1454 (m); 1382 (m, C-N<sub>arom</sub>); 1087 (vs, Si-OR); 806 (m); 617 (m); 455 (m).

#### Synthesis of MSNPs-[C<sub>4</sub>MIM][OH]



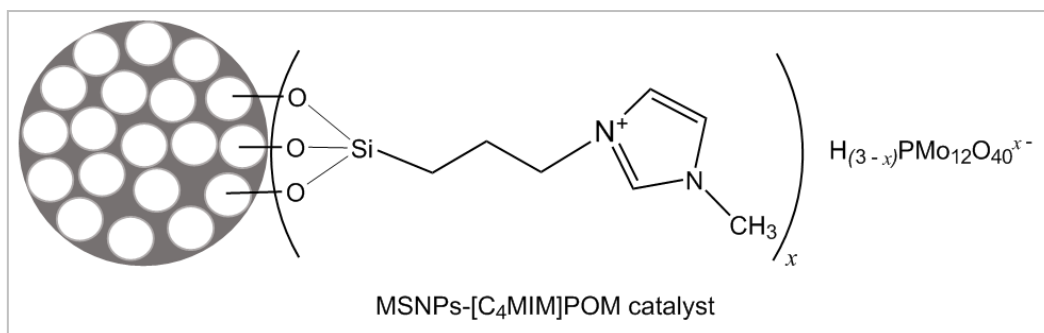
To change the anion I<sup>-</sup> to OH<sup>-</sup>, MSNPs-[C<sub>4</sub>MIM][I] was treated with a NaOH solution (0.025 M) for 3 h, and then centrifuged and washed with distilled water. The product was then dried at 80 °C (0.25 g, 71 %).

<sup>1</sup>H NMR (400.13 MHz, D<sub>2</sub>O + NaOH, 25 °C) δ = 7.33 (s, 1H), 7.28 (s, 1H), 4.05 (t, J = 8.0 Hz, 2H), 3.75 (s, 3H), 2.06 (s, 1H), 1.84 (m, 2H), 0.29 (t, J = 8.0 Hz, 2) ppm. FTIR (KBr,  $\bar{\nu}/\text{cm}^{-1}$ ): 3450 (s); 1640 (m, C=N); 1573 (m); 1456 (m); 1428 (m, C-N<sub>arom</sub>); 1086 (vs, Si-OR); 963 (m, C-N<sub>alif</sub>); 798 (m); 620 (m); 558 (m); 460 (s).

#### Synthesis of MSNPs-[C<sub>4</sub>MIM]POM

H<sub>3</sub>PMo<sub>12</sub>O<sub>40</sub> (0.1501 mg) was dissolved in 10 mL of ethanol and then added to MSNPs-[C<sub>4</sub>MIM][OH] with constant stirring at room temperature. After centrifugation and washings with ethanol several times, the final product was dried under vacuum for a few hours (0.20 g, 59 %).

<sup>1</sup>H NMR (400.13 MHz, D<sub>2</sub>O + NaOH, 25 °C) δ = 7.34 (s, 1H), 7.28 (s, 1H), 4.05 (t, J = 8.0 Hz, 2H), 3.75 (s, 3H), 3.53 (s, 1H), 1.84 (m, 2H), 0.29 (m, 2H) ppm.



**Solid State <sup>13</sup>C CP MAS NMR** (100,61 MHz, 25 °C)  $\delta$  = 137.28, 124.17, 52.65, 36.65, 24.24, 9.72 ppm. **Solid State <sup>31</sup>P CP MAS NMR** (162 MHz, 25 °C)  $\delta$  = -3.67 ppm. **FTIR** (KBr,  $\bar{\nu}/\text{cm}^{-1}$ ): 3423 (s); 3164 (m, -CH<sub>2</sub>); 2976 (m, -CH<sub>2</sub>); 2923 (m, -CH<sub>3</sub>); 2361 (m); 1636 (m, C=N); 1575 (m); 1457 (m); 1089 (vs, Si-OR); 961 (m, C-N<sub>alif</sub>); 803 (m); 620 (m); 462 (s). **Elemental analysis** (%) found: C, 7.60; H, 1.63; N, 2.27.

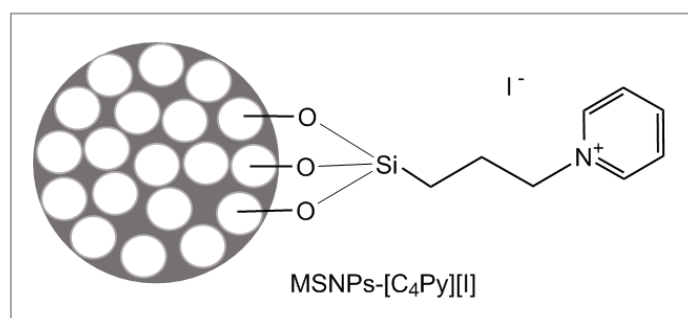


**Fig. 2.3.** – FTIR tablet preparation using KBr as a solid solvent.

- **Synthesis of MSNPs-[C<sub>4</sub>Py]POM catalyst**

**Synthesis of MSNPs-[C<sub>4</sub>Py][I]**

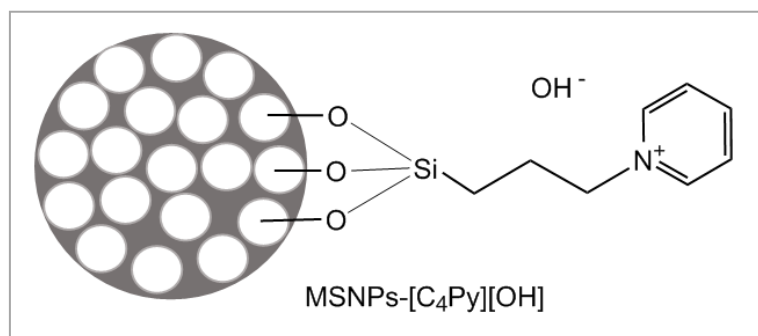
After drying 0.4014 mg of MSNPs at 180 °C for 2 h in vacuum conditions, it was added to 1-(3-trimethoxysilylpropyl)-3-pyridinium iodide dissolved in 20 mL of acetonitrile. The reaction was left for 24 hours at 85 °C, under stirring conditions and nitrogen atmosphere (0.58 g, 52 %).



**<sup>1</sup>H NMR** (400.13 MHz, D<sub>2</sub>O + NaOH, 25 °C)  $\delta$  = 8.42 (t, J = 8.0 Hz, 1H), 7.93 (d, J = 8.0 Hz, 2H), 4.46 (t, J = 8.0 Hz, 2H), 3.20 (s, 1H), 1.97 (m, 2H), 0.31 (t, J = 12.0 Hz, 2H) ppm. **FTIR** (KBr,  $\bar{\nu}/\text{cm}^{-1}$ ): 3443 (s); 2950 (m, -CH<sub>2</sub>); 2923 (m, -CH<sub>2</sub>); 2850 (m, -CH<sub>2</sub>);

2354 (m); 2333 (m); 1865 (m); 1635 (m,  $C=N_{\text{arom}}$ ); 1488 (m); 1456 (m); 1379 (m,  $C-N_{\text{arom}}$ ); 1090 (s,  $Si-OR$ ); 958 (m,  $C-N_{\text{alif}}$ ); 801 (m); 673 (m); 561 (m); 460 (s).

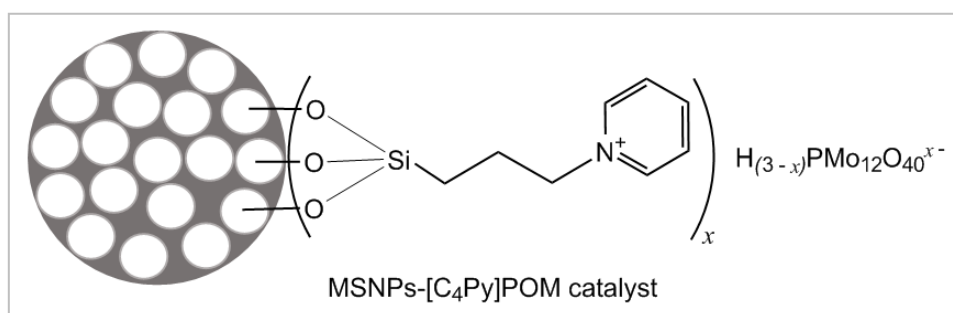
### Synthesis of MSNPs-[C<sub>4</sub>Py][OH]



MSNPs-[C<sub>4</sub>Py][I] (0.4000 g) was then treated with a NaOH solution (0.025 M) for 2 h with constant stirring. The product was then centrifuged for 15 minutes several times at 5.000 rpm, and washed with distilled water. The product was then dried in the oven at 80 °C (0.28 g, 69 %).

<sup>1</sup>H NMR (400.13 MHz, D<sub>2</sub>O + NaOH, 25 °C)  $\delta$  = 8.60 (d, J = 8.0 Hz, 1H), 8.39 (t, J = 4.0 Hz, 1H), 7.90 (d, J = 8.0 Hz, 2H), 4.43 (t, J = 8.0 Hz, 2H), 1.94 (m, 2H), 0.23 (t, J = 4.0 Hz, 2H) ppm. FTIR (KBr,  $\bar{\nu}/\text{cm}^{-1}$ ): 3442 (s); 2356 (m); 2335 (m); 1637 (m,  $C=N_{\text{arom}}$ ); 1490 (m); 1090 (s,  $Si-OR$ ); 960 (m,  $C-N_{\text{alif}}$ ); 796 (m); 678 (m); 533 (m); 463 (s).

### Synthesis of MSNPs-[C<sub>4</sub>Py]POM



$H_3PMo_{12}O_{40}$  (0.2 mmol, 0.3804 g) was in contact with exchange ion resin DOWEX® 50WX8-100 ( $H^+$ ) (0.6 mL, 1 mmol) for 30 min. It was then dissolved in methanol and added to MSNPs-[C<sub>4</sub>Py][OH] (0.2511 g) with stirring conditions for 2 days. The mixture was washed and centrifuged several times (5.000 rpm for 20 min). The solid was dried at 80 °C for 24 hours. At this point, after the <sup>31</sup>P NMR results being analyzed, it was discovered that the salt  $Na_3PMo_{12}O_{40}$  used was contaminated, so it was necessary to repeat the NaOH treatment for 4 h to eliminate the polyoxometalate ion from the sample. The blue mixture was then centrifuged at 5.000 rpm and washed with distilled water several times. The white solid was left to dry for 24 hours at 80 °C. A different  $H_3PMo_{12}O_{40}$  (0.1190 g) dissolved in methanol was added to MSNPs-[C<sub>4</sub>Py][OH] (0.1299 g) for 2 days with constant stirring. The whitish-green solid was left to dry at the oven at 80 °C, after being centrifuged and washed with methanol for several times (0.13 g, 51 %). Several analysis were performed, including X-Ray Fluorescence Spectroscopy (**Fig. 2.4**).

<sup>1</sup>H NMR (400.13 MHz, D<sub>2</sub>O + NaOH, 25 °C)  $\delta$  (ppm) = 8.43 (t, J = 8.0 Hz, 1H), 7.94 (d, J = 4.0 Hz, 2H), 4.48 (t, J = 8.0 Hz, 2H), 3.22 (s, 1H), 2.02 (m, 2H), 0.32 (t, J = 8.0 Hz, 2H) ppm. FTIR (KBr,  $\bar{\nu}/\text{cm}^{-1}$ ): 3441 (s); 2952 (m,  $-CH_2$ ); 2926 (m,  $-CH_2$ ); 2852 (m,  $-CH_2$ ); 2360 (m); 2337 (m); 1636 (m,  $C=N_{\text{arom}}$ ); 1489 (m); 1457 (m); 1091 (s,  $Si-OR$ );

960 (m, C-N<sub>alif</sub>); 801 (m); 680 (m); 551 (m); 465 (s). **Elemental analysis (%)** found: C, 8.58; H, 1.65; N, 1.03.

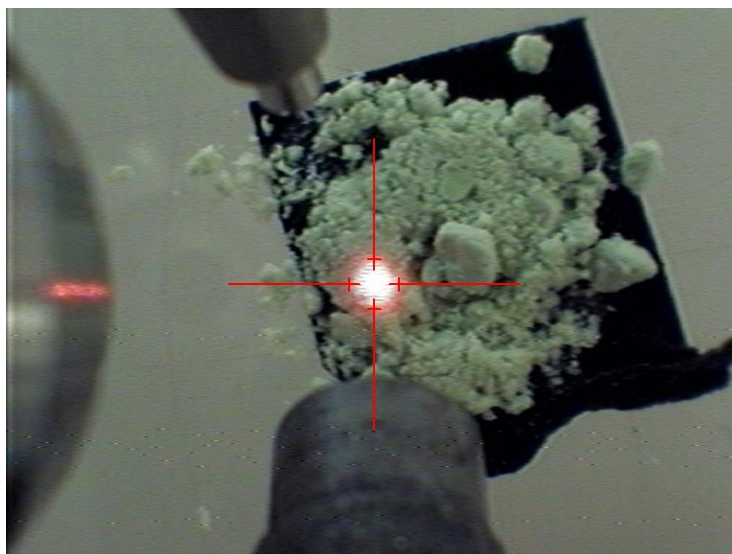
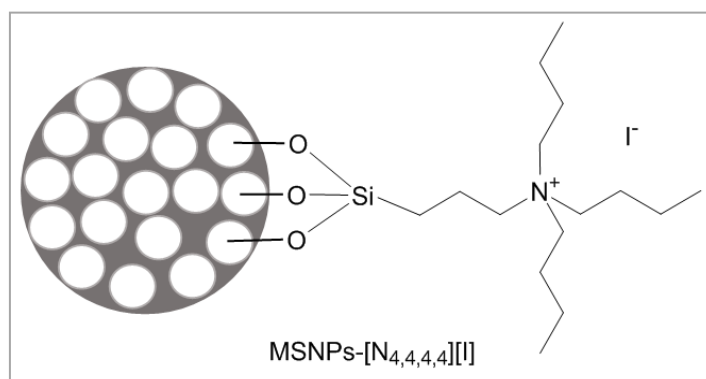


**Figure 2.4.** - X-Ray Fluorescence Spectroscopy preparation of the heterogeneous catalyst MSNPs-[C<sub>4</sub>MIM]POM.

- **Synthesis MSNPs-[N<sub>4,4,4,4</sub>]POM catalyst**

**Synthesis of MSNPs-[N<sub>4,4,4,4</sub>][I]**



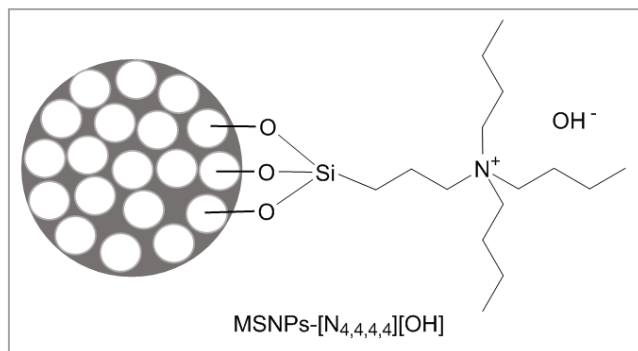
After drying MSNPs (0.4011 g) for 2 hours, it was added to the previously prepared ionic liquid N-(3-trimethoxysilylpropyl)tributylammonium iodide dissolved in acetonitrile for 48 h. The white mixture was centrifuged at 5.000 rpm and washed with methanol several times. The resulting white solid was dried at the oven at 80 °C (0.46 g, 51 %).

**<sup>1</sup>H NMR** (400.13 MHz, D<sub>2</sub>O + NaOH, 25 °C) δ = 3.02 (m, 8H), 1.58 (m, 8H), 1.23 (m, 6H), 0.80 (t, J = 8.0 Hz, 9H), 0.22 (t, J = 4.0 Hz, 2H) ppm. **FTIR** (KBr,  $\bar{\nu}/\text{cm}^{-1}$ ): 3452 (s); 2964 (m, -CH<sub>3</sub>); 2877 (m, -CH<sub>2</sub>); 2347 (m); 1634 (m); 1481 (m); 1463 (m); 1380 (m); 1087 (s, Si-OR); 968 (m, C-N<sub>alif</sub>); 804 (m); 561 (m); 458 (m).

**Synthesis of MSNPs-[N<sub>4,4,4,4</sub>][OH]**

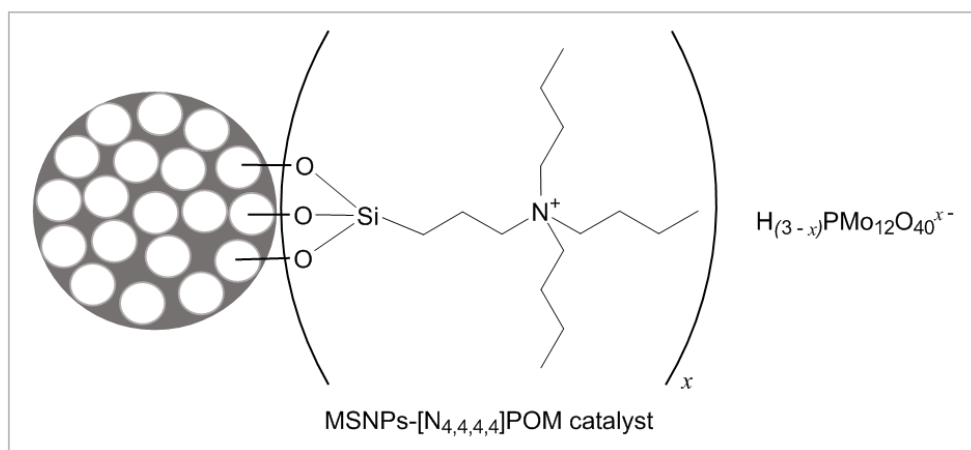
To change the anion I<sup>-</sup> by OH<sup>-</sup>, 0.4006 g of MSNPs-[N<sub>4,4,4,4</sub>][I] was treated with a NaOH solution (0.025 M) for 2 h, and then centrifuged and washed with distilled water. The product was then dried in the oven at 80 °C (0.3601 g, 89.89 %).

**FTIR** (KBr,  $\bar{\nu}/\text{cm}^{-1}$ ): 3452 (s); 2964 (m,  $-\text{CH}_3$ ); 2877 (m,  $-\text{CH}_2$ ); 2347 (m); 1634 (m); 1481 (m); 1463 (m); 1380 (m); 1087 (s,  $\text{Si-OR}$ ); 968 (m,  $\text{C-N}_{\text{alif}}$ ); 804 (m); 561 (m); 458 (m).



### **Synthesis of MSNPs-[N<sub>4,4,4,4</sub>]POM**

$\text{H}_3\text{PMo}_{12}\text{O}_{40}$  (0.9011 g) was in contact with exchange ion resin DOWEX® 50WX8-100 ( $\text{H}^+$ ) (1.4 mL, 2.38 mmol) for 30 min. It was then dissolved in methanol and added to MSNPs-[N<sub>4,4,4,4</sub>][OH] (0.3364 g) with stirring conditions for 2 days. The greenish-yellow mixture was washed and centrifuged several times. The yellow and green solid was dried at 80 °C for 24 hours, resulting in a two-layered color solid (blue and green). Like it was mentioned before, it was necessary to repeat the NaOH treatment (for 5 h) to eliminate the ion  $\text{H}_2\text{PMo}_{12}\text{O}_{40}^-$  from the sample.



The blue mixture was then centrifuged at 5.000 rpm and washed with distilled water several times until pH was 8.11. The grey solid was left to dry for 24 hours at 80 °C. A different  $\text{H}_3\text{PMo}_{12}\text{O}_{40}$  (0.2323 g) dissolved in methanol was added to MSNPs-[N<sub>4,4,4,4</sub>][OH] (0.2494 g) for 2 days with constant stirring. The whitish-green solid was left to dry at the oven at 80 °C, after being centrifuged and washed with methanol for several times (0.26 g, 54 %).

**<sup>1</sup>H NMR** (400.13 MHz,  $\text{D}_2\text{O} + \text{NaOH}$ , 25 °C)  $\delta$  = 3.08 (m, 8H), 1.56 (m, 8H), 1.26 (m, 6H), 0.84 (t,  $J = 8.0$  Hz, 9H), 0.30 (t,  $J = 8.0$  Hz, 2H) ppm. **Solid State <sup>13</sup>C CP MAS NMR** (100,61 MHz, 25 °C)  $\delta$  = 59.27, 24.61, 20.35, 13.57, 9.12 ppm. **Solid State <sup>31</sup>P CP MAS NMR** (162 MHz, 25 °C)  $\delta$  = -3.55, -4.12 ppm. **FTIR** (KBr,  $\bar{\nu}/\text{cm}^{-1}$ ): 3423 (s); 2965 (m,  $-\text{CH}_3$ ); 2879 (m,  $-\text{CH}_2$ ); 2360 (m); 2341 (m); 1868 (m); 1635 (m); 1467 (m); 1382 (m); 1089 (vs,  $\text{Si-OR}$ ); 959 (s,  $\text{C-N}_{\text{alif}}$ ); 890 (s); 810 (s); 667 (s); 545 (s); 462 (s). **Elemental analysis** (%) found: C, 11.11; H, 2.41; N, 0.70.

## 2.4. Catalytic Reactions

### 2.4.1. Oxidation of Lignin Model Compounds

#### 2.4.1.1. Conventional Heating using acetonitrile as solvent

- **Oxidation of Cinnamyl Alcohol**

The oxidation reactions of cinnamyl alcohol were performed based on *Badamali et al*<sup>55</sup> experimental procedure.

##### Catalyst H<sub>3</sub>PMo<sub>12</sub>O<sub>40</sub> with H<sub>2</sub>O<sub>2</sub>

Cinnamyl alcohol (1 mmol) was dissolved in 10 mL of acetonitrile with hydrogen peroxide (3 mmol) and H<sub>3</sub>PMo<sub>12</sub>O<sub>40</sub> (1 mmol). The mixture was stirred for 47 h at 80 °C. After the reaction, the solvent was removed by evaporation in *rota-vapor* and dried under vacuum conditions. No reaction was observed by NMR spectroscopy.

##### Catalyst H<sub>3</sub>PMo<sub>12</sub>O<sub>40</sub> without H<sub>2</sub>O<sub>2</sub>

For this oxidation reaction, cinnamyl alcohol (1 mmol) was dissolved in 10 mL of acetonitrile and H<sub>3</sub>PMo<sub>12</sub>O<sub>40</sub> (1 mmol). The mixture was stirred for 47 h at a temperature of 80 °C. After the reaction, the solvent was removed by evaporation in *rota-vapor* and dried under vacuum conditions. The reaction was checked by NMR spectroscopy from final crude.

##### Catalyst [N<sub>4,4,4,4</sub>]<sub>3</sub>[PMo<sub>12</sub>O<sub>40</sub>] with H<sub>2</sub>O<sub>2</sub>

Cinnamyl Alcohol (0.5 mmol) was dissolved in 5 mL of acetonitrile with hydrogen peroxide (3 mmol) and [N<sub>4,4,4,4</sub>]<sub>3</sub>[PMo<sub>12</sub>O<sub>40</sub>] (0.5 mmol). The mixture was maintained at the same conditions as the previous reaction, being stirred for 47 h at a temperature of 80 °C. After the reaction, the solvent was removed by evaporation in *rota-vapor* and dried under vacuum conditions as well. No reaction was observed by NMR.

- **Oxidation of Guaiacol**

The oxidation reactions of Guaiacol were performed based on *Hwang et al*<sup>56</sup> experimental protocol.

##### Catalyst H<sub>3</sub>PMo<sub>12</sub>O<sub>40</sub> with H<sub>2</sub>O<sub>2</sub>

For this oxidation reaction, guaiacol (1 mmol) was dissolved in 10 mL of acetonitrile with hydrogen peroxide (3 mmol) and the H<sub>3</sub>PMo<sub>12</sub>O<sub>40</sub> (1 mmol). The mixture was stirred for 47 h at a temperature of 80 °C. After the reaction, the solvent was removed by evaporation in *rota-vapor* and dried under vacuum conditions.

### **Catalyst [H<sub>3</sub>PMo<sub>12</sub>O<sub>40</sub>] without H<sub>2</sub>O<sub>2</sub>**

For this oxidation reaction, guaiacol (1 mmol) was dissolved in 10 mL of acetonitrile with H<sub>3</sub>PMo<sub>12</sub>O<sub>40</sub> (1 mmol). The mixture was stirred for 47 h at a temperature of 80 °C. After the reaction, the solvent was removed by evaporation in *rota-vapor* and dried under vacuum conditions.

### **Catalyst [N<sub>4,4,4,4</sub>]<sub>3</sub>[PMo<sub>12</sub>O<sub>40</sub>] with H<sub>2</sub>O<sub>2</sub>**

Guaiacol (0.5 mmol) was dissolved in 5 mL of acetonitrile with hydrogen peroxide (3 mmol) and [N<sub>4,4,4,4</sub>]<sub>3</sub>[PMo<sub>12</sub>O<sub>40</sub>] (0.5 mmol). The mixture was maintained at the same conditions as the previous reaction, being stirred for 47 h at a temperature of 80 °C. After the reaction, the solvent was removed by evaporation in *rota-vapor* and dried under vacuum conditions as well.

## **2.4.1.2. Microwave Heating using acetonitrile as solvent**

- **Oxidation of Cinnamyl Alcohol**

### **Catalyst H<sub>3</sub>PMo<sub>12</sub>O<sub>40</sub> with H<sub>2</sub>O<sub>2</sub>**

For this oxidation reaction, cinnamyl alcohol (0.62 mmol) was dissolved in 10 mL of acetonitrile with hydrogen peroxide (0.31 mmol) and H<sub>3</sub>PMo<sub>12</sub>O<sub>40</sub> (0.031 mmol). The reaction occurred during 1 minute in a domestic microwave, stirring after each 20 seconds. It was necessary to keep adding acetonitrile, since it is removed quickly after a few seconds. The color changed from yellow to dark green. The addition of K<sub>2</sub>CO<sub>3</sub> to solution was performed to eliminate H<sub>2</sub>O<sub>2</sub> residues. The final crude was obtained after evaporation of the solvent in *rota-vapor*.

### **Catalyst [C<sub>4</sub>MIM]<sub>3</sub>[PMo<sub>12</sub>O<sub>40</sub>] with H<sub>2</sub>O<sub>2</sub>**

For this oxidation reaction, cinnamyl alcohol (0.62 mmol) was dissolved in 10 mL of acetonitrile with hydrogen peroxide (0.31 mmol) and [C<sub>4</sub>MIM]<sub>3</sub>[PMo<sub>12</sub>O<sub>40</sub>] (0.031 mmol). The reaction occurred during 1 minute in a domestic microwave, stirring after each 20 seconds. It was necessary the addition of more acetonitrile. The color changed from yellow to dark blue. The addition of K<sub>2</sub>CO<sub>3</sub> to solution was performed to eliminate H<sub>2</sub>O<sub>2</sub> residues. The final crude was obtained after evaporation of the solvent in *rota-vapor*.

### **Catalyst [C<sub>4</sub>Py]<sub>3</sub>[PMo<sub>12</sub>O<sub>40</sub>] with H<sub>2</sub>O<sub>2</sub>**

For this oxidation reaction, cinnamyl alcohol (0.62 mmol) was dissolved in 10 mL of acetonitrile with hydrogen peroxide (0.31 mmol) and [C<sub>4</sub>Py]<sub>3</sub>[PMo<sub>12</sub>O<sub>40</sub>] (0.031 mmol). The reaction occurred during 1 min in a domestic microwave, stirring after each 20 seconds. It was necessary to keep adding acetonitrile. The color was yellow before and after the reaction. The addition of K<sub>2</sub>CO<sub>3</sub> to solution was performed to eliminate H<sub>2</sub>O<sub>2</sub> residues. The final crude was obtained after evaporation of the solvent in *rota-vapor*.

## 2.4.2. Oxidative Desulfurization of a Model Diesel

### Synthesis of Model Oil (2000 ppm)

In order to obtain a Model oil (2000 ppm) with the 4 main sulfur compounds present in petroleum, 1-benzothiophene (1-BT) (500 ppm), 4,6-dimethyldibenzothiophene (4,6-DMDBT) (500 ppm), 4-methyldibenzothiophene (4-MDBT) (500 ppm) and dibenzothiophene (DBT) (500 ppm) were mixed at room temperature.

### Synthesis of Internal Standard solution

Tetradecane and n-octane were mixed in same molar proportions (1:1) at room temperature.

### 2.4.2.1. Homogeneous Catalysts

#### Catalyst [N<sub>4,4,4,4</sub>]<sub>3</sub>[PMo<sub>12</sub>O<sub>40</sub>]

Homogeneous catalyst [N<sub>4,4,4,4</sub>]<sub>3</sub>[PMo<sub>12</sub>O<sub>40</sub>] (3 μmol) was used for the reaction of 750 μl of model oil, in 750 μl of acetonitrile. The mixture was stirred at 70 °C for 15 min. After the first 15 min, it was added 75 μl of H<sub>2</sub>O<sub>2</sub> 30% (w/w).

Meanwhile, Gas Chromatography (GC) equipment was prepared and an acetonitrile sample was measured to clean the equipment and an internal standard. The analysis tubes were previously filled with 20 μl of internal standard. After adding hydrogen peroxide to the reactor, samples of 20 μl were taken and measured after 10, 30 and 60 min. The GC measurements continued to be taken after each 60 min for a total of 6 h of measurements.

#### Catalyst [C<sub>4</sub>MIM]<sub>3</sub>[PMo<sub>12</sub>O<sub>40</sub>]

Catalyst [C<sub>4</sub>MIM]<sub>3</sub>[PMo<sub>12</sub>O<sub>40</sub>] (3 μmol) was added to 750 μl of model oil in 750 μl of acetonitrile. The mixture was stirred at 70 °C for 15 min, and after that phase, it was added 75 μl of H<sub>2</sub>O<sub>2</sub> 30% (w/w). The analysis tubes were previously filled with 20 μl of internal standard.

Samples of 20 μl were taken and measured after 10, 30 and 60 min of adding the hydrogen peroxide. The GC measurements continued to be taken after each 60 min for a total of 6 h of measurements.

#### Catalyst [C<sub>4</sub>Py]<sub>3</sub>[PMo<sub>12</sub>O<sub>40</sub>]

Homogeneous catalyst [C<sub>4</sub>Py]<sub>3</sub>[PMo<sub>12</sub>O<sub>40</sub>] (3 μmol) was used for the reaction of 750 μl of model oil, with 750 μl of acetonitrile as solvent. The mixture was stirred at a temperature of 70 °C for 15 min. After adding 75 μl of H<sub>2</sub>O<sub>2</sub> 30% (w/w), samples of 20 μl were taken and measured after 10, 30 and 60 min. The GC measurements continued to be taken after each 60 min for a total of 6 h of measurements.



## 2.4.2.2. Heterogeneous Catalysts

MSNPs-[C<sub>4</sub>MIM]POM, MSNPs-[C<sub>4</sub>Py]POM and MSNPs-[N<sub>4,4,4,4</sub>]POM catalysts were used in three different cycles in the same conditions. The following method describes each reaction of the three repeated cycles.

Heterogeneous catalyst (3 μmol of active center, 59 mg) was used in reaction of 750 μl of model oil, with 750 μl of 1-butyl-3-methylimidazolium hexafluorophosphate as an ionic liquid solvent. The mixture was stirred at a temperature of 70 °C for 15 min. After adding 75 μl of H<sub>2</sub>O<sub>2</sub> 30% (w/w), samples of 20 μl were taken and measured after 10, 30 and 60 min. The GC measurements continued to be taken after each 60 min for a total of 6 h of measurements.

Additionally, there were also two more studies applied to catalyst MSNPs-[C<sub>4</sub>MIM]POM, using half of solvent quantity and half the oxidant quantity used previously. The methods are described below.

### - Half Solvent quantity

Catalyst (3 μmol of active center, 19.5 mg) was used for the reaction of 250 μl of model oil, with 125 μl of 1-butyl-3-methylimidazolium hexafluorophosphate as an ionic liquid solvent. The mixture was stirred at a temperature of 70 °C for 15 min. After adding 25 μl of H<sub>2</sub>O<sub>2</sub> 30% (w/w), samples of 20 μl were taken and measured after 10, 30 and 60 min. The GC measurements continued to be taken after each 60 min for a total of 3 h of measurements.

### - Half Oxidant quantity

Catalyst (3 μmol of active center, 19.5 mg) was used for the reaction of 250 μl of model oil, with 250 μl of 1-butyl-3-methylimidazolium hexafluorophosphate as an ionic liquid solvent. The mixture was stirred at a temperature of 70 °C for 15 min. After adding 12.5 μl of H<sub>2</sub>O<sub>2</sub> 30% (w/w), samples of 20 μl were taken and measured after 10, 30 and 60 min.



### 3. Results and Discussion

#### 3.1. Objectives

The main objective of this thesis is focused on the development of efficient and environmental-friendly homogeneous and heterogeneous catalysts to apply in oxidative processes, focusing in the oxidations of lignin and a model diesel.

The first phase of the experimental work comprised the synthesis and characterization of the ionic liquids (new homogeneous catalyst) based on the polyoxometalate phosphomolybdate ( $[\text{PMo}_{12}\text{O}_{40}]^{3-}$ ) anion with different organic cations as counter ions, as well as their analogous heterogeneous catalysts through their immobilization in mesoporous silica nanoparticles. Therefore, different ionic liquids were prepared with tetra-alkylammonium ( $[\text{N}_{4,4,4,4}]^+$ ), alkylpyridinium ( $[\text{C}_4\text{Py}]^+$ ) and methylimidazolium ( $[\text{C}_4\text{MIM}]^+$ ) cations combined with chloride ( $\text{Cl}^-$ ) and iodide ( $\text{I}^-$ ) anions. The prepared ionic liquids were characterized by  $^1\text{H}$  NMR and FTIR to attest the desired molecular structures.

After preparing different ionic liquids, their halogen anions were changed to  $[\text{PMo}_{12}\text{O}_{40}]^{3-}$  anion. In parallel, heterogeneous catalytic materials were prepared using mesoporous silica nanoparticles (MSNs) as supports to functionalized selected organic cations. This experimental protocol is divided in three steps: first the cations of the ionic liquids was immobilized through covalent linkage to the mesoporous surface using iodide as counter ion, then the iodide anions were exchanged by hydroxyl groups and finally by an acid-base reaction with the phosphomolybdic acid the final heterogeneous catalyst was achieved.

The second part of the work was dedicated to test the prepared Homogeneous and Heterogeneous Catalysts in two different preliminary oxidation reactions: a) the oxidation of Lignin model compounds such as cinammyl alcohol and guaiacol using the homogeneous catalysts by conventional heating and microwave heating ( $^1\text{H}$  NMR technique was used to confirm the presence of oxidation products); b) the oxidative desulfurization (ODS) of petroleum model compounds using heterogeneous catalysts and checking the catalytic performance by Gas Chromatography analysis.

## 3.2. Preparation and characterization of IL and POM-IL catalysts

### 3.2.1. Preparation and characterization of Ionic Liquids

In order to prepare POM-IL catalysts, the first step was the synthesis of the ionic liquids based on cations tetra-alkylammonium ( $[N_{4,4,4,4}]^+$ ), alkylpyridinium ( $[C_4Py]^+$ ) and methylimidazolium ( $[C_4MIM]^+$ ), combined with chloride ( $Cl^-$ ) and iodide ( $I^-$ ) anions (**Fig. 3.1.**).

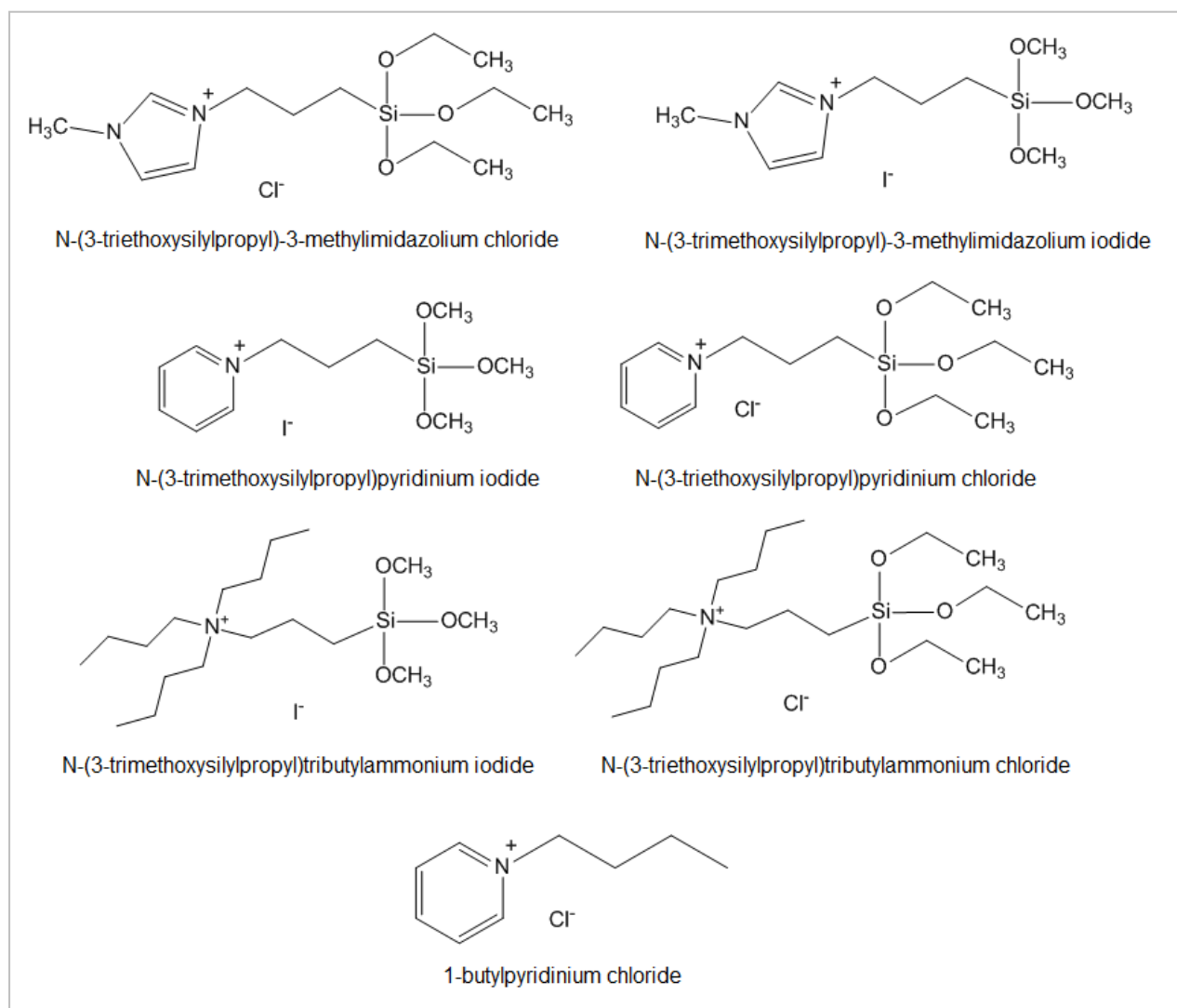


**Fig. 3.1.** - Chemical structures of the desired Ionic Liquids.

The different chloride and iodide salts were firstly prepared and summarized in the following table (**Table 3.1.**). This table describes some details related to synthetic method such as temperature ( $^{\circ}C$ ), reaction time (hours) and molar proportion of the reagents as well as the yield (%) and physical state of the final product.

**Table 3.1.** - Reaction conditions and results of the synthesis of the prepared ionic liquids.

Ionic Liquid	T (°C)	t (h)	proportion of reagents	$\eta$ (%)	Physical state of the product
N-(3-trimethoxysilylpropyl)pyridinium iodide	80	3	1:1	94	Viscous yellow oil
N-(3-triethoxysilylpropyl)pyridinium chloride	80	24	1:1	-	No reaction
N-(3-trimethoxysilylpropyl)-3-methylimidazolium iodide	100	24	1:1	98	Brown liquid
N-(3-triethoxysilylpropyl)-3-methylimidazolium chloride	100	24	1.5:1	95	Pale yellow liquid
N-(3-trimethoxysilylpropyl)tributylammonium iodide	80	24	1:1	50	Non-coloured liquid
N-(3-triethoxysilylpropyl)tributylammonium chloride	100	48	1:1	80	Viscous Brown oil
1-butylpyridinium chloride	100	48	1.4:1	28	Brown solid

All prepared ionic liquids were characterized by  $^1\text{H}$  NMR and Fourier-Transform Infrared Spectroscopy (FTIR) spectroscopies in order to prove the desired chemical structures as well as the final relative purity of the products.

### 3.2.1.1. N-(3-trimethoxysilylpropyl)pyridinium iodide

The synthesis of the desired salt was performed following a method already described in the literature by *Cho et al*<sup>57</sup>, by reflux of pyridine with 3-iodopropyltrimethoxysilane in 1:1 of molar ration according to **Figure 3.2.** The product was obtained as viscous yellow oil in high yield (94%).

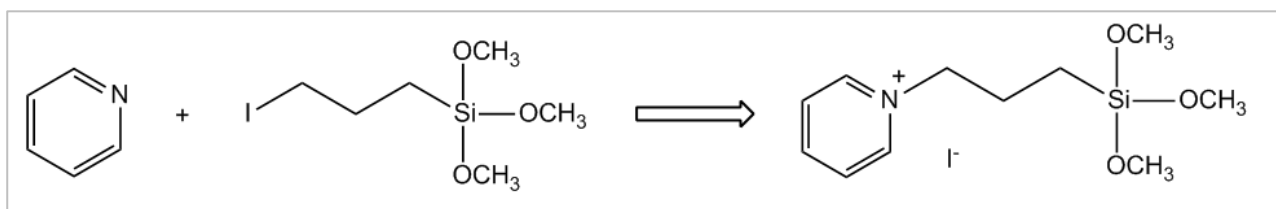


**Fig. 3.2.** - Schematic representation of the synthesis of ionic liquid N-(3-trimethoxysilylpropyl)pyridinium iodide with pyridine and 3-iodopropyltrimethoxysilane.

The FTIR spectra of the obtained product and reactants are represented in **Fig. 3.3.**

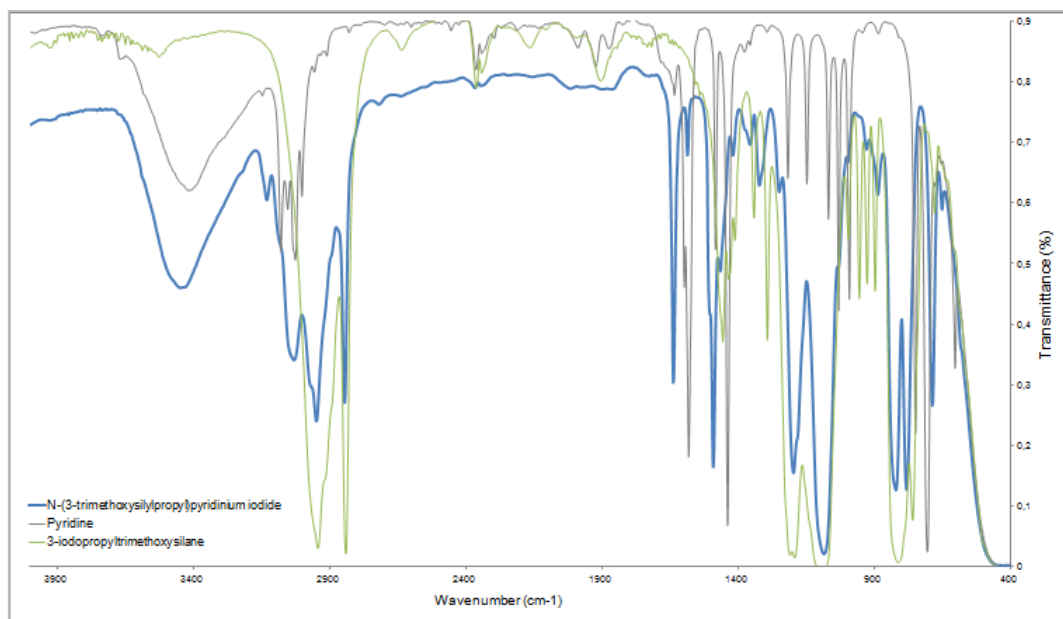


**Fig. 3.3.** - Fourier-Transform Infrared Spectrum of N-(3-trimethoxysilylpropyl)pyridinium iodide (blue), pyridine (grey) and 3-iodopropyltrimethoxysilane (green).

According to *Jovanovski et al*<sup>68</sup>, the dominant modes of  $-\text{OCH}_3$  groups are shown in 2844, 1194, 1080, 820 and 775  $\text{cm}^{-1}$ . When analyzing the obtained FTIR spectrum, it is possible to observe that the bands 2839, 1191, 1079, 815 and 776  $\text{cm}^{-1}$  are present in the final product, as it was expected. Also, according to *Urbanks*<sup>69</sup>, the ranges 3250-3000  $\text{cm}^{-1}$  bands correspond to the C—H aromatic bond vibrations of pyridine, and 1650-1400  $\text{cm}^{-1}$  bands correspond to aromatic C—C, C=C and C=N vibrations. These bands are present in the obtain spectrum at 3128, 3028, 1632, 1579, 1486, 1460 and 1413  $\text{cm}^{-1}$ .

To prove the desired chemical structure,  $^1\text{H}$  NMR spectra of the final compound was performed as indicated in **Figure 3.4**.

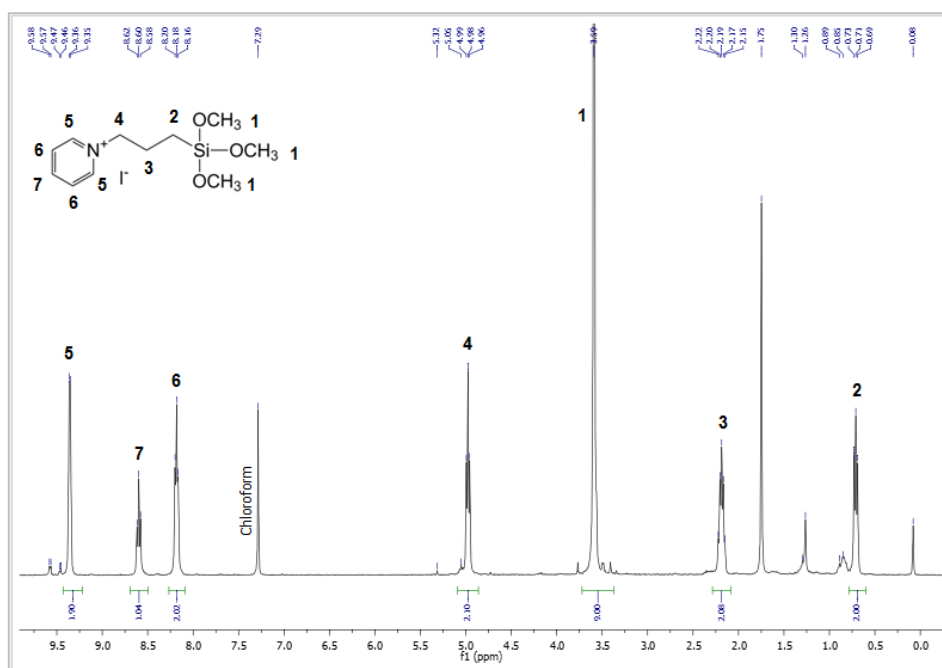


**Fig. 3.4.** - Solution  $^1\text{H}$  NMR Spectrum of N-(3-trimethoxysilylpropyl)pyridinium iodide, in deuterated chloroform.

Analyzing the obtained spectrum it is possible to confirm the structure of N-(3-trimethoxysilylpropyl)pyridinium iodide where all protons from organic cations were attributed in the spectra (the numerated peaks correspond to the numbers of the structure presented). From  $^1\text{H-NMR}$  is possible to confirm the chemical structure of the compound as well as to check the relative purity (no significant additional peaks were observed).

### 3.2.1.2. N-(3-trimethoxysilylpropyl)-3-methylimidazolium iodide

The synthesis of the desired salt was performed following a method (**Fig. 3.5.**) already described in the literature by *Jovanovski et al*<sup>60</sup>. The product was obtained in very high yield (98%) and relatively good purity level.

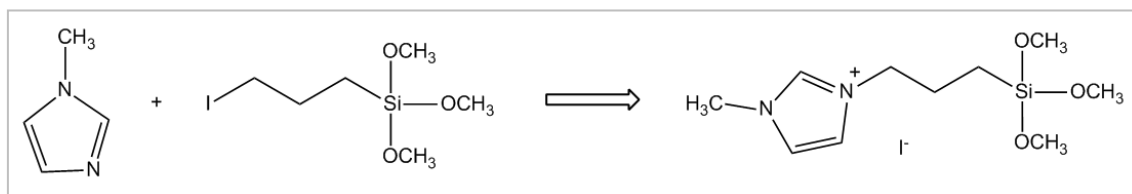


**Fig. 3.5.** - Schematic representation of the synthesis of ionic liquid N-(3-trimethoxysilylpropyl)-3-methylimidazolium iodide using 1-methylimidazole and 3-iodopropyltrimethoxysilane.

The obtained FTIR spectrum of N-(3-trimethoxysilylpropyl)-3-methylimidazolium iodide is overlapped with the spectra of the reactants 1-methylimidazole and 3-iodopropyltrimethoxysilane, represented in the following figure (**Fig. 3.6.**).

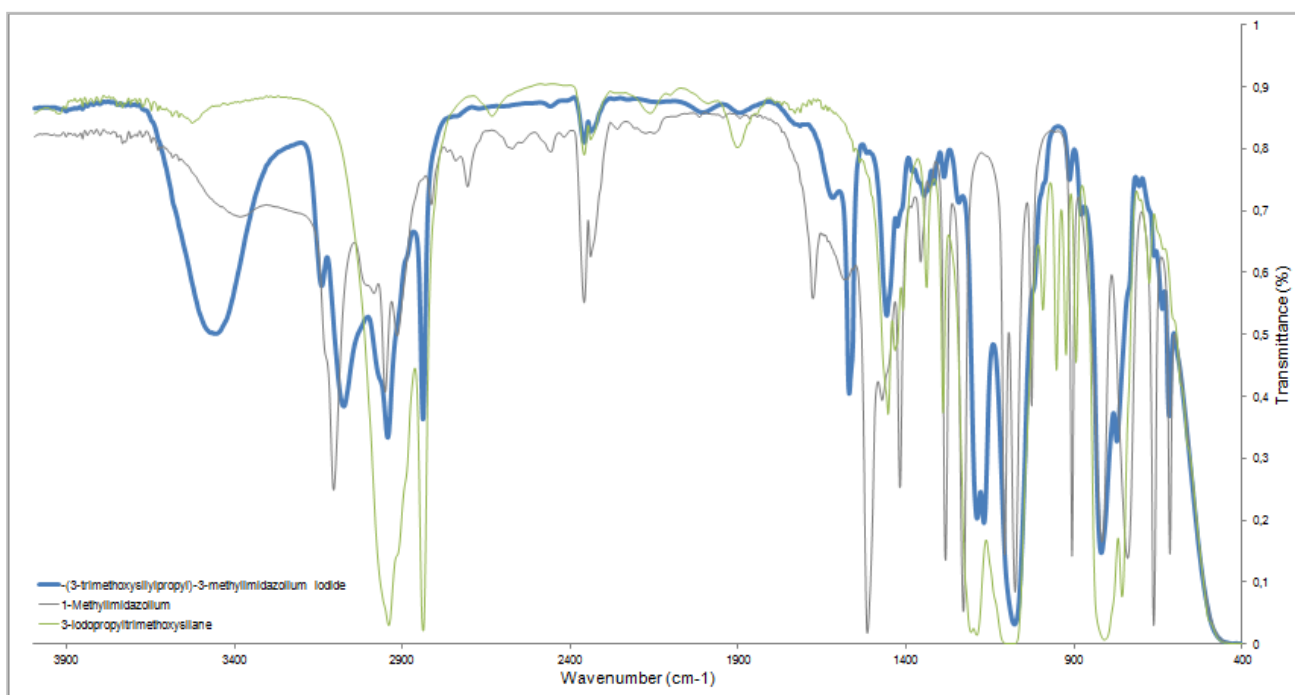


**Fig. 3.6.** - Fourier-Transform Infrared Spectra of N-(3-trimethoxysilylpropyl)-3-methylimidazolium iodide (blue), 1-methylimidazole (grey) and 3-iodopropyltrimethoxysilane (green).

According to *Jovanovski*, the dominant modes of  $-\text{OCH}_3$  groups are shown in 2844, 1194, 1080, 820 and 775  $\text{cm}^{-1}$ . When analyzing the obtained FTIR spectrum, it is possible to observe that the bands 2945, 1188, 1079 and 821 and 775  $\text{cm}^{-1}$  are present

in the final product, as it was expected. Comparing the spectra from the product and the reagents, it is possible to observe that the bands at 2360 and 2356  $\text{cm}^{-1}$  are maintained. The ring modes at 1575 and 1170  $\text{cm}^{-1}$  bands also described by *Jovanovski*, are also part of the product spectrum at 1571 and 1170  $\text{cm}^{-1}$ . According to the experimental work of *Jovanovski*, the cation imidazolium was assigned to the bands at 3140 and 3078  $\text{cm}^{-1}$  and the aliphatic stretching modes appeared at 2976 and 2945  $\text{cm}^{-1}$ . According to the spectrum obtained, 3142, 3076 and 2945  $\text{cm}^{-1}$  are present in the product. Having characteristics bands from both reactants, it is possible to affirm that the desired product was synthesized.

The NMR spectra of the final compound is indicated in **Fig.3.7**.

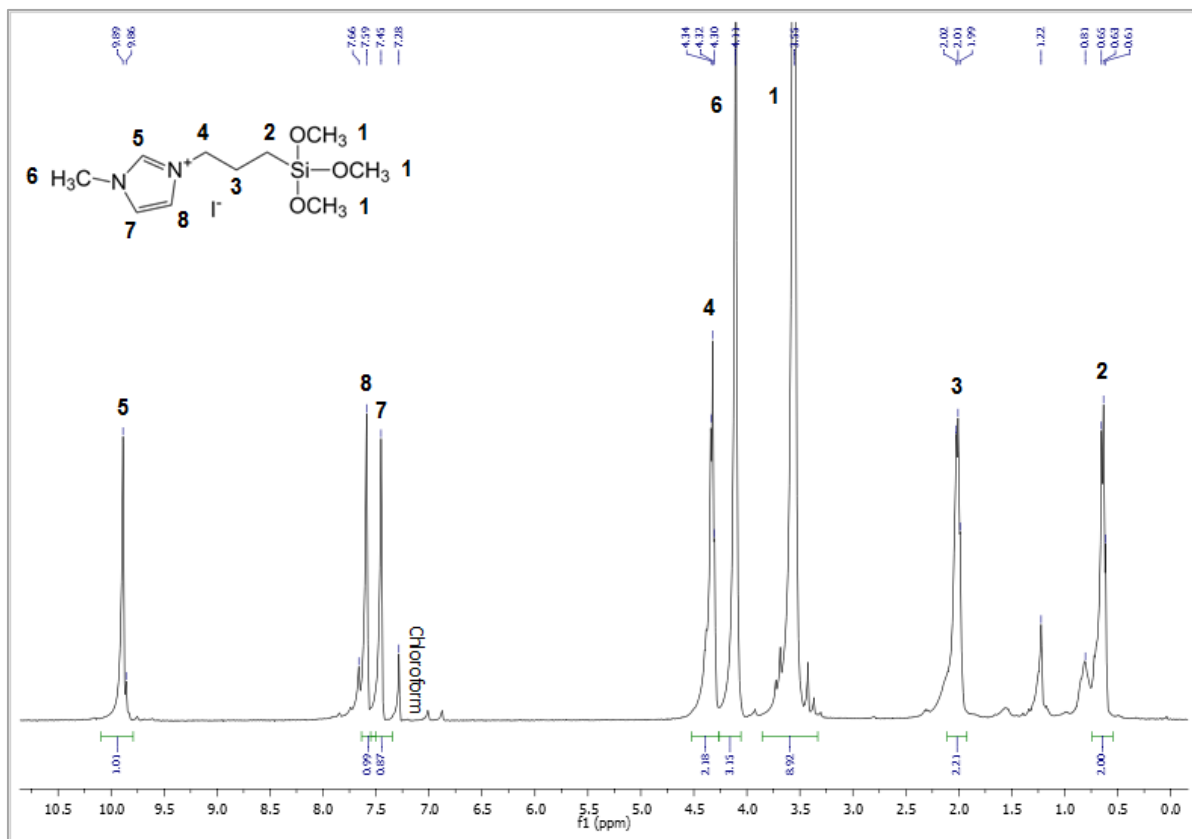


**Fig. 3.7.** - Liquid State  $^1\text{H}$  NMR Spectrum of N-(3-trimethoxysilylpropyl)-3-methylimidazolium iodide, in deuterated chloroform.

Peak **2** corresponds to the protons of the propyl chain. It is represented as an asymmetric triplet, but it proves the proton neighbors. The remaining protons of the propyl chain are represented by numbers **3** and **4**.

The singlet represented by the number **1** corresponds to the nine protons of the methoxy groups, and the singlet from number **6** corresponds to the three protons of the methyl group of the aromatic ring.

The numbers **5**, **7** and **8** represent, respectively, the single protons of the aromatic ring. Even though the numbers **7** and **8** are represented in the spectrum as singlets, they should be represented as duplets because of their neighbor protons.

The peak presented in 7.28 corresponds to the deuterated chloroform used as solvent for the  $^1\text{H}$  NMR analysis. There are also a few extra peaks that don't correspond to the structure of the ionic liquid prepared, which implies that there were still present some impurities or some residues of the reagents used.



### 3.2.1.3. N-(3-trimethoxysilylpropyl)tributylammonium iodide

The synthesis was performed by reflux of tributylamine with 3-iodopropyltrimethoxysilane according to **Fig.3.8.** Contrarily to previous reactions the desired salt based on functionalized ammonium cation was obtained in low yield (49%) according to the reactivity of the tertiary amine.

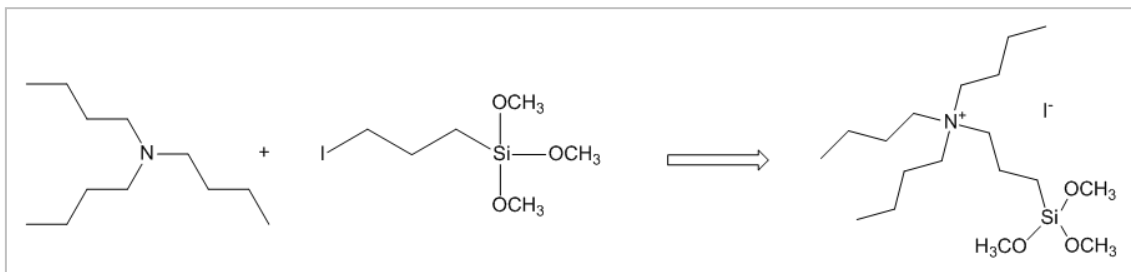


**Fig. 3.8.** - Schematic representation of the synthesis of ionic liquid N-(3-trimethoxysilylpropyl)tributylammonium iodide using tributylamine and 3-iodopropyltrimethoxysilane.

In the following obtained FTIR spectra (**Fig. 3.9.**), ionic liquid N-(3-trimethoxysilylpropyl)tributylammonium iodide is represented in green, and the reagents used, tributylamine and 3-iodopropyltrimethoxysilane, are represented in blue and grey.

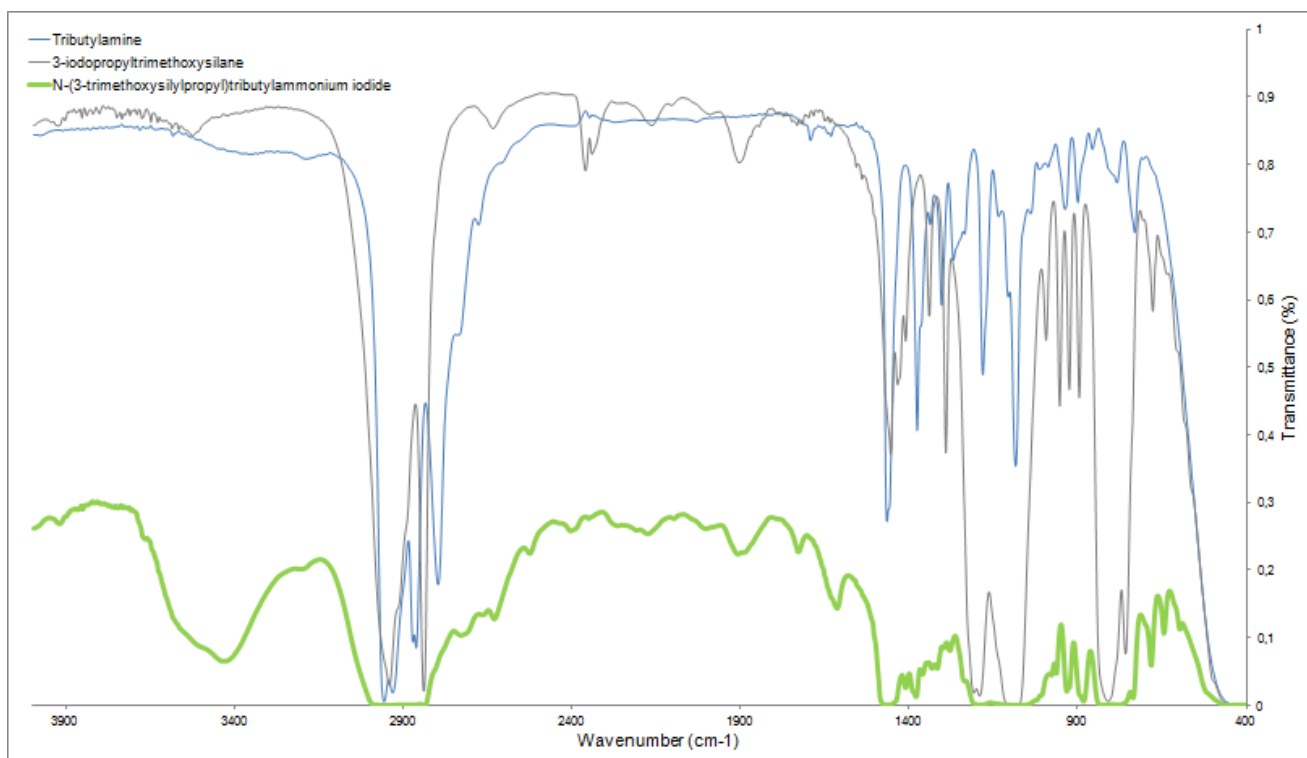


**Fig. 3.9.** - Fourier-Transform Infrared Spectrum of N-(3-trimethoxysilylpropyl)tributylammonium iodide (green), tributylamine (blue) and 3-iodopropyltrimethoxysilane (grey).

Since the product is very concentrated, analyzing the obtained spectrum is difficult. According to *Jovanovski*, the dominant modes of  $-OCH_3$  groups are shown in 2844, 1194, 1080, 820 and 775  $cm^{-1}$ . When analyzing the obtained FTIR spectrum, it is

possible to observe that only the bands 1077 and 823  $\text{cm}^{-1}$  are present in the final product.

$^1\text{H}$  NMR Spectroscopy analysis was performed with deuterated chloroform as solvent. The obtained spectrum is presented in the following figure (**Fig. 3.10**).

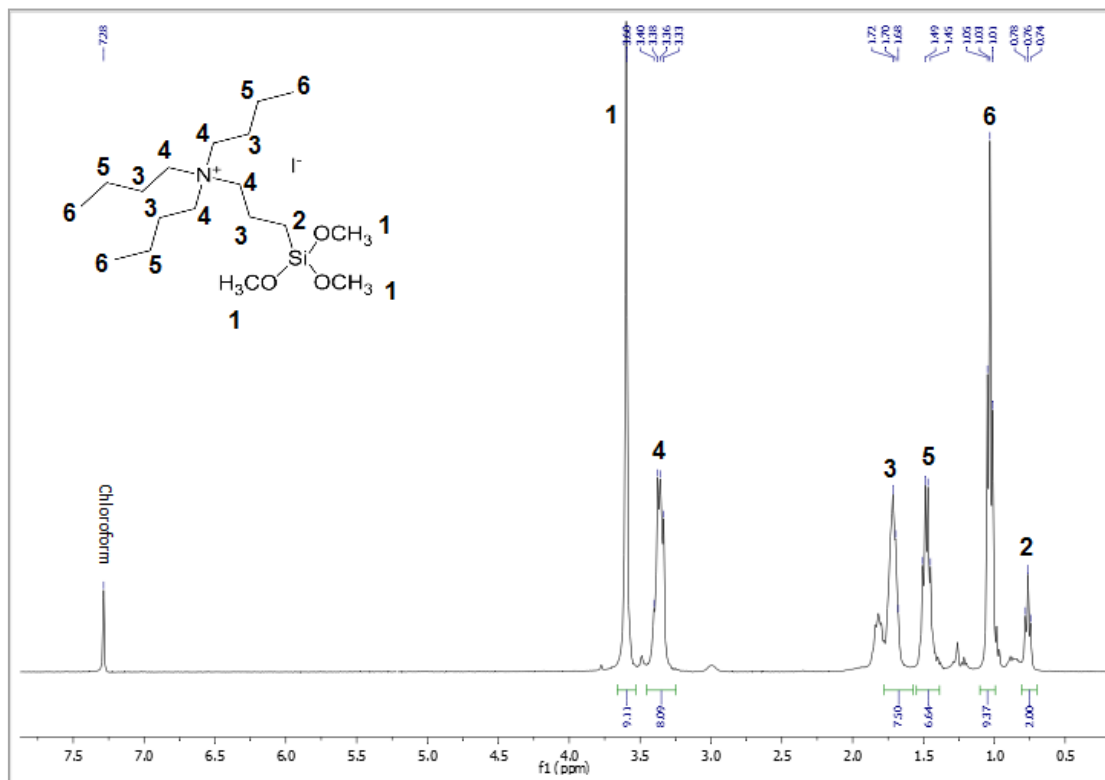


**Fig. 3.10.** - Liquid State  $^1\text{H}$  NMR Spectrum of N N-(3-trimethoxysilylpropyl)tributylammonium iodide, in deuterated chloroform.

Analyzing the obtained spectrum it is possible to confirm the structure of N-(3-trimethoxysilylpropyl)tributylammonium iodide where all protons from organic cations were attributed in the spectra (the numerated peaks correspond to the numbers of the structure presented). From  $^1\text{H}$ -NMR is possible to confirm the chemical structure of the compound as well as to check the relative purity.

### 3.2.1.4. 1-butylpyridinium chloride

This synthesis was performed in 1.4:1 molar ratio, by reflux of 1-chlorobutane and pyridine (**Fig. 3.11**.) following the method described in the literature by *Cho et al*<sup>58</sup>,

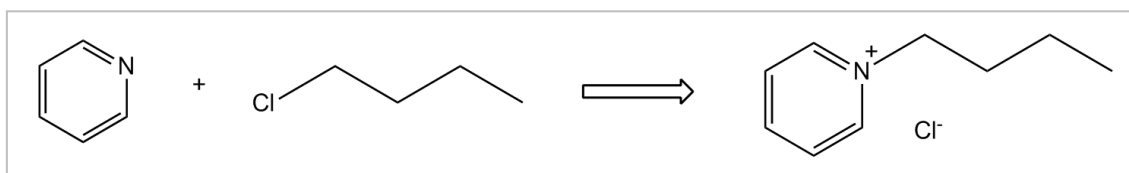


**Fig. 3.11.** - Schematic representation of the synthesis of ionic liquid 1-butylpyridinium chloride using pyridine and 1-chlorobutane.

The desired salt based on functionalized pyridinium cation was obtained in a very low yield (28%) according the reactivity of the ion chloride.

The liquid phase and solid phase of 1-butylpyridinium chloride are represented in dark blue and green, and the reagents used, pyridine and 1-chlorobutane, are represented in grey and light blue in the FTIR spectrum presented (**Fig.3.12.**).

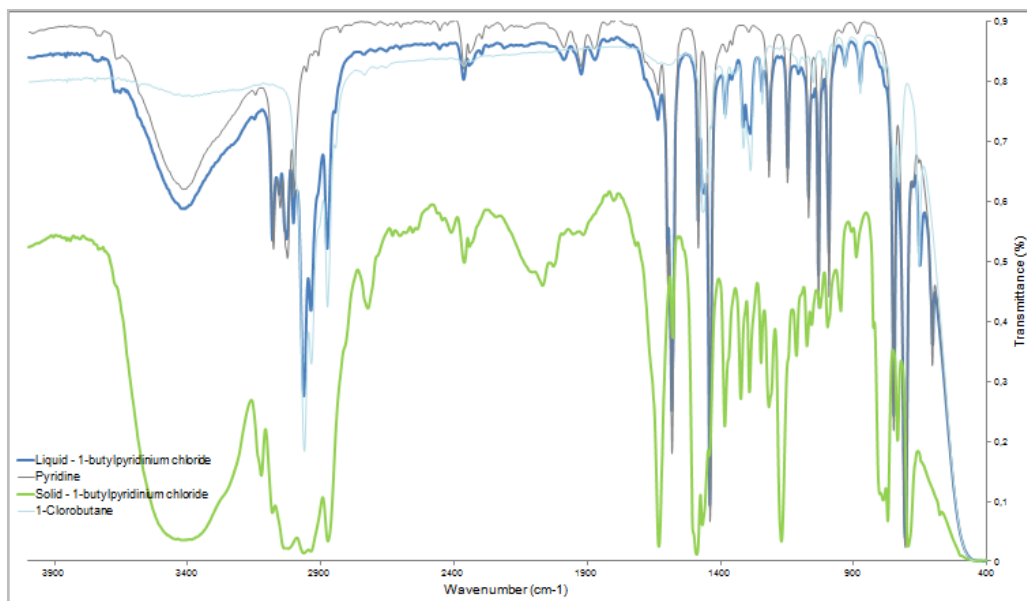


**Fig. 3.12.** - Fourier-Transform Infrared Spectrum of solid 1-butylpyridinium chloride (blue), pyridine (grey), liquid 1-butylpyridinium chloride (green) and 1-chlorobutane (light blue).

By analyzing the spectrum, it is possible to observe that the product has characteristic bands from 1-chlorobutane at 2961, 2934 and 2874  $\text{cm}^{-1}$ . Also, according to *Urbanksi*, the ranges 3250-3000  $\text{cm}^{-1}$  bands correspond to the C—H aromatic bond vibrations of pyridine, and 1650-1400  $\text{cm}^{-1}$  bands correspond to aromatic C—C, C=C and C=N vibrations. These bands are present in the obtain spectrum at 3079, 3025, 3000, 1580, 1482 and 1438  $\text{cm}^{-1}$ .

To prove its molecular structure, a  $^1\text{H}$  NMR Spectroscopy analysis was performed, and the obtained spectrum is presented in the following figure (**Fig. 3.13.**).

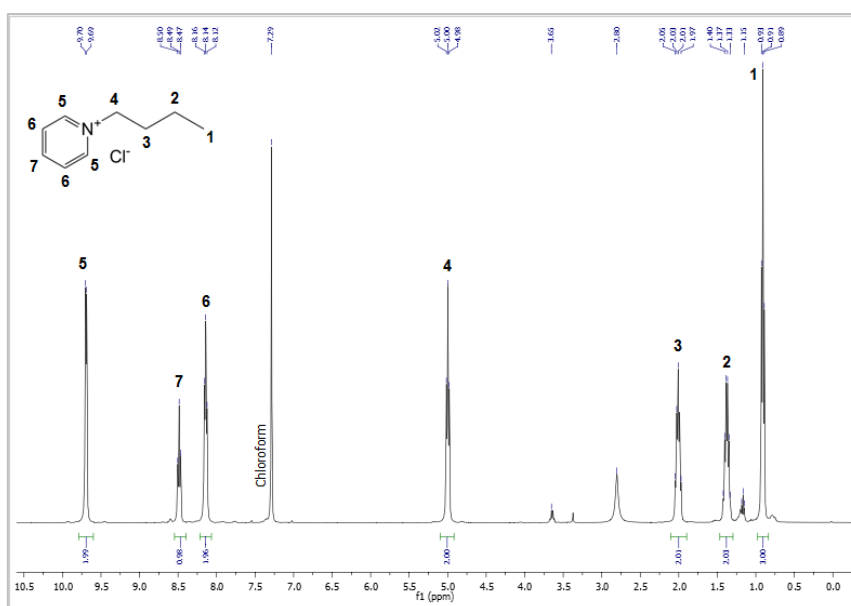


**Fig. 3.13.** - Liquid State  $^1\text{H}$  NMR Spectrum of 1-butylpyridinium chloride, in deuterated chloroform.

The structure of 1-butylpyridinium chloride is represented in the upper left corner. The triplet that appears at 0.93 ppm, represented by peaks at **1**, corresponds to the three protons of the methyl group. Peaks **2**, **3** and **4** correspond, each, to two protons of remaining part the aliphatic butyl chain. Numbers **2** and **3** are represented as quintuplets and number **3** as a triplet in the spectrum, validating the proton neighbors. The aromatic ring peaks arise as duplet at 9.70 ppm corresponding to the protons **5** and as two triplets for protons **6** and **7**, respectively. The peak presented at 7.29 ppm corresponds to the deuterated chloroform used as solvent for the  $^1\text{H}$  NMR analysis. There are also a few extra peaks that don't correspond to the structure of the ionic liquid prepared, which implies that there were still present some impurities or some residues of the reagents used. This way, with the  $^1\text{H}$  NMR analysis, it is possible to confirm that the expected product was form, with the right structure.

### 3.2.2. Preparation and characterization of POM-IL catalysts

The three Homogeneous catalysts prepared are constituted by cations ammonium ( $[N_{4,4,4,4}]$ ), pyridinium ( $[C_4Py]$ ) and imidazolium ( $[C_4MIM]$ ) with phosphomolybdate  $[PMo_{12}O_{40}]^{3-}$  as anion (**Fig. 3.14.**)

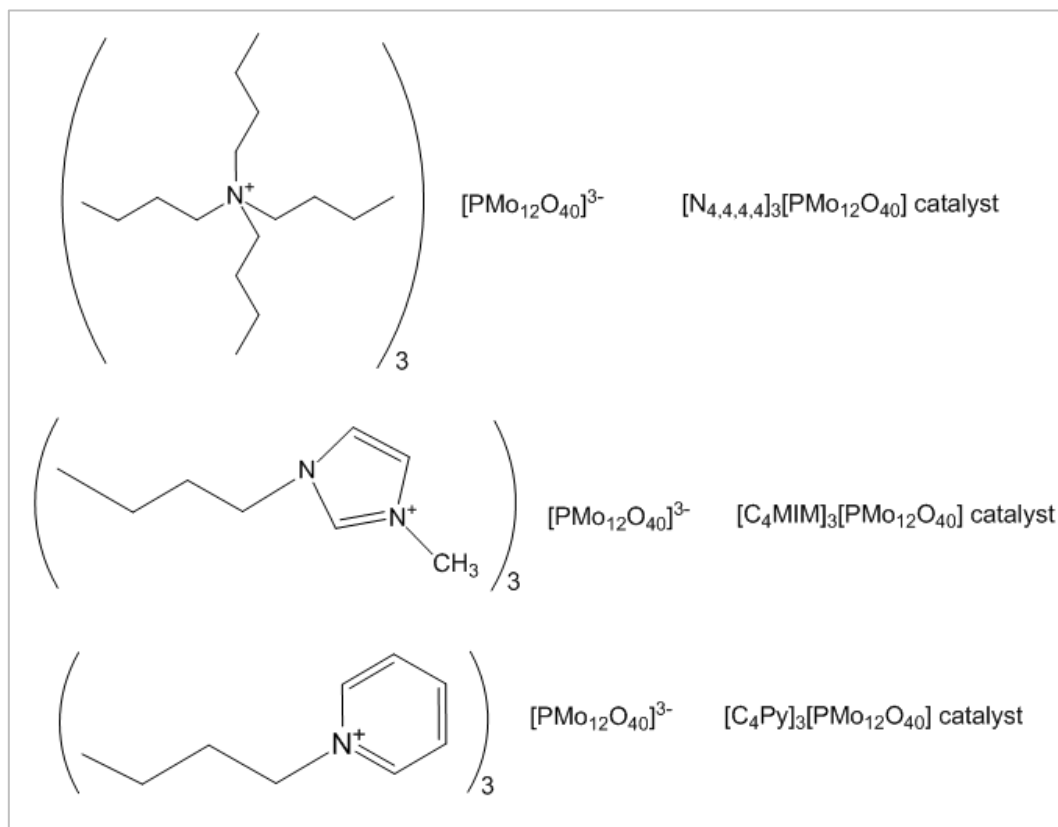


**Fig. 3.14.** - Chemical structures of the prepared Homogeneous Catalysts,  $[N_{4,4,4,4}]_3[PMo_{12}O_{40}]$ ,  $[C_4MIM]_3[PMo_{12}O_{40}]$  and  $[C_4Py]_3[PMo_{12}O_{40}]$ .

The catalysts were then characterized by Elemental Analysis (EA), Fourier-Transform Infrared Spectroscopy (FTIR) and Solution  $^1H$  NMR and  $^{31}P$  NMR Spectroscopy.

#### 3.2.2.1. $[N_{4,4,4,4}]_3[PMo_{12}O_{40}]$ catalyst

The synthesis of catalyst  $[N_{4,4,4,4}]_3[PMo_{12}O_{40}]$  was performed by changing the bromide anion,  $Br^-$ , from tetrabutylammonium bromide,  $[N_{4,4,4,4}][Br]$  to the final anion, phosphomolybdate  $[PMo_{12}O_{40}]^{3-}$  (**Fig.3.15.**).

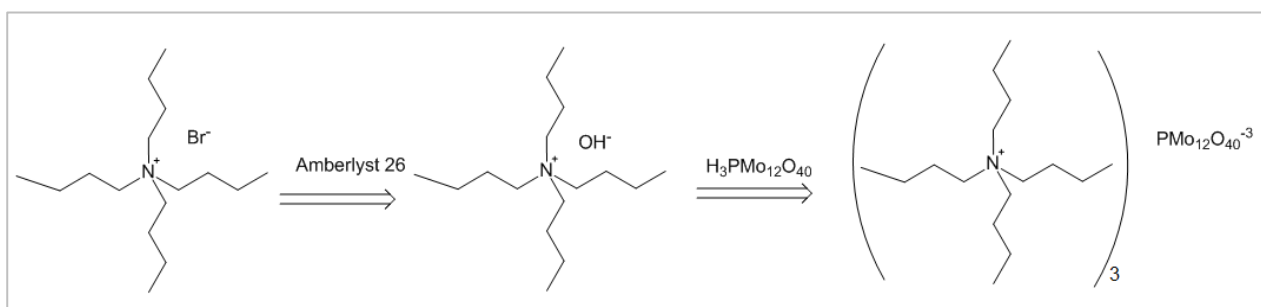


**Fig. 3.15.** - Schematic representation of ion exchange from  $[N_{4,4,4,4}][Br]$  to  $[N_{4,4,4,4}]_3[PMo_{12}O_{40}]$ , using ion exchange resin Amberlyst® A26 ( $OH^-$ ) and polyoxometalate  $H_3PMo_{12}O_{40}$ .

The product was characterized by Elemental Analysis, Fourier-Transform Infrared (FTIR) and  $^1\text{H}$  NMR and  $^{31}\text{P}$  NMR Spectroscopies. In **Table 3.2.** are shown the calculated values of C, H and N for each possible structure. Elemental analysis allowed to conclude that the salt with the molecular structure  $[\text{N}_{4,4,4,4}]_3[\text{PMo}_{12}\text{O}_{40}]$  was formed.

**Table 3.2.** - Elemental Analysis calculated and determined results (C, N and H) for  $[\text{N}_{4,4,4,4}]_3[\text{PMo}_{12}\text{O}_{40}]$  catalyst.

	C (%)		N (%)		H (%)	
	Calc.	Exp.	Calc.	Exp.	Calc.	Exp.
$[\text{N}_{4,4,4,4}][\text{H}_2\text{PMo}_{12}\text{O}_{40}]$	9.21	23.18	0.67	1.65	1.82	4.39
$[\text{N}_{4,4,4,4}]_2[\text{HPMo}_{12}\text{O}_{40}]$	16.39		1.20		3.11	
$[\text{N}_{4,4,4,4}]_3[\text{PMo}_{12}\text{O}_{40}]$	22.14		1.61		4.15	

The FTIR spectra of the catalyst  $[\text{N}_{4,4,4,4}]_3[\text{PMo}_{12}\text{O}_{40}]$  and reagents tetrabutylammonium  $[\text{N}_{4,4,4,4}][\text{Br}]$  and polyoxometalate  $\text{H}_3\text{PMo}_{12}\text{O}_{40}$  are represented respectively in blue, green and grey in figure **Fig. 3.16.**

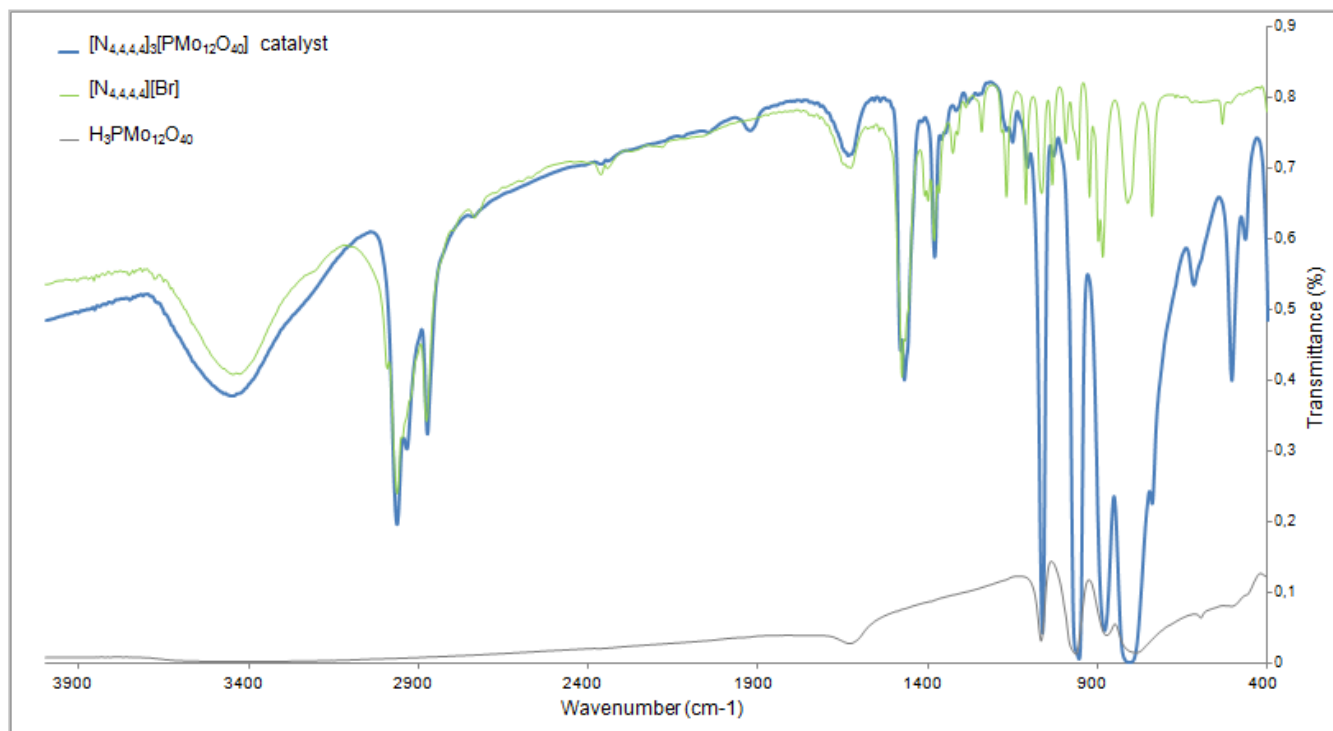


**Fig. 3.16.** - Fourier-Transform Infrared Spectra of catalyst  $[\text{N}_{4,4,4,4}]_3[\text{PMo}_{12}\text{O}_{40}]$  (blue),  $[\text{N}_{4,4,4,4}][\text{Br}]$  (green) and polyoxometalate  $\text{H}_3\text{PMo}_{12}\text{O}_{40}$  (grey).

The characteristic bands from  $\text{H}_3\text{PMo}_{12}\text{O}_{40}$  are from 1014, 976, 890 and 790  $\text{cm}^{-1}$ , that can be observed in 1030, 954, 880 and 740  $\text{cm}^{-1}$ .

The  $^1\text{H}$  NMR spectrum of  $[\text{C}_4\text{MIM}]_3[\text{PMo}_{12}\text{O}_{40}]$  is shown in **Fig 3.17.**

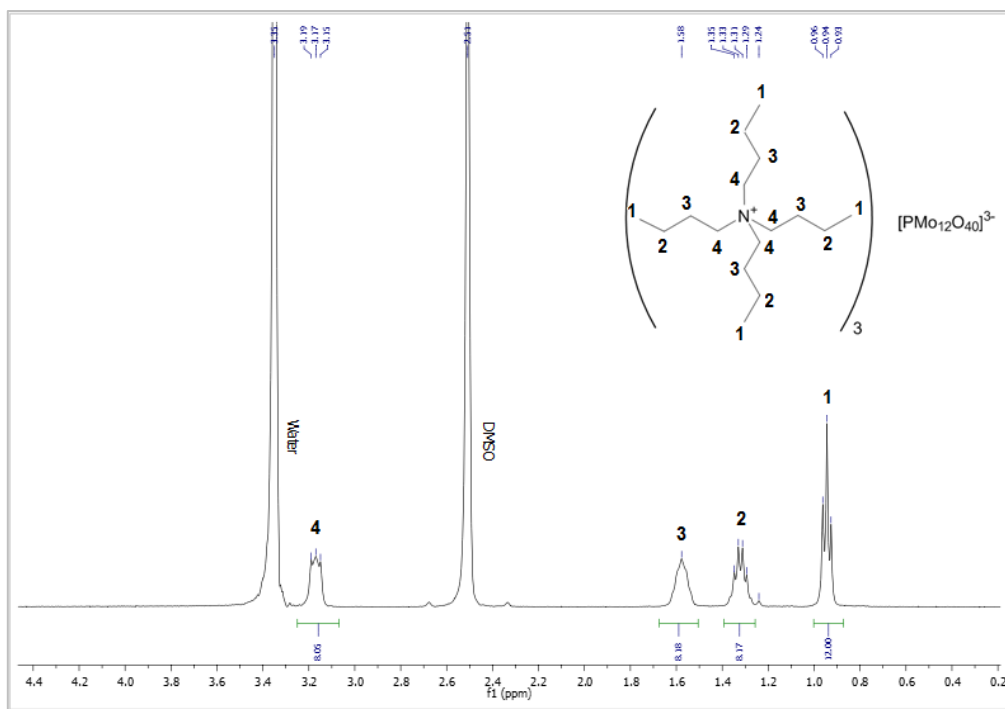


**Fig. 3.17.** - Solution  $^1\text{H}$  NMR Spectrum of  $[\text{N}_{4,4,4,4}]_3[\text{PMo}_{12}\text{O}_{40}]$ , in DMSO-d<sub>6</sub>.

With the obtained spectrum, it is possible to observe that the triplet at 0.96 ppm, represented by number 1, corresponds to the twelve protons of the  $\text{CH}_3$  terminations of the cation  $[\text{N}_{4,4,4,4}]^+$ . Even though numbers 2 and 3 represent correctly eight protons of the two  $\text{CH}_2$  in the middle of the chain, they should be represented respectively as sextuplet and as a quintuplet. The triplet represented at 3.19 ppm of the spectrum by number 4 corresponds to the eight protons closer to the nitrogen atom. It is possible to conclude that the chemical structure obtained is the expected.

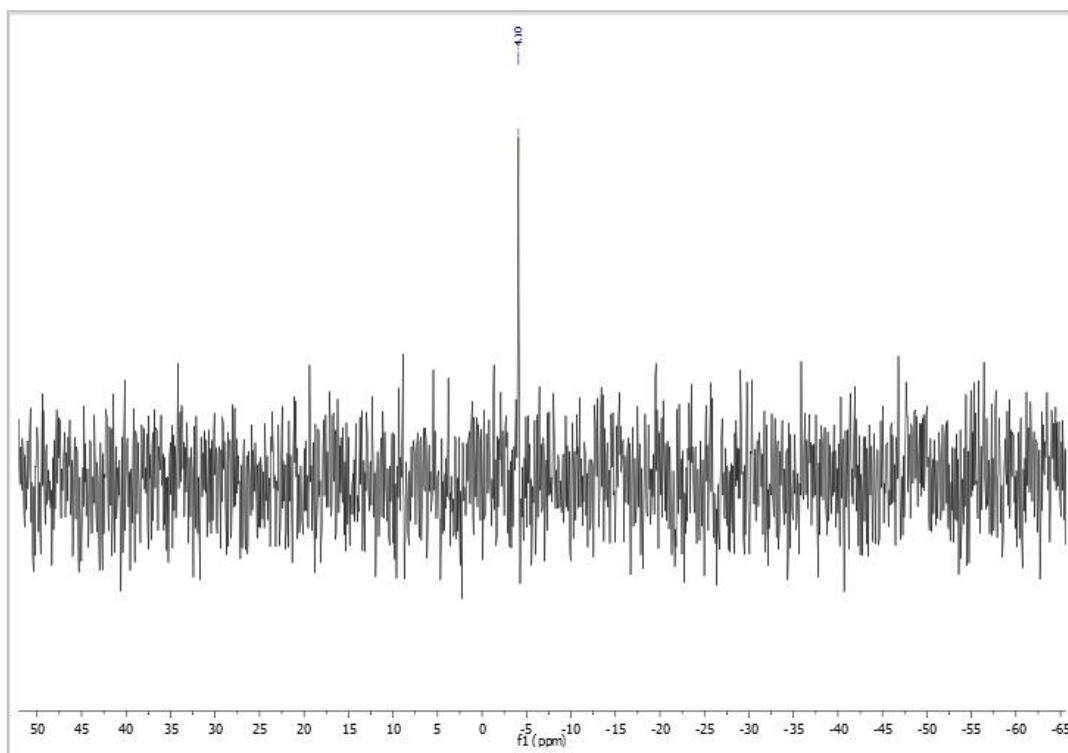


**Fig. 3.18.** - Solution  $^{31}\text{P}$  NMR Spectrum of  $[\text{N}_{4,4,4,4}]_3[\text{PMo}_{12}\text{O}_{40}]$ , in DMSO-d<sub>6</sub>.

The  $^{31}\text{P}$  NMR spectroscopy is very common used to characterize phosphopolyoxometalates and it has been shown that the chemical shift of  $^{31}\text{P}$  in the anion is highly sensitive to structural changes. The spectrum of the catalyst  $[\text{N}_{4,4,4,4}]_3[\text{PMo}_{12}\text{O}_{40}]$  contains a peak at -4.10 ppm which is in agreement with the values reported in literature for the same solvent.<sup>58</sup> (**Fig. 3.18**).

### 3.2.2.2. $[\text{C}_4\text{MIM}]_3[\text{PMo}_{12}\text{O}_{40}]$ catalyst

The synthesis of catalyst  $[\text{C}_4\text{MIM}]_3[\text{PMo}_{12}\text{O}_{40}]$  was performed by exchanging the chloride anion,  $\text{Cl}^-$ , from 1-butyl-3-methylimidazolium chloride,  $[\text{C}_4\text{MIM}][\text{Cl}]$ , to the final anion, phosphomolybdate  $[\text{PMo}_{12}\text{O}_{40}]^{3-}$  (**Fig.3.19**).

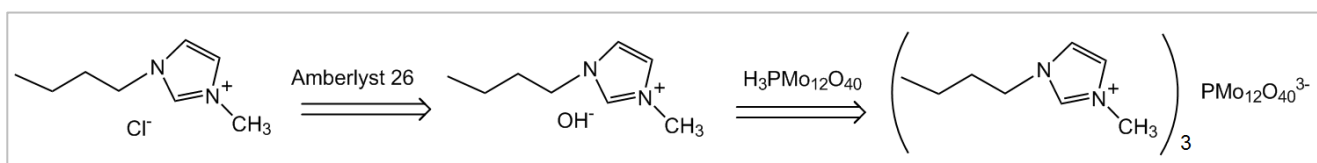


**Fig. 3.19.** - Schematic representation of ion exchange from  $[\text{C}_4\text{MIM}][\text{Cl}]$  to  $[\text{C}_4\text{MIM}]_3[\text{PMo}_{12}\text{O}_{40}]$ , using ion exchange resin Amberlyst® A26 ( $\text{OH}^-$ ) and polyoxometalate  $\text{H}_3\text{PMo}_{12}\text{O}_{40}$ .

The product obtained was characterized by elemental analysis, FTIR,  $^1\text{H}$  and  $^{31}\text{P}$  NMR spectroscopies. In **Table 3.3**, the calculated values of C, H and N for different structures that could be formed and the experimental values obtained by elemental analysis are shown. With the first look at the table, it is possible to see that the closest results to the experimental value are the values obtained for the structure  $[\text{C}_4\text{MIM}]_3[\text{PMo}_{12}\text{O}_{40}]$ .

**Table 3.3.** - Elemental Analysis calculated and determined results (C, N and H) for  $[\text{C}_4\text{MIM}]_3[\text{PMo}_{12}\text{O}_{40}]$  catalyst.

	C (%)		N (%)		H (%)	
	Calc.	Exp.	Calc.	Exp.	Calc.	Exp.
$[\text{C}_4\text{MIM}][\text{H}_2\text{PMo}_{12}\text{O}_{40}]$	4.89	13.20	1.43	3.72	0.87	1.99
$[\text{C}_4\text{MIM}]_2[\text{HPMo}_{12}\text{O}_{40}]$	9.14		2.66		1.48	
$[\text{C}_4\text{MIM}]_3[\text{PMo}_{12}\text{O}_{40}]$	12.86		3.75		2.00	

The infrared spectra of the reactants  $[\text{C}_4\text{MIM}][\text{Cl}]$  and  $\text{H}_3\text{PMo}_{12}\text{O}_{40}$ , and the synthesized catalyst  $[\text{C}_4\text{MIM}]_3[\text{PMo}_{12}\text{O}_{40}]$  are represented respectively in blue, green and grey in **Fig. 3.20**.



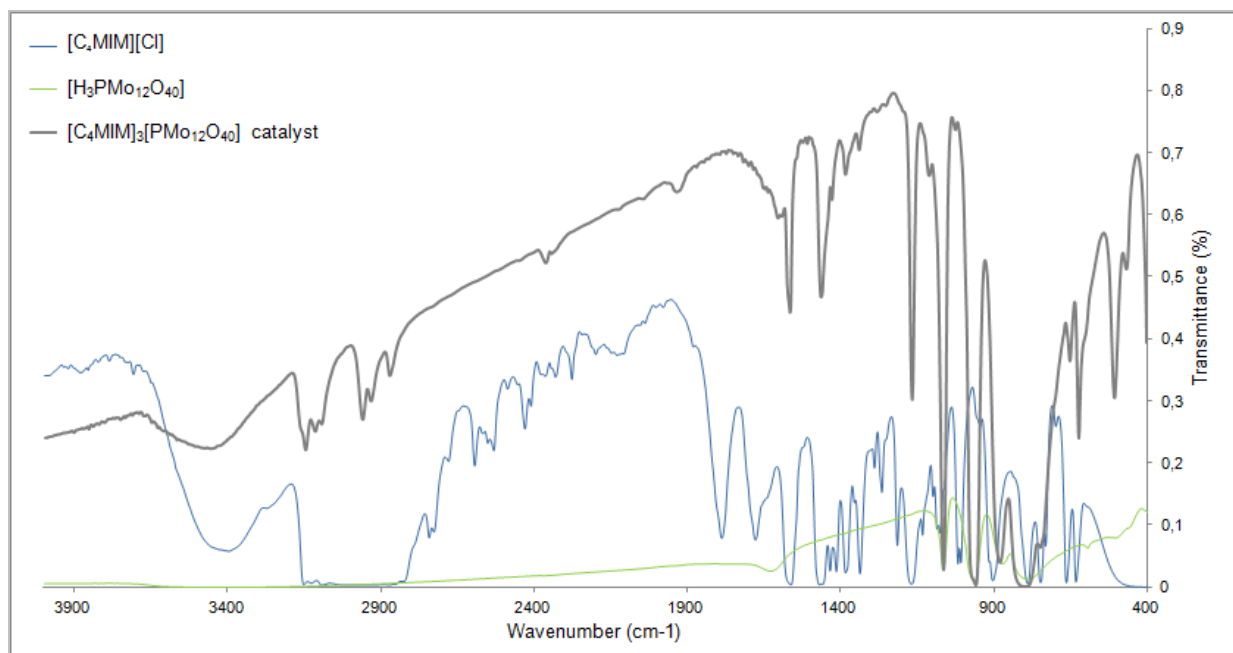


**Fig. 3.20.** - Fourier-Transform Infrared Spectra of  $[C_4MIM][Cl]$  (blue), polyoxometalate  $H_3PMo_{12}O_{40}$  (green) and catalyst  $[C_4MIM]_3[PMo_{12}O_{40}]$  (grey).

The characteristic bands from  $H_3PMo_{12}O_{40}$  are from 1014, 976, 890 and 790  $cm^{-1}$ , that can be observed in 1020, 956, 878 and 796  $cm^{-1}$ .

The  $^1H$  NMR spectrum of  $[C_4MIM]_3[PMo_{12}O_{40}]$  is shown in **Fig 3.21**.

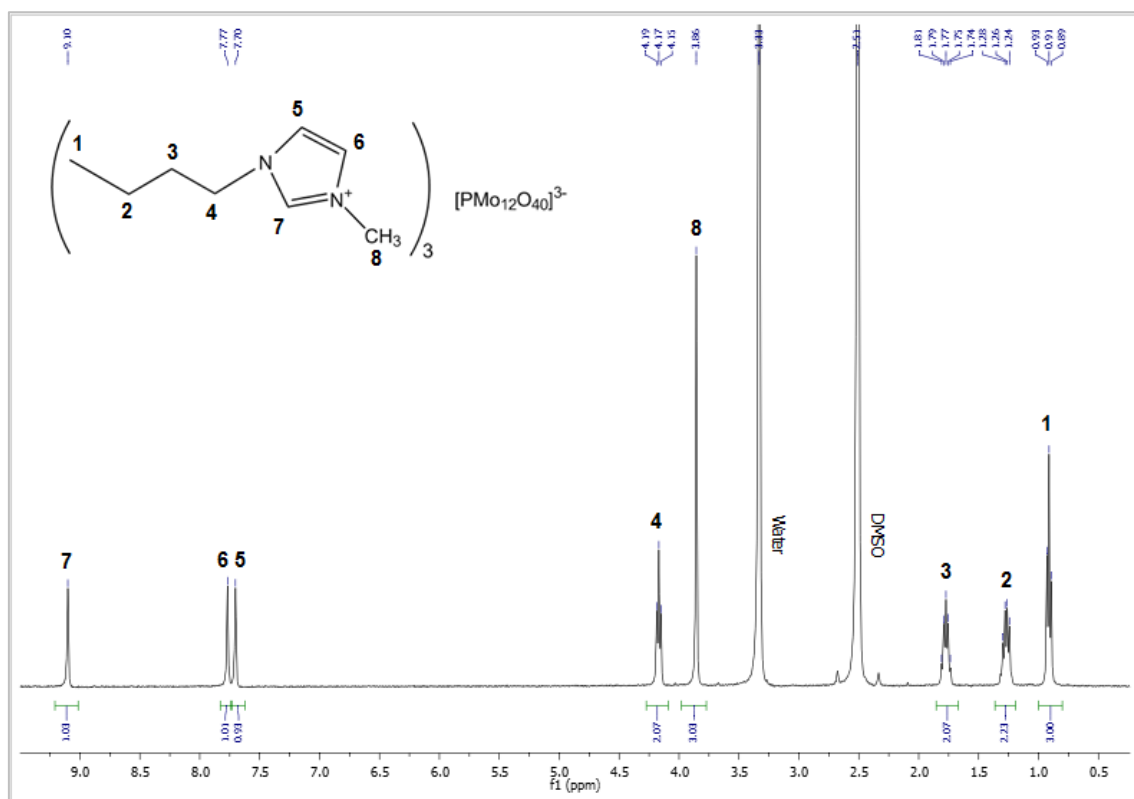


**Fig. 3.21.** - Solution  $^1H$  NMR Spectrum of  $[C_4MIM]_3[PMo_{12}O_{40}]$ , in  $DMSO-d_6$ .

The triplet of number 1 represent the  $CH_3$  termination of the aliphatic chain, and numbers 2, 3 and 4, represent the remaining eight protons. Numbers 5 and 6 represent

the two atoms of the aromatic ring with the proton of number 7. The singlet represented in number 8 corresponds to the methyl in the aromatic ring, with a total of three protons. In conclusion, the chemical structure of  $[C_4MIM]_3[PMo_{12}O_{40}]$  is proven.

The following  $^{31}P$  NMR spectrum was obtained using DMSO-d6 as deuterated solvent (**Fig. 3.22.**).

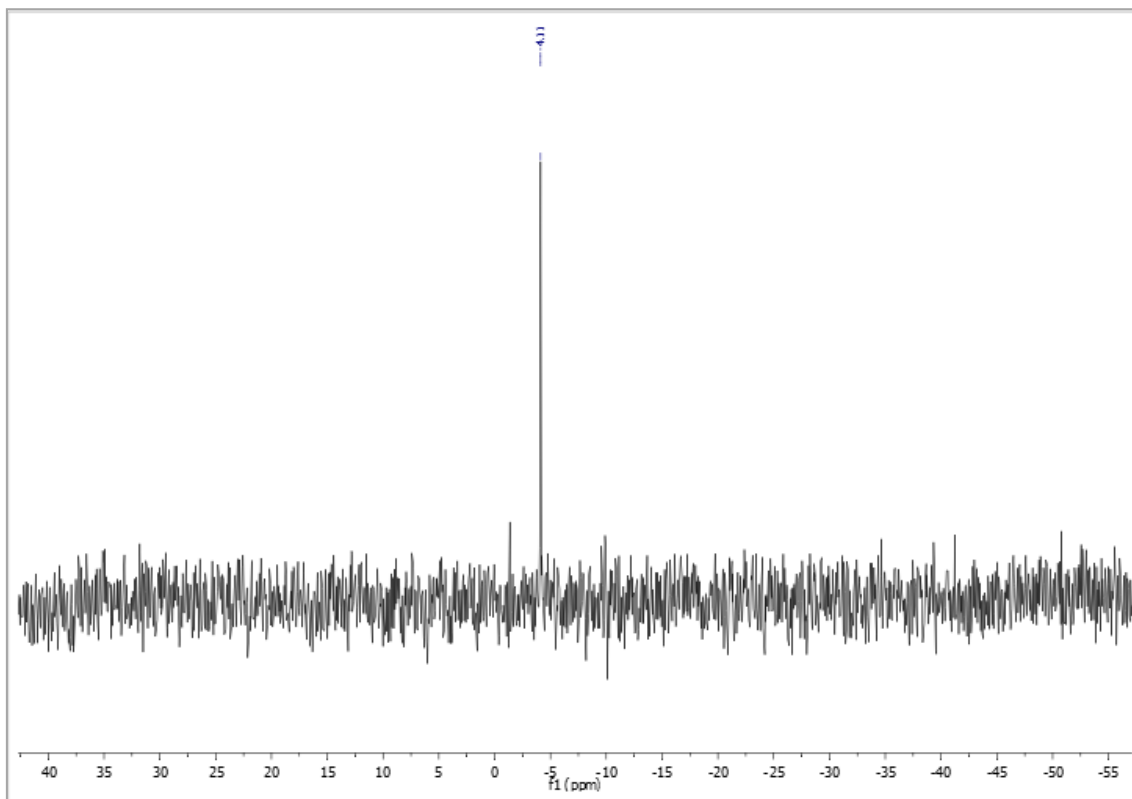


**Fig. 3.22.** - Solution  $^{31}P$  NMR Spectrum of  $[C_4MIM]_3[PMo_{12}O_{40}]$ , in DMSO-d6.

The  $^{31}P$  NMR spectrum obtained of  $[C_4MIM]_3[PMo_{12}O_{40}]$  catalyst proves the presence of phosphorus at 4.11 ppm in the product obtained. The obtained spectrum is similar to the previous catalyst prepared, the chemical drift is probably due to the effect of the counter-ion in the structure. This is a good sign in proving the expected chemical structure, showing that there was a reaction with the polyoxometalate used.

### 3.2.2.3. $[C_4Py]_3[PMo_{12}O_{40}]$ catalyst

The synthesis of catalyst  $[C_4Py]_3[PMo_{12}O_{40}]$  was performed by exchanging the chloride anion,  $Cl^-$ , from 1-butylpyridinium chloride,  $[C_4Py][Cl]$ , to the final anion, phosphomolybdate  $[PMo_{12}O_{40}]^{3-}$  (**Fig.3.23.**).

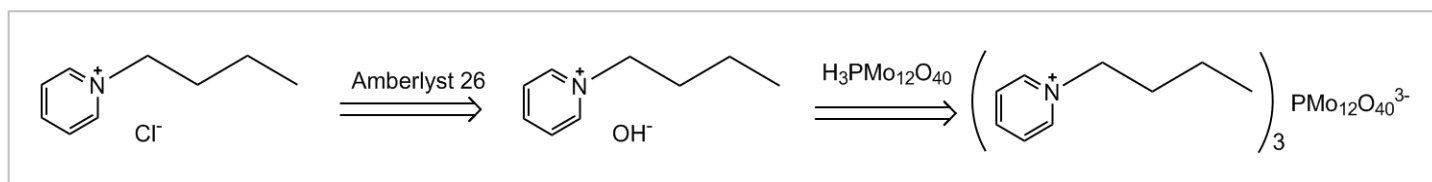


**Fig. 3.23.** - Schematic representation of ion exchange from  $[C_4Py][Cl]$  to  $[C_4Py]_3[PMo_{12}O_{40}]$ , using ion exchange resin Amberlyst® A26 ( $OH^-$ ) and polyoxometalate  $H_3PMo_{12}O_{40}$ .

The product obtained was characterized by elemental analysis, FTIR,  $^1\text{H}$  and  $^{31}\text{P}$  NMR spectroscopies. In **Table 3.4** the calculated values of C, H and N for different structures that could be formed and the experimental values obtained by elemental analysis are shown. With the first look at the table, it is possible to see that the closest results to the experimental value are the values obtained for the structure  $[\text{C}_4\text{Py}]_3[\text{PMo}_{12}\text{O}_{40}]$ .

**Table 3.4.** - Elemental Analysis calculated and determined results (C, N and H) for  $[\text{C}_4\text{Py}]_3[\text{PMo}_{12}\text{O}_{40}]$  catalyst.

	C (%)		N (%)		H (%)	
	Calc.	Exp.	Calc.	Exp.	Calc.	Exp.
$[\text{C}_4\text{Py}][\text{H}_2\text{PMo}_{12}\text{O}_{40}]$	5.39	15.04	0.70	1.88	0.80	1.87
$[\text{C}_4\text{Py}]_2[\text{HPMo}_{12}\text{O}_{40}]$	9.88		1.28		1.33	
$[\text{C}_4\text{Py}]_3[\text{PMo}_{12}\text{O}_{40}]$	13.70		1.78		1.78	

With the first look at the table, it is possible to see that the closest results to the experimental value are the values obtained for the structure  $[\text{C}_4\text{Py}]_3[\text{PMo}_{12}\text{O}_{40}]$ .

FTIR spectra of the reactants 1-butylpyridinium chloride  $[\text{C}_4\text{Py}][\text{Cl}]$  and polyoxometalate  $\text{H}_3\text{PMo}_{12}\text{O}_{40}$ , and the synthesized catalyst  $[\text{C}_4\text{Py}]_3[\text{PMo}_{12}\text{O}_{40}]$  (represented respectively in blue, green and grey) in represented in **Fig. 3.24**.

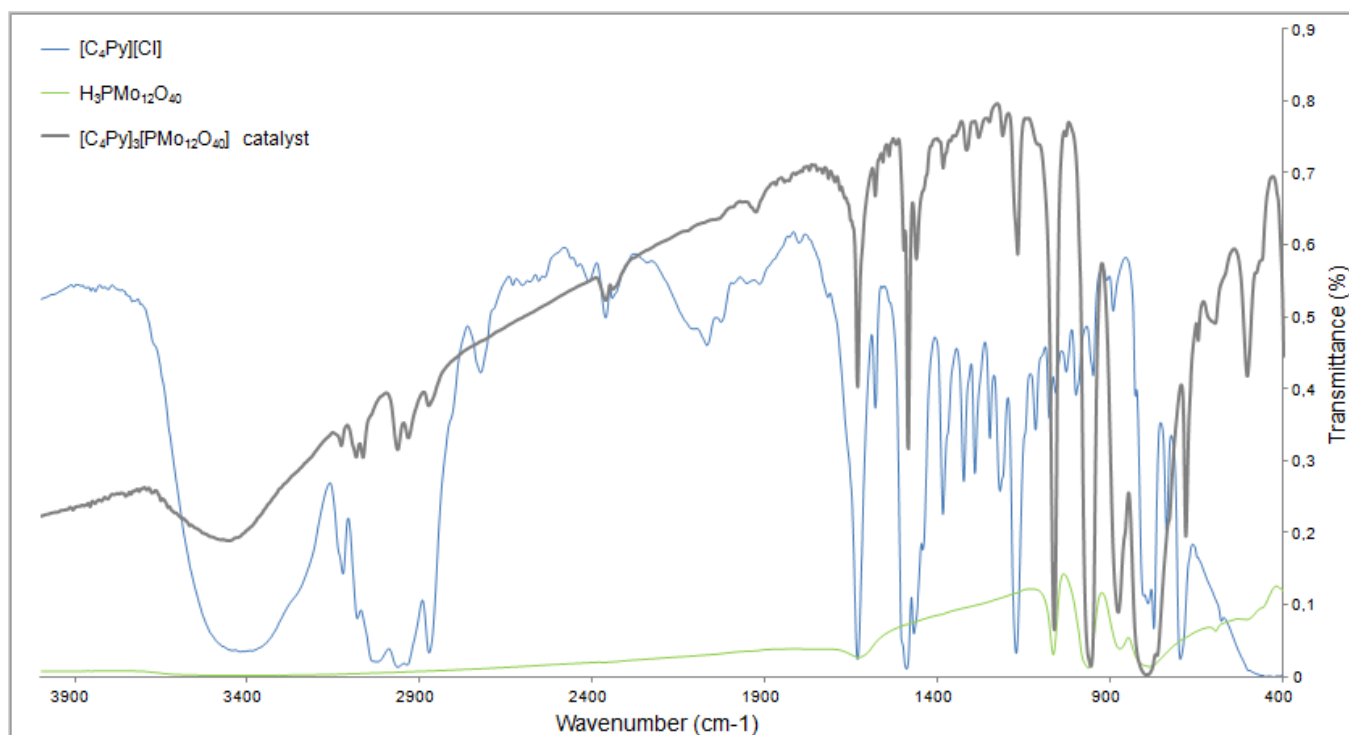


**Fig. 3.24.** - Fourier-Transform Infrared Spectra of 1-butylpyridinium chloride  $[\text{C}_4\text{Py}][\text{Cl}]$  (blue), polyoxometalate  $\text{H}_3\text{PMo}_{12}\text{O}_{40}$  (green) and catalyst  $[\text{C}_4\text{Py}]_3[\text{PMo}_{12}\text{O}_{40}]$  (grey).

The characteristic bands from  $\text{H}_3\text{PMo}_{12}\text{O}_{40}$  are from 1014, 976, 890 and 790  $\text{cm}^{-1}$ , that can be observed in 1063, 956, 878 and 795  $\text{cm}^{-1}$ .

$^1\text{H}$  NMR spectrum of catalyst  $[\text{C}_4\text{Py}]_3[\text{PMo}_{12}\text{O}_{40}]$  is presented in **Fig. 3.25**.

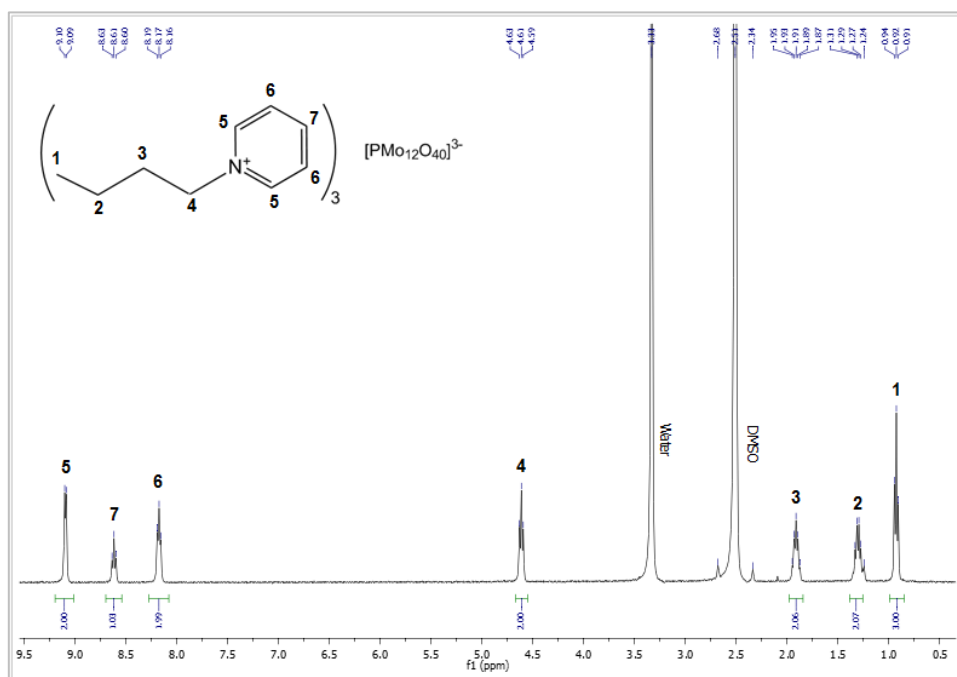


**Fig. 3.25.** - Solution  $^1\text{H}$  NMR Spectrum of  $[\text{C}_4\text{Py}]_3[\text{PMo}_{12}\text{O}_{40}]$ , in  $\text{DMSO-d}_6$ .

The triplet at 0.94 ppm, represented by number 1, represents the three protons of the end of the  $\text{CH}_3$  aliphatic chain. Numbers 2 (quintuplet at 1.31 ppm), 3 (quintuplet at 1.95 ppm) and 4 (triplet at 4.63 ppm) represent the two protons present in each carbon atom of the aliphatic chain. On the left side of the spectrum, numbers 5, 6 and 7, represent the protons of the aromatic ring. The duplet of number 5 represents the two protons closer to nitrogen at 9.10 ppm, and the triplets of number 6 (at 8.19 ppm) and 7 (at 8.63 ppm) represent, respectively, the two middle protons and the further single proton. In conclusion, it is possible to confirm that the chemical structure obtained with the synthesis process expected is correct.

The following  $^{31}\text{P}$  NMR spectrum was obtained using  $\text{DMSO-d}_6$  as deuterated solvent (**Fig. 3.26**).

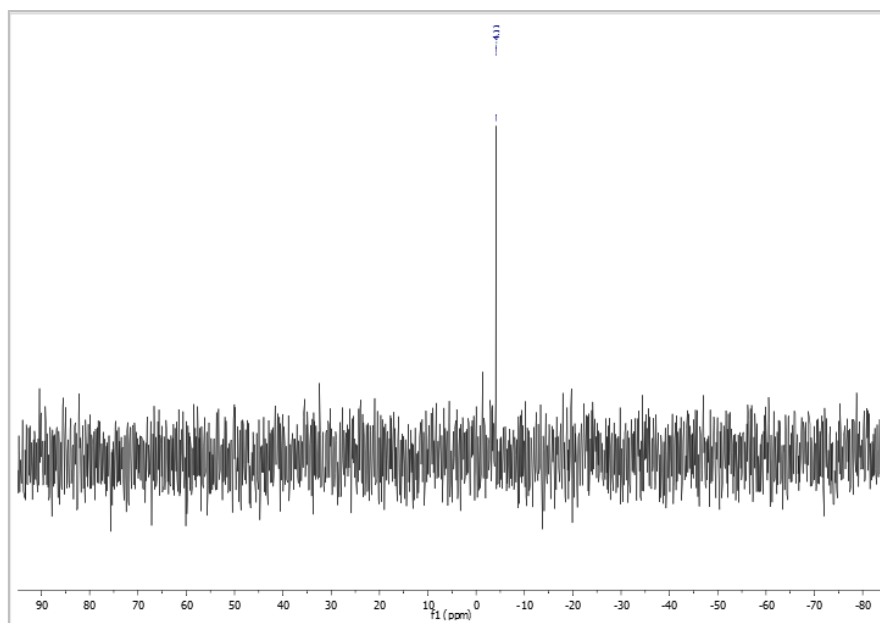


**Fig. 3.26.** - Solution  $^{31}\text{P}$  NMR Spectrum of  $[\text{C}_4\text{Py}]_3[\text{PMo}_{12}\text{O}_{40}]$ , in DMSO- $d_6$ .

The  $^{31}\text{P}$  NMR spectrum obtained of  $[\text{C}_4\text{Py}]_3[\text{PMo}_{12}\text{O}_{40}]$  catalyst proves the presence of phosphorus at peak -4.11 ppm in the product obtained. It is a good sign, since the obtained spectrum is similar to the previous spectrums presented of the other two catalysts. As it was already mentioned before, the chemical drift from the first one is probably due to the effect of the counter-ion in the structure.

### 3.3. Preparation and characterization of MSNPs and MSNPs-POM-IL catalysts

#### 3.3.1. Preparation and characterization of Mesoporous Silica Nanoparticles (MSNPs)

Mesoporous silica nanoparticles of the type MCM-48 were synthesized following a method described in the literature by Bouchoucha et al.<sup>58</sup>, that uses a mixture of two surfactants, Pluronic F127 and Hexadecyltrimethylammonium bromide (CTAB), and triethanolamine to control the particle size. After the reaction of formation of MSNPs, the colloidal solution obtained was centrifuged and washed several times with water and the powder obtained was dried in an oven. To remove the surfactants and triethanolamine from the pores, the material was calcinated. The experimental procedure followed in this work<sup>61</sup> reported a size distribution of 45 nm.

Mesoporous Silica Nanoparticles were characterized by Dynamic Light Scattering (DLS), Fourier-Transform Infrared Spectroscopy (FTIR) and Transmission Electron Microscopy (TEM).

After analyzing the results from the DLS study (**Fig. 3.27**), it is possible to observe that, after three measurements, the experimental size obtained was in the range 90-110 nm

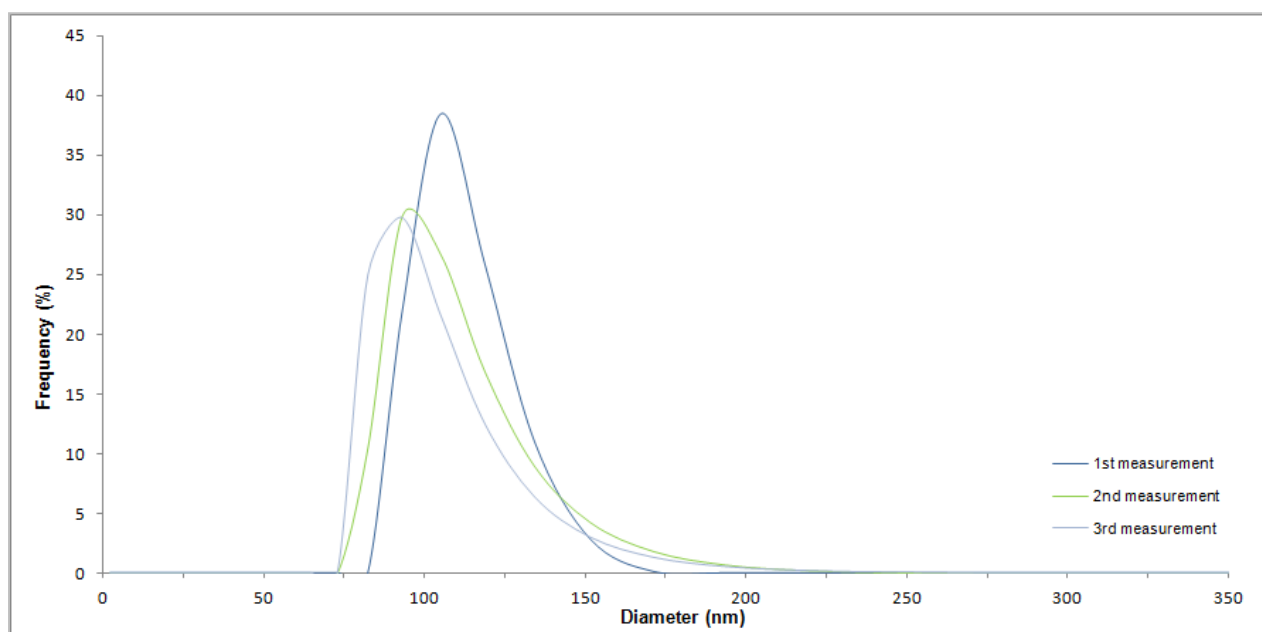


**Fig. 3.27** - DLS analysis of the Mesoporous Silica Nanoparticles size distribution with three measurements.

The discrepancy in these values can be justified by the existence of nanoparticle aggregates in the samples during the analysis.

Transmission Electron Microscopy images were obtained at resolutions of 500 nm, 200 nm and 100 nm using water as solvent. In **Fig. 3.28**, it is possible to observe that the nanoparticle sizes obtained are approximately between 80 nm to 100 nm (supporting the DLS results), having small variations in size. It is also possible to observe the pore distribution in the 100 nm resolution, confirming the existence of pores in the material.

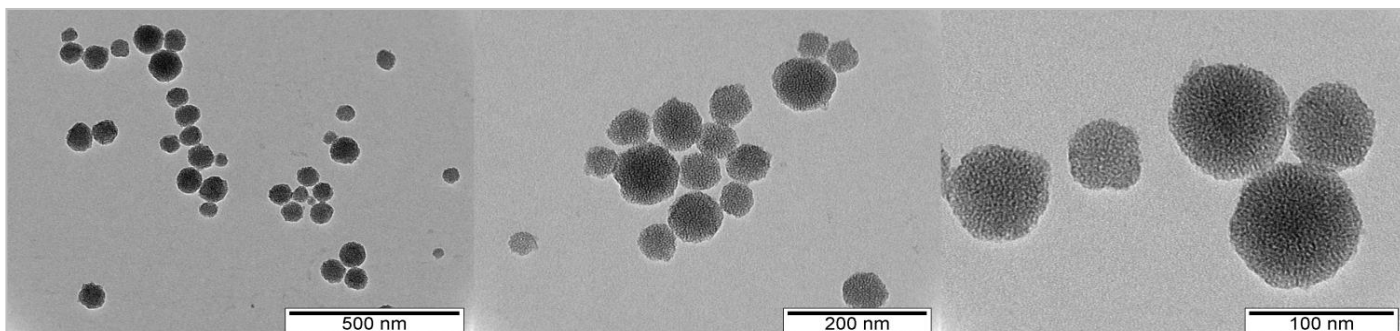


**Fig. 3.28.** - TEM images of the Mesoporous Silica Nanoparticles used for the production of the catalysts magnified to 500 nm, 200 nm and 100 nm, using water as solvent.

The Fourier-Transform Infrared spectra obtained for the mesoporous silica nanoparticles before and after the calcination process are presented in the **Figure 3.29.** below.

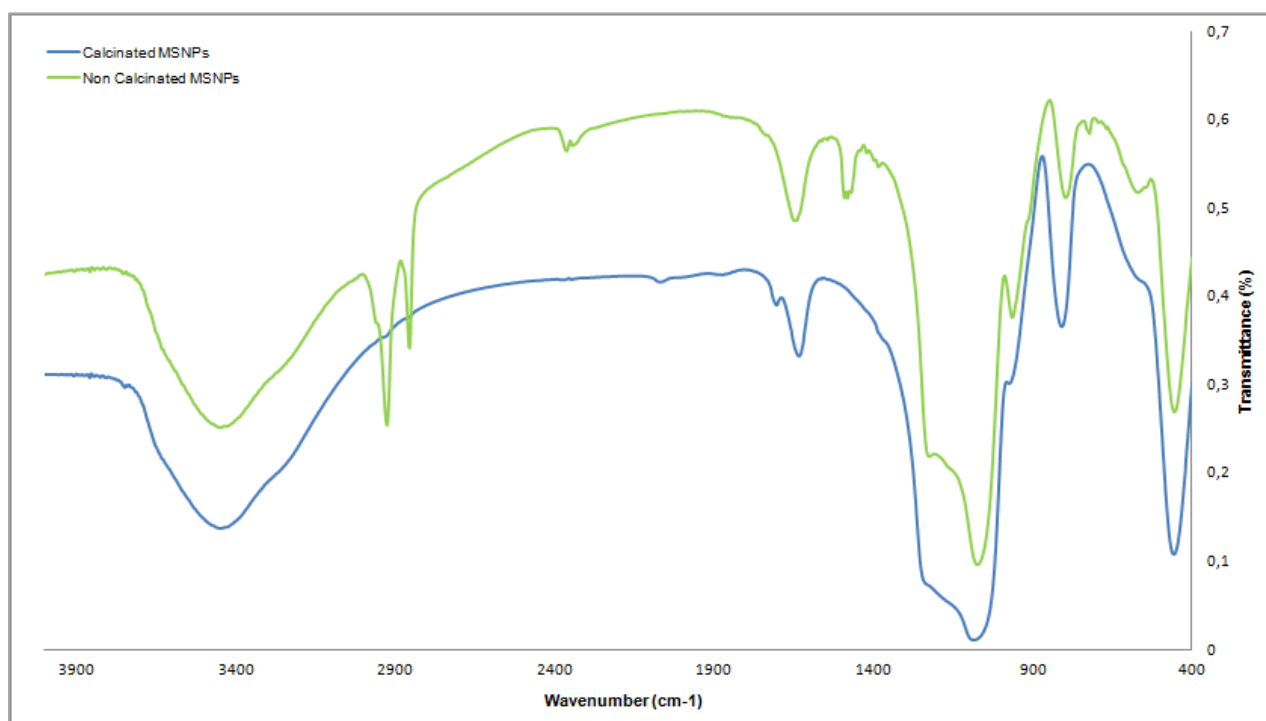


**Fig. 3.29.** - Fourier-Transform Infrared Spectra of Mesoporous Silica Nanoparticles before (green) and after (blue) calcination process.

The two spectra obtained are very similar, and have the characteristic signature bands in the range  $1000 - 400 \text{ cm}^{-1}$ , corresponding to the molecular vibrations of silica network. The broad band at  $3443 \text{ cm}^{-1}$  is attributed to the stretching vibration of the OH bond which indicates the presence of adsorbed water and silanol groups (Si-OH). The band at  $1635 \text{ cm}^{-1}$  corresponds to the bending modes of water. The bands at  $1200-1084 \text{ cm}^{-1}$  are assigned to the asymmetric stretching vibrations of Si-O-Si, the band at  $960 \text{ cm}^{-1}$  corresponds to the stretching vibration of the surface Si-OH, the band at  $808 \text{ cm}^{-1}$  is due to the symmetric stretching vibration of Si-O-Si, and the band at  $455 \text{ cm}^{-1}$  is assigned to bending vibration of Si-O-Si.<sup>60</sup> By this way, it is possible to confirm that the structure of the silica nanoparticles was not damaged and there was no degradation. The non-calcinated nanoparticles spectrum has some additional bands at  $2924 \text{ cm}^{-1}$ , and at  $2853 \text{ cm}^{-1}$  attributed to the stretching vibrations modes of CH<sub>3</sub>, CH<sub>2</sub> and CH,

groups and at  $1490\text{ cm}^{-1}$  and at  $728\text{ cm}^{-1}$  due to the bending vibration modes of  $\text{CH}_3$  and  $\text{CH}_2$  from Pluronic F127 and CTAB surfactants.

### 3.3.2. Preparation and characterization of MSNPs-POM-IL catalysts

The prepared Heterogeneous catalysts were characterized by Transmission Electron Microscopy (TEM), Scanning Electron Microscopy (SEM), Energy Dispersive X-Ray Spectroscopy (EDS), X-Ray Fluorescence Spectroscopy (XRF), Inductively Coupled Plasma Mass Spectrometry (ICP-MS), Elemental Analysis (EA), Fourier-Transform Infrared Spectroscopy (FTIR) and NMR Spectroscopy (Solution  $^1\text{H}$  NMR, and solid state  $^{13}\text{C}$  CP MAS and  $^{31}\text{P}$  NMR).

#### 3.3.2.1. MSNPs-[C<sub>4</sub>MIM]POM

The heterogeneous catalyst MSNPs-[C<sub>4</sub>MIM]POM was prepared via the three steps method shown in **Fig.3.30.**

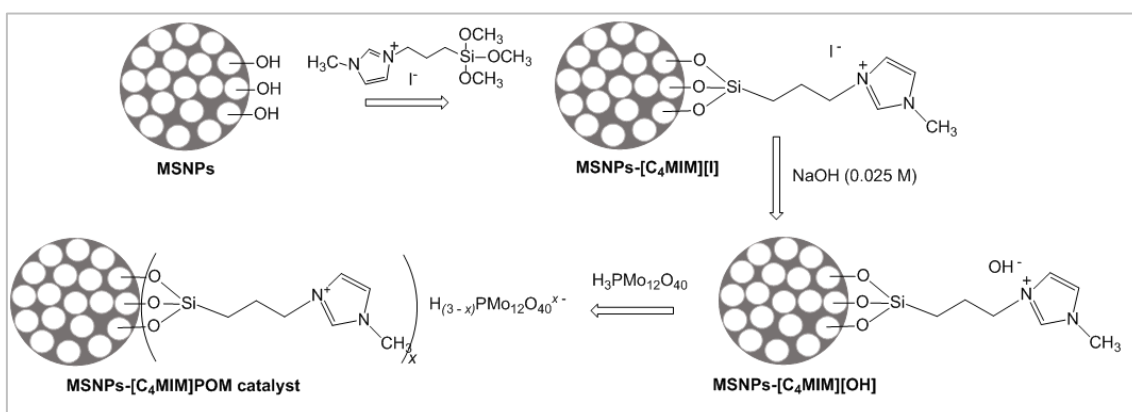


**Fig. 3.30.** - Schematic representation of the three-step synthesis method of heterogeneous catalyst MSNPs-[C<sub>4</sub>MIM]POM.

First, the surface of the pristine MSNPs was functionalized with N-(3-trimethoxysilylpropyl)-3-methylimidazolium iodide and then the iodide anions were exchanged by OH<sup>-</sup> anions using a NaOH solution (0.025M) following the method described by *Udayakumar et al*<sup>61</sup>. Finally, to this last material phosphomolybdic acid was added and through an acid-base reaction the catalyst was obtained.

The intermediates materials were characterized by FTIR and solution  $^1\text{H}$  NMR spectroscopies to verify the integrity of the functionalized cation [C<sub>4</sub>MIM] (see experimental section). The final material was characterized by Transmission Electron Microscopy (TEM), Scanning Electron Microscopy (SEM), Energy Dispersive X-Ray Spectroscopy (EDS)

In order to evaluate if the catalyst produced had the desired morphology, size and porosity, a TEM analysis was performed. In the **Figure 3.31.** presented below, it is possible to observe the catalyst prepared, MSNPs-[C<sub>4</sub>MIM]POM in two different resolutions, 100 nm and 500 nm. The color contrast in the obtained 100 nm images show the existence of multiple pores, resulting in a highly mesoporous structure of the catalyst. In general, the particles sizes are in the range 60-80 which is in agreement with the DLS results.



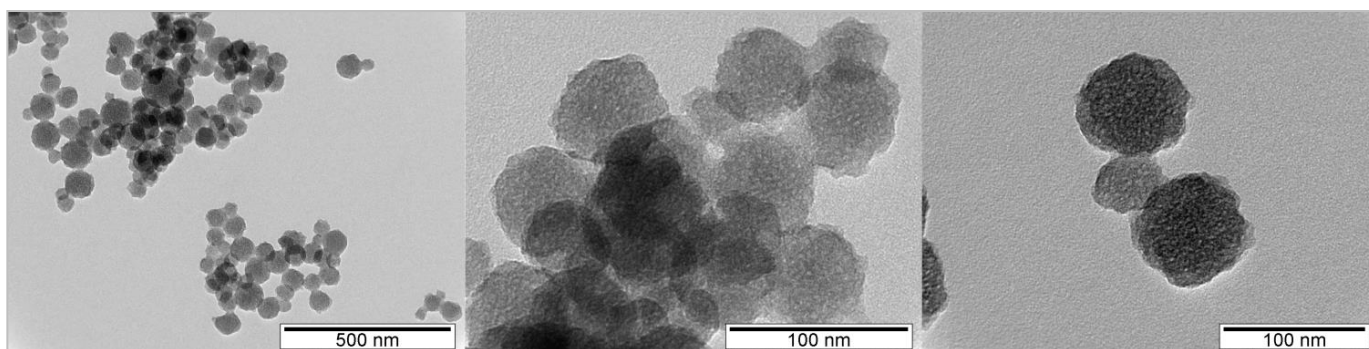


**Fig. 3.31.** - TEM images of the heterogeneous catalyst MSNPs-[C<sub>4</sub>MIM]POM, in resolutions 500 nm and 100 nm, using water as solvent.

SEM gives information about the surface topography of the sample and local in EDS mode. In the **Figure 3.32.** presented below, it is possible to observe the catalyst prepared, MSNPs-[C<sub>4</sub>MIM]POM, in three different resolutions, 4 μm, 1 μm and 500 nm.

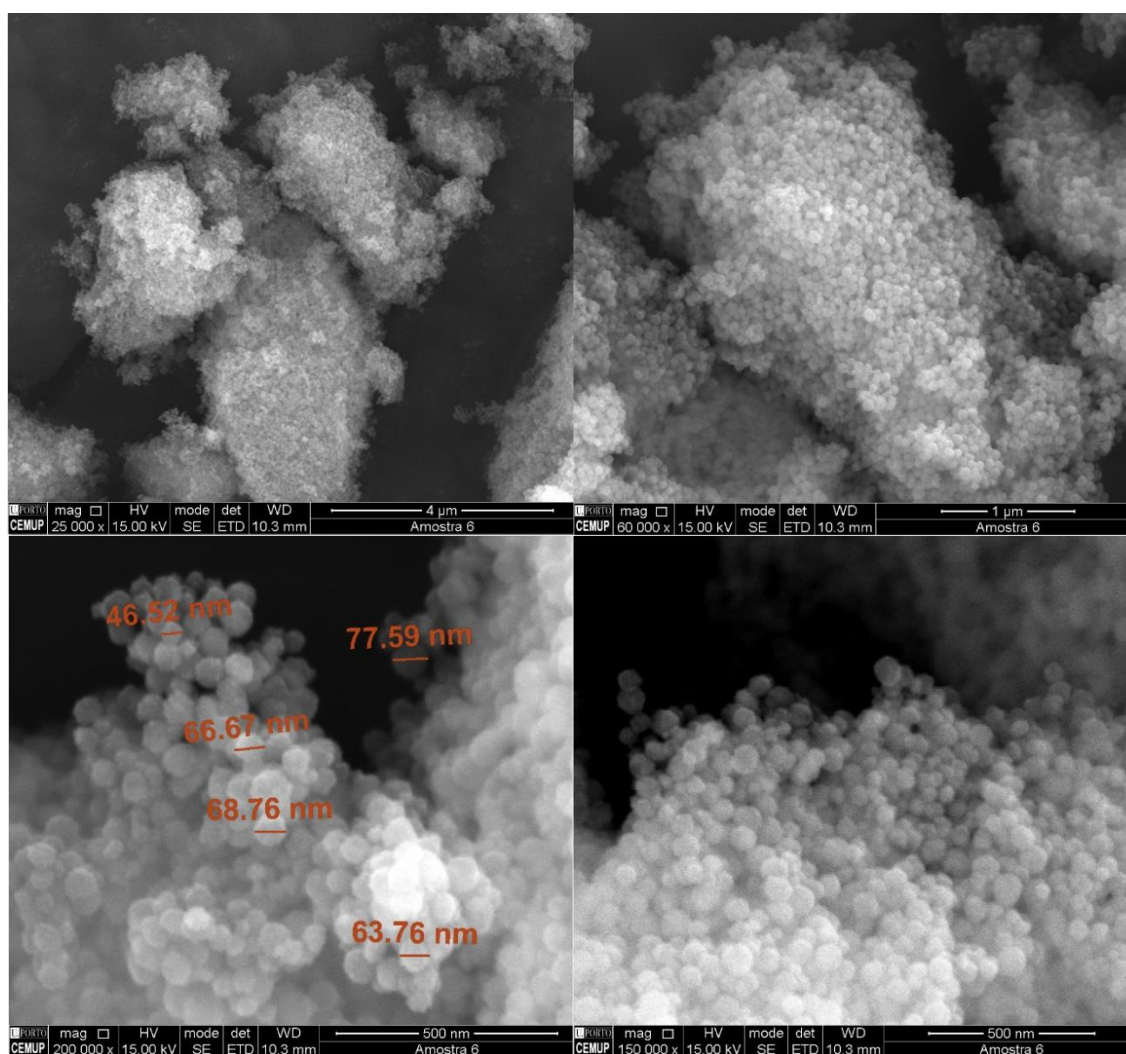


**Fig. 3.32.** - SEM images of heterogeneous catalyst MSNPs-[C<sub>4</sub>MIM]POM, magnified in resolutions 4 μm, 1 μm and 500 nm.

The images allowed to observe that the material consists of small spherical particles with their size in the range 60-80 nm. In the closest resolution (500 nm) it is possible to see that there was no degradation of the catalyst morphology and shape, which means

that the catalyst structure and morphology were kept after the basic treatment with NaOH solution and after the functionalization.

By Energy Dispersive X-Ray Spectroscopy, it is possible to identify the present elements in the analyzed sample. The obtained spectrum is presented in the following figure (**Fig. 3.33.**).

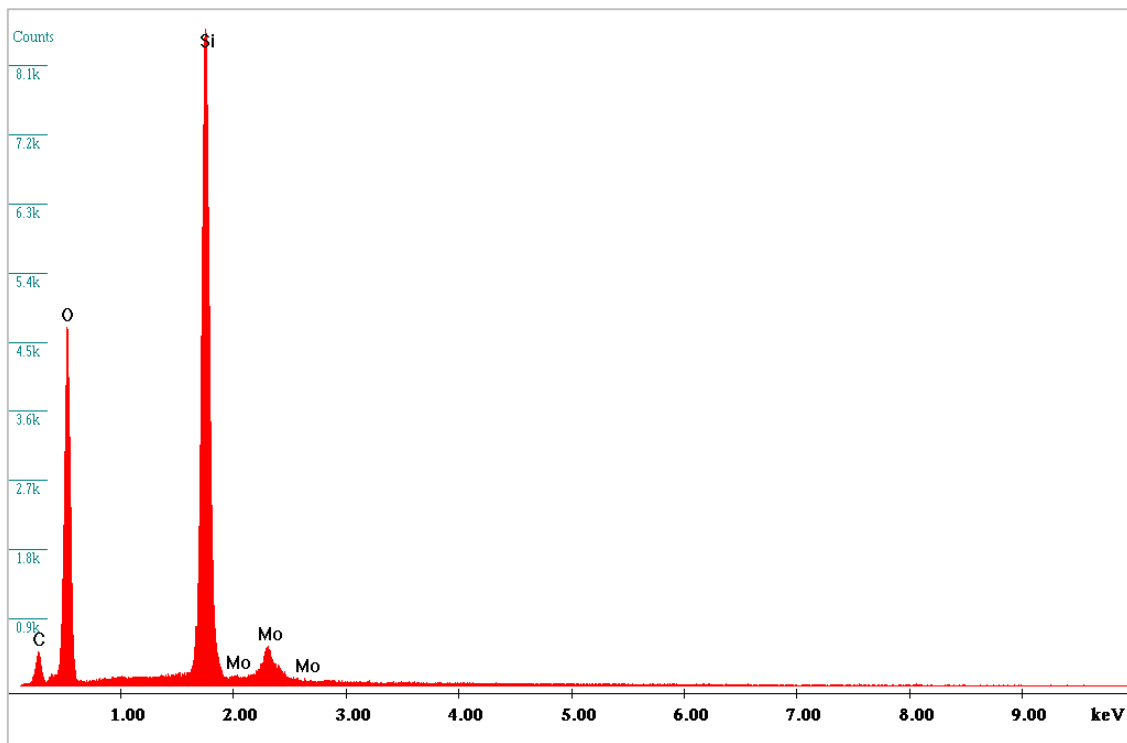


**Fig. 3.33.** - EDS analysis of the elements present in the heterogeneous catalyst MSNPs-[C<sub>4</sub>MIM]POM prepared.

The main peaks correspond to Silicon (Si) and Oxygen (O), which was expected since they are the main constituents of the silica nanoparticles. The presence of Molybdenum (Mo) is also observed which confirm the presence of the anion in the catalyst composition. (A presença de carbono não é indicadora da presença do catião uma vez que a amostra é preparada em fita de carbono). The presence of Phosphorus (P) is not observed because it is in a small quantity in comparison with Molybdenum. The EDS results proved the functionalization of the silica nanoparticles with the anion.

X-Ray Fluorescence Spectroscopy analysis of catalyst MSNPs-[C<sub>4</sub>MIM]POM was performed in order to prove the elemental composition of the catalyst prepared. The following figures (**Fig. 3.34.** and **Fig. 3.35.**) show the results of the x-ray fluorescence spectroscopy of the heterogeneous catalyst MSNPs-[C<sub>4</sub>MIM]POM.

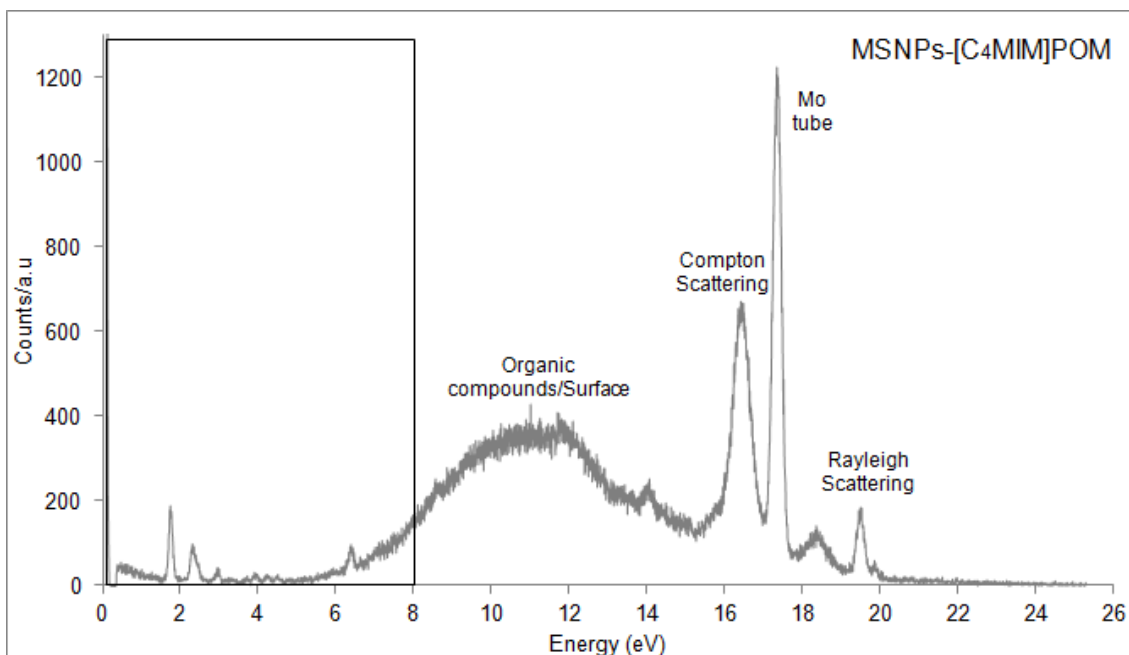


**Fig. 3.34.** - X-Ray Fluorescence Spectroscopy results of the heterogeneous catalyst MSNPs-[C<sub>4</sub>MIM]POM.

After magnifying the first spectrum (**Fig. 3.35.**), it is possible to observe, as expected, the evidence of Silicon (Si) and Molybdenum (Mo) in the sample. These elements confirm the presence of the silica network of the nanoparticles and their successful functionalization with the anion.

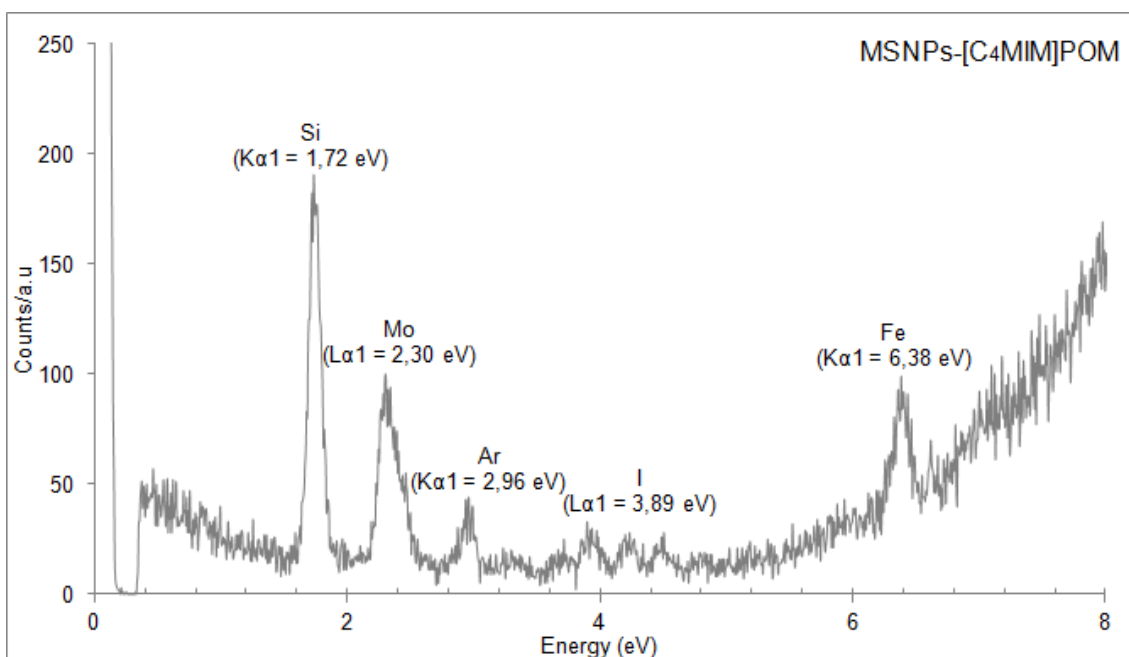


**Fig. 3.35.** - X-Ray Fluorescence Spectroscopy results magnified, of the heterogeneous catalyst MSNPs-[C<sub>4</sub>MIM]POM.

In the analysis, it was not visible the element Phosphorus (P). There is also Iodine (I) in the sample, which means that there is still a residue of iodine present in the sample from the first step of functionalization. There are also trace elements of Argon (Ar) and Iron (Fe) in the sample from impurities.

It was performed an ICP-MS analysis for the heterogeneous catalyst MSNPs-[C<sub>4</sub>MIM]POM to study the presence of phosphorus (P) and molybdenum (Mo). The following tables (**Table 3.5.** and **Table 3.6.**) show the obtained results from the analysis.

**Table 3.5.** - ICP-MS results for P and Mo for MSNPs-[C<sub>4</sub>MIM]POM catalyst.

	Element	Concentration (g/Kg)
MSNPs-[C <sub>4</sub> MIM]POM	P line (214.914)	1.45
	Mo line (202.031)	58.44

The molybdenum (Mo) content is significantly superior to the phosphorus (P) content. After obtaining the proportion mol (Molybdenum)/g (product), this relation can give the information of mol (POM)/g (product), knowing that there are twelve atoms of molybdenum per POM molecule. This way, it is possible to determine the active site quantity. Therefore, there are 0.05 mmol of POM in 1 g of catalyst.

**Table 3.6.** - ICP-MS results for Mo content of MSNPs-[C<sub>4</sub>MIM]POM catalyst.

	g(Mo)/Kg(prod)	g(Mo)/g(prod)	mmol(Mo)/g(prod)	mmol(POM)/g(prod)
MSNPs-[C <sub>4</sub> MIM]POM	58.44	0.06	0.60	0.05

The results obtained for N content allowed to conclude that the loading cation [C<sub>4</sub>MIM] is about 0.8 mmol per g of material (**Table 3.7.**). This means that only about 6% of the total cation anchored is balanced with the POM. The obtained C/N ratio is 3.9, higher than the expected value of 3,5 if the three alkoxysilane groups react with the silanol surface groups, this indicates that probably there is some cations present that are not covalently bounded to the surface and/or there is an incomplete condensation of the alkoxysilane with the surface.

**Table 3.7.** - Elemental Analysis results in mmol/g of material for C and N content in MSNPs-[C<sub>4</sub>MIM]POM catalyst.

	C	N
	mmol / g prod	mmol / g prod
MSNPs-[C <sub>4</sub> MIM]POM	0.91	0.81

The synthesized catalyst MSNPs-[C<sub>4</sub>MIM]POM, polyoxometalate H<sub>3</sub>PMo<sub>12</sub>O<sub>40</sub> and MSNPs-[C<sub>4</sub>MIM][OH], are represented respectively in blue, green and grey in the FTIR spectra presented (**Fig. 3.36.**).

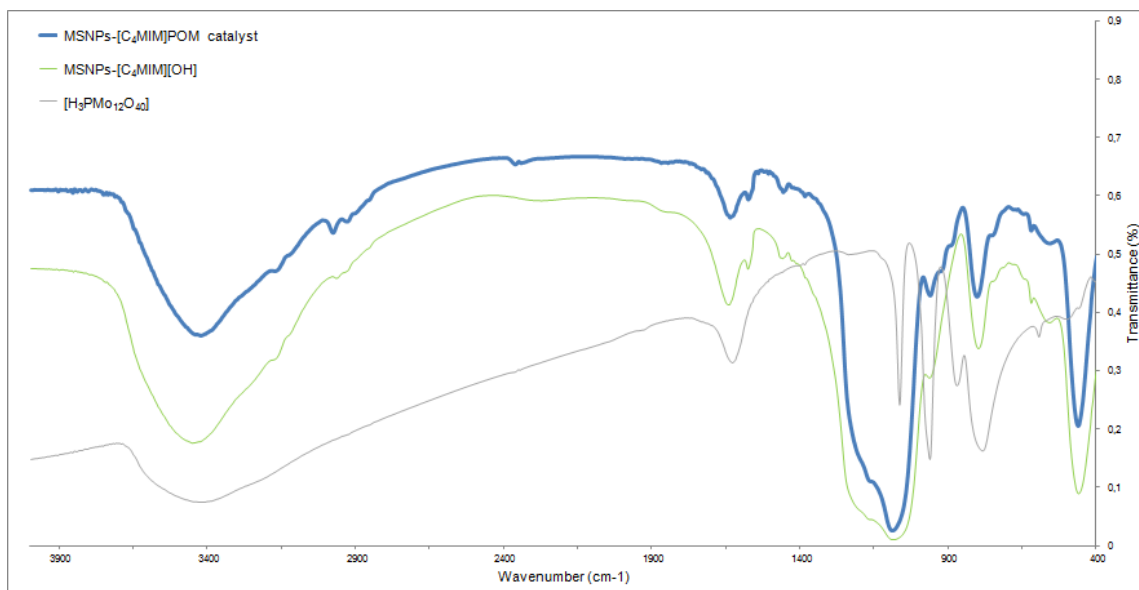


**Fig. 3.36.** - Fourier-Transform Infrared Spectra of MSNPs-[C<sub>4</sub>MIM]POM catalyst (blue), MSNPs-[C<sub>4</sub>MIM][OH] (green) and polyoxometalate H<sub>3</sub>PMo<sub>12</sub>O<sub>40</sub> (grey).

The characteristic bands from H<sub>3</sub>PMo<sub>12</sub>O<sub>40</sub> are from 1014, 976, 890 and 790 cm<sup>-1</sup>, that can be observed 1089, 961 and 803 in cm<sup>-1</sup>. There are some bands in the 900 cm<sup>-1</sup> area, that could represent part of linkage Mo-O.

The catalyst was characterized by solution <sup>1</sup>H NMR following a method described in the literature by *Crucho et al*<sup>62</sup> that uses a high basic solution of deuterium oxide with sodium hydroxide to destroy the silica network and to release the ligand anchored into solution. This strategy allows to quantify the loading of ligand in the material by using an internal standard (1,3,5-trioxane). The following figure (**Fig. 3.37.**) represents the <sup>1</sup>H NMR spectrum obtained of MSNPs-[C<sub>4</sub>MIM]POM.

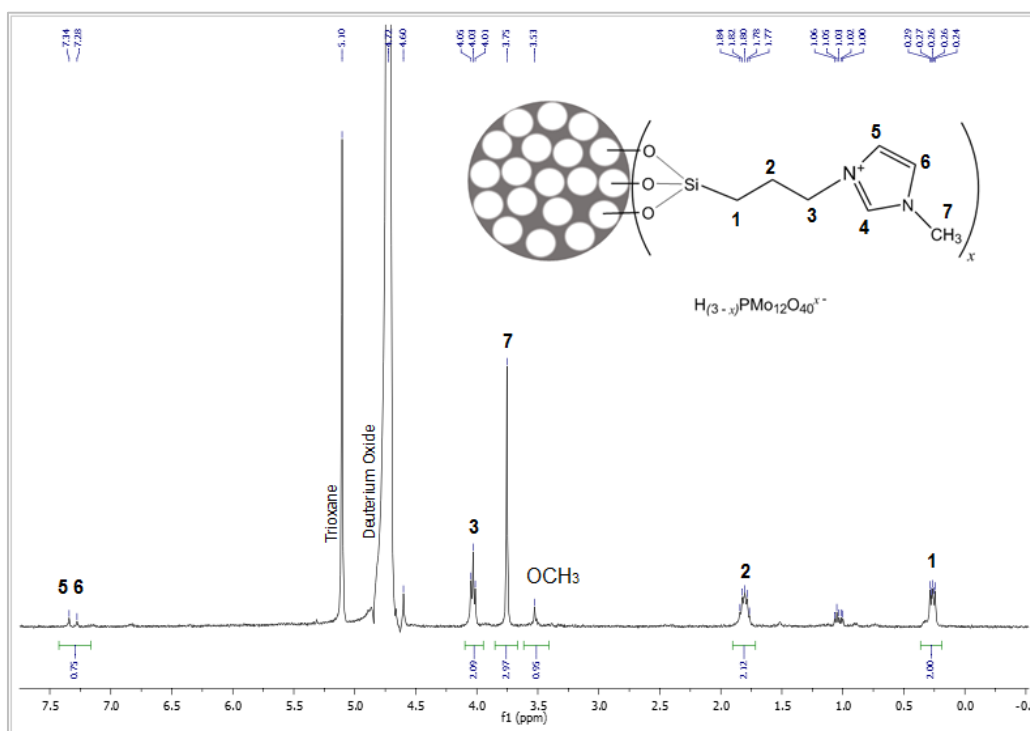


**Fig. 3.37.** - Solution <sup>1</sup>H NMR Spectrum of MSNPs-[C<sub>4</sub>MIM]POM, in Deuterium Oxide basified with sodium hydroxide and 1,3,5-trioxane as internal standard.

The spectrum contains peaks at 0.29 ppm, 1.84 ppm and 4.05 ppm that are attributed to the protons **1**, **2** and **3** of the alkyl chain, respectively. The singlet at 3.53 ppm can be due to the methoxy groups resulting from the incomplete condensation of the alkoxysilane with the surface silanols which is in agreement with the results obtained from elemental analysis. The singlet at 3.75 ppm is attributed to the methyl group of methylimidazol. The protons of the imidazol ring are not resistant to a high basic medium. The peak represented with "OCH<sub>3</sub>" is derivated, propably, from the methoxy group from the alkoxysilane that did not reacted to the surface of the MSNPs. Aromatic protons appear above 6 ppm, and, as it was possible to see, protons from number **5** and **6** were degraded with the basicity of the solution as it was verified.

The following spectrum represents the Solid State <sup>13</sup>C CP MAS NMR (**Fig. 3.38**).

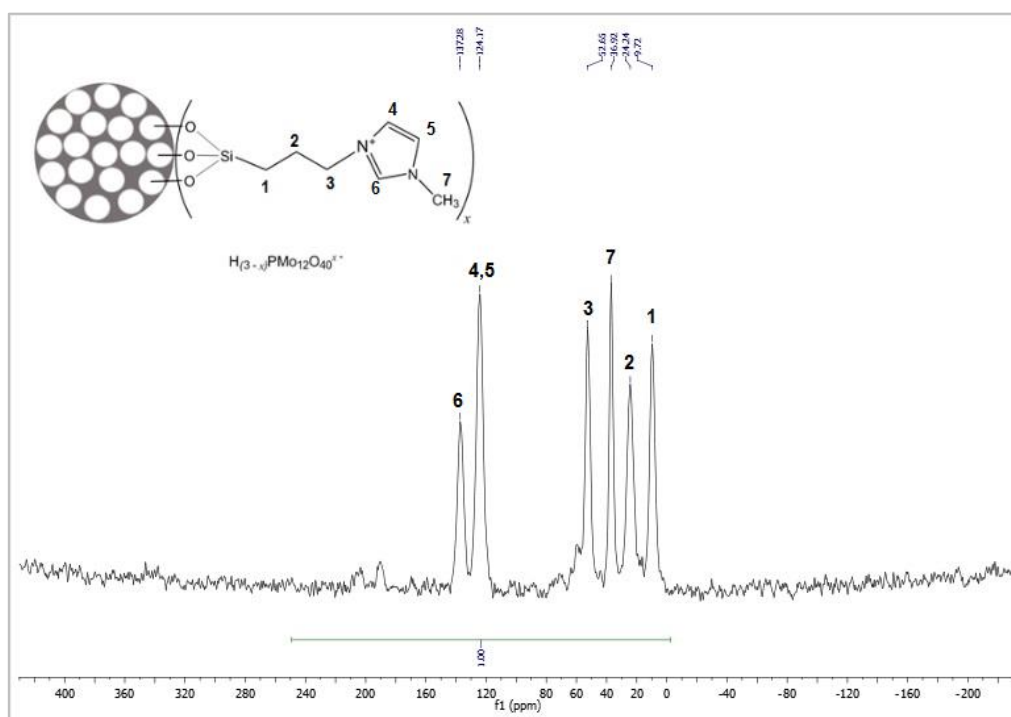


**Fig. 3.38.** - Solid State <sup>13</sup>C CP MAS NMR Spectrum of MSNPs-[C<sub>4</sub>MIM]POM.

The peaks at 9.72 ppm, 24.24 ppm and 52.65 ppm are assigned to the carbons numbered as **1**, **2** and **3** of the alkyl chain, respectively. The peak at 36.65 ppm is attributed to the carbon of methyl group numbered as **7**. The peaks at 124.17 ppm and 137.28 ppm correspond to the carbons of imidazol ring numbered as **4**, **5** and **6**. The spectrum shows that the integrity of the cation is preserved after the treatment with the phosphomolybdic acid.

The following spectrum represents the Solid State <sup>31</sup>P NMR obtained (**Fig. 3.39**).

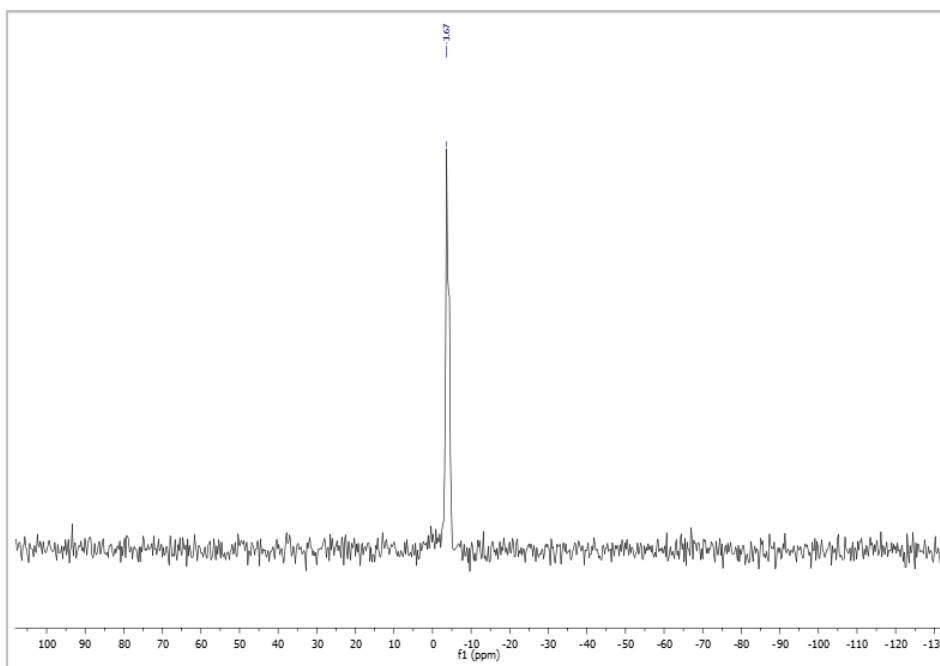


**Fig. 3.39.** - Solid State  $^{31}\text{P}$  NMR Spectrum of MSNPs-[C<sub>4</sub>MIM]<sub>3</sub>[PMo<sub>12</sub>O<sub>40</sub>].

The  $^{31}\text{P}$  NMR spectrum obtained of MSNPs-[C<sub>4</sub>MIM]POM contain a peak at -3.67 ppm which is close to the chemical shift of -3.20 ppm reported in the literature for the same POM immobilized in a silica hybrid material containing the same cation (*Wang et al*<sup>63</sup>). This proves the successful immobilization of the POM in the final material.

### 3.3.2.2. MSNPs-[C<sub>4</sub>Py]POM catalyst

The heterogeneous catalyst MSNPs-[C<sub>4</sub>Py]POM was prepared using the same three steps method used for MSNPs-[C<sub>4</sub>MIM]POM (**Fig.3.40.**).

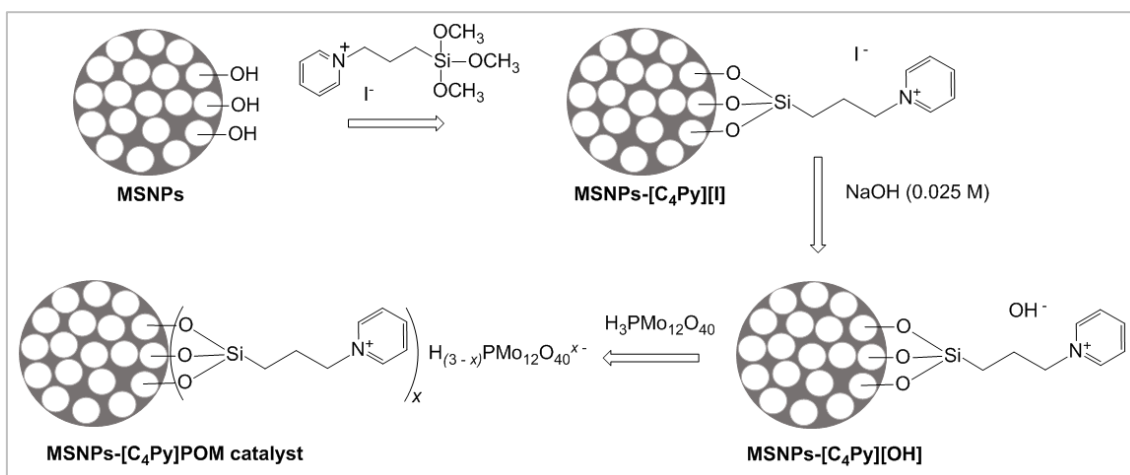


**Fig. 3.40.** - Schematic representation of the three-step synthesis method of heterogeneous catalyst MSNPs-[C<sub>4</sub>Py]POM.

A TEM analysis was performed to study the morphology, size and porosity. In the **Figure 3.41.** presented below, it is possible to observe the catalyst prepared, MSNPs-[C<sub>4</sub>Py]POM in the resolutions, 100 nm, 200 nm and 500 nm.

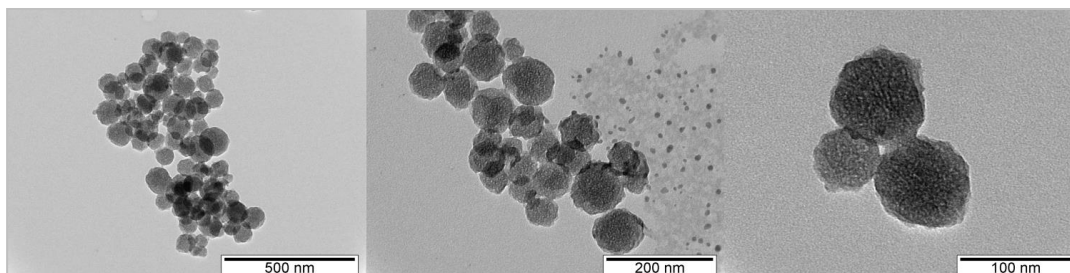


**Fig. 3.41.** - TEM images of the heterogeneous catalyst MSNPs-[C<sub>4</sub>Py]POM, in resolutions 500 nm, 200 nm and 100 nm, using water as solvent.

The 100 nm image shows the existence of pores in the nanoparticle structure. According to the images obtained, there was no degradation of the catalyst particles, which means, just like the other catalysts, the structure and morphology were intact after the basic treatment with NaOH solution and after the functionalization. As it also possible to observe, the nanoparticles size is not homogeneous, having a size distribution of approximately 50 to 100 nm.

It was performed an ICP-MS analysis for the heterogeneous catalyst MSNPs-[C<sub>4</sub>Py]POM to study the presence of molybdenum (Mo). The following tables (**Table 3.8.** and **Table 3.9.**) show the obtained results from the analysis.

**Table 3.8.** - ICP-MS results for Molybdenum for MSNPs-[C<sub>4</sub>Py]POM catalyst.

	Element	Conc. (g/Kg)
MSNPs-[C <sub>4</sub> Py]POM	Mo line (202,031)	28,99

After obtaining the proportion mmol (Molybdenum)/g (product), this relation can give the information of mol (POM)/g (product), knowing that there are twelve atoms of molybdenum per POM molecule. By this way, it is possible to determine the active site quantity. Therefore, there are 0.025 mmol of POM in 1 g of catalyst.

**Table 3.9.** - ICP-MS results for Molybdenum for MSNPs-[C<sub>4</sub>Py]POM catalyst.

	g(Mo)/Kg(prod)	g(Mo)/g(prod)	mmol(Mo)/g(prod)	mmol(POM)/g(prod)
MSNPs-[C <sub>4</sub> Py]POM	28,99	0,029	0.30	0.025

The results obtained for N content allowed to conclude that the loading cation [C<sub>4</sub>Py][ is about 0.7 mmol per g of material (**Table 3.10.**) This means that only about 3.6% of the total cation anchored is balanced with the POM. The obtained C/N ratio is 9.7, higher than the expected value of 8 if the three alkoxy silane groups react with the silanol surface groups, this indicates that probably there are some cations groups present that are not covalently bounded to the surface and/or there is an incomplete condensation of the alkoxy silane with the surface.

**Table 3.10.** - Elemental Analysis results in mmol/g of material for C and N content in MSNPs-[C<sub>4</sub>Py]POM catalyst.

	C	N
	mmol / g prod	mmol / g prod
MSNPs-[C <sub>4</sub> Py]POM	7.15	0.74



The spectra of polyoxometalate  $H_3PMo_{12}O_{40}$ , MSNPs-[C<sub>4</sub>Py][OH], and the synthesized catalyst MSNPs-[C<sub>4</sub>Py]POM are represented respectively in blue, green and grey in **Fig. 3.42**.

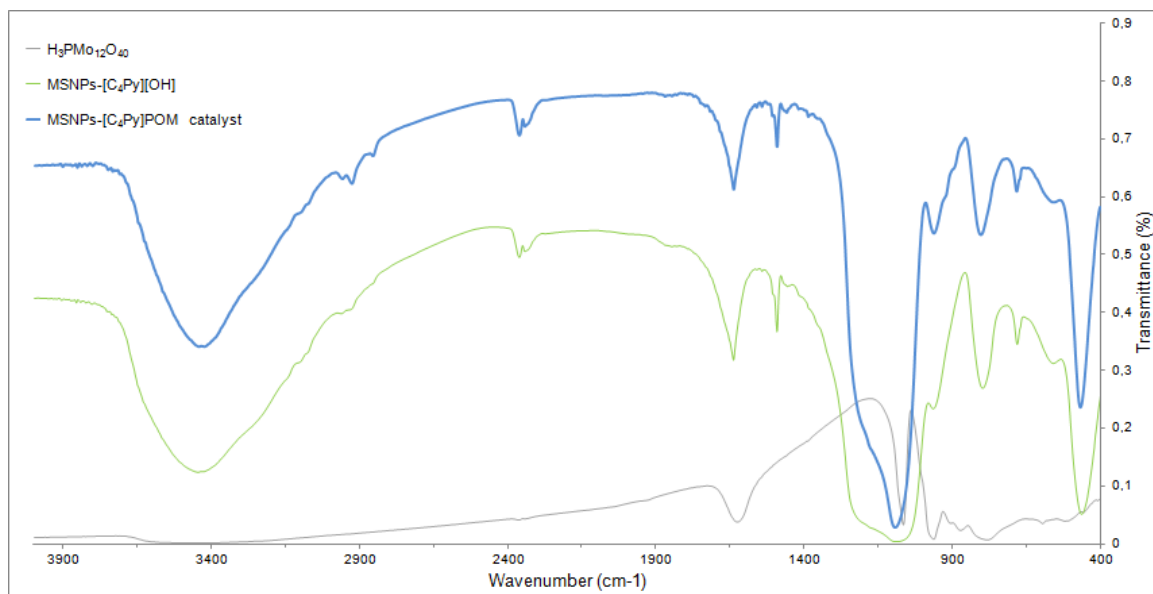


**Fig. 3.42.** - Fourier-Transform Infrared Spectra of MSNPs-[C<sub>4</sub>Py]POM catalyst (blue), MSNPs-[C<sub>4</sub>Py][OH] (green) and polyoxometalate  $H_3PMo_{12}O_{40}$  (grey).

The characteristic bands from  $H_3PMo_{12}O_{40}$  are from 1014, 976, 890 and 790  $cm^{-1}$ , that can be observed in 1091, 960 and 801  $cm^{-1}$ .

There are some bands in the 900  $cm^{-1}$  area, that could represent part of linkage Mo-O.

The following solution  $^1H$  NMR spectrum was obtained for the heterogeneous catalyst MSNPs-[C<sub>4</sub>Py]POM (**Fig. 3.43**).

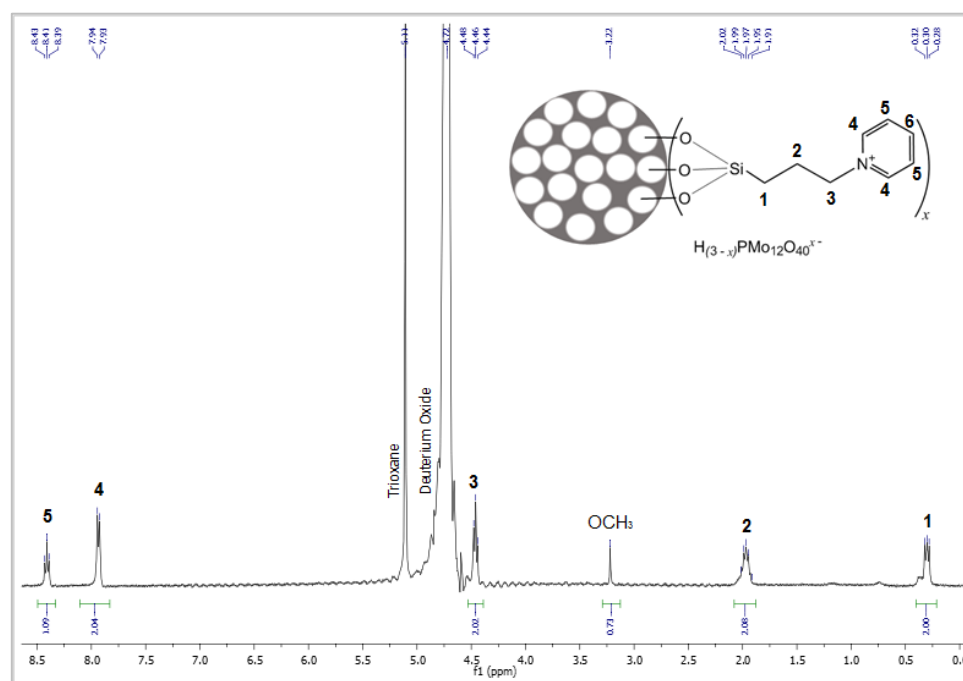


**Fig. 3.43.** - Solution  $^1H$  NMR Spectrum of MSNPs-[C<sub>4</sub>Py]POM, in Deuterium Oxide basified with sodium hydroxide and 1,3,5-trioxane as internal standard.

The spectrum contains peaks at 0.32 ppm, 2.02 ppm and 4.48 ppm that are attributed to the protons 1, 2 and 3 of the alkyl chain, respectively. The singlet at 3.22 ppm can be due to the methoxy groups resulting from the incomplete condensation of the alkoxy silane with the surface silanols which is in agreement with the results obtained from elemental analysis. As it was previously seen in the previous catalyst, the peak represented with "OCH3" is derived, probably, from the methoxy group from the alkoxy silane that did not react to the surface of the MSNPs.

### 3.3.2.3. MSNPs-[N<sub>4,4,4,4</sub>]POM

The catalyst MSNPs-[N<sub>4,4,4,4</sub>]POM was prepared in the same way indicated for the previous heterogeneous catalysts (**Fig. 3.44.**).

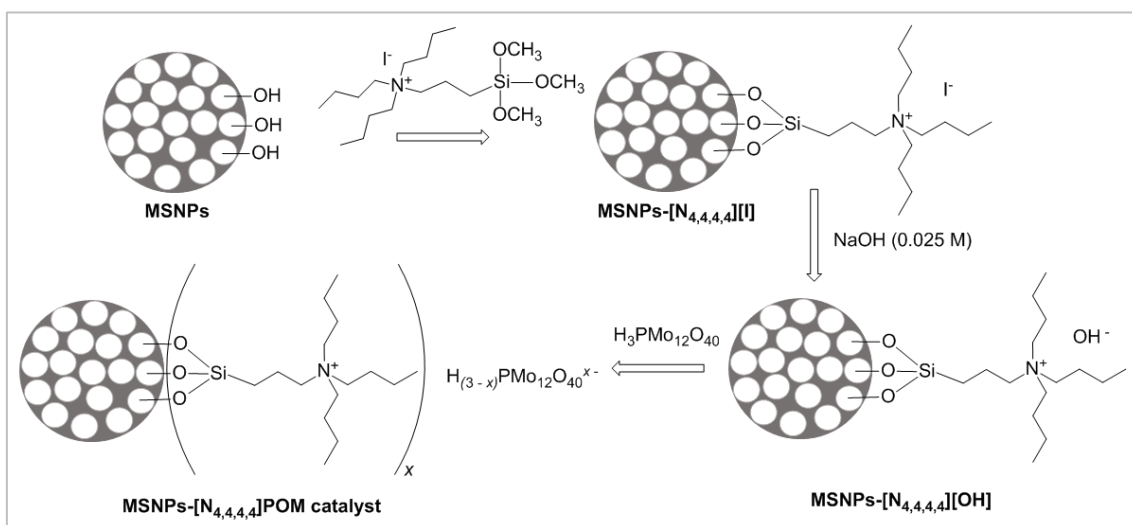


**Fig. 3.44.** - Schematic representation of the three-step synthesis method of heterogeneous catalyst MSNPs-[N<sub>4,4,4,4</sub>]POM.

Just like it was made to the two previous heterogeneous catalysts, a TEM analysis was performed to study of morphology, size and porosity. In the **Figure 3.45.** presented below, different images were taken of MSNPs-[N<sub>4,4,4,4</sub>]POM in the resolutions 100 nm, 200 nm and 500 nm.

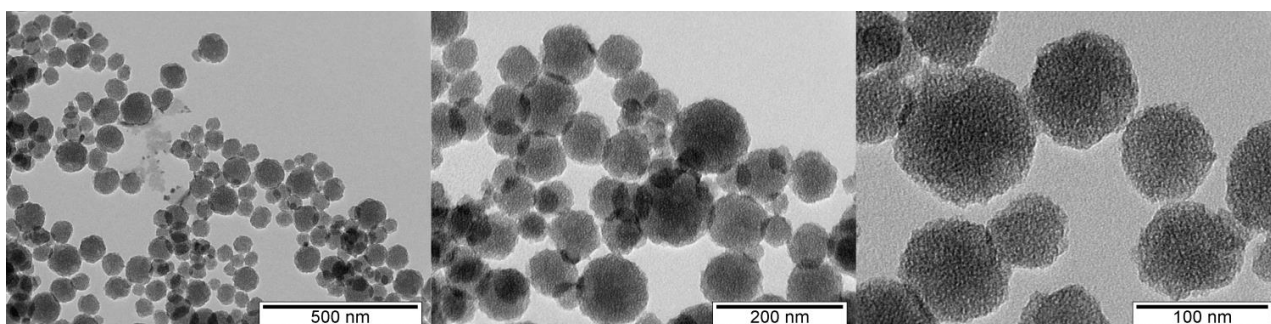


**Fig. 3.45.** - TEM images of the heterogeneous catalyst MSNPs-[N<sub>4,4,4,4</sub>]POM, in resolutions 500 nm, 200 nm and 100 nm, using water as solvent.

The images show the existence of pores, especially in the 100 nm resolution. There was some aggregation, but it is possible to see that there was no degradation of the catalyst particles, which means the catalyst structure and morphology were intact after the basic treatment with NaOH solution and after the functionalization with the phosphomolybdic acid. As it also possible to observe, the nanoparticles size is not

homogeneous, having a size distribution of approximately 50 to 90 nm. Even having a round shape, the form is not regular.

It was performed an ICP-MS analysis for the heterogeneous catalyst MSNPs-[N<sub>4,4,4,4</sub>]POM to study the presence of molybdenum (Mo). The following tables (**Table 3.11.** and **Table 3.12.**) show the obtained results from the analysis.

**Table 3.11.** - ICP-MS results for Molybdenum of MSNPs-[N<sub>4,4,4,4</sub>]POM catalyst.

	Element	Conc. (g/Kg)
MSNPs-[N <sub>4,4,4,4</sub> ]POM	Mo line (202.03)	64.11

After obtaining the proportion mol (Molybdenum)/g (product), this relation can give the information of mol (POM)/g (product), knowing that there are twelve atoms of molybdenum per POM molecule. This way, it is possible to determine the active site quantity. Therefore, there are 0.06 mmol of POM in 1 g of catalyst.

**Table 3.12.** - ICP-MS results for Molybdenum for MSNPs-[N<sub>4,4,4,4</sub>]POM catalyst.

	g(Mo)/Kg(prod)	g(Mo)/g(prod)	mmol(Mo)/g(prod)	mmol(POM)/g(prod)
MSNPs-[N <sub>4,4,4,4</sub> ]POM	64.11	0.06	0.67	0.06

An elemental analysis for the elements C, N and H was performed to MSNPs-[N<sub>4,4,4,4</sub>]POM catalyst.

The results obtained for N content allowed to conclude that the loading cation [N<sub>4,4,4,4</sub>] is 0.5 mmol per g of material (**Table 3.13.**) This means that about 12% of the total cation anchored is balanced with the POM. The obtained C/N ratio is 18.5, higher than the expected value of 15 if the three alkoxysilane groups react with the silanol surface groups, this indicates that probably there is some cations groups present that are not covalently bounded to the surface and/or there is an incomplete condensation of the alkoxysilane with the surface.

**Table 3.13.** - Elemental Analysis results in mmol/g of material for C and N content for MSNPs-[N<sub>4,4,4,4</sub>]POM catalyst.

	C	N
	mmol / g prod	mmol / g prod
MSNPs-[N <sub>4,4,4,4</sub> ]POM	9.26	0.50

The FTIR spectra of Polyoxometalate H<sub>3</sub>PMo<sub>12</sub>O<sub>40</sub>, MSNPs-[N<sub>4,4,4,4</sub>][OH], and the synthesized catalyst MSNPs-[N<sub>4,4,4,4</sub>]POM are represented respectively in blue, green and grey in (**Fig. 3.46.**)

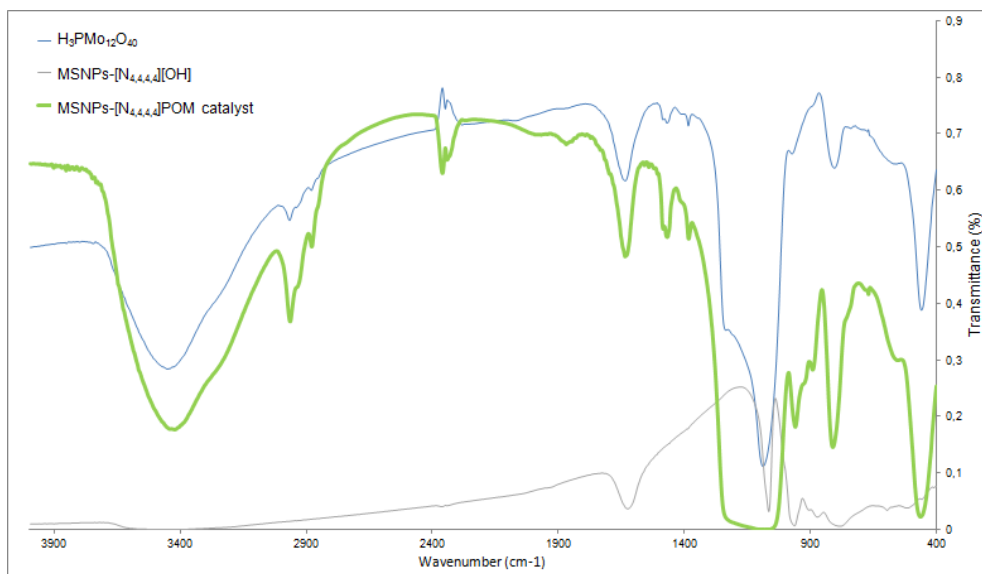


**Fig. 3.46.** - Fourier-Transform Infrared Spectra of MSNPs-[N<sub>4,4,4,4</sub>]POM catalyst (blue), MSNPs-[N<sub>4,4,4,4</sub>][OH] (green) and polyoxometalate H<sub>3</sub>PMo<sub>12</sub>O<sub>40</sub> (grey).

The characteristic bands from H<sub>3</sub>PMo<sub>12</sub>O<sub>40</sub> are from 1014, 976, 890 and 790 cm<sup>-1</sup>, that can be observed in 1089, 959, 890 and 810 cm<sup>-1</sup>.

There are some bands in the 900 cm<sup>-1</sup> area, that could represent part of linkage Mo-O. The <sup>1</sup>H NMR spectrum of MSNPs-[N<sub>4,4,4,4</sub>]POM is shown in **Fig. 3.47**. The spectrum contains the peak at 0.30 ppm attributed to the two protons numbered as **5**, the triplet at 0.84 ppm, the quartet at 1.26 ppm and the multiplet at 1.56 ppm are assigned to the protons numbered as **1** (nine protons), **2** (six protons) and **3** (six protons) of the butyl chains, respectively. The multiplet at 3.08 ppm corresponds to the eight protons numbered as **4**.

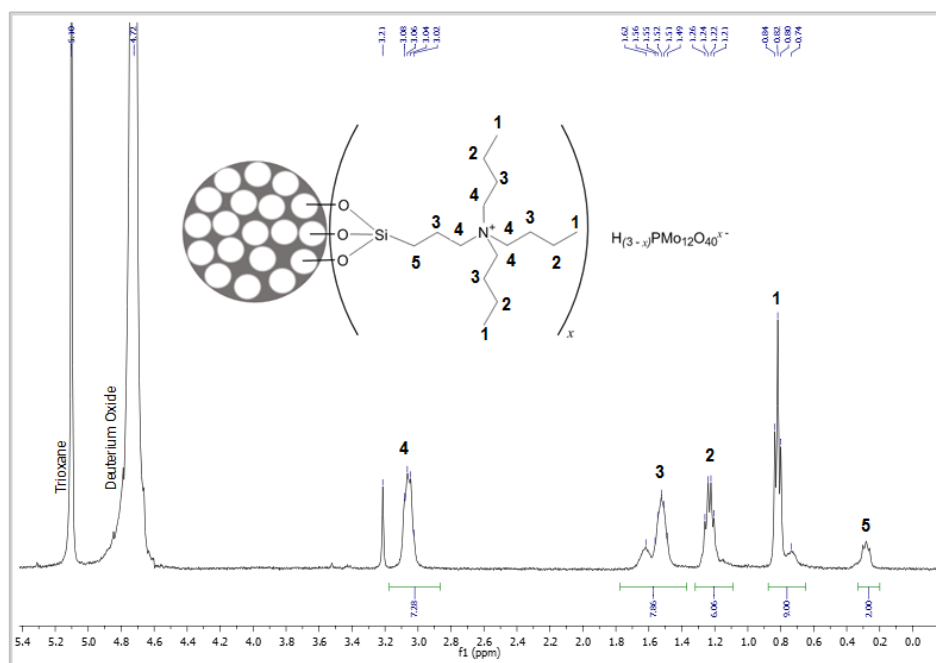


**Fig. 3.47.** - Solution <sup>1</sup>H NMR Spectrum of MSNPs-[N<sub>4,4,4,4</sub>]POM, in Deuterium Oxide basified with sodium hydroxide and 1,3,5-trioxane as internal standard.

With the obtained spectrum, it is possible to observe that the triplet that is represented by number **1** corresponds to the nine protons of the CH<sub>3</sub> terminations. Numbers **3** and

4 represent eight protons of the two CH<sub>2</sub> in the middle of the chains. The multiplet is represented by number 2 corresponds to six protons and number 5 corresponds to the two protons closer to the Si atom. The <sup>13</sup>C NMR spectrum of MSNPs-[N<sub>4,4,4,4</sub>]POM is shown in **Fig. 3.48**.

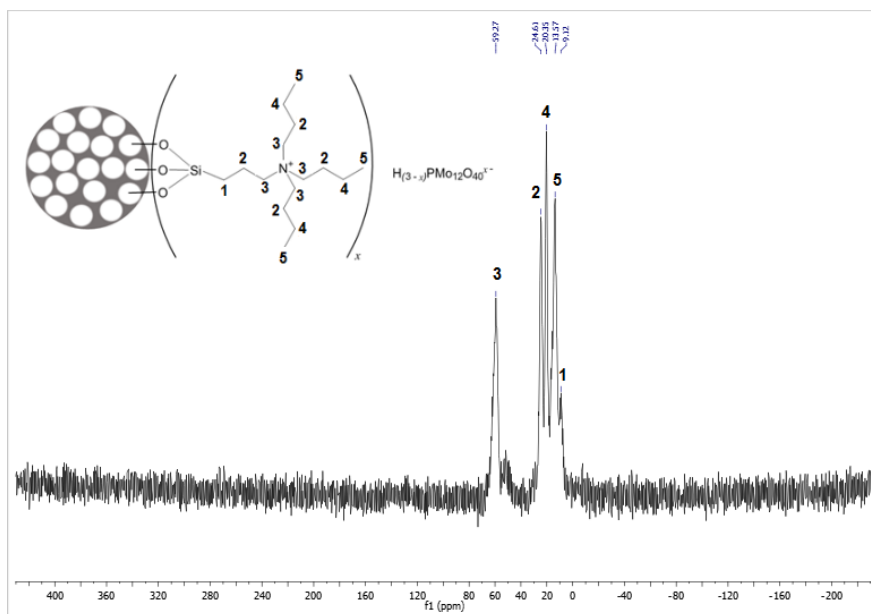


**Fig. 3.48.** - Solid State <sup>13</sup>C CP MAS NMR Spectrum of MSNPs-[N<sub>4,4,4,4</sub>]POM

The obtained spectrum contains a peak at 9.12 ppm which is attributed to the carbon of the CH<sub>2</sub> group numbered as 1. The peaks observed at 13.57 ppm, 20.35 ppm, 24.61 ppm and 59.27 ppm are assigned to the methyl groups of butyl chains numbered as 5, and to the CH<sub>2</sub> groups numbered as 4, 2 and 3, respectively. The spectrum confirms the successful immobilization of the cation. The following spectrum represents the Solid State <sup>31</sup>P NMR (**Fig. 3.49**).

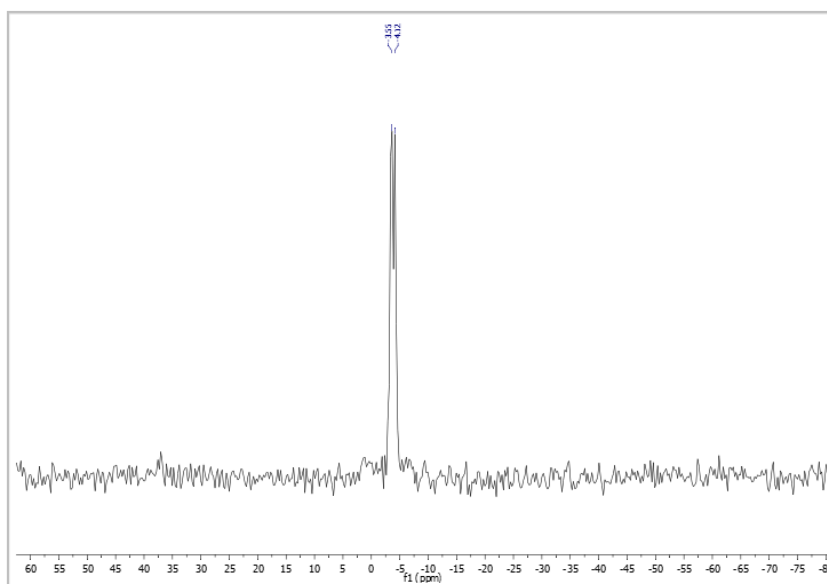


**Fig. 3.49.** - Solid State <sup>31</sup>P NMR Spectrum of MSNPs-[N<sub>4,4,4,4</sub>]POM.

The <sup>31</sup>P NMR spectrum obtained of MSNPs-[N<sub>4,4,4,4</sub>]POM catalyst shows a peak splitted into two at -4.12 ppm and -3.55 ppm which means that there is two different phosphorous coordination environments.

## 3.4. Catalysis

### 3.4.1. Oxidation of Lignin Model Compounds

The obtained results of the following catalytic oxidations of lignin model compounds, guaiacol and cinnamyl alcohol, were characterized by  $^1\text{H}$  NMR spectroscopy.

#### 3.4.1.1. Conventional Heating

##### ➤ Oxidation of Guaiacol using acetonitrile

As it was described in the Experimental Section, a study was performed in order to oxidize guaiacol with conventional heating using polyoxometalate  $\text{H}_3\text{PMo}_{12}\text{O}_{40}$  (with and without hydrogen peroxide) and  $[\text{N}_{4,4,4,4}]_3[\text{PMo}_{12}\text{O}_{40}]$  as catalysts.

In all three reactions, there was no sign of a new product after the oxidation process in the  $^1\text{H}$  NMR spectra obtained. This gives the indication that guaiacol was not oxidized, and no oxidation products were formed.

##### ➤ Oxidation of Cinnamyl Alcohol with using acetonitrile

The study of the oxidation of cinnamyl alcohol was performed in the same conditions and with the same catalysts as the study of guaiacol, as it was previously described in the Experimental Section.

##### • Catalyst $[\text{H}_3\text{PMo}_{12}\text{O}_{40}]$

In the first oxidation reaction, cinnamyl alcohol, hydrogen peroxide (3 mmol) and  $\text{H}_3\text{PMo}_{12}\text{O}_{40}$  were dissolved in acetonitrile.

According to the  $^1\text{H}$  NMR results, there were no oxidized products obtained. This means that cinnamyl alcohol was not oxidized and no oxidation products were formed. With the  $^1\text{H}$  NMR results, it was also possible to observe that the peaks gave the information that the product was degraded. The probable reason for these results is the high quantity of hydrogen peroxide used in the reaction.

Therefore, a new study was performed in the same conditions without adding hydrogen peroxide to the mixture (**Fig.3.50**).

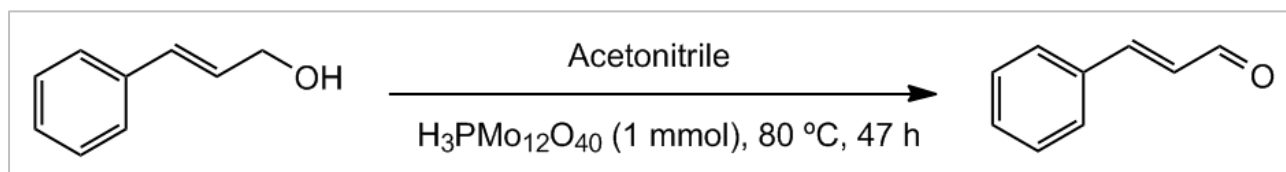


**Fig. 3.50.** - Oxidation of cinnamyl alcohol using polyoxometalate  $\text{H}_3\text{PMo}_{12}\text{O}_{40}$  as catalyst, without using hydrogen peroxide, with conventional heating.

In this study, the  $^1\text{H}$  NMR spectrum obtained (**Fig A.1.7.**, in Annexes) showed the presence of a new peak, representing the new product formed (in comparison to the  $^1\text{H}$  NMR spectrum of model compound cinnamyl alcohol).

Comparing the integrals of the obtained product and the model compounds, it was obtained a yield of 10%. It is interesting to observe that this reaction had better results than the previous one. This confirms that the oxidizing power of the polyoxometalate is enough to oxidize cinnamyl alcohol, while using 3 mmol of hydrogen peroxide degrades the model compound.

- **Catalyst [N<sub>4,4,4,4</sub>]<sub>3</sub>[PMo<sub>12</sub>O<sub>40</sub>]**

Another study was performed in the same conditions and with hydrogen peroxide to the mixture, with catalyst [N<sub>4,4,4,4</sub>]<sub>3</sub>[PMo<sub>12</sub>O<sub>40</sub>] (**Fig.3.51**).

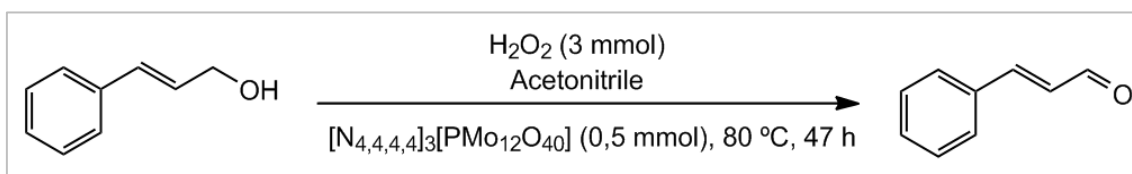


**Fig. 3.51.** - Oxidation of cinnamyl alcohol using catalyst [N<sub>4,4,4,4</sub>]<sub>3</sub>[PMo<sub>12</sub>O<sub>40</sub>], using hydrogen peroxide with conventional heating.

In this study, the <sup>1</sup>H NMR spectrum obtained (**Fig A.1.8.**, in Annexes) showed the presence of a new peak, representing the new product formed (in comparison to the <sup>1</sup>H NMR spectrum of model compound cinnamyl alcohol). Comparing the integrals of the obtained product and the model compounds, it was obtained a yield of 43%.

In terms of using conventional heating for the oxidation processes, it is possible to observe that the homogeneous catalyst with hydrogen peroxide had better results than using polyoxometalate without hydrogen peroxide.

### 3.4.1.2. Microwave Heating

- **Oxidation of Cinnamyl Alcohol using acetonitrile**

Since the oxidation results of cinnamyl alcohol were more promising than the results of oxidation of guaiacol, the application of the catalysts was only performed in the first model compound.

- **Catalyst [H<sub>3</sub>PMo<sub>12</sub>O<sub>40</sub>]**

For this oxidation reaction, cinnamyl alcohol was oxidized in acetonitrile with hydrogen peroxide (0.31 mmol) and H<sub>3</sub>PMo<sub>12</sub>O<sub>40</sub> as catalyst (**Fig. 3.52**).

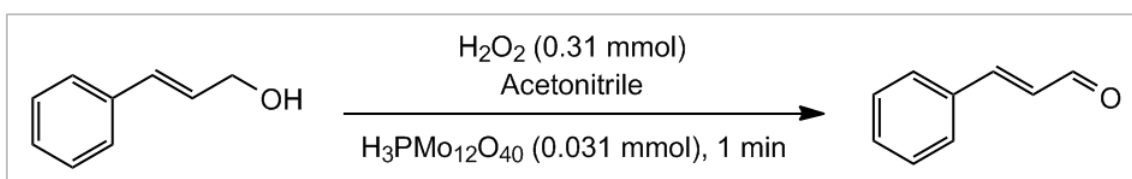


**Fig. 3.52.** - Oxidation of cinnamyl alcohol using polyoxometalate H<sub>3</sub>PMo<sub>12</sub>O<sub>40</sub>, using hydrogen peroxide and microwave heating.

The <sup>1</sup>H NMR spectrum obtained (**Fig A.1.9.**, in Annexes) showed the presence of a new peak, representing the new product formed. Comparing the integrals of the obtained product and the model compounds, it was obtained a yield of 37%.

- **Catalyst [C<sub>4</sub>MIM]<sub>3</sub>[PMo<sub>12</sub>O<sub>40</sub>]**

This oxidation reaction, cinnamyl alcohol was oxidized in the same conditions as the last reaction, using [C<sub>4</sub>MIM]<sub>3</sub>[PMo<sub>12</sub>O<sub>40</sub>] as catalyst (**Fig. 3.53**).

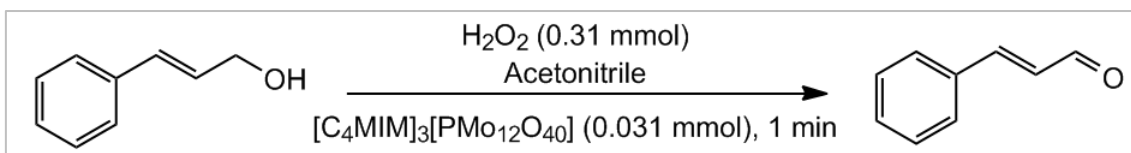


**Fig. 3.53.** - Oxidation of cinnamyl alcohol using catalyst  $[\text{C}_4\text{MIM}]_3[\text{PMo}_{12}\text{O}_{40}]$ , using hydrogen peroxide and microwave heating.

The  $^1\text{H}$  NMR spectrum obtained showed the presence of more than one new peaks, showing that new products were formed. Therefore, it was not possible to compare the integrals, since it is not possible to know which product belongs to each peak.

- **Catalyst  $[\text{C}_4\text{Py}]_3[\text{PMo}_{12}\text{O}_{40}]$**

This oxidation reaction, cinnamyl alcohol was oxidized in the same conditions as the last reaction, using  $[\text{C}_4\text{Py}]_3[\text{PMo}_{12}\text{O}_{40}]$  as catalyst (**Fig. 3.54.**).

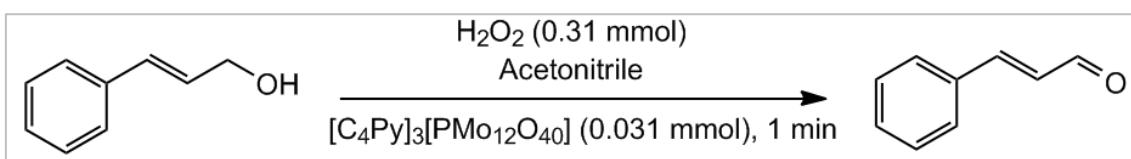


**Fig. 3.54.** - Oxidation of cinnamyl alcohol using catalyst  $[\text{C}_4\text{Py}]_3[\text{PMo}_{12}\text{O}_{40}]$ , using hydrogen peroxide and microwave heating.

Just like it happened in the last reaction, the  $^1\text{H}$  NMR spectrum obtained showed the presence of more than one new peaks, showing that new products were formed. As it was said before, it was not possible to compare the integrals, since it is not possible to know which product belongs to each peak.

Comparing the results obtained from microwave heating, it is possible to observe that the use of  $\text{H}_3\text{PMo}_{12}\text{O}_{40}$  only oxidizes into 1 product, while the use of the homogenous catalysts facilitate the oxidation of more than one product.



### 3.4.2. Oxidative Desulfurization of a multicomponent model diesel

Oxidative Desulfurization is a process that consists in the oxidation of sulfur compounds by turning them into sulfoxides and sulfones (**Fig. 3.55**). It is particularly important in the oxidation of benzothiophene compounds, since it is a difficult oxidation process. The following study was performed at Faculdade de Ciências in Universidade do Porto.

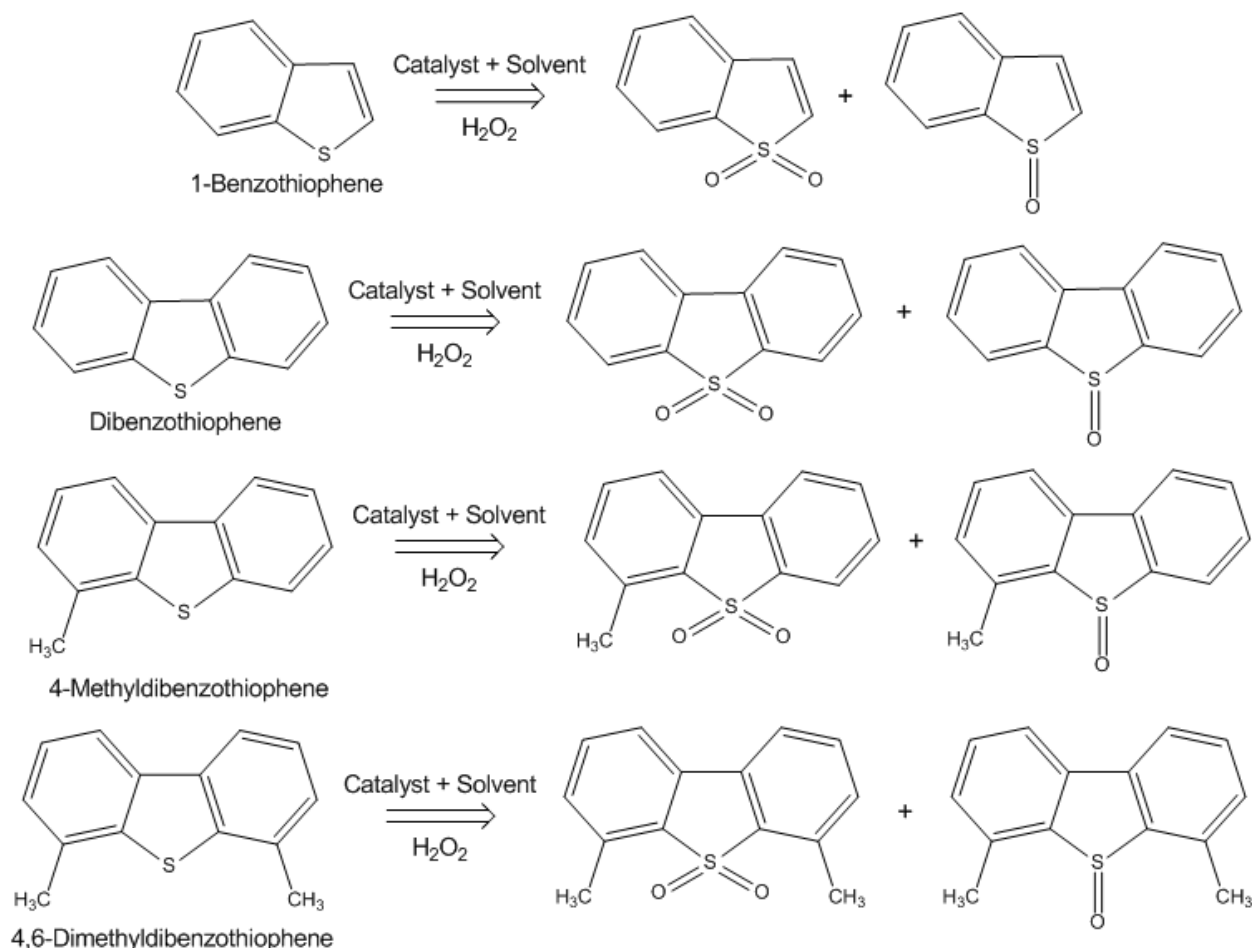


**Fig. 3.55.** - Schematic representation of Oxidative Desulfurization (ODS) of 1-benzothiophene (1-BT), dibenzothiophene (DBT), 4-methyldibenzothiophene (4-MDBT) and 4,6-dimethyldibenzothiophene (4,6-DMDBT) using a catalyst, a solvent and an oxidant.

For this study, it was necessary to prepare a stock solution (2000 ppm) of the four model compounds (1-BT, DBT, 4-MDBT and 4,6-DMDBT) with 500 ppm each to produce the model oil used in the process. It was also prepared a standard solution of n-octane and tetradecane to control the gas chromatography results. The Oxidative Desulfurization process is divided in two different stages.

- First Stage: Initial Extraction

After the addition of solvent (in this work, acetonitrile for homogeneous catalysts and ionic liquid 1-butyl-3-methylimidazolium hexafluorophosphate ([BMIM][PF<sub>6</sub>]) for the heterogeneous catalyst), model oil prepared and respective catalyst to a reactor at a temperature of 70 °C in paraffin bath for 10 minutes, the first stage of the process begins. This stage consists of the initial extraction of the sulfur compounds to the solvent phase of the reactor (**Fig. 3.56**).

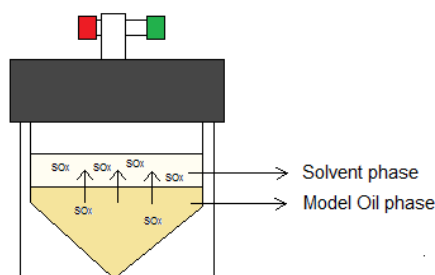


**Fig. 3.56.** - Representation of the initial extraction of the Oxidative Desulfurization of sulfur compounds.

- Second Stage: Catalytic phase

In this stage, the oxidant (oxygen peroxide 30%) is added to the reactor, and the oxidation of sulfur compounds begins. After the moment the oxygen peroxide is added to the reactor, samples are taken after for a few hours (up to 6 hours) and are analyzed in a Gas Chromatograph.

In the following section, it is presented a study on the application and performance comparison in the use of homogeneous and heterogeneous catalysts in the oxidative desulfurization of the petroleum model compounds presented previously (1-BT, DBT, 4-MDBT and 4,6-DMDBT).

### 3.4.2.1. Homogeneous Catalysts in ODS

In the oxidative desulfurization using homogeneous catalysts it was used acetonitrile as extraction solvent. Acetonitrile has been used as a solvent in these oxidation processes since it has a high extraction potential. Though it is an excellent extraction solvent, acetonitrile is not a “green” choice, since it is toxic, volatile and flammable.

In the initial extraction, the model oil prepared, catalyst and standard solution were put in a reactor in the described quantities in **Table 3.14**.

**Table 3.14.** - Quantities of solvent (acetonitrile), oxidant (hydrogen peroxide), model oil and standard solution used in the study of the Homogeneous catalysts in ODS.

	Homogeneous Catalysts		
	$[N_{4,4,4,4}]_3[PMo_{12}O_{40}]$	$[C_4MIM]_3[PMo_{12}O_{40}]$	$[C_4Py]_3[PMo_{12}O_{40}]$
Acetonitrile ( $\mu$ l)	750	750	750
H <sub>2</sub> O <sub>2</sub> ( $\mu$ l)	75	75	75
Catalyst (mg)	7.62	6.72	6.70
Model Oil ( $\mu$ l)	750	750	750
Standard solution ( $\mu$ l)	20	20	20

The mixture was kept under stirring conditions at a temperature of 70 °C in paraffin bath for 10 minutes. In this stage, the sulfur compounds transfer to the solvent phase (**Fig. 3.57**).



**Fig. 3.57.** - Reactors with acetonitrile, model oil and standard solution used in the study of the Homogeneous catalysts in ODS.

The initial point ( $t = 0$  min) represents the time when the oxidant, hydrogen peroxide at 30%, is added to the reactor to begin the second stage, the oxidation phase. After 10 minutes of adding the oxygen peroxide, the first sample of oil is taken and is analyzed in a Gas Chromatograph for 20 minutes. The next samples were taken after 30, 60, 120, 180, 240, 300, 360 and 420 minutes after the addition of oxidant to the reactor.

Taking the example of the ODS catalysis using  $[N_{4,4,4,4}]_3[PMo_{12}O_{40}]$  as catalyst, it is possible to observe that after a few hours, the content of 1-BT, DBT, 4-MDBT and 4,6-DMDBT has decreased (**Fig. 3.58**). The different colors represent the different samples taken after a specific amount of time. For example, the bright blue color represents the highest peaks that correspond to the addition of oxygen peroxide to the mixture and the point when the oxidation began. After continuing taking samples for the next hours, the curves start to show lower intensity, proving that the sulfur compounds are being oxidized and its content in the sample is decreasing.

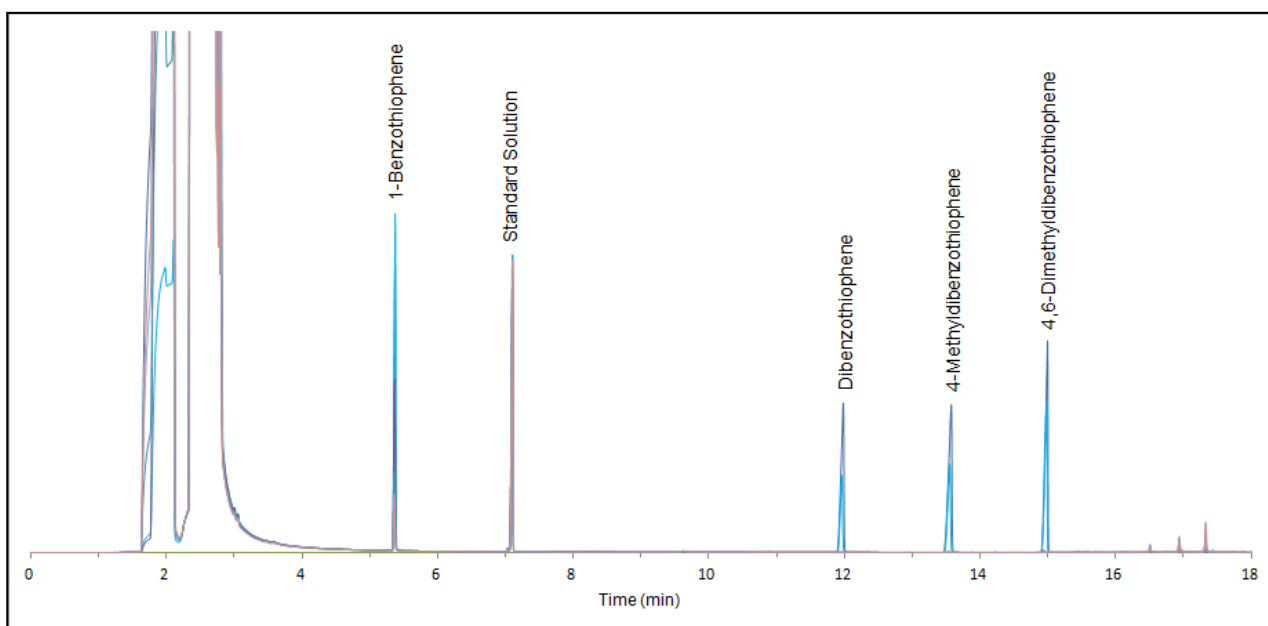


**Fig. 3.58.** - Graphic of the development of the Oxidative Desulfurization process of sulfur compounds using  $[N_{4,4,4,4}]_3[PMo_{12}O_{40}]$  catalyst.

The following table (**Table 3.15**) shows the gas chromatography results of the oxidations performed using the homogeneous catalysts ( $[N_{4,4,4,4}]_3[PMo_{12}O_{40}]$ ,  $[C_4MIM]_3[PMo_{12}O_{40}]$ , and  $[C_4Py]_3[PMo_{12}O_{40}]$ ) from the initial addition of hydrogen peroxide ( $t = 0$  min) up to 7 hours later ( $t = 420$  min), representing the quantity of sulfur compounds present in the sample (ppm) and total desulfurization (%).

**Table 3.15.** - Results and comparison of the performance of Homogeneous catalysts in ODS. Representation of the oxidation of the model oil compounds (ppm) and total desulfurization (%), over time (min).

Time (min)	Homogeneous Catalysts					
	[N <sub>4,4,4,4</sub> ] <sub>3</sub> [PMo <sub>12</sub> O <sub>40</sub> ] catalyst		[C <sub>4</sub> MIM] <sub>3</sub> [PMo <sub>12</sub> O <sub>40</sub> ] catalyst		[C <sub>4</sub> Py] <sub>3</sub> [PMo <sub>12</sub> O <sub>40</sub> ] catalyst	
	ppm	Total Dessulf (%)	ppm	Total Dessulf (%)	ppm	Total Dessulf (%)
0	2016	0	1538	0	1538	0
10	929	53	-	-	901	41
30	631	68	581	62	665	56
60	-	-	291	81	275	82
120	149	92	258	83	265	82
180	61	96	239	84	257	83
240	39	98	322	79	273	82
300	43	97	223	85	336	78
360	41	97	232	84	206	86
420	49	97	-	-	254	83

Some of the points taken are represented with a “-”, since the results were inconclusive or were not taken.

Comparing the three catalysts at the last common analyzed time (t = 360 min, 6 hours), it is possible to conclude that the best performing catalyst is [N<sub>4,4,4,4</sub>]<sub>3</sub>[PMo<sub>12</sub>O<sub>40</sub>], with a total desulfurization rate of 97.96% (remaining 41.12 ppm of model compounds in the sample), followed by [C<sub>4</sub>Py]<sub>3</sub>[PMo<sub>12</sub>O<sub>40</sub>] with a total desulfurization rate of 86.61% (remaining 206.00 ppm of model compounds in the sample) and [C<sub>4</sub>MIM]<sub>3</sub>[PMo<sub>12</sub>O<sub>40</sub>] with a total desulfurization rate of 84.90% (remaining 232.31 ppm of model compounds in the sample).

When comparing the results of both catalysts [N<sub>4,4,4,4</sub>]<sub>3</sub>[PMo<sub>12</sub>O<sub>40</sub>] and [C<sub>4</sub>Py]<sub>3</sub>[PMo<sub>12</sub>O<sub>40</sub>] after t = 420 min, 7 hours, it is also possible to see that there is not a significant alteration in the results comparing with the previous hour, since [N<sub>4,4,4,4</sub>]<sub>3</sub>[PMo<sub>12</sub>O<sub>40</sub>] performed a total desulfurization of 97.52 %, remaining 49.94 ppm of sulfur compounds in that sample, and [C<sub>4</sub>Py]<sub>3</sub>[PMo<sub>12</sub>O<sub>40</sub>] performed a total desulfurization of 83.43 % remaining 254.83 ppm of sulfur compounds in the sample.

Overall, all three catalysts had a good performance in the oxidative desulfurization of petroleum model compounds.

In the next graph (**Fig. 3.59.**) it is possible to see the oxidative reactions using the three catalysts [N<sub>4,4,4,4</sub>]<sub>3</sub>[PMo<sub>12</sub>O<sub>40</sub>], [C<sub>4</sub>MIM]<sub>3</sub>[PMo<sub>12</sub>O<sub>40</sub>] and [C<sub>4</sub>Py]<sub>3</sub>[PMo<sub>12</sub>O<sub>40</sub>] (respectively represented in blue, green and grey).

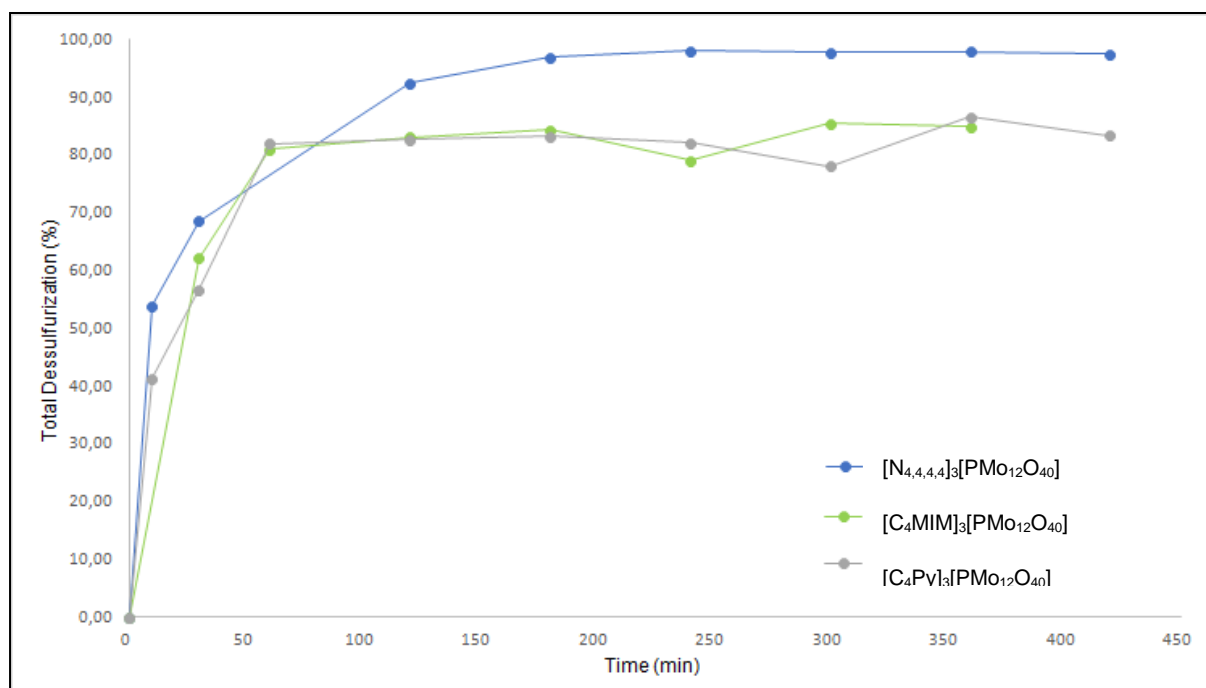


**Fig. 3.59.** - Graphic representation of the Gas Chromatography results of the Oxidative Desulfurization of petroleum model compounds using Homogeneous Catalysts.

### 3.4.2.2. Heterogeneous Catalyst in ODS

In the oxidative desulfurization using three heterogeneous catalysts, an ionic liquid was used as extraction solvent (1-butyl-3-methylimidazolium hexafluorophosphate, [BMIM][PF<sub>6</sub>]). Ionic Liquids have been used as solvents in these oxidation processes for its sustainability and for its capacity to increase the extraction of sulfur compounds to the solvent phase.

- **MSNPs-[C<sub>4</sub>MIM]POM catalyst**

In the table below (**Table 3.16.**) are presented the quantities of solvent, oxidant, model oil and standard solution used in each study. Since MSNPs-[C<sub>4</sub>MIM]POM catalyst quantity was becoming very low after its use for the three cycles, it was necessary to reduce to 1/3 of the quantities of solvent, oxidant, model oil and standard solution used, in order to have enough catalyst to apply in the two remaining studies. This way, the same proportion was still kept in the last studies performed with half solvent quantity and half oxidant quantity.

**Table 3.16.** - Quantities of solvent ([BMIM][PF<sub>6</sub>]), oxidant (hydrogen peroxide), model oil and standard solution used in the study of the Heterogeneous catalyst in ODS, in 3 equal cycles, half the solvent quantity and half oxidant quantity studies.

	Heterogeneous Catalyst				
	MSNPs-[C <sub>4</sub> MIM]POM				
	1st Cycle	2nd Cycle	3rd Cycle	Half Solvent	Half Oxidant
[BMIM][PF <sub>6</sub> ] (μl)	750	750	750	125	250
H <sub>2</sub> O <sub>2</sub> (μl)	75	75	75	25	12.5
Catalyst (mg)	59	59	59	19.5	19.5
Model Oil (μl)	750	750	750	250	250
Standard solution (μl)	20	20	20	6.7	6.7

To initiate the first stage of each study, the initial extraction, the model oil prepared, catalyst and standard solution were put in a reactor in the described quantities previously. The mixture was kept under stirring conditions at a temperature of 70 °C in paraffin bath for 10 minutes. In this stage, the sulfur compounds transfer to the solvent phase (**Fig. 3.60**).

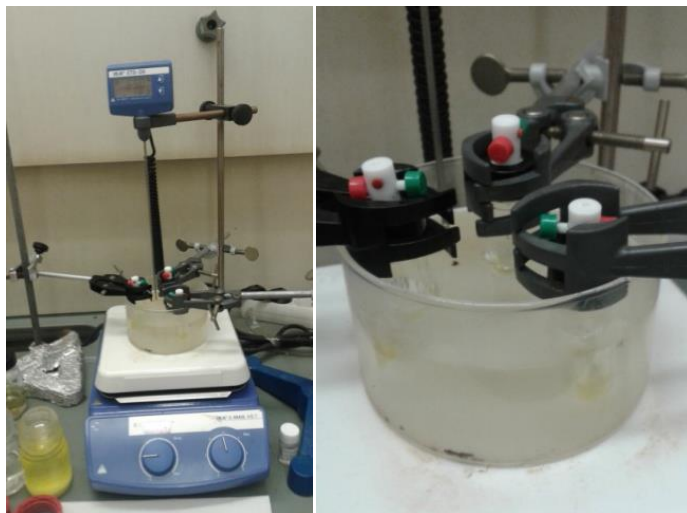


**Fig. 3.60.** - Paraffin bath setting for the ODS reactions.

The initial point ( $t = 0$  min) represents the time when the oxidant, hydrogen peroxide at 30%, is added to the reactor to begin the second stage, the oxidation phase. After 10 minutes of adding the oxygen peroxide, the first sample of oil is taken and is analyzed in a Gas Chromatograph for 20 minutes. The next samples were taken after 30, 60, 120, 180, 240, 300, 360 and 420 minutes after the addition of oxidant to the reactor (**Fig. 3.61**).



**Fig. 3.61.** - Gas Chromatograph used to analyze the ODS samples.

The following table (**Table 3.17**) shows the gas chromatography results of the oxidations performed (three cycles and the studies of half solvent quantity and half oxidant quantity) from the initial addition of hydrogen peroxide ( $t = 0$  min) up to 7 hours later ( $t = 420$  min), representing the quantity of sulfur compounds still present in the oil sample (ppm) and total desulfurization (%).

**Table 3.17.** - Results and comparison of the performance of the Heterogeneous catalyst in ODS in 3 cycles and half the solvent quantity and half oxidant quantity. Representation of the oxidation of the model oil compounds (ppm) and total desulfurization (%), over time (min).

MSNPs-[C <sub>4</sub> MIM]POM catalyst										
t (min)	1st Cycle		2nd Cycle		3rd Cycle		Half Solvent		Half Oxidant	
	ppm	Des. (%)	ppm	Des. (%)	ppm	Des. (%)	ppm	Des. (%)	ppm	Tot. D. (%)
0	1871	0	1824	0	2166	0	2016	0.00	2016	0.00
10	1166	37.65	1060	41.89	1081	50.07	-	-	-	-
30	697	62.75	336	81.57	406	81.22	1220	39.47	815	59.55
60	440	76.46	182	89.98	160	92.60	1490	-	-	-
120	318	82.99	86	95.25	104	95.17	768	61.88	494	75.46
180	284	84.80	56	96.90	64	97.03	593	70.54	-	-
240	-	-	39	97.81	53	97.55	935	-	-	-
300	262	85.95	26	98.55	23	98.94	336	83.30	-	-
360	213	88.60	20	98.88	20	99.05	-	-	-	-
420	243	86.97	-	-	-	-	-	-	-	-

As it was previously explained, some of the points are represented with a “-“, since some results were inconclusive or were not taken.

The three first studies compared the application of the heterogeneous catalyst in the same conditions of solvent quantity, oxidant quantity and model oil quantity. In conclusion, comparing the last sample common time (t = 300 min, 5 hours), it is possible to observe that the 1<sup>st</sup> cycle has the worst results of the three applications, having a total desulfurization of 85.95 %, and the 3<sup>rd</sup> cycle has the best results having a total desulfurization of 98.94 %.

Comparing the same common time samples (t = 120 min, 2 hours), it is confirmed that the use of half the solvent and oxidant quantities in the oxidation processes had the worst results in all of the heterogeneous catalyst application studies, in comparison to the “integral” use in the three cycles. Even having similar results, the use of half solvent quantity had better results having a total desulfurization of 75.46 %, remaining 494.67 ppm of model compounds in the sample, in comparison to the use of half solvent, having a total desulfurization of 61.88 %, remaining 768.57 ppm of model compounds in the sample.

The last two studies performed with half solvent and oxidant quantities applied were problematic since there were used very small quantities of model oil, in comparison to the cycles with optimized quantities. Since there was few oil in the reactors, the oil extraction process was very difficult to keep. Therefore, only a few samples were taken for half solvent (for 5 hours) and for half oxidant (for 2 hours). The fact that an ionic liquid was used as extraction solvent also contributed to the difficult oil extraction process with a syringe.

Overall, comparing all catalyst studies at the same common time (t = 120 min, 2 hours), the best performance catalyst application was the application in the 2<sup>nd</sup> cycle with a total desulfurization of 95.25 % and 86.65 ppm of sulfur compounds remaining in the sample after only 120 minutes.

In the next graph (**Fig. 3.62.**) it is possible to observe the evolution of oxidative reactions using the same catalyst MSNPs-[C<sub>4</sub>MIM]POM, in three equal condition studies, half the solvent quantity study and half the oxidant quantity study (respectively represented in blue, dark green, grey, light green and light blue).

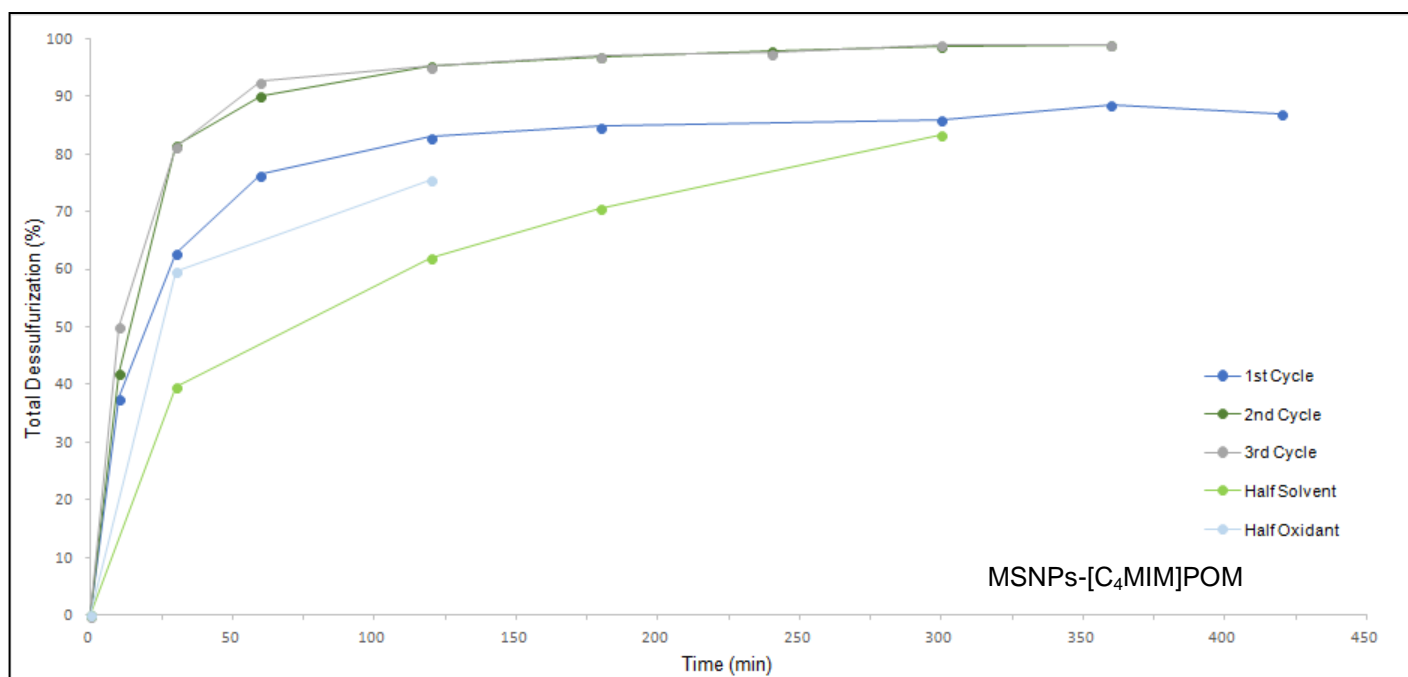


**Fig. 3.62.** - Graphic representation of the Gas Chromatography results of the Oxidative Desulfurization of petroleum model compounds using MSNPs-[C<sub>4</sub>MIM]POM as a Heterogeneous Catalyst.

- **MSNPs-[C<sub>4</sub>Py]POM catalyst**

The experimental protocol was the same as the MSNPs-[C<sub>4</sub>MIM]POM catalyst, using 750 ul of solvent, 75 ul of hydrogen peroxide, 3 mmol of catalyst, 750 ul of model oil and 20 ul of standard solution.

The following table (**Table 3.18.**) shows the gas chromatography results of the three cycle oxidations performed from the initial addition of hydrogen peroxide (t = 0 min) up to 2 hours later (t = 120 min), representing the total desulfurization (%) that occurred.

**Table 3.18.** - Results and comparison of the performance of MSNPs-[C<sub>4</sub>Py]POM catalyst in ODS in 3 cycles Representation of the oxidation of the model oil compounds (ppm) and total desulfurization (%), over time (min).

Time (min)	MSNPs-[C <sub>4</sub> Py]POM catalyst		
	1st Cycle Des. (%)	2nd Cycle Des. (%)	3rd Cycle Des. (%)
0	0.00	0.00	0.00
10	43.42	60.27	48.73
30	93.40	96.16	93.23
60	96.24	98.38	94.57
120	97.82	99.37	94.83

In the next graph (**Fig. 3.63.**) it is possible to observe the evolution of oxidative reactions using the same catalyst MSNPs-[C<sub>4</sub>Py]POM, in three equal condition studies (represented in blue, grey and green).



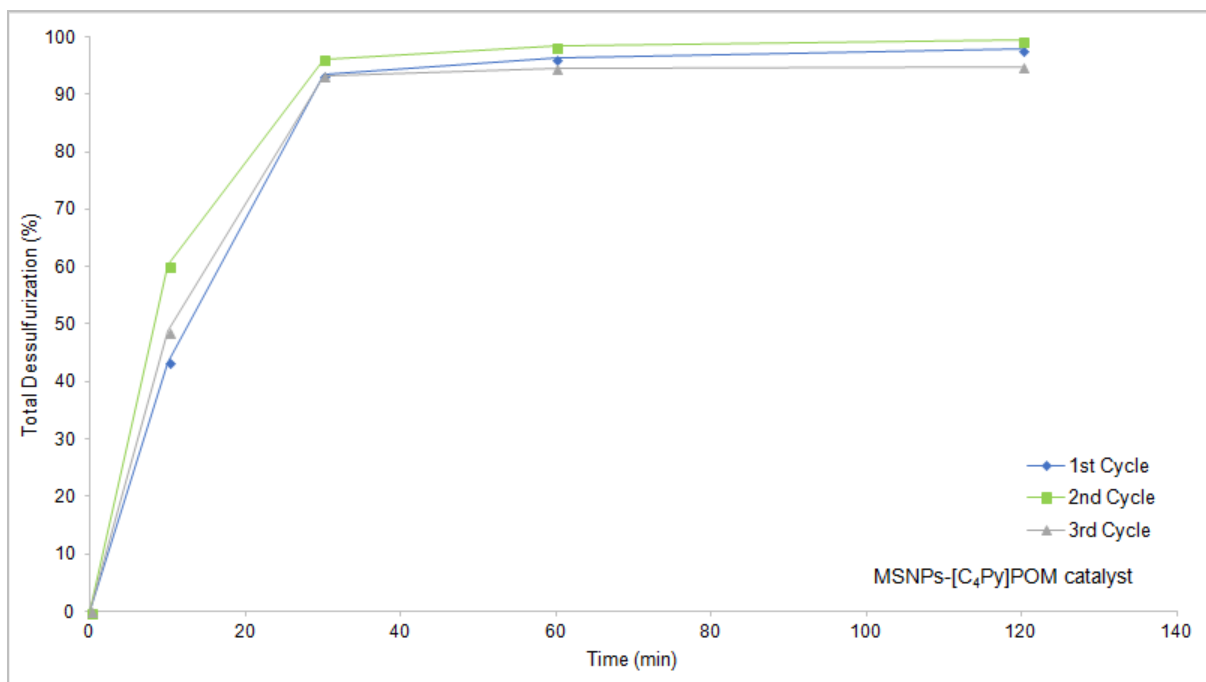


**Fig. 3.63.** - Graphic representation of the Gas Chromatography results of the Oxidative Desulfurization of petroleum model compounds using MSNPs-[C<sub>4</sub>Py]POM as a Heterogeneous Catalyst.

The three studies compared the application of the heterogeneous catalyst in the same conditions of solvent quantity, oxidant quantity and model oil quantity. In conclusion, comparing the last sample common time (t = 120 min, 2 hours), it is possible to observe that the 3<sup>rd</sup> cycle has the worst results of the three applications, having a total desulfurization of 94.83 %, and the 2<sup>nd</sup> cycle has the best results having a total desulfurization of 99.37 %.

- **MSNPs-[N<sub>4,4,4,4</sub>]POM catalyst**

The experimental protocol was the same as the MSNPs-[C<sub>4</sub>MIM]POM catalyst, using 750 ul of solvent, 75 ul of hydrogen peroxide, 3 mmol of catalyst, 750 ul of model oil and 20 ul of standard solution.

The following table (**Table 3.19.**) shows the gas chromatography results of the three cycle oxidations performed from the initial addition of hydrogen peroxide (t = 0 min) up to 3 hours later (t = 180 min), representing the total desulfurization (%) that occurred.

**Table 3.19.** - Results and comparison of the performance of MSNPs-[N<sub>4,4,4,4</sub>]POM catalyst in ODS in 3 cycles Representation of the oxidation of the model oil compounds (ppm) and total desulfurization (%), over time (min).

Time (min)	MSNPs-[N <sub>4,4,4,4</sub> ]POM catalyst		
	1st Cycle Des. (%)	2nd Cycle Des. (%)	3rd Cycle Des. (%)
0	0.00	0.00	0.00
10	34.14	85.76	80.07
30	66.33	95.13	93.32
60	88.53	98.40	98.39
120	97.98	100.00	100.00
180	100.00	100.00	100.00

In the next graph (**Fig. 3.64.**) it is possible to observe the evolution of oxidative reactions using the same catalyst MSNPs-[C<sub>4</sub>Py]POM, in three equal condition studies (represented in blue, grey and green).

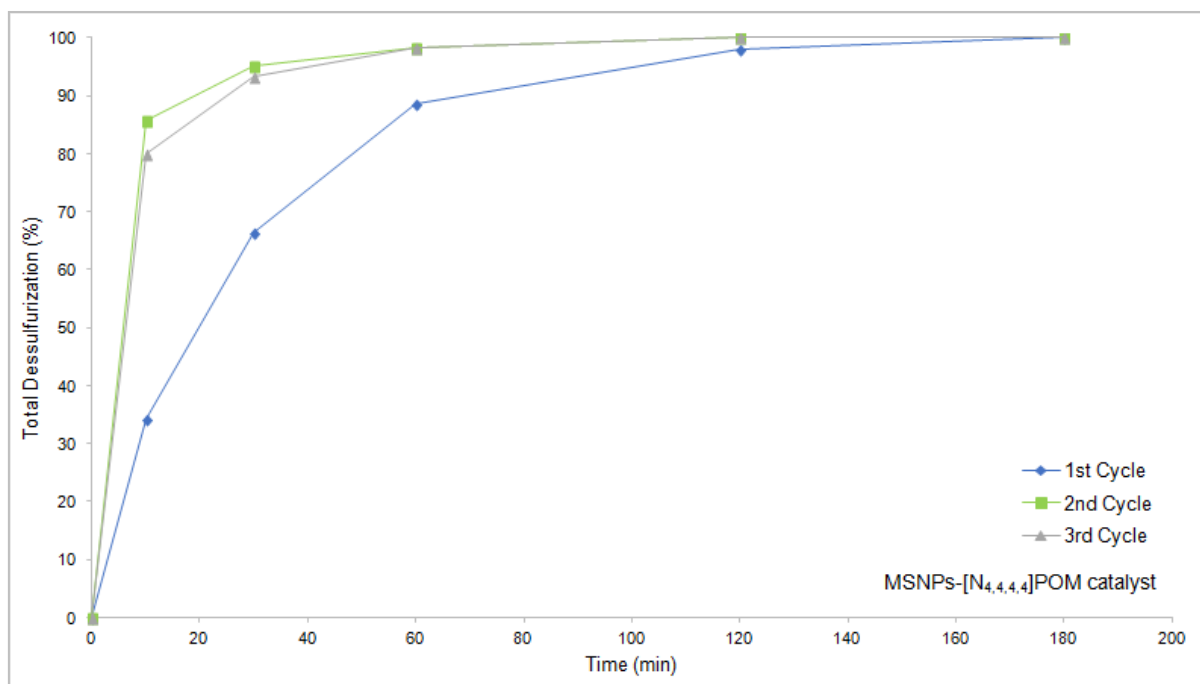


**Fig. 3.64.** - Graphic representation of the Gas Chromatography results of the Oxidative Desulfurization of petroleum model compounds using MSNPs-[N<sub>4,4,4,4</sub>]POM as a Heterogeneous Catalyst.

The three studies compared the application of the heterogeneous catalyst in the same conditions of solvent quantity, oxidant quantity and model oil quantity. In conclusion, comparing the last sample common time (t = 180 min, 3 hours), it is possible to observe that all the three catalysts achieved 100 % of desulfurization. The 2<sup>nd</sup> and 3<sup>rd</sup> cycle had the best results, already achieving 100 % 1 hour before.

After analyzing the final results of the study of the Homogenous and Heterogeneous catalysts used in the Oxidative Desulfurization of 1-BT, DBT, 4-MDBT and 4,6-DMDBT, it is possible to conclude that the Heterogeneous catalysts (specifically MSNPs-[N<sub>4,4,4,4</sub>]POM) had the best performance of the six catalysts studied, reaching a total desulfurization of 100% after only 2 hours (**Table 3.20.**).

**Table 3.20.** - Comparison of the performance of Homogeneous catalysts in ODS, over time (min).

t (min)	Homogeneous Catalysts		
	[N <sub>4,4,4,4</sub> ] <sub>3</sub> [PMo <sub>12</sub> O <sub>40</sub> ]	[C <sub>4</sub> MIM] <sub>3</sub> [PMo <sub>12</sub> O <sub>40</sub> ]	[C <sub>4</sub> Py] <sub>3</sub> [PMo <sub>12</sub> O <sub>40</sub> ]
0	0.00	0.00	0.00
10	53.92	-	41.37
30	68.66	62.16	56.72
60	-	81.03	82.08
120	92.60	83.19	82.72
180	96.95	84.40	83.26
240	98.06	79.04	82.24
300	97.86	85.47	78.11
360	97.96	84.90	86.61

Comparing the three Homogeneous catalysts, it is also possible to conclude that after 6 hours the catalyst with best performance was  $[N_{4,4,4,4}]_3[PMo_{12}O_{40}]$  with 97.96% of total desulfurization, followed by  $[C_4Py]_3[PMo_{12}O_{40}]$  (86.61 %) and  $[C_4MIM]_3[PMo_{12}O_{40}]$  (84.90 %) (**Fig. 3.65**).

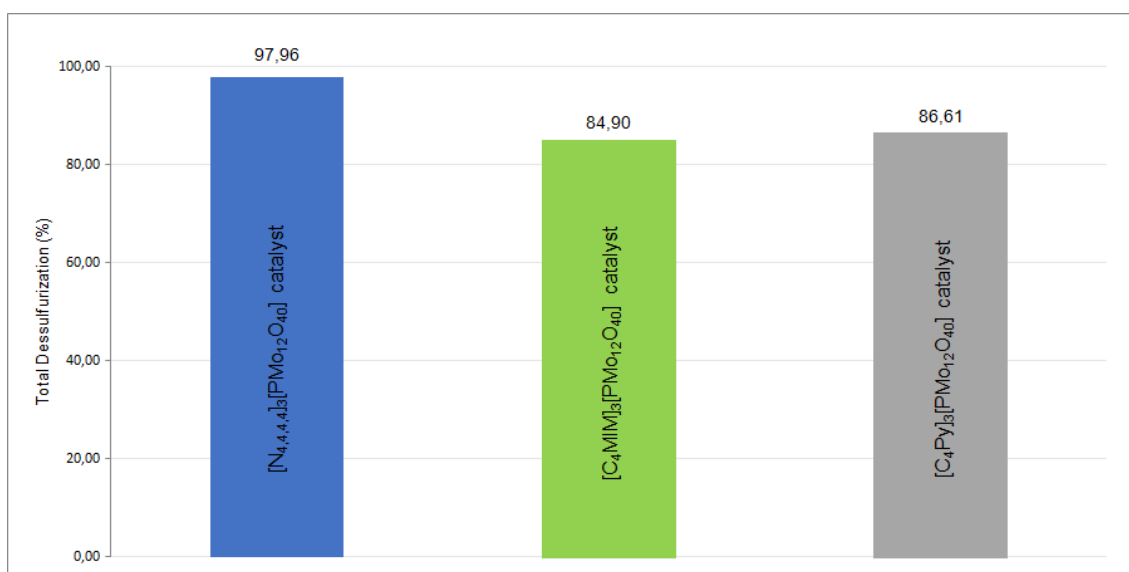


**Fig. 3.65.** - Graphic representation of the total desulfurization obtained (in percentage) of Homogeneous Catalysts after 6 hours of oxidation.

**Table 3.21.** - Comparison of the performance of Heterogeneous catalysts and Heterogeneous catalyst in ODS, over time (in minutes).

t (min)	Heterogeneous Catalysts		
	MSNPs- $[N_{4,4,4,4}]POM$	MSNPs- $[C_4MIM]POM$	MSNPs- $[C_4Py]POM$
0	0.00	0.00	0.00
10	85.76	50.07	60.27
30	95.13	81.22	96.16
60	98.4	92.60	98.38
120	100.0	95.17	99.37
180	100.0	97.03	-

Comparing the three Heterogeneous catalysts, it is also possible to conclude that after only 2 hours the catalyst with best performance was MSNPs- $[N_{4,4,4,4}]POM$  achieving 100% of total desulfurization, followed by MSNPs- $[C_4Py]POM$  (99.37 %) and MSNPs- $[C_4MIM]POM$  (95.25 %) (**Fig. 3.66**).

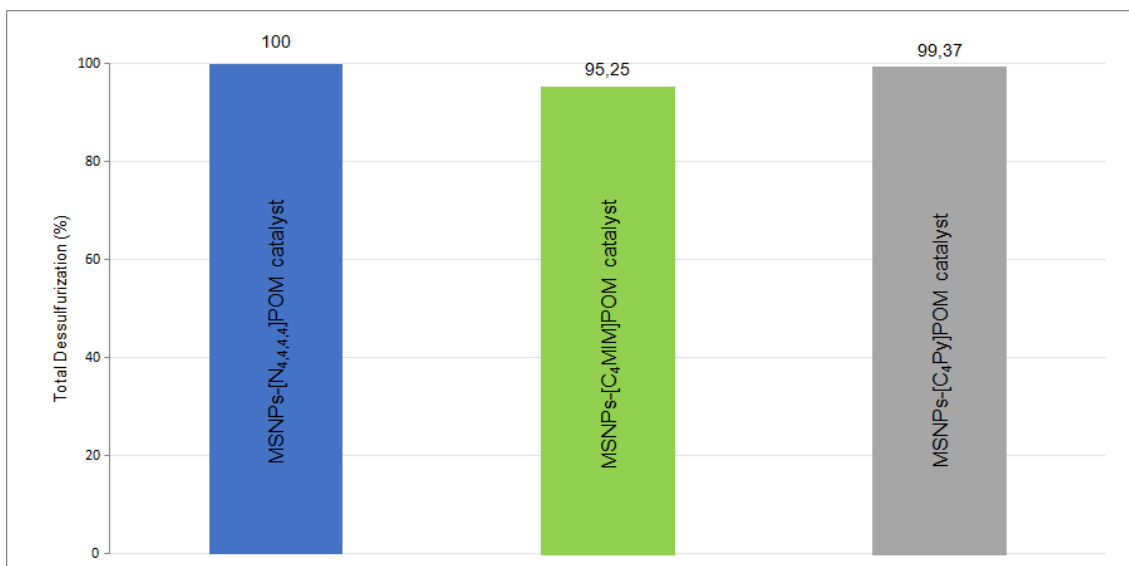


**Fig. 3.66.** - Graphic representation of the total desulfurization obtained (in percentage) of Heterogeneous Catalysts after 2 hours of oxidation.

The results obtained show that cation tetrabutylammonium  $[N_{4,4,4,4}]^+$  had the best results in both forms of catalyst, followed by cation pyridinium  $[C_4Py]^+$ . Heterogeneous catalysts have also confirmed to be the best catalysts in the Oxidative Desulfurization reactions performed

In the end, all six catalysts had excellent results and have a promising future as catalysts in the oxidative desulfurization of petroleum model compounds for a “greener” future.





## 4. Conclusion

In this work, new heterogeneous catalysts based on mesoporous silica nanoparticles (MSNPs) with different cations of ionic liquids (ILs) covalently bonded to their surface, 1-Butyl-3-methylimidazolium ([C<sub>4</sub>MIM]), 1-butylpyridinium ([C<sub>4</sub>Py]) and Tetrabutylammonium ([N<sub>4,4,4,4</sub>]), and with the polyoxometalate (POM) derived from phosphomolybdic acid ([H<sub>(3-x)</sub>PMo<sub>12</sub>O<sub>40</sub>]<sup>x-</sup>) as anions were prepared. Their analogous homogeneous compounds were also prepared for comparison (POM-ILs): [N<sub>4,4,4,4</sub>]<sub>3</sub>[PMo<sub>12</sub>O<sub>40</sub>], [C<sub>4</sub>MIM]<sub>3</sub>[PMo<sub>12</sub>O<sub>40</sub>] and [C<sub>4</sub>Py]<sub>3</sub>[PMo<sub>12</sub>O<sub>40</sub>]. All catalysts were characterized by several solution and solid state techniques that confirm their successful preparation.

The homogeneous catalysts and the polyoxometalate H<sub>3</sub>PMo<sub>12</sub>O<sub>40</sub> were tested in the catalytic oxidation of lignin model compounds: cinnamyl alcohol and guaiacol. The cinnamyl alcohol oxidations had promising results in comparison to the guaiacol oxidation. The first tests applied to the model compounds using conventional heating were performed in equal conditions in order to compare the results. <sup>1</sup>H NMR spectroscopy allowed to observe that for the guaiacol oxidation no product was formed. Therefore, it is possible to conclude that maybe the conditions that were used in this study, e.g. oxidant quantity, were not optimized to continue the study of this oxidation reaction.

The study continued with the oxidation of cinnamyl alcohol since it had promising results. By analyzing the obtained <sup>1</sup>H NMR spectra when using conventional heating, it was possible to observe that there was product formed when using [N<sub>4,4,4,4</sub>]<sub>3</sub>[PMo<sub>12</sub>O<sub>40</sub>] as catalyst with hydrogen peroxide, and H<sub>3</sub>PMo<sub>12</sub>O<sub>40</sub> as catalyst without hydrogen peroxide. Also, when using oxidant H<sub>2</sub>O<sub>2</sub> and microwave heating, new products were formed when using catalysts H<sub>3</sub>PMo<sub>12</sub>O<sub>40</sub>, [C<sub>4</sub>MIM]<sub>3</sub>[PMo<sub>12</sub>O<sub>40</sub>] and [C<sub>4</sub>Py]<sub>3</sub>[PMo<sub>12</sub>O<sub>40</sub>]. In ODS studies, both heterogeneous and homogeneous catalysts were tested.

Comparing the performance of the different catalysts, it was shown that the application of the heterogeneous catalysts had better results in less reaction time, in comparison to the application of homogeneous catalysts. Interestingly, the cation tetrabutylammonium had the best results in both homogeneous and heterogeneous catalysts, achieving, respectively, 98% (in 6 hours) and 100% (in 2 hours) of total desulfurization. The recycling study of the ODS process was also performed, showing that the catalytic activity was improved in second and third cycles for MSNPs-[N<sub>4,4,4,4</sub>]POM.

Two additional studies of the application of the heterogeneous catalyst based on cation imidazolium, MSNPs-[C<sub>4</sub>MIM]POM, with half the solvent and half oxidant (comparing to the three "normal" cycles) were performed. These studies had the worst results compared to the others, obtaining only 83% and 75% of total desulfurization. Even though the values obtained are low compared to the others studies, the results are still very positive. By this way, it is possible to conclude that these new materials can be promising in ODS catalysis, since excellent results in the removal of 1-benzothiophene and derivatives from the petroleum model oil were obtained.





## **5. Future Perspectives**

The prepared heterogeneous and homogeneous catalysts had interesting results in both applications tested: the catalytic oxidation of cinnamyl alcohol (a lignin model compound) and the oxidative desulfurization of a petroleum model oil.

In terms of the oxidation of cinnamyl alcohol, if there was more time to optimize the conditions of the catalytic processes tested, the first test that would be made is to change the solvent used, using an ionic liquid as a solvent instead of acetonitrile in microwave heating. When acetonitrile was used in a domestic microwave, it was necessary to constantly stop the microwave heating process to stir the mixture. Therefore, the advantage of using an ionic liquid is that it wouldn't be necessary to stop the reaction to stir the mixture after only a few seconds, making it possible to perform a continuous oxidation process.

In the future, new catalytic oxidations of model compounds of lignin can be explored and optimized in order to answer some questions such as: What can influence the efficiency of the catalytic process? Are the heterogeneous catalysts more promising than the homogeneous catalysts? Is it better the use of an ionic liquid or a conventional solvent for applying these materials into the catalytic process? Is it better to use conventional heating or microwave heating in these processes? If microwave heating is used, what is the best time?

The results obtained prove that it is possible to apply the innovative catalysts in the catalytic oxidation of lignin model compound cinnamyl alcohol. By this way, it is possible to affirm that the future is promising for these new catalysts in the valorization of lignin.

When referring to the ODS process of a petroleum model compound, both homogeneous and heterogeneous catalysts had excellent results. As it was mentioned before, all heterogeneous catalysts achieved almost 100 % of total desulfurization in only a few hours, and homogeneous catalysts about 80% to 95%. The performance and stability of the heterogeneous catalysts should be studied in more detail using a higher number of consecutive cycles and characterizing the catalyst after the cycles. These results are very interesting for the future of oil desulfurization and, consequently, for reducing SO<sub>x</sub> compounds released to the atmosphere from combustion of fuels. It would be very interesting to apply these new catalysts in a real sample of diesel.

With the obtained results, it is possible to affirm that the new heterogeneous and homogeneous catalysts prepared based on ionic liquids and polyoxometalates have a bright future in Green Chemistry, contributing to a greener future.



# Annexes

## A.1. NMR Spectroscopy

### Solution NMR Spectroscopy

#### - $^1\text{H}$ NMR

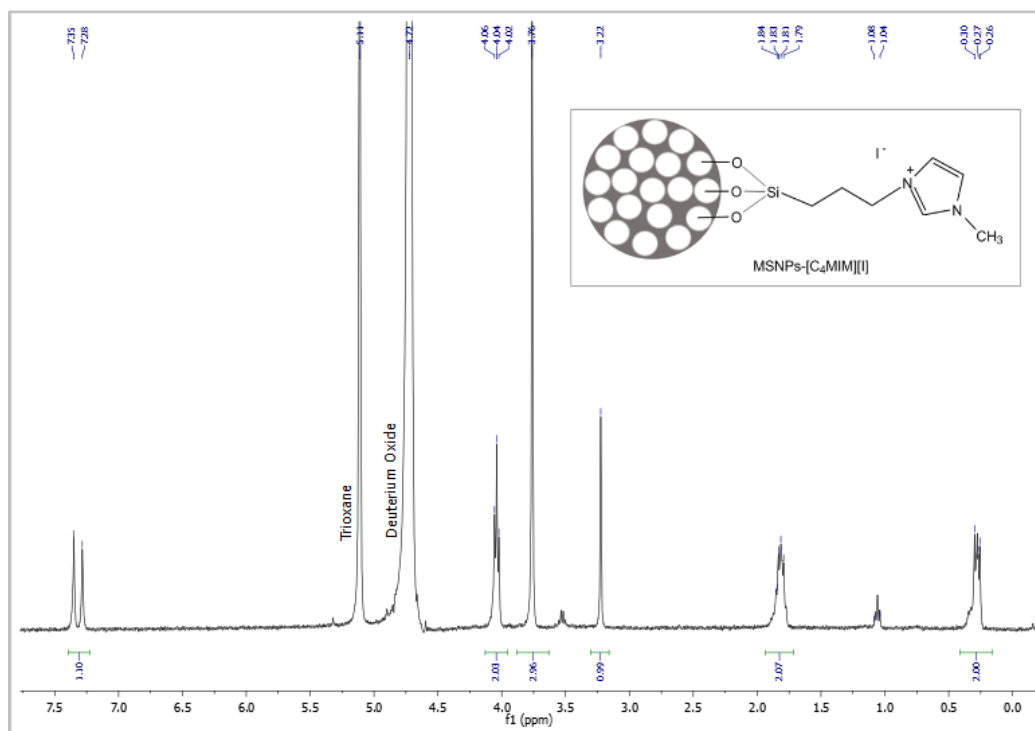


Fig. A.1.1. -  $^1\text{H}$  NMR (400.13 MHz, D<sub>2</sub>O + NaOH, 25 °C) of MSNPs-[C<sub>4</sub>MIM][I].

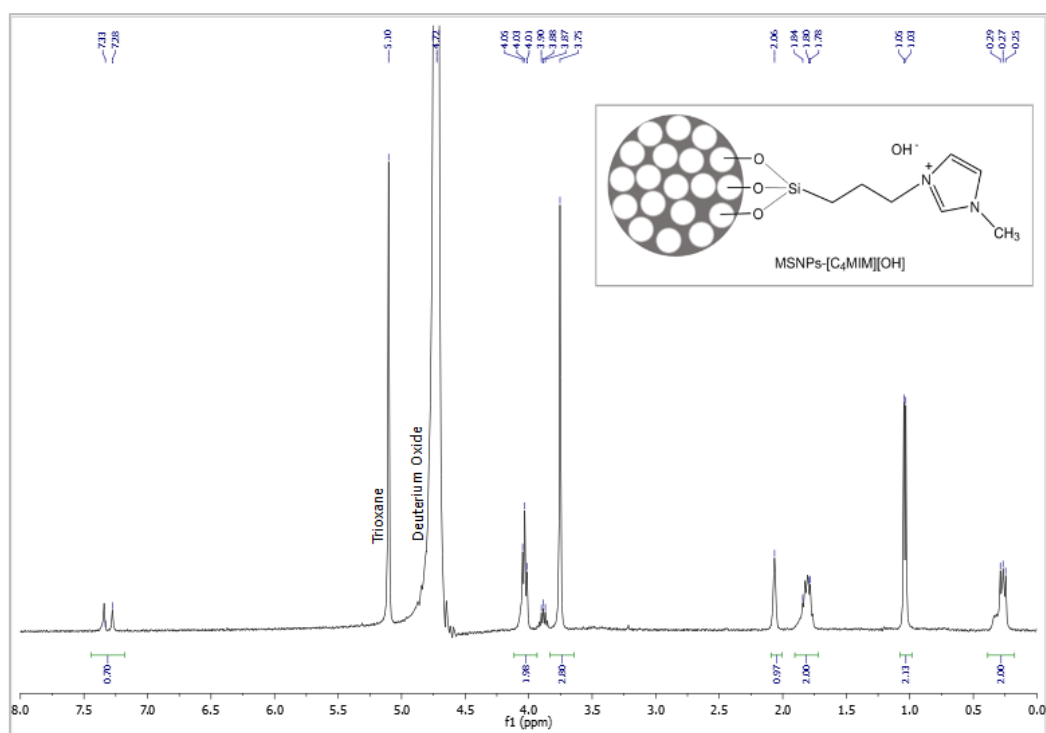
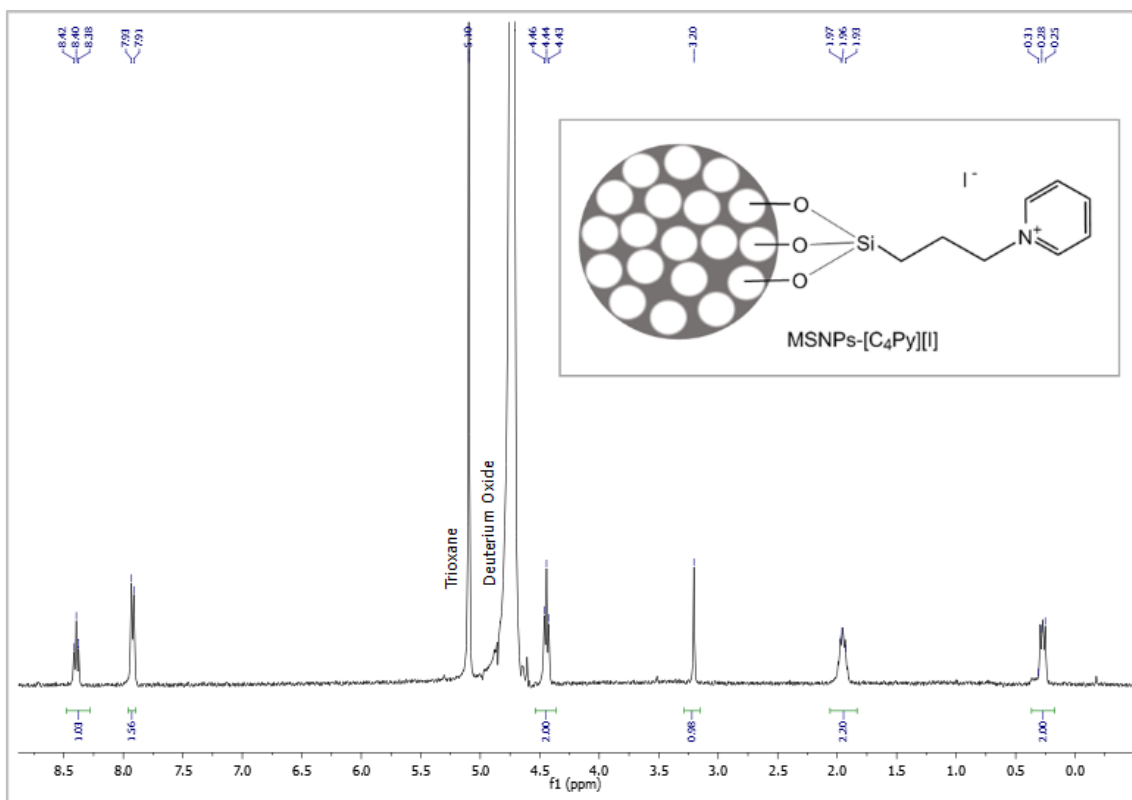
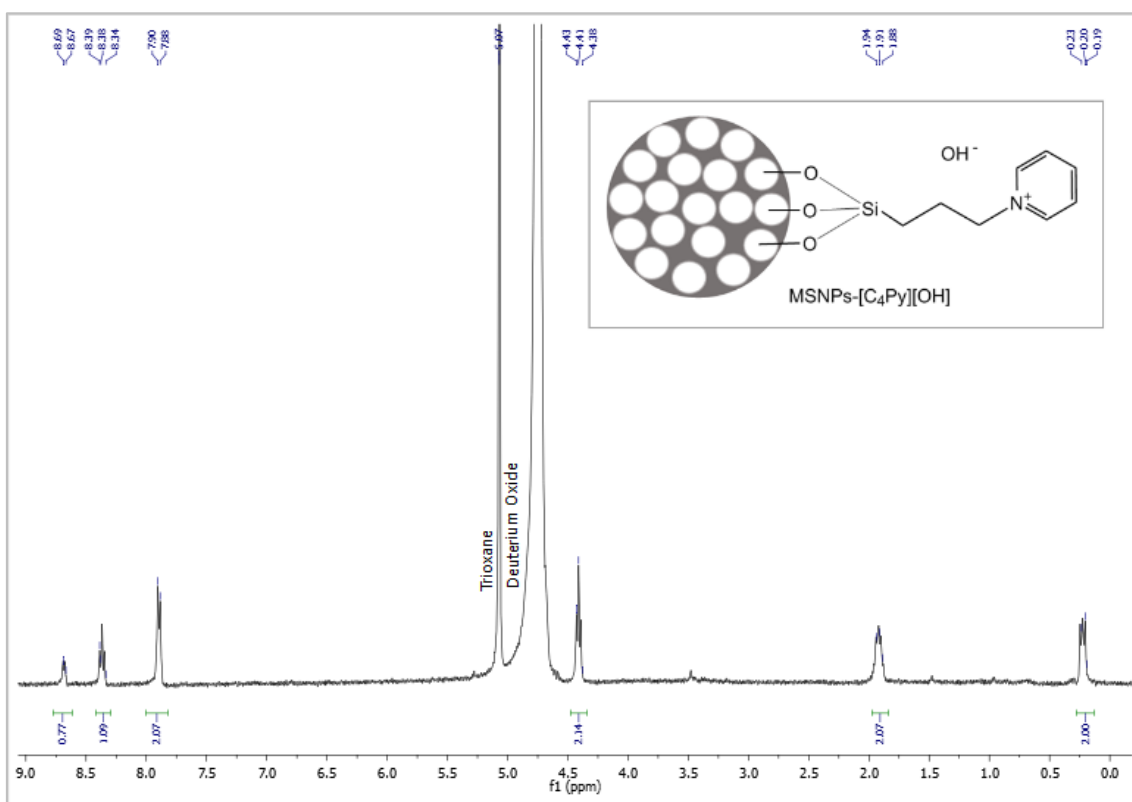


Fig. A.1.2. -  $^1\text{H}$  NMR (400.13 MHz, D<sub>2</sub>O + NaOH, 25 °C) of MSNPs-[C<sub>4</sub>MIM][OH].



**Fig. A.1.3.** - <sup>1</sup>H NMR (400.13 MHz, D<sub>2</sub>O + NaOH, 25 °C) of MSNPs-[C<sub>4</sub>Py][I].



**Fig. A.1.4.** - <sup>1</sup>H NMR (400.13 MHz, D<sub>2</sub>O + NaOH, 25 °C) of MSNPs-[C<sub>4</sub>Py][OH].

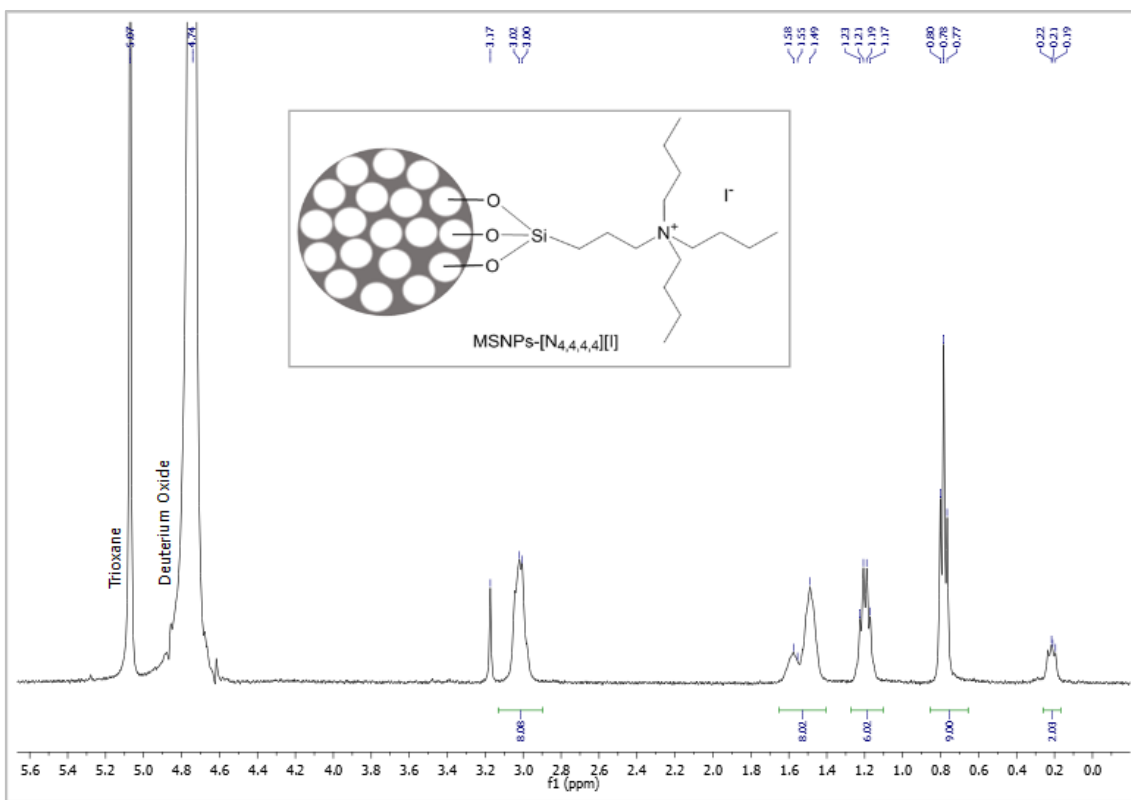


**Fig. A.1.5.** -  $^1\text{H}$  NMR (400.13 MHz, D<sub>2</sub>O + NaOH, 25 °C) of MSNPs-[N<sub>4,4,4,4</sub>][I].

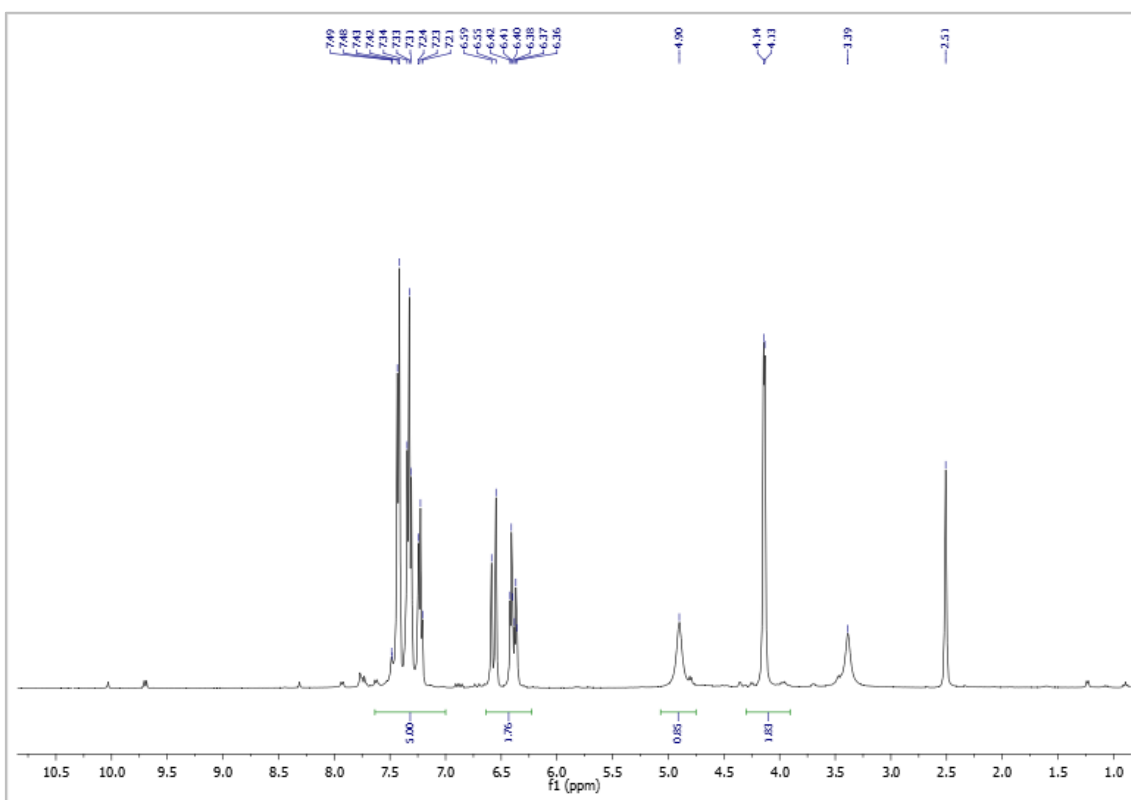


**Fig. A.1.6.** -  $^1\text{H}$  NMR (400.13 MHz, DMSO d<sub>6</sub>, 25 °C) of lignin model compound, cinnamyl alcohol.

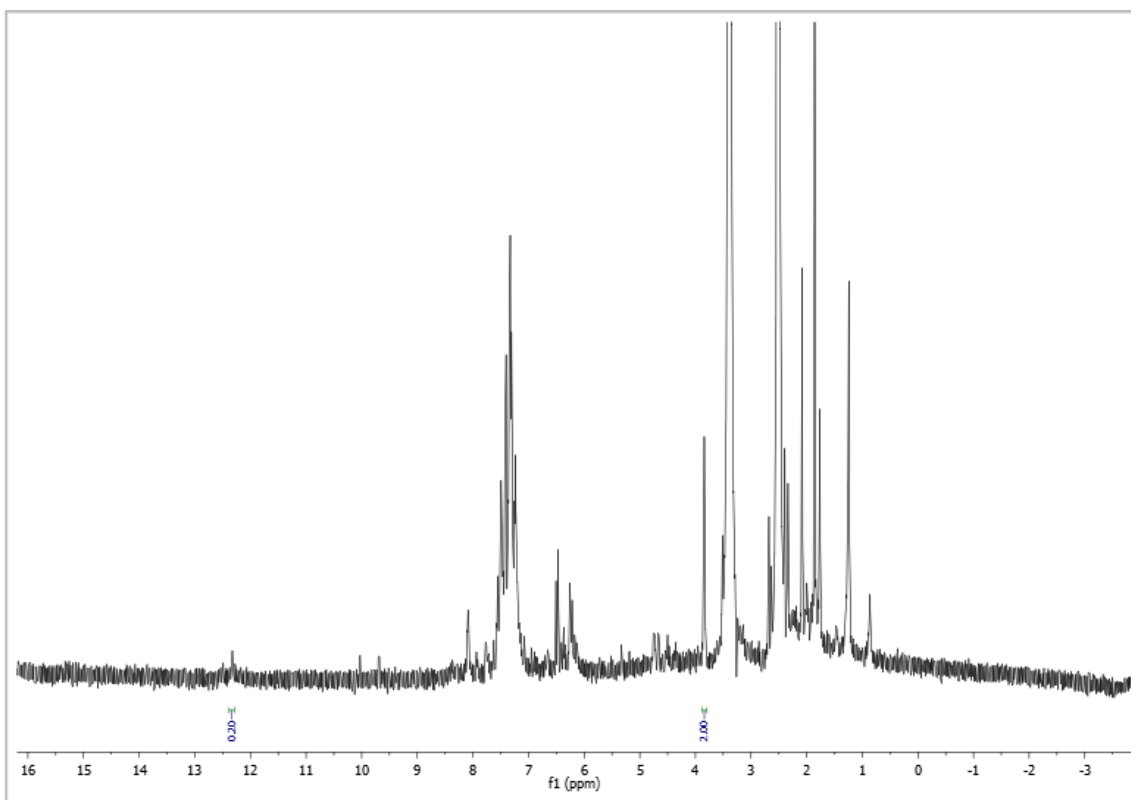


**Fig. A.1.7.** - <sup>1</sup>H NMR (400.13 MHz, DMSO d<sub>6</sub>, 25 °C) of the catalysis of cinnamyl alcohol using H<sub>3</sub>PMo<sub>12</sub>O<sub>40</sub> as catalyst, in conventional heating.

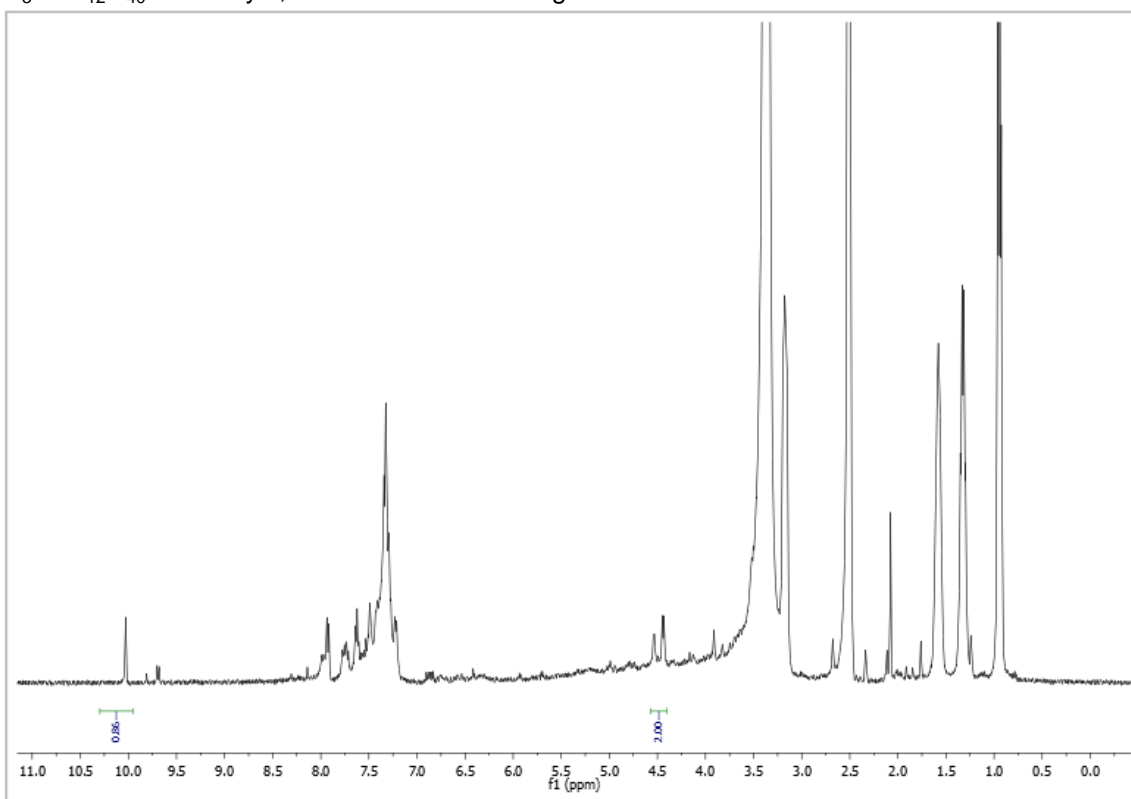


**Fig. A.1.8.** - <sup>1</sup>H NMR (400.13 MHz, DMSO d<sub>6</sub>, 25 °C) of the catalysis of cinnamyl alcohol using H<sub>2</sub>O<sub>2</sub> (30%) and [N<sub>4,4,4,4</sub>]<sub>3</sub>[PMo<sub>12</sub>O<sub>40</sub>] as catalyst, in conventional heating.

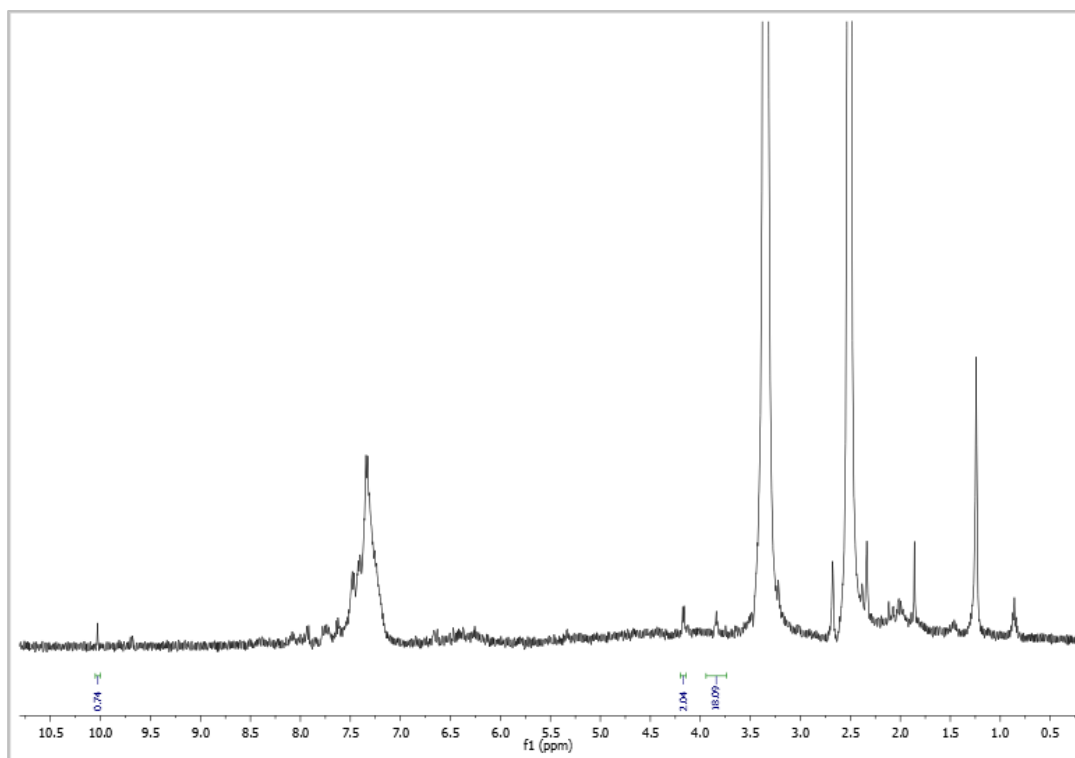


**Fig. A.1.9.** -  $^1\text{H}$  NMR (400.13 MHz, DMSO  $d_6$ , 25 °C) of the catalysis of cinnamyl alcohol using  $\text{H}_3\text{PMo}_{12}\text{O}_{40}$  as catalyst, in microwaves.

-  $^{31}\text{P}$  NMR

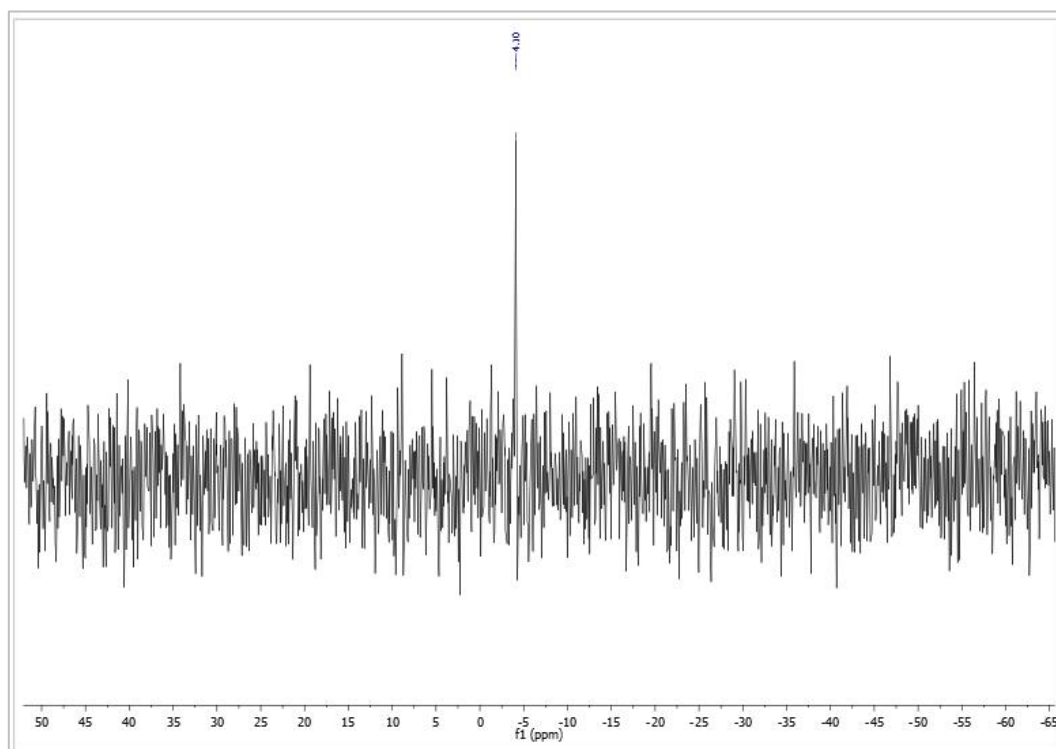


**Fig. A.1.10.** -  $^{31}\text{P}$  NMR (100.61 MHz, DMSO  $d_6$ , 25 °C) of  $[\text{N}_{4,4,4,4}]_3[\text{PMo}_{12}\text{O}_{40}]$  catalyst.

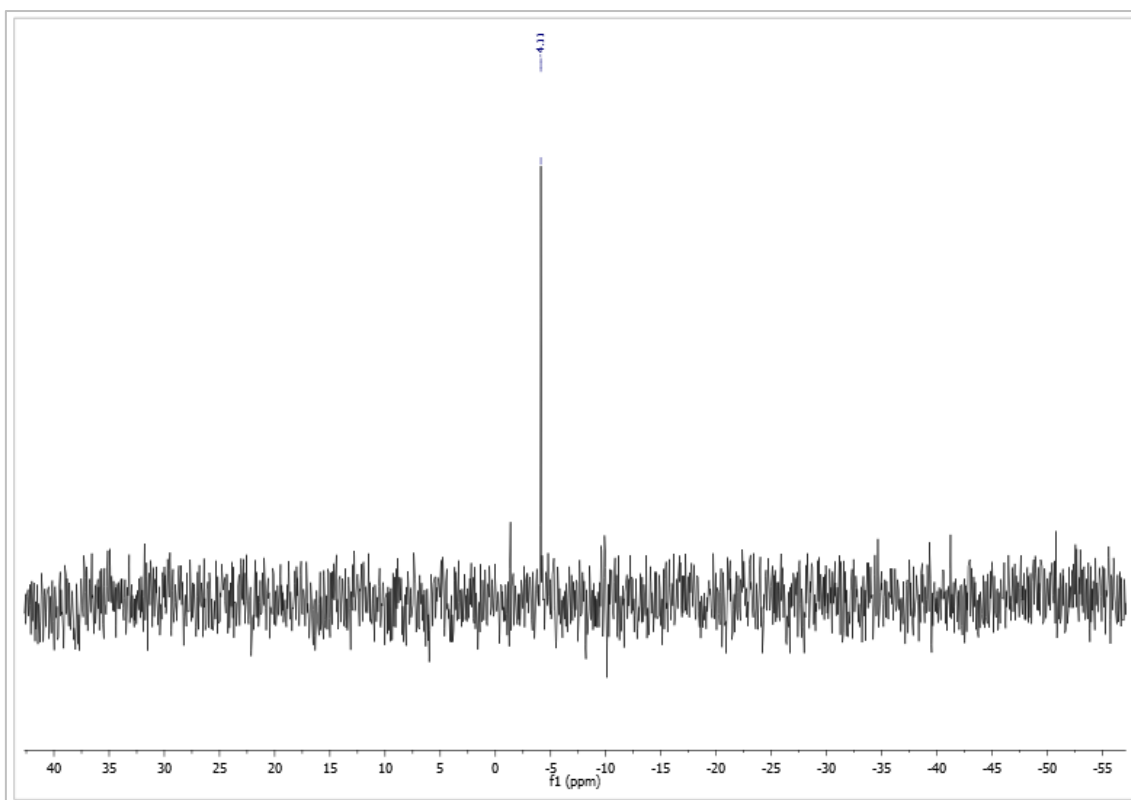


**Fig. A.1.11.**  $^{31}\text{P}$  NMR (100.61 MHz, DMSO  $d_6$ , 25  $^\circ\text{C}$ ) of  $[\text{C}_4\text{MIM}]_3[\text{PMo}_{12}\text{O}_{40}]$  catalyst.

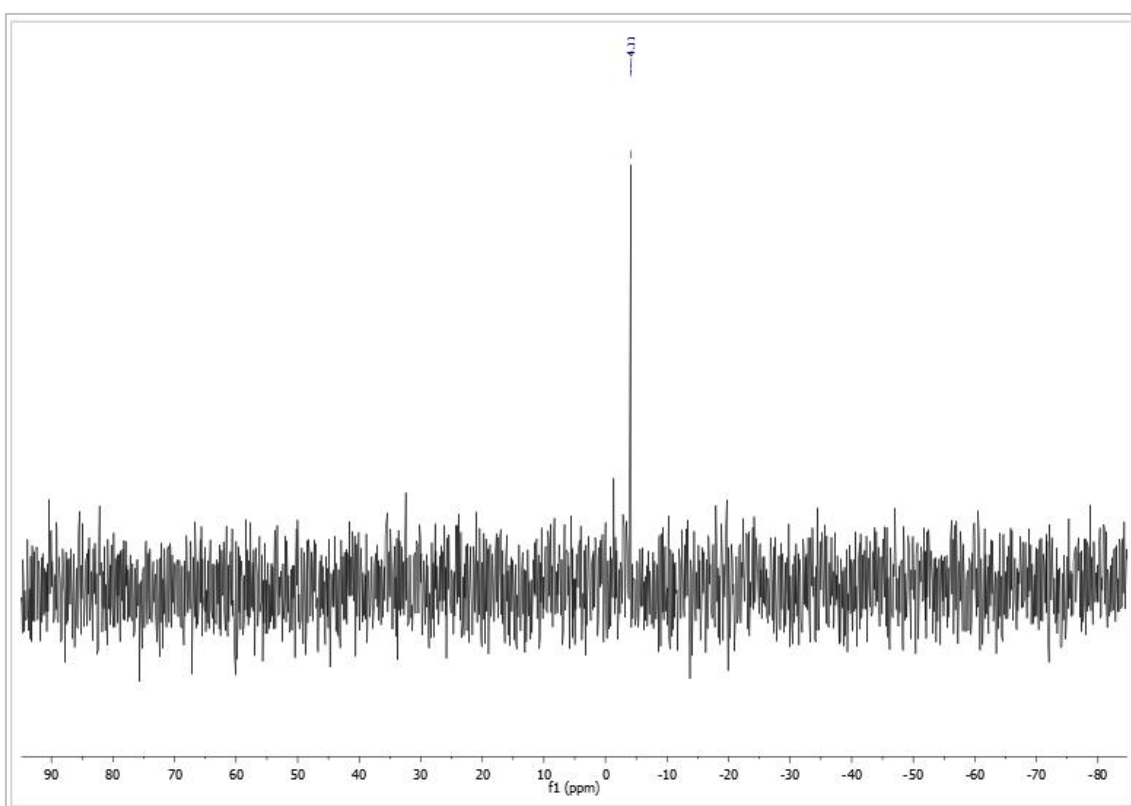


**Fig. A.1.12.**  $^{31}\text{P}$  NMR (100.61 MHz, DMSO  $d_6$ , 25  $^\circ\text{C}$ ) of  $[\text{C}_4\text{Py}]_3[\text{PMo}_{12}\text{O}_{40}]$  catalyst.



## Solid State CP MAS NMR

### - $^{13}\text{C}$ CP MAS NMR

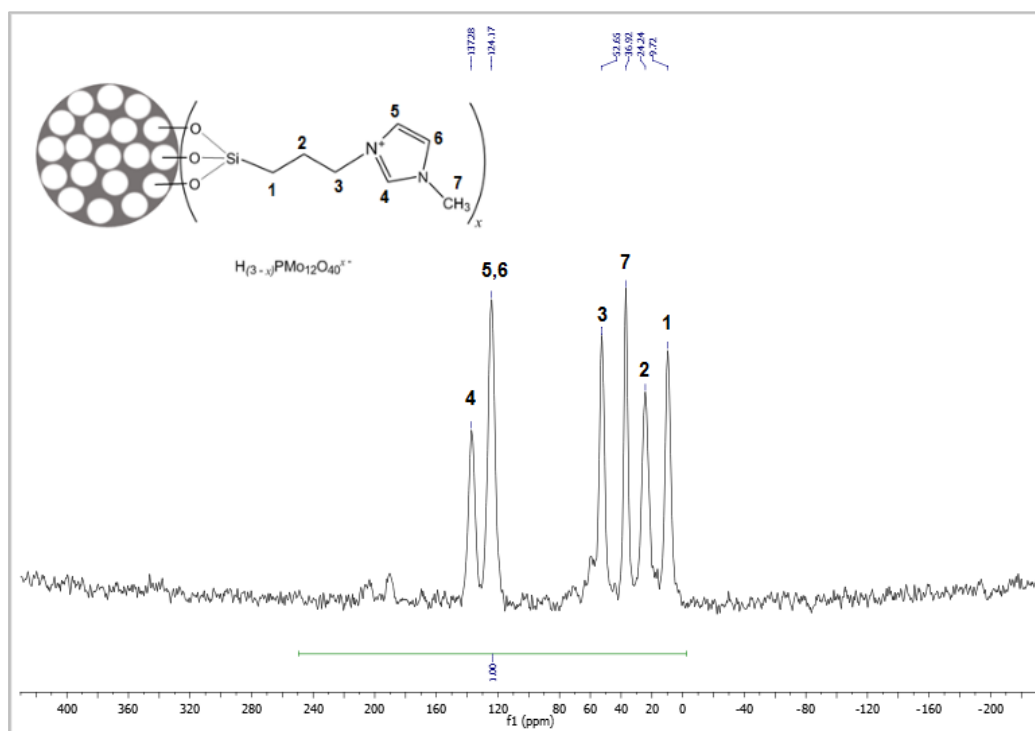


**Fig. A.1.13.** - Solid State  $^{13}\text{C}$  CP MAS NMR (162 MHz, 25 °C) of MSNPs-[C<sub>4</sub>MIM]POM catalyst.

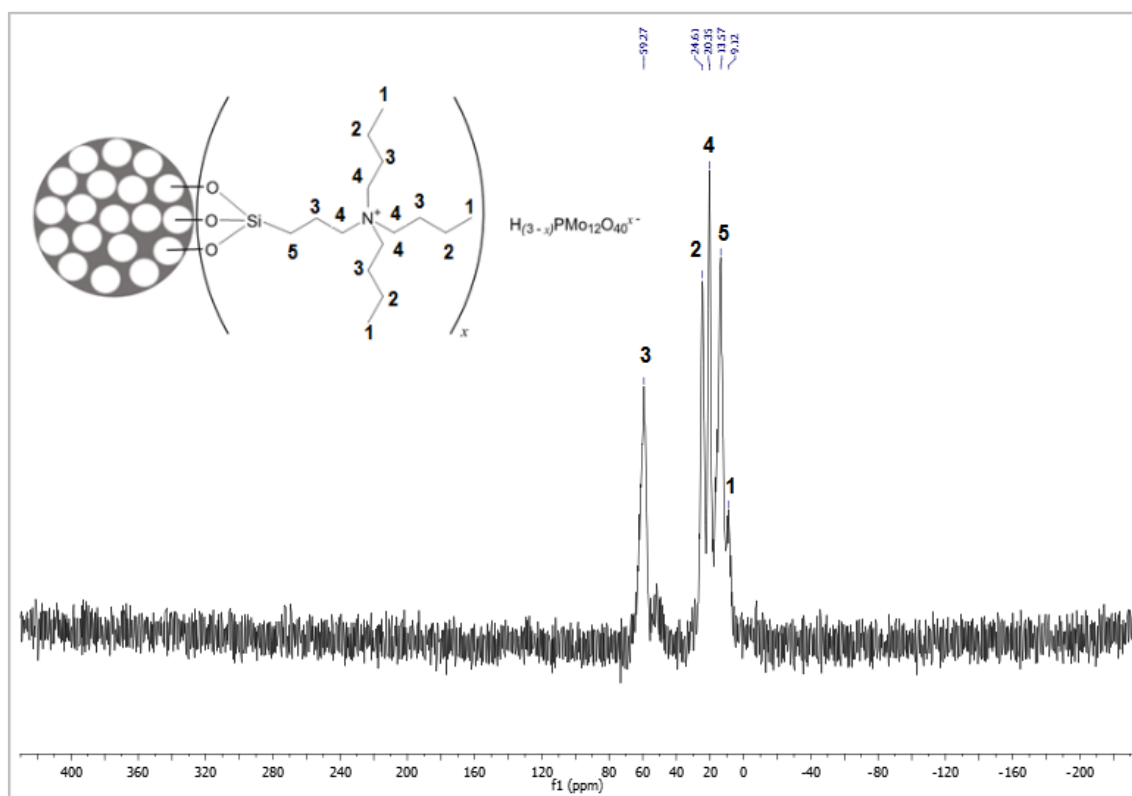


**Fig. A.1.14.** - Solid State  $^{13}\text{C}$  CP MAS NMR (162 MHz, 25 °C) of MSNPs-[N<sub>4,4,4,4</sub>]POM catalyst.

-  $^{31}\text{P}$  CP MAS NMR

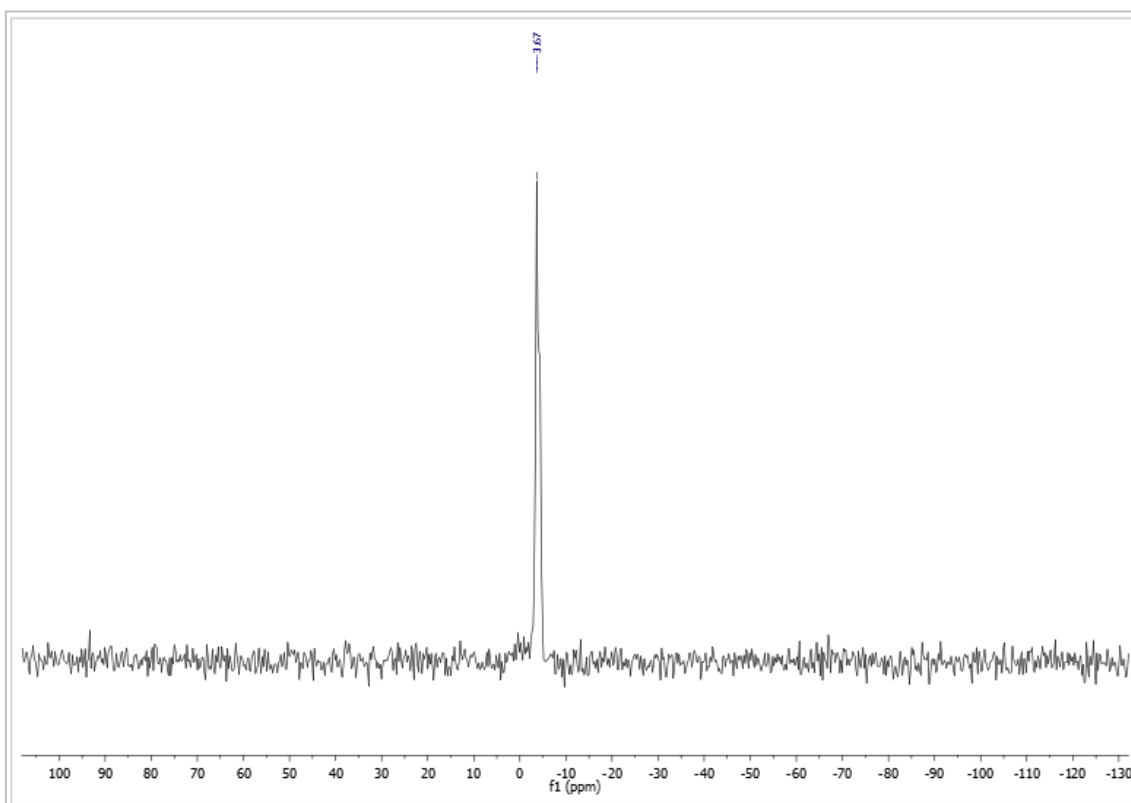


**Fig. A.1.15.** - Solid State  $^{31}\text{P}$  CP MAS NMR (100.61 MHz, 25 °C) of MSNPs-[C<sub>4</sub>MIM]POM catalyst.

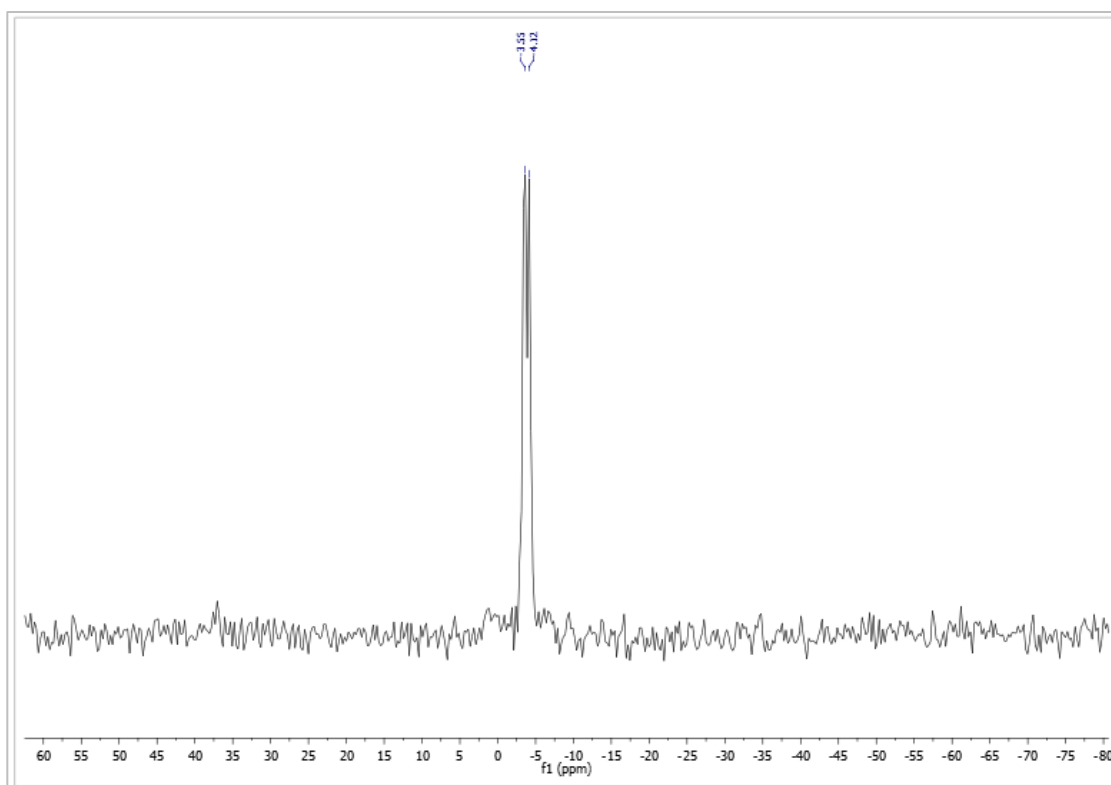


**Fig. A.1.16.** - Solid State  $^{31}\text{P}$  CP MAS NMR (100.61 MHz, 25 °C) of MSNPs-[N<sub>4,4,4,4</sub>]POM catalyst.

## A.2. Fourier-Transform Infrared (FTIR) Spectroscopy

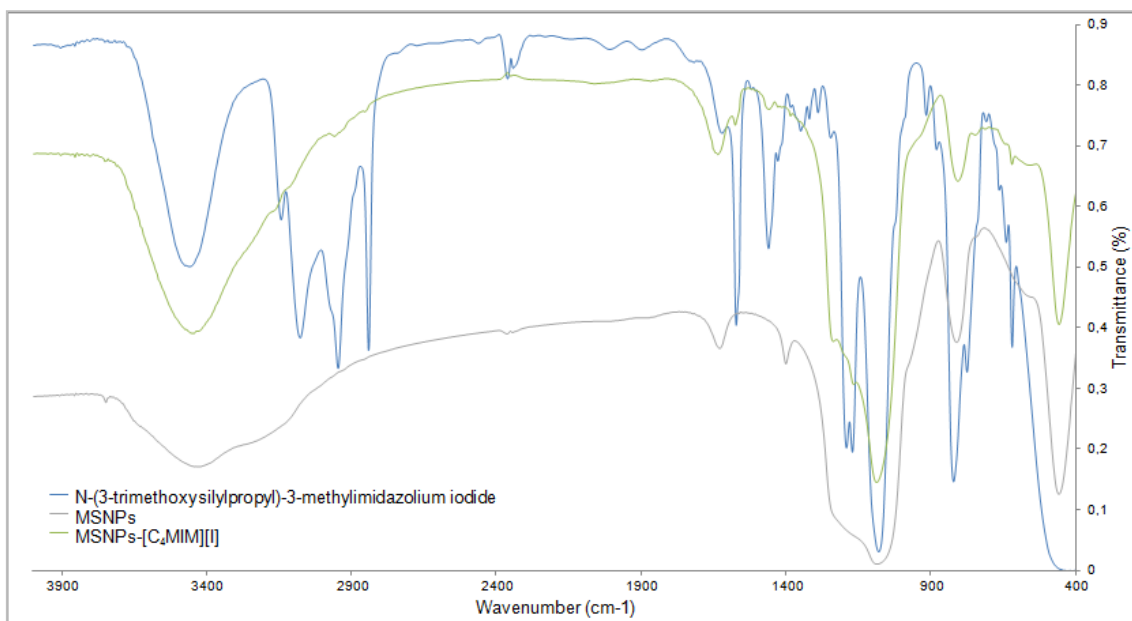


**Fig. A.2.1.** – FTIR spectra of MSNPs-[C<sub>4</sub>MIM][I], N-(3-trimethoxysilylpropyl)-3-methylimidazolium iodide and MSNPs.

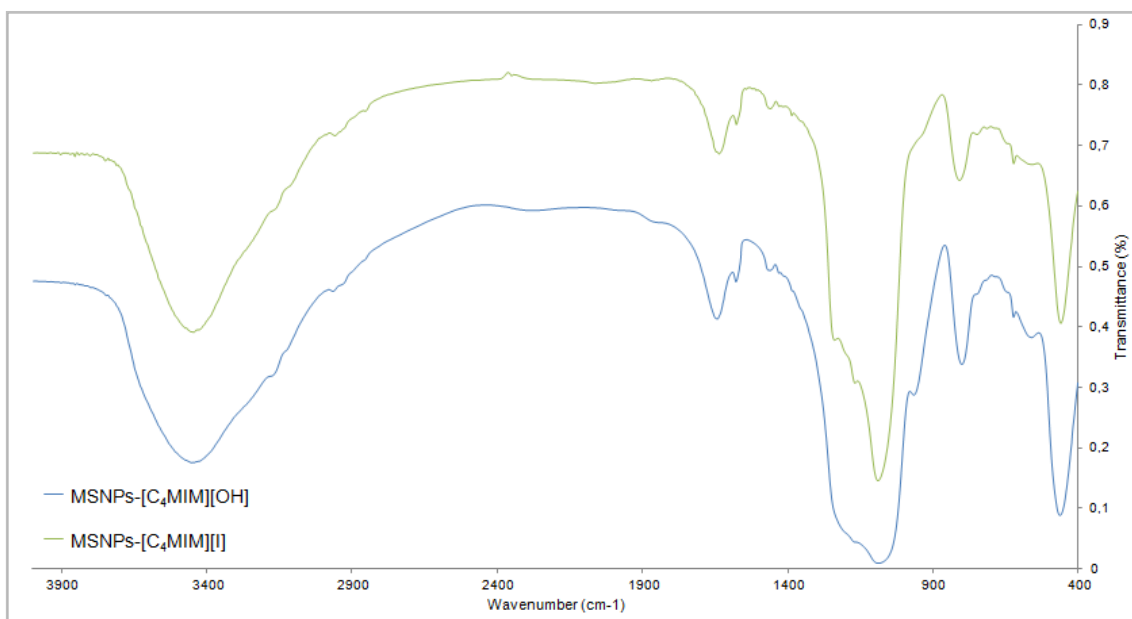


**Fig. A.2.2.** – FTIR spectra of MSNPs-[C<sub>4</sub>MIM][I] and MSNPs-[C<sub>4</sub>MIM][OH].

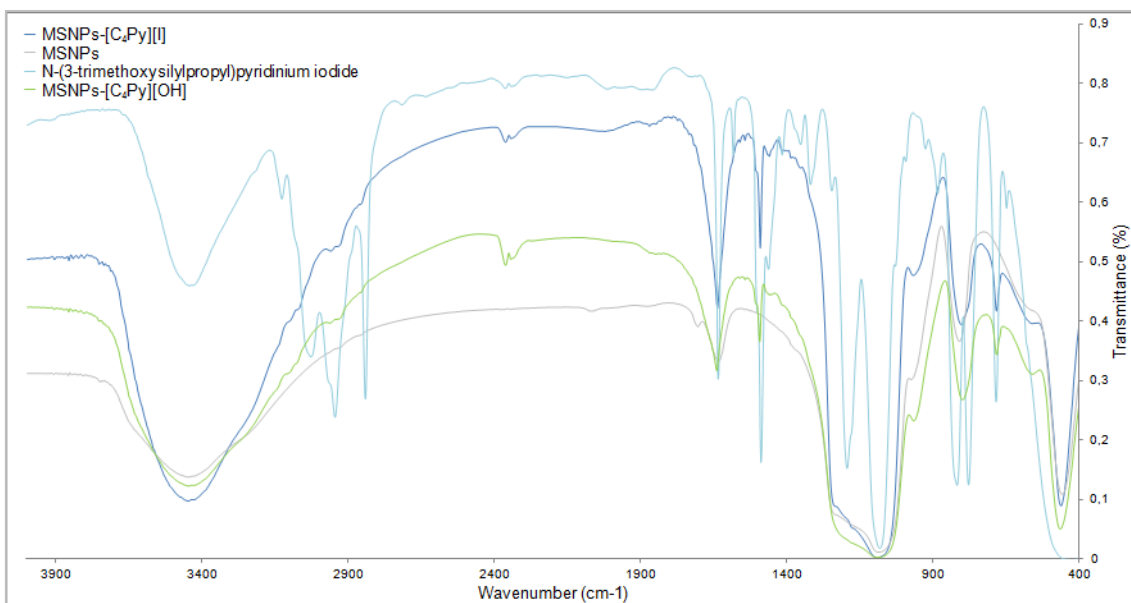


**Fig. A.2.3.** – FTIR spectra of MSNPs-[C<sub>4</sub>Py][I], MSNPs-[C<sub>4</sub>Py][OH], MSNPs and N-(3-trimethoxysilylpropyl)pyridinium iodide.

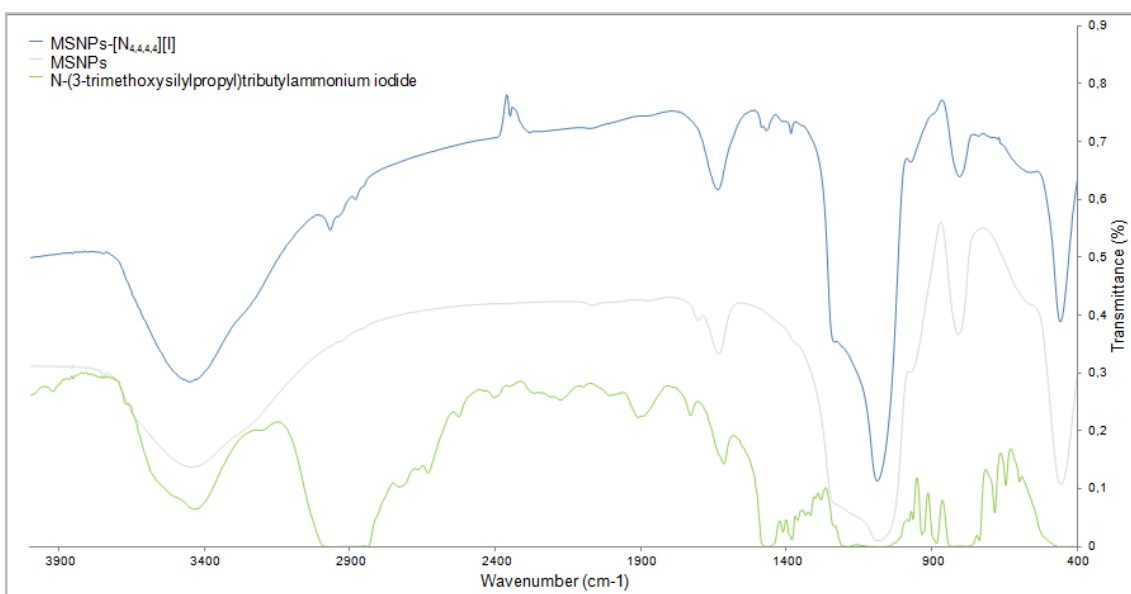


**Fig. A.2.4.** – FTIR spectra of MSNPs-[N<sub>4,4,4,4</sub>][I], MSNPs and N-(3-trimethoxysilylpropyl)tributylammonium iodide.

## **Bibliography**

- [1] Collins, T.; *Science*, **2001**, 48, 291.
- [2] Agency, U. S. E. P., EPA, Available at <http://www.epa.gov/>
- [3] Zimmerman, J. B.; Anastas, P. T.; *Environmental Science And Technology*, **2003**, 37, 94A.
- [4] Tang, S.; Bourne, R.; Smith, R.; Poliakoff, M.; *Green Chemistry*, **2008**, 10, 268.
- [5] Anastas, P. T.; Warner, J. C., *Oxford University Press: New York*, **1998**, p.30.
- [6] ACS Chemistry For Life, Examples of Green Chemistry. Available on: <https://www.acs.org/content/acs/en/greenchemistry/what-is-green-chemistry/examples.html>
- [7] Independent Statistics & Analysis U.S. Energy Information Administration, *Biomass Explained*, **2017**. Available at [https://www.eia.gov/energyexplained/?page=biomass\\_home](https://www.eia.gov/energyexplained/?page=biomass_home)
- [8] PT. Biomassa Jatim Energy, 2016. Available at <http://punakawansejati.co.id/category/pt-biomassa-jatim-energy/>
- [9] P. Mckendry, *Bioresource Technology*, **2002**, 83, 37-46.
- [10] Union of Concerned Scientists, *How Biopower Works*, **2015**. Available at [http://www.ucsusa.org/clean\\_energy/our-energy-choices/renewable-energy/how-biomass-energy-works.html#.Wa7K9dQrlrg](http://www.ucsusa.org/clean_energy/our-energy-choices/renewable-energy/how-biomass-energy-works.html#.Wa7K9dQrlrg)
- [11] M. Anissimov, What is Photosynthesis, 2017. Available at <http://www.wisegeek.com/what-is-photosynthesis.htm>
- [12] GLW Energy. Available at: <https://glwenergy.com/biomass/>
- [13] W. G. Glasser and S. Sarkane, *American Chemical Society*, **1989**, 560 pp.
- [14] J. H. Lora and W. G. Glasser, *J. Polym. Environ.*, **2002**, 10, 39–48.
- [15] J. Zakzeski, P. C. A. Bruijninx, A. L. Jongerius and B. M. Weckhuysen, *Chem. Rev.*, **2010**, 110, 3552–3599.
- [16] T. Gomiero, M. G. Paoletti and D. Pimentel, *J. Agric. Environ. Ethics*, **2010**, 23, 403-434.
- [17] W. Boerjan, J. Ralph and M. Baucher, *Annu. Rev. Plant Biol.*, **2003**, 54, 519–546.
- [18] R. Ma, Y. Xu and X. Zhang, *ChemSusChem.*, **2014**, 7, 1–29.
- [19] H. Lange, S. Decina and C. Crestini, *Eur. Polym. J.*, **2013**, 49, 1151–1173.
- [20] M. A. Eisenstadt and K. G. Bogolitsyn, *Russ. J. Bioorg. Chem.*, **2010**, 36, 802–815.

- 
- [21] A. D. Adler, R. F. Longo, F. Kampas and J. Kim, J., *Inorg. Nucl. Chem.*, **1970**, 32, 2443–2445.
- [22] Lignowork. What is Lignin?. Available at: <http://www.icfar.ca/lignoworks/content/what-lignin.html>
- [23] G. Chatel et al., *Green Chem.*, **2016**, 18, 1839.
- [24] E. Farnetti, R. Di Monte, J. Kašpar, *Inorganic and Bio-Inorganic Chemistry, Homogeneous and Heterogeneous Catalysis, Vol. II.*
- [25] X. Ma, K. Sakanishi, I. Mochida, *Ind. Eng. Chem. Res.*, **1994**, 33 (2), 218–222.
- [26] M. Muzic, K. Sertic-Bionda, Z. Gomzi, S. Podolski, S. Telen. *Chemical Engineering Research and Design*, **2010**, 88, 4, 487-495.
- [27] U. Domańska, K. Walczak, M. Królikowski, *The Journal of Chemical Thermodynamics*, **2014**, 77, 40–45.
- [28] M. Soleimani, A. Bassi, A. Margaritis, *Biotechnology Advances*, **2007**, 25, 6, 570-596.
- [29] Wilkes, J.; *Green Chemistry*, **2002**, 4, 73.
- [30] Parshall, G. W.; *Journal of the American Chemical Society*, **1972**, 94, 8716.
- [31] Koch, V. R.; Miller, L. L.; Osteryoung, R. A.; *Journal of the American Chemical Society*, **1976**, 98, 5277.
- [32] L. Branco. Líquidos Iônicos: Aplicações e Perspectivas Futuras. *Química*, **2015**., 139
- [33] M. Freemantle, *RSC Publishing*, **2010**.
- [34] Plechkova, N.; Seddon, K.; *Chemical Society Review*, **2008**, 37, 123.
- [35] Sigma-Aldrich, Chemfiles Volume 5, Article 6.
- [36] MacFarlane, D. R.; Pringle, J. M.; Johansson, K. M.; Forsyth, S. A.; Forsyth, M.; *Chemical Communications*, **2006**, 1905.
- [37] P. Wasserkeid, T. Welton, Wiley-VCH, **2007**.
- [38] D. Cole-Hamilton, R. Tooze, *Springer*, **2006**.
- [39] S. Keskin, D. Kayrak-Talay, U. Akuran, O. Hortaçsu, J. *Supercritical Fluids*, **2007**, 43, 150-180.
- [40] Aldrich, Ionic Liquids - Enabling Technologies, *ChemFiles*, **2005**, 5.
- [41] S. Omwoma, C.T. Gore, Y. Ji, C. Hu, Y.-F. Song, *Coordination Chemistry Reviews*, **2015**, 286, 17-29.

- 
- [42] X. Chen, H. Li, P. Yin, T. Liu, "Design of polystyrene latex particles covered with polyoxometalate clusters via multiple covalent bonding", *Chemical Communications*, **2015**, 51, 6104-6107.
- [43] C. Granadeiro, S. Ribeiro, S. Balula and L. Cunha-Silva, "Polyoxometalates@MOFs Composites: Efficient and Versatile Heterogeneous Catalysts for Sustainable Oxidative Systems", **2014**.
- [44] D.C. Julião, "Novos Catalisadores Heterogêneos Contendo Polioxometalatos: Preparação e Aplicação Catalítica", *Universidade do Porto*, **2013**.
- [45] A. Libermana, N. Mendez, W. Troglerb, & A. Kummelb, *Surf Sci Rep*, **2014**, 69, 132–158.
- [46] I. Slowing, B. Trewyn, S. Giri, & V. Lin, *Adv. Funct. Mater*, **2007**, 17, 1225–1236.
- [47] U. Zulfikar, T. Subhani, S. Wilayat Husain, *Journal of Asian Ceramic Societies*, **2016**, 4, 91–96.
- [48] Li, Z. X.; Barnes, J. C.; Bosoy, A.; Stoddart, J. F.; Zink, J. I. *Chem. Soc. Ver.*, **2012**, 41, 2590–2605.
- [49] Meng, H.; Xue, M.; Xia, T.; Ji, Z. X.; Tarn, D. Y.; Zink, J. I.; Nel, A. E. *ACS Nano*, **2011**, 5, 4131–4144.
- [50] Napierska, D.; Thomassen, L. C. J.; Rabolli, V.; Lison, D.; Gonzalez, L.; Kirsch-Volders, M.; Martens, J. A.; Hoet, P. H. *Small*, **2009**, 5, 846–853.
- [51] Bouchoucha M., Côté M., C.-Gaudreault R., Fortin M., Kleitz F., *Chem. Mater*, **2016**, 28, 4243–4258.
- [52] Kim, T. W.; Chung, P. W.; Lin, V. S. Y. *Chem. Mater.*, **2010**, 22, 5093–5104.
- [53] Wu, S., Moua C.Y., Lin H.P.. *Chem. Soc. Rev.*, **2013**, 42, 3862.
- [54] Freire C., Pereira C., Rebelo S., *Catalysis*, **2002**, 24, 116-203.
- [55] Badamali et al. *Cat. Commun.*, **2013**, 31, 1-4.
- [56] Hwang et al. *J. Molecular Catalysis A: Chem.*, **2004**, 208, 195-202.
- [57] Cho et al. *Bull. Korean Chem. Soc.* **2011**, Vol 32, 6.
- [58] Jovanovski et al. *J. Phys. Chem. B*, **2005**, 109, 14387-14395.
- [59] Katcka, M. and Urbanski T., *Bull. L'Academie Pol. Sciences*, **1984**, Vol XII, 9.
- [60] L.S. Nogueira, S. Ribeiro, C.M. Granadeiro, E. Pereira, G. Feio, L. Cunha-Silva, S.S. Balula, *Dalton Trans*, 43, 9518-9528, **2014**.
- [61] Udayakumar, S.; Park, S.W.; Park, D.W.; Choi, B.S. Immobilization of ionic liquid on hybrid MCM-41 system for the chemical fixation of carbon dioxide on cyclic carbonate. *Catalysis Communications*, **2008**, 9, 1563–1570.

---

[62] Crucho et al., *Anal. Chem.*, **2017**, 89, 681–687.

[63] Wang et al. *Chinese Journal of Catalysis*, **2014**, 35, 532–539.